The Geology and Petrochemistry of the Sisson Brook W-Cu-Mo Deposit, New Brunswick

by

Heidi J. Nast
Department of Geological Sciences
McGill University, Montreal
August, 1985

A thesis submitted to the faculty of Graduate Studies and Research in partial fulfillment of the requirements for the degree of Master of Science.

ABSTRACT

The Sisson Brook W-Cu-Mo deposit is located in central New Brunswick. Four phases of deformation and/or metamorphism have affected the surrounding area. The last event (M4) probably occurred during Upper Devonian to Lower Carboniferous time. It was associated with development of a steeply-dipping foliation surface, E-trending faults, and intrusion of a feldspar-quartz-biotite porphyry. The latter led to mineralization and hydrothermal alteration.

Potentially economic mineralization occurs in four vein sets (VI to VIV), concentrated in two N-trending zones which extend northward (Zone A) and flank the western edge of (Zone B) the porphyry. Zone A occurs in metavolcano-sediments and Zone B is hosted by gabbro and metavolcano-sediments. The economically important mineralization in Zone A consists of chalcopyrite and wolframite in VIV quartz stockworks and veins; in Zone B it consists mostly of yellow fluorescent (molybdenum-bearing) scheelite in VI amphibole and VII quartz vein(let)s, and white fluorescent (pure $CaWO_4$) scheelite and molybdenite in VIII and VIV quartz veins and stockworks.

Each vein set is associated with specific alteration minerals which occur pervasively in and near the deposit, and in vein haloes. These associations are: VI - hornblende and sodic plagioclase (A1); VII and VIII - biotite, K-feldspar and sodic plagioclase (A2); and VIV - sericite and pyrite (A3). Vein set VI and A1 alteration are host rock specific, occurring largely in mafic units. A2 and A3 alteration are

most intense in Zones B and A, respectively.

An electron microprobe study of vein and alteration phases shows compositional changes in the amphiboles and biotites southward across Zone A and eastward into Zone B: VI/A1 amphiboles are enriched in Al, Fe, and alkalies and VII, VIII/A2 biotites are enriched in Fe. In addition, the most sodic A1 and A2 plagioclases occur in Zone B.

An fO2-fS2 phase diagram for the H-O-S-Fe system showing contours of XFe in amphibole, indicates that the Fe-enrichment of A1 amphibole resulted in part, from host rock buffering of fO2. This, as well as the dependence of VI/A1 mineral compositions on host rock lithology suggest that the fluid to rock ratio was low during their formation. In contrast, a high fluid to rock ratio is inferred for the VII, VIII/A2 assemblages from the low Kd value for Fe/Mg between A2 biotite and the A1 amphibole it replaces. VIV/A3 minerals probably formed when the fluid to rock ratio was at its highest as evidenced by the abundance and large-scale nature of VIV quartz stockworks.

The composition and association of vein/alteration minerals show that the minerals formed under changing fO2/fS2 conditions. VI/A1 minerals formed under oxygenating conditions; VII, VIII/A2 minerals formed under decreased fO2/fS2 conditions; and VIV/A3 minerals precipitated following increases in fO2 and fS2.

Mass balance equations show that VI and A1 assemblages formed from silica-undersaturated, moderately alkali-enriched fluids and that the A2 assemblage formed from silica-saturated, highly potassic fluids.

Fluid inclusion data indicate that VI through VIV mineralization and associated alteration occurred between 350°C and 450°C, and that orthomagmatic fluids may have been present during formation of vein sets VIII and VIV.

Significant drops in pressure and temperature followed formation of vein set VIV and led to widespread deposition of massive carbonate (vein set VV) and collapse of the hydrothermal system.

RESUME

Le gîte de W-Cu-Mo de Sisson Brook est situé dans la région centrale du Nouveau-Brunswick. Quatre phases de déformation et/ou de métamorphisme ont affecté la région. La dernière phase (M4) a probablement eu lieu pendant l'intervalle du Dévonien supérieur au Carbonifère inférieur. Elle s'est accompagnée du développement d'une foliation a fort pendage, de failles d'orientation est-ouest et de l'intrusion d'un porphyre à feldspath-quartz-biotite. Cette dernière a produit la minéralisation et l'altération hydrothermale.

La minéralisation économique potentielle est localisée dans quatre groupes de filons (VI a VIV) concentrés en deux zones d'orientation nord-sud; la Zone A s'étire vers le nord et la zone B flanque la bordure ouest du porphyre. La Zone A se trouve dans des terrains sédimentaires et métavolcaniques et la Zone B dans un gabbro et des roches sédimentaires et métavolcaniques. Dans la Zone A, la minéralisation d'importance économique consiste en chalcopyrite et wolframite dans des filons et des stockwerks a quartz VIV; dans la Zone B, elle consiste en scheelite à fluorescence jaune dans des filons à amphibole VI et a quartz VII, et en scheelite à fluorescence blanche et en molybdénite dans des filons et stockwerks à quartz VIV.

Chaque groupe de filons est associé à des minéraux d'altération spécifiques qui sont abondamment disséminés dans

le gîte et aux abords, et dans les halos filoniens. Ces associations sont: VI - hornblende et plagioclase sodique (A1); VII et VII - biotite, feldspath potassique et plagioclase sodique (A2); et VIV séricite et pyrite (A3). Les filons VI et A1 sont généralement restreints aux unités mafiques encaissantes. Les altérations A2 et A3 sont plus intenses dans les Zones B et A respectivement. Une étude a la microsonde des minéraux filoniens et d'altération montrent des variations dans la composition des amphiboles et des biotites vers le sud dans la Zone A et vers l'est dans la Zone B: les amphiboles VI/A1 s'enrichissent en Al, Fe et en métaux alcalins et les biotites s'enrichissent en Fe. Enfin, les plagioclases A1 et A2 les plus sodiques se trouvent dans la Zone B.

Un diagramme de phase de fO2-fS2 du système H-O-S-Fe, avec isoplèthes du XFe de l'amphibole, indique que l'enrichissement en Fe de l'amphibole A1 résulte probablement en partie d'un effet tampon de la roche encaissante sur fO2. Ceci, comme la dépendance des compositions minérales VI/A1 de la nature de la roche encaissante, suggère un rapport fluide:roche peu élevé pendant leur formation. Par contre, d'après le Kd peu élevé du rapport Fe/Mg entre la biotite A2 et l'amphibole A1 qu'elle remplace, on infère un rapport fluide:roche élevé pour les assemblage VII, VIII. Les minéraux VIV/A3 ont probablement été formés lors du rapport fluide:roche maximal comme l'indiquent l'abondance et la grande taille des stockwerks à quartz VIV.

La composition et l'association des minéraux filoniens et d'altération montrent que les minéraux ont été formés dans des conditions variables relatives au rapport fO2/fS2. Les minéraux VI/A2 ont été formés dans des conditions oxygénées; les minéraux VII, VIII/A2 ont été formés dans des conditions de fO2/fS2 décroissant et les minéraux VIV/A3 ont été précipités à la suite d'élévations de fO2 et fS2 (Chap. 7).

Les équations de balance massique montrent que les assemblages VI et A1 proviennent de fluides sous-saturés en silice et modérément alcalins alors que l'assemblage A2 provient de fluides saturés en silice et fortement potassiques. Les données d'inclusions fluides indiquent que les épisodes minéralisants VI à VIV et leur altération ont eu lieu entre 350°C et 450°C et que les fluides orthomagmatiques auraient pu être présents pendant la formation des filons VIII et VIV.

A la suite de la formation des filons VIV, des chutes significatives de pression et de temperature ont mené à la précipitation généralisée de calcaires massifs (filons VV) et à l'effondrement du système hydrothermal.

Table of Contents

Page

Chapter 1. Introduction

Chapter 2. Geologic setting

Chapter 3. Mineralization

Chapter 4. Hydrothermal alteration

Chapter 5. Chemistry

Chapter 6. Fluid inclusions

Chapter 7. Petrogenesis of the vein and alteration assemblages

List of Figures

List of Tables

ACKNOWLEDGEMENTS

The author gratefully acknowledges the financial support of Kidd Creek Mines, Ltd. throughout the entirety of this project. Special thanks to Dr. R.L. Moore for his continued interest in the project, and who was especially helpful in sending pertinent company data to the author throughout the project duration. The author also wishes to thank Mr. R. Mann for his assistance in orienting the author in the field and his hospitality, to Mr. W. Gardiner for sharing his insights and data from independent work in the surrounding areas, and to Dr. D. Scott for sharing his chemical data of some of the mineral phases.

The author also gratefully acknowledges the one year fellowship and award with the Mineral Exploration Research Institute (IREM/MERI).

The author is especially grateful for her advisor, Prof. A.E. Williams-Jones, who not only gave thoughtful guidance and editing throughout the project, but provided the author with the space necessary to learn.

The author also wishes to thank her contemporaries: Dr. Iain Samson for his numerous discussions and expertise in fluid inclusions, Mr. Bob Linnen for his encouragement and discussions on thermodynamics, Mr. George Cutter for sharing his expertise in key thermodynamic concepts, to Mr. Ian Graham for generously sharing his knowledge of mathematics, to Ms. Susan Stodder for giving of her time and knowledge of physical chemistry, and to Ms. Isabelle Cadieux for her interesting and enlivening discussions on geology and life.

Lastly, the author offers her heartfelt thanks to Mr. Richard Yates. With characteristic precision and care, he taught the author how to draft, and listened painstakingly to the many groans and cursings which ensued.

CHAPTER 1. INTRODUCTION

1.1 INTRODUCTION

The Sisson Brook deposit is a promising W-Cu-Mo prospect that is located in the southern part of the Miramichi Zone of central New Brunswick (Fig. 1.1). The deposit occurs within the eastern part of the thermal aureole of the (post-Acadian) Nashwaak granite, and is adjacent to an elongate geophysical anomaly, believed to represent the near surface extent of a feldspar-quartz-biotite porphyry (Chap. 2).

The deposit comprises two mineralized vein- and stockwork-filled fracture zones hosted by metavolcano-sediments in the north (Zone A), and gabbro and metavolcano-sediments in the south (Zone B; Fig. 2.1). It is estimated that Zone A contains 7.5 million tons grading 0.35% Cu as chalcopyrite and 0.21% WO3 as wolframite. Reserves have not been calculated for Zone B, in which the mineralization grades approximately 0.10% WO3 and/or 0.10% Mo, as scheelite and molybdenite, respectively.

Sisson Brook is one of sixteen similarly mineralized vein and/or stockwork zones in New Brunswick which comprise an arc-shaped W ± Mo ± Cu ± Sn metallogenic province of probable Upper Devonian to Lower Carboniferous age. The metallogenic province is bounded along most of its length by faults interpreted as reactivated Acadian and transecting shear structures which formed during a late distentional event (Fig. 2 in Ruitenberg and Fyffe, 1982). Although all the showings occur within the thermal aureoles of Devonian-

Figure 1.1 Location map of the Sisson Brook deposit. Inset shows the approximate location of the Sisson Brook deposit within the major tectonostratigraphic zones of New Brunswick.

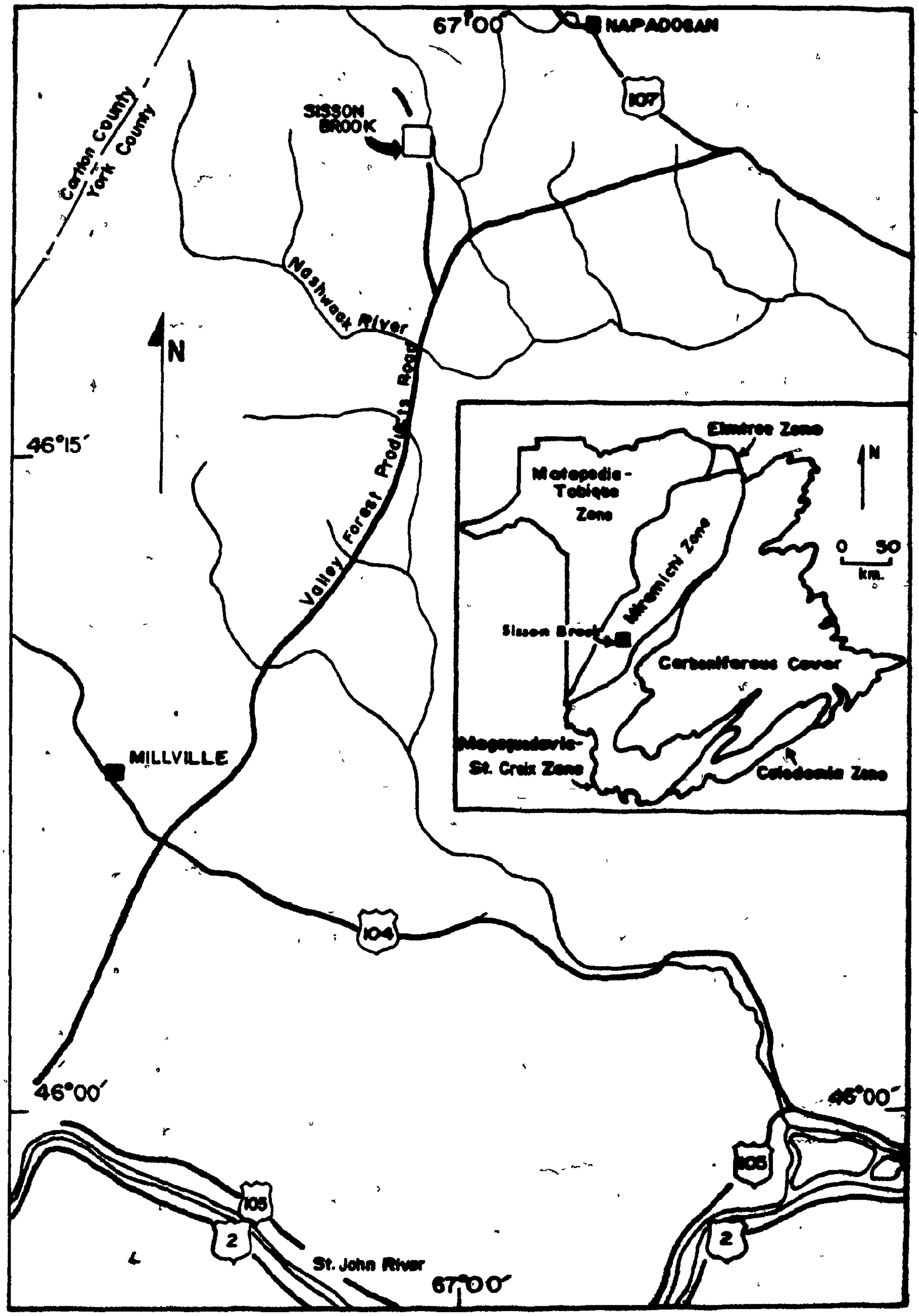
67°00'
NAPADOGAN
107
SISSON BROOK
Carlton County
York County
Nashwaak River
N
46°15'
Valley Forest Products Road
MILLVILLE
104
46°00'
46°00'
105
2
105
2
St. John River
67°00'
Elmtree Zone
Matapedia-Tobique Zone
Miramichi Zone
N
0 50 km.
Sisson Brook
Carboniferous Cover
Magaguadavic-St. Croix Zone
Caledonia Zone

age post-Acadian granites, they appear to be genetically associated with a later tectonic event of probable Middle Devonian to Early Carboniferous age. At Sisson Brook, the late event is manifested in the intrusion of a small feldspar-quartz-biotite porphyry which crosscuts the thermal aureole of the Nashwaak granite. Similar late granite porphyries have been found at several other showings (e.g., Burnt Hill, Rocky Brook, Square Lake, in Ruitenberg and Fyffe, 1982).

This thesis presents a geologic map of the Sisson Brook area based upon a petrographic and field examination of the structural, metamorphic, and hydrothermal features observed in drill core and outcrop; a detailed comparative study of the petrography and geometry of the mineralization and host rock alteration in the two main mineralized zones at Sisson Brook; and a working hypothesis and model for the type and evolution of the mineralizing system.

1.2 LOCATION AND ACCESS

The Sisson Brook mining license is located 60km northwest of Fredericton, New Brunswick, 8km along a fire access road approximately 27km north of the intersection of the Valley Forest Products Road and highway 104 (Fig 1.1). All outcrops are easily accessible by foot and most are within a kilometer of a small lumber road. Access is facilitated by the good condition of grid lines, low relief, and lack of dense underbrush. Good outcrop occurs over approximately five percent of the area.

1.3 EXPLORATION HISTORY

The earliest published report of mineral exploration predates the first geologic description of the Sisson Brook area (Nashwaak Pulp and Paper Co., 1960; Anderson, 1968). The report includes the results of an aeromagnetic survey conducted as part of the exploration program, and delineates an anomaly coincident with what is now known as Zone A (Mann, 1980). In 1967-69 Penarroya Ltee., initiated a more extensive exploration program and drilled four holes which intersected several, meter wide, intervals of scheelite-tungsten mineralization (Rabinovitch, 1969).

In 1978 Texasgulf Inc. noted a correlation between high Mo values in stream sediments near and west of Sisson Brook (NBDNR map sheet 21J/6E, 1974) and the enriched molybdenum-tungsten intervals in the Penarroya drill holes (Moore, 1978). Fifteen claims were subsequently staked. A soil geochemical survey conducted in part of the claim group (McQuade, 1979) and a regional tin-tungsten stream-sediment survey conducted by Texasgulf, Inc., showed a correlation between high Cu, Bi, W, Mo values and high tungsten values in parts of the Sisson, Napadogan, and Bird Brook drainage basins.

In 1979 Texasgulf staked 88 additional claims north and south of the original claim group, and initiated an exploration program consisting of detailed mapping, soil sampling, and a geophysical survey. Eleven holes (SSN 1-11) were drilled along three geophysical anomalies (Moore, 1979) and intersected significant Cu-W mineralization in two NNW-trending quartz stockwork zones (Zone A; Mann, 1980; see Fig. 3.9). In 1980, twelve holes (SSN 12-23) were drilled under and laterally offset from drill holes SSN 1-11 in an attempt to define the three dimensional nature of this fracture system.

In 1981, nine holes were drilled 0.5km south of Zone A (SSN 24-32). Five of these intersected abundant scheelite-molybdenite mineralization in what was interpreted to be a single, semi-continuous, quartz vein system, and one drill hole intersected more than 40m of relatively unaltered unfoliated feldspar-quartz-biotite (FQB) porphyry (Mann, 1981b). In 1982, eight additional holes (SSN 33-40) were drilled along strike of the above mineralization, and helped define several scheelite and crosscutting scheelite-molybdenite mineralized fracture zones over 1.5 km long and 0.5km wide (Zone B; Fig. 1.2; see Fig. 3.10).

Numerous short reports have been prepared on the petrography and mineralization of the rocks at Sisson Brook since 1978. These include a report of the general geology and mineralization of Sisson Brook, made prior to Texasgulf drilling (McQuade, 1979), a mineralogic and electron microprobe study of selected samples from drill holes 1-19 (Hak and Watkinson, 1981), two short petrographic reports (Abbott, 1981; Williams-Jones, 1981), two geophysical survey reports (Gasteiger, 1982; Ravenhurst, 1982), an investigation of the geochemical variance of the plutonic rocks (Lougheed, 1982), and a comprehensive fluorescence, microprobe and petrographic study of scheelite-bearing samples from Zone B (Scott, 1982); the latter samples were analyzed for major elements, %Mo and %W .

1.4 METHODS

A geological map was compiled by the author during the summer of 1982. All samples collected from the field were slabbed and photographed to facilitate identification, review, and later reclassification if necessary. Geological reports by workers who independently mapped various sectors of the property provided the basis for distinguishing the major units (McQuade, 1979; Lutes, 1981; Lougheed, 1982). Geophysical reports aided in the placement of major faults and interpretation of local structures (Gasteiger, 1982; Ravenhurst, 1982).

Drill holes SSN 1, 5, 11, 13, 19, 25, 26 were relogged in detail to document occurrences of vein or stockwork gangue and associated mineralization as well as the degree and nature of related local and/or pervasive alteration. A significant correlation was discovered between the color of a particular unit and the type and degree of alteration. This correlation was used to derive a hydrothermal alteration color index by which all colors recorded in previous drill logs were related to a specific type and intensity of wallrock alteration (Chap. 4).

A three-dimensional analysis of the mineralization and some of the associated hydrothermal alteration was made by constructing two (2) three-dimensional models of Zones A and

B at scales of 1:500 and 1:1000, respectively. This was achieved by projecting wt.% WO_3, MoS_2, and Cu values and alteration intensity onto two separate sets of semi-transparent vertical drill hole sections. (Vertical sections were computer-generated and supplied by Kidd Creek Mines, Ltd.).

Ten parallel vertical sections which trend 084° were made for Zone A. This orientation subparallels the strike of the drill holes and is approximately perpendicular to the strike of Zone A mineralization. The sections were drawn at ~100m intervals and extend from L8N to L3S.

Eight parallel vertical sections trending 090° were made for Zone B. The 090° orientation crosscuts the mineralization at a high angle (70° to 90°) and subparallels the strike of the drill holes. The sections were drawn at 50 to 100m intervals and extend from L6 to 12S.

The vertical sections from each zone were then hung to scale in three dimensions and used to derive the plan and cross sections of mineralization and alteration presented in Chapters 3 and 4

Drill hole SSN 13, the most heavily mineralized in Zone A, SSN 26, heavily mineralized and containing the largest intervals of the FQB porphyry in Zone B, and SSN 25, within the periphery of Zone B were sampled and studied in the greatest detail. All samples collected from these drill holes were slabbed, polished, and stained. The latter was accomplished by etching each sample for thirty seconds in

60% hydrofluoric acid and staining it in a saturated solution of sodium cobaltinitrate.

Vein and host rock materials from all drill holes were collected for general petrographic study, and representative samples were collected from drill holes SSN 1, 2, 3, 8, 9, 11, 13, 25, 26, 28, 31, 33, 36, 37, 38 for microprobe and/or fluid inclusion study. In total, 331 thin-, 82 polished thin-, 40 polished thick-, and 29 doubly polished fluid inclusion sections were examined using a Leitz HM-POL polarizing microscope with a Leitz Wetzlar GMBH epi-illuminator.

Microphotographs were made using Kodacolor 64 or 100 ASA film with a blue filter, or Ektachrome 160 or 400 ASA film and no filter on an Ultraphot. Scheelite identification was accomplished using UVGL-48, M-12, and MSL48 6V Mineralight Lamp models of Ultra Violet Products, Inc., San Gabriel, California and model F-8 of Raytech, Inc. of Stratford, Conn. The sliding filter was removed in models MSL48 and UVGL48 to increase overall ultraviolet output.

Fluid inclusion work was done on a SGE model III freezing and heating stage with a Leitz SMLUX polarizing microscope and a high intensity type 3M-ENX 160W projection lamp. The apparatus was previously calibrated from -50 to 500 C using organic compounds and native metals of known melting points.

Electron microprobe analyses were carried out on a wavelength dispersive Camebax model MB1 microbeam by Cameca at 15 kV and 5 to 10nA.

Bulk rock analyses were done by X-Ray Assay laboratories of Don Mill, Ontario. Bondar-Clegg of Ottawa, Ontario conducted most of the chemical analyses of trace elements.

Correlation coefficients between mineralization and alteration (Chap. 4) were derived using a McGill main frame statistical program, STATPAK. Stoichiometric calculations of amphiboles, biotites and plagioclase were made on an IBM-PC using published or in-house programs, and are referred to in full in Chapter 5. Graphical depiction of electron microprobe data (Chap. 5) was done using an in-house program, ROCGRAF2, which employs an IBM-PC and EPSON printer. Iterative calculations used in the construction of phase diagrams were made using a program written in Fortran, COMP, on McGill's main frame (Chap. 7).

CHAPTER 2. GEOLOGIC SETTING

2.1 TECTONOSTRATIGRAPHIC SETTING

The Sisson Brook deposit is located within the southern portion of the Miramichi Zone, also known as the Miramichi Anticlinorium (Anderson, 1968; Rodgers, 1970), the Miramichi Massif (Fyffe, 1981) and Zone 3 (Ruitenberg, et.al., 1977; see Fig. 1.1). The Miramichi Zone consists of a thick sequence of continental, marine, and volcanosediments, intruded by polydeformed foliated Ordovician granites, numerous unfoliated to weakly foliated Devonian granites, and minor felsic stocks and porphyries of probable Upper Devonian to Lower Carboniferous age.

The oldest exposed rocks in the zone belong to the Cambro-Ordovician Lower Tetagouche Group, to which Unit I at Sisson Brook is tentatively assigned. The rocks comprise a thick succession of quartz-wackes, quartzites, and slates, which are interpreted to be continental wedge sediments shed off the Avalon microcontinent during a period of late Hadrynian-Cambrian distension (Ruitenberg, et.al., 1977). The sequence is capped by Lower Ordovician calcareous slates or an unconformable pebble conglomerate, and is overlain by the Upper Tetagouche Group, an intercalated sequence of pillow basalts, felsic volcanics, feldspathic graywackes, red and gray slates, and limestone.

The Tetagouche Group underwent intense folding and polydeformation as a result of the closing of the Iapetus ocean during the Late Ordovician Taconic orogeny (Rodgers, 1970). Abundant flysch sedimentation ensued during Siluro-Devonian time in marginal basins which developed off either side of the Miramichi Zone, which is considered to have acted as the main axis of an upraised geanticline.

Voluminous quantities of granitic material were emplaced semi-continuously throughout early Devonian-Carboniferous times along two belts: the Central Plutonic Belt which lies within the Miramichi zone and includes the Nashwaak granite, <100 to 750m west of the deposit, and the Southern Plutonic Belt which lies in the Fredericton Trough. The igneous activity was succeeded by a late tectonic event of probable Upper Devonian to Lower Carboniferous age.

About 15 tungsten showings, similar to Sisson Brook have been found in New Brunswick and define a northerly trending, arc-shaped W ± Mo ± Cu ± Sn metallogenic province which crosscuts the Central and Southern Plutonic belts. The showings are hosted by Cambrian to Silurian age metasediments and occur near intersections of the late shear structures and thermal aureoles of granites in the Southern or Central Plutonic belts. Late porphyritic stocks are spatially associated with some of the showings, including Sisson Brook. This suggests that small-scale plutonism was associated with the late faulting and may have been responsible for the mineralization (see Table 1 in Ruitenberg and Fyffe, 1982).

2.2 LOCAL GEOLOGY

2.2.1 STRATIGRAPHY

A geological map of the Sisson Brook area was compiled during the summer of 1982 (Fig. 2.1). This endeavor was facilitated by field checking and sampling areas in the mining license which had been mapped previously by other workers (Mann, 1979; McQuade, 1979; Lougheed, 1981). Major lithologic units were distinguished by compositional and textural differences observed in the field.

Unit I is comprised of quartzitic sediments with lesser amounts of siltstones, pelites, and argillites. It is believed to be the oldest unit in the area and to comprise the axial zone of a regional anticline. Unit I is overlain to the east and west by what are considered to be stratigraphically equivalent shales (Unit IIa) and volcanosediments (Unit II b), respectively (Lutes, 1981). The eastern boundary of the Sisson Brook Mining License occurs within the western part of the shale unit.

Unit IIb is crosscut by massive metagabbro (Unit III) to the west which is, in turn, crosscut by leucogranite dykes and stringers (Unit IVb), that are increasingly abundant to the west. Further west, Unit III is intruded by the pink, coarse grained Nashwaak granite (Unit IVa).

An unfoliated and unmetamorphosed feldspar-quartz-biotite porphyry (Unit V) is found in drill core from SSN 26, 28, 33, 36 and 37, near the Unit III-IIb contact which suggests it intruded along the gabbro-sediment contact. The porphyry is believed to post-date intrusion of the Nashwaak granite, and to have been responsible for the mineralization at Sisson Brook.

Figure 2.1 Geological map of the Sisson Brook area showing major stratigraphic units and location of main mineralized zones, A and B.

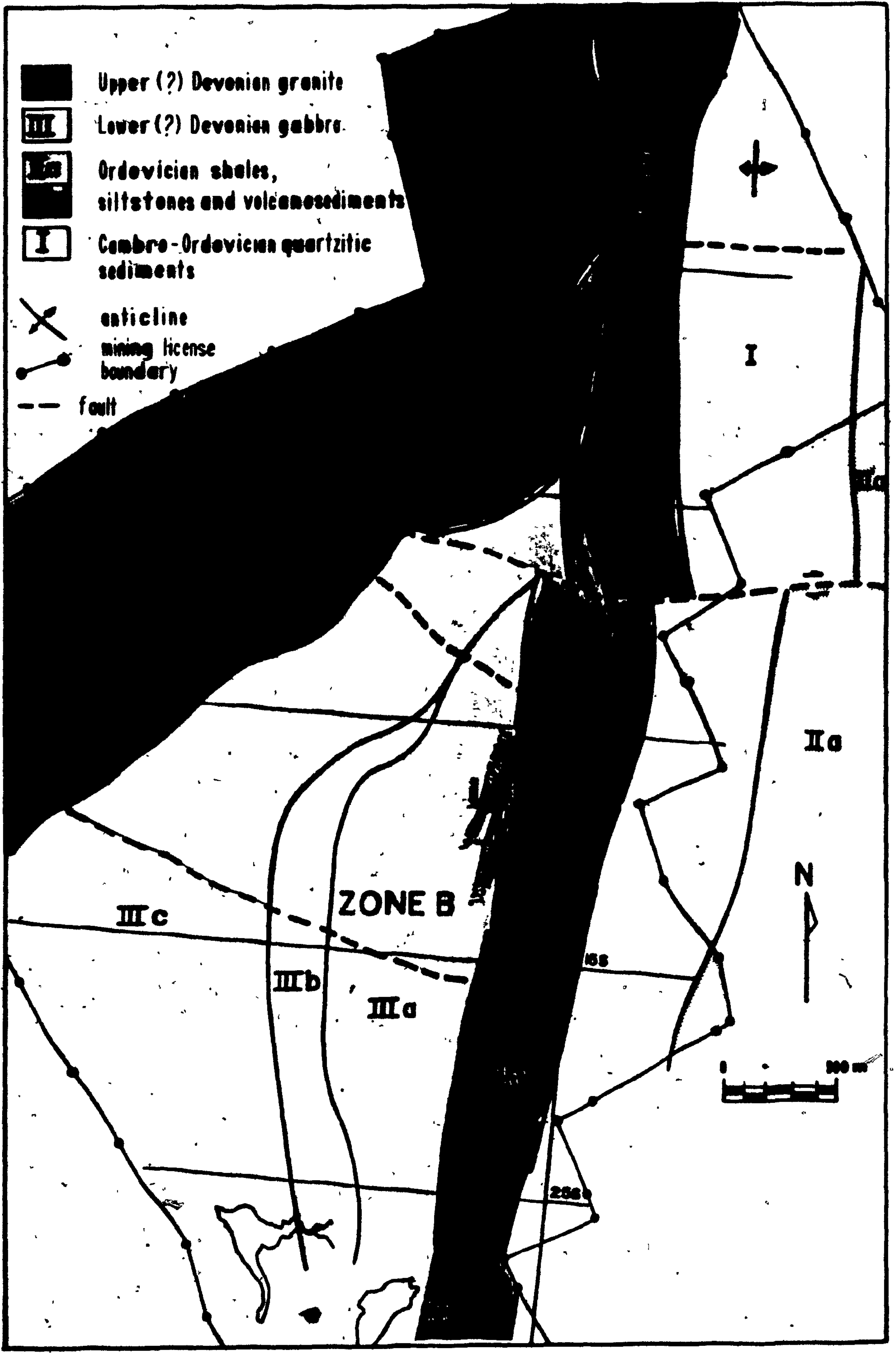
Upper (?) Devonian granite
III Lower (?) Devonian gabbro
IIa Ordovician shales, siltstones and volcanosediments
I Cambro-Ordovician quartzitic sediments
anticline
mining license boundary
fault
I
IIIa
IIa
ZONE B
IIIc
IIIb
IIIa
158
258
N
0
300 m

2.2.1a UNIT I

SUBUNIT IA

Two subunits, A and B, are recognized within Unit I. Subunit IA comprises most of the outcrops and consists of thin (<1.5cm thick) alternating beds of 60% to >90% pink quartzite and black argillite. The subunit also contains thickly bedded (>3.0 cm thick) units of massive, pale blue, quartzites up to >1m wide which contain thin, rare, argillaceous laminae (see Fig. 2.7). In thin section, the quartz within the blue quartzites is subangular and unsorted which indicates that it was locally derived or that there was rapid sediment supply.

A zone of outcrops containing almost no blue quartzites and the highest ratio of pink to black beds occurs semi-continuously along the contact between Units I and IIb (to the west) from L26N to L9N. No outcrops of subunit IA were found south of L3S. Numerous angular boulders comprised of the thinly interlayered pink and black member of subunit A were found, however, between lines L10 to 13S and are interpreted as suboutcrop.

A variant which bears little resemblance in outcrop to subunit A is exposed between L4+50 and 8+50N. The outcrops are highly sheared, schistose, blue-black in color, and exhibit a knotted or bulbous texture. The latter is due to the presence of coarse grained hydrothermal biotite and transposition of the dominant (S2) foliation along a late (S3) crenulation cleavage. However, close inspection reveals that the outcrops comprise the interbedded pink quartzite and black argillite units that characterize subunit IA.

SUBUNIT IB

Subunit IB is exposed along Sisson Brook, and is made up of interbedded argillaceous and silty laminae which weather to form tan and blue-black gritty surfaces. The easternmost outcrop consists of isolated shale rip-up fragments in a dark blue-black silty matrix indicating that the unit formed in a subaerial to shallow water environment. The latter unit probably represents a transitional facies into the Unit IIa black slates to the east.

Westward, subunit IB grades imperceptibly into Unit IIb pelites. The only megascopic difference between the two units is the paucity of fine grained lapilli tuffs and absence of medium or coarse grained ones in Unit I (a single fine grained lapilli tuff was found in drill hole SSN 19). For this reason the first occurrence of medium grained lapilli tuff was chosen to mark the boundary between Unit IIb (below) and subunit IB.

2.2.1b UNIT IIa

Unit IIa occupies the eastern sector of the Sisson Brook area. It is believed to be part of the east limb of a regional anticline (above), and the stratigraphic equivalent of Unit IIb (Lutes, 1981). The unit consists of pyrite-bearing black slates, gray to green-gray silty slates, and minor volcanics. Three subfacies are recognized.

The basal subfacies, C, is composed mostly of graphitic, pyrite-bearing, black slates. In outcrops where late-stage shearing is evident, the slates are highly silicified and contain abundant, commonly contorted and/or ptygmatically folded, thin lenses of white quartz. The unit is overlain by subfacies B, a succession of gray to green silty slates in which no shearing or ptygmatically folded quartz lenses were found. The uppermost subfacies, A, consists of several gray-green volcanic units intercalated with and overlain by slates macroscopically similar to those of subfacies C.

2.2.1c UNIT IIb

Unit IIb consists of mafic and felsic volcanic rocks interbedded with tan to olive silty sandstones, pelites and finely crystalline, deep green-colored, banded or massive (FGA) amphibolitic units. No exposures of Unit IIb were found south of L3+00S. The eastern contact with Unit I is drawn at the base of the last occurrence of a medium-grained lapilli tuff or at the first occurrence of subunit IA. The western contact is intrusive with the Nashwaak granite in the north and the metagabbro in the south.

Two main rock divisions are recognized based upon the presence of a dominant lithology. Subunit IIb1 consists mostly of tan, thinly bedded silty quartzites, lesser pelitic metasediments, and minor volcanics. The quartzites are found mainly along the edge of the Nashwaak granite between L5 and 26N, but minor amounts are also found within the metavolcano-sedimentary-rich subunit described below.

Subunit IIb2 consists of interbedded felsic and intermediate lapilli tuffs, pelites, argillites, minor quartzites, bright green, banded, amphibolitic metasediments, and massive fine grained, dark green, amphibolitic units (FGA). In general, pelitic metasediments increase in abundance to the west and FGA units increase in abundance eastward.

FGA units have a markedly consistent mineralogy composed of fine grained actinolite and plagioclase. Many of the FGA units have finely crystalline textures, suggesting that they are dykes or welded mafic crystal tuffs. FGA units are present in Zones A and B, and are easily recognized in drill core because of their distinct color, massive texture, and consistent mineralogy. For these reasons, the units were used to study and compare the relative amount and type of hydrothermal alteration present in Zones A and B and in the mineralogically similar gabbro (Chaps. 4 and 5).

The interlayering of the sediments and volcanics suggests that the latter were deposited subaerially or in a shallow water environment. It is noteworthy that the quartz-hosted wolframite mineralization in Zone A (Mann, 1980) dies out northward within the volcanosedimentary-rich subunit IIb2 at the interface with subunit IIb1. Copper mineralization, however, continues northward, well into quartzite-rich subunit, IIb1 (Chap. 4).

2.2.1d UNIT III

Unit III comprises the large body of gabbro east of the Nashwaak granite which consists primarily of 40% to 70%

actinolite, and plagioclase. It is divided into three subgroups, a, b, and c based upon variations in metamorphic mineral assemblages and rock fabrics. Subgroups b and c are further divided into two and three variants, respectively.

Field identification of the subgroups was based on textural evidence alone. If an unfoliated equicrystalline texture was apparent, it was identified as IIIa; if the aforementioned texture was difficult to ascertain in outcrop or handsample, but easily recognizable on a sawn surface, it was classified as IIIb. Rocks east of the Nashwaak granite (Unit IVb) and west of Unit IIIb which were relatively mafic and crystalline, but not easily recognizable as gabbro in the field, were classified as Unit IIIc.

UNIT IIIa

Unit IIIa hosts the majority of early scheelite mineralization in Zone B (Chap. 3). Modal analyses of five relatively unaltered Unit IIIa gabbro samples (Table 2.2) show that plagioclase and actinolite make up ~56% and 38% of the gabbro, respectively. The remainder comprises mostly M3 brown biotite which topotaxially replaces the actinolite. Minor opaques are also present and locally outline and/or are concentrated within the actinolite cores. Microprobe analyses reveal that some of the actinolite is cored by relict ferroaugite (Scott, 1983, pers. comm.). Thin section and microprobe data show that the plagioclase has an An content of 50 to 65. The unit locally contains felsic and mafic horizons which define a foliation subparallel to S2.

Table 2.1 Modal analyses of 5 relatively pristine Unit IIIa gabbro samples from drill hole SSN 25. Numbers represent downhole depth, in meters.

Sample	8.34	18.8	20.55	31.20	75.50	Avg.
Actinolite	36%	33%	30%	40%	49%	38%
Plagioclase	54%	60%	66%	56%	45%	56%
M3 Biotite	7%	7%	4%	¼3%	4%	5%
Opaques	< 3%	<1%	>1%	>1%	<2%	1%
Sphene	-	tr.	-	-	-	-

UNIT IIIb

Unit IIIb is lobate-shaped and rims Unit IIIa to the west. The unit is moderately to highly foliated and outcrops for an area over two kilometers in length and 300m in width, pinching out to the north and south. Two subgroups are recognized. The first is equigranular and composed mainly of altered plagioclase and amphibole. The second subgroup has bimodal grain sizes ranging from 0.5to 2mm and 0.25 to 4mm, respectively, and is composed mostly of plagioclase 1 to 2mm across, <25% fine grained amphibole, and minor quartz.

UNIT IIIc

Unit IIIc, located between Unit IIIb and the Nashwaak granite, is over 0.5km in width and several kilometers in length. Unit IIIc is a hybridized version of the gabbro which shows gradual and increasing amounts of hybridization with, and assimilation by, Unit IVb to the west (see Dietrich, 1973, for a summary of hybridization and assimilation criteria).

Some outcrops which contain abundant plastic mixing of Units IIIc and IVb, are patchily to completely hybridized to a marbled felsic-mafic rock showing extreme compositional and textural inhomogeneity, or an equicrystalline rock resembling granodiorite, respectively. The large compositional and textural variations help explain why it has been described as a gneiss (Rabinovitch, 1969), a hybrid rock (McQuade, 1979), an augen gneiss (Mann, 1980), a quartz diorite and diorite (Lougheed, 1981), and a granodiorite (Lutes, 1981).

Subunit IIIc is divided into three metamorphic variants, 1, 2, and 3, located between L7N and L9S, L9S and L17S, and south of L17S, respectively. The contacts between the variants are probably gradational and were not observed in the field.

VARIANT 1

Variant 1 is mineralogically similar to Unit IIIb, but is pervasively silicified, locally has an irregular or cauliflower-like recrystallization texture, and contains pervasive brown biotite alteration (Fig. 2.2a). North of L0+00 discrete domains of Unit IIIb, 1-2m across, grade gradually or sharply into outcrops of variant 1.

A few small variant 1 outcrops near L5S/11W appear to comprise a silicified gneissose rock containing felsic and mafic horizons, <1 to 4cm across. The horizons look like the metamorphic foliation found in Unit IIIa. Alternatively, the layers may represent plastic admixing of gabbro and

Figure 2.2 (a) Biotitized Unit IIIc gabbro (variant 1) crosscut by VII quartz vein. Note irregular recrystallization texture. (b) Unit IIIc gabbro blocks (variant 2) brittly crosscut by/and in matrix of Unit IVb leucogranite. Note the thick biotite selvedges along the interfaces of the granite and gabbro. (c) Unit IIIc gabbro (variant 2) plastically crosscut by leucogranite. (d) Unit IIIc gabbro (variant 3). The unit is dioritic in appearance and contains large knobs of M3 actinolite up to several centimeters in length.

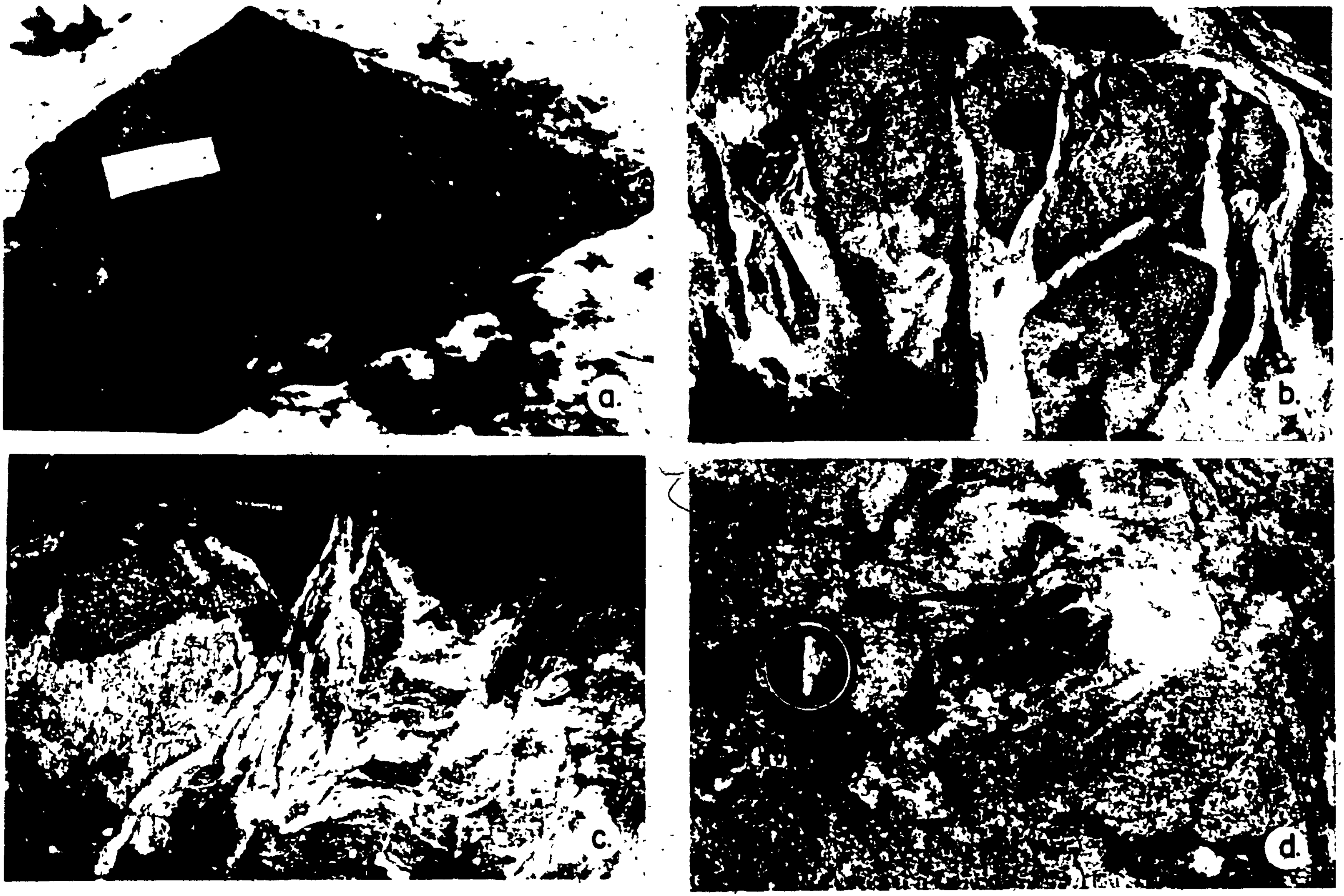
a.
b.
c.
d.

leucogranite.

VARIANT 2

Variant 2 consists mostly of gabbro which is partially, and in places, completely hybridized by the leucogranite. In some places it consists of massive or banded, rectangular to subrounded blocks of Unit IIIa, <1 to 2m across, in a matrix of coarse grained leucogranite (Unit IVb; Fig. 2.2b), large Unit IIIa or b gabbro outcrops locally hybridized by numerous Unit IVb dykes and stringers, or a relatively homogeneous granodioritic phase believed to be completely hybridized gabbro. The latter grades locally into a more mafic counterpart which resembles gabbro, in the same outcrop.

Where variant 2 is crosscut in a brittle way by Unit IVb (Fig. 2.2b), the blocks are more easily recognized as gabbro. In outcrops crosscut in a ductile fashion, however, the gabbro is altered locally to a more leucocratic rock with a heterogeneous 1 to 3mm crystal size, and is less easily identified as gabbro (Fig. 2.2c).

VARIANT 3

Variant 3, which occurs south of variant 2, extends southward off the map area and grades imperceptibly into Unit IIIb to the east. It is the most hybridized part of the gabbro which, in outcrop, resembles a mafic fine grained version of the Nashwaak granite or a granodiorite similar to the locally hybridized patches found in variant 2. The rocks are massive, composed mostly of plagioclase and subrounded quartz grains in a mafic biotite-rich matrix, and have a grainy or a cauliflower-like crystalline texture. South of L25S, large knobs of actinolite, up to 1.0cm across grow locally out of the matrix (Fig. 2.2d).

2.2.1g UNIT IVa

The Nashwaak granite is one of many unfoliated Acadian granites found in the Central Plutonic Belt of New Brunswick (Fyffe, et.al., 1981). It is pink, medium to coarse grained and equicrystalline (average crystal size 1cm), and contains about equal amounts of plagioclase, orthoclase, and quartz, and <8% biotite. Numerous (0.25 to 0.50m wide) dykes crosscut several gabbro outcrops near the Unit IIIc-IVb contact.

The Nashwaak has an extensive thermal aureole which is evidenced by porphyryoblast development in metasediments, and amphibolitization of gabbro, fine grained amphibolitic (FGA) and other mafic units. In addition, it is locally silicic, foliated, subporphyritic and marginally contaminated by gabbro along its border. The latter is evidenced by the presence of abundant biotite (up to 25%) where it crosscuts Unit III.

Analyses of unaltered Nashwaak granite from in and near the Sisson Brook area fall along the upper end of regional Na + K enrichment (Fig. 2.3) and Ca-depletion trends outlined by analyses of other Central Plutonic granites (Table 2.2). The biotite-rich granite, adjacent to gabbro (above) plots between pristine gabbro and Nashwaak analyses, indicating that it is probably contaminated.

Figure 2.3 Wt. % SiO2 versus Na2O + K2O in Central Plutonic Belt granites near Sisson Brook area and Unit IIIa gabbro.

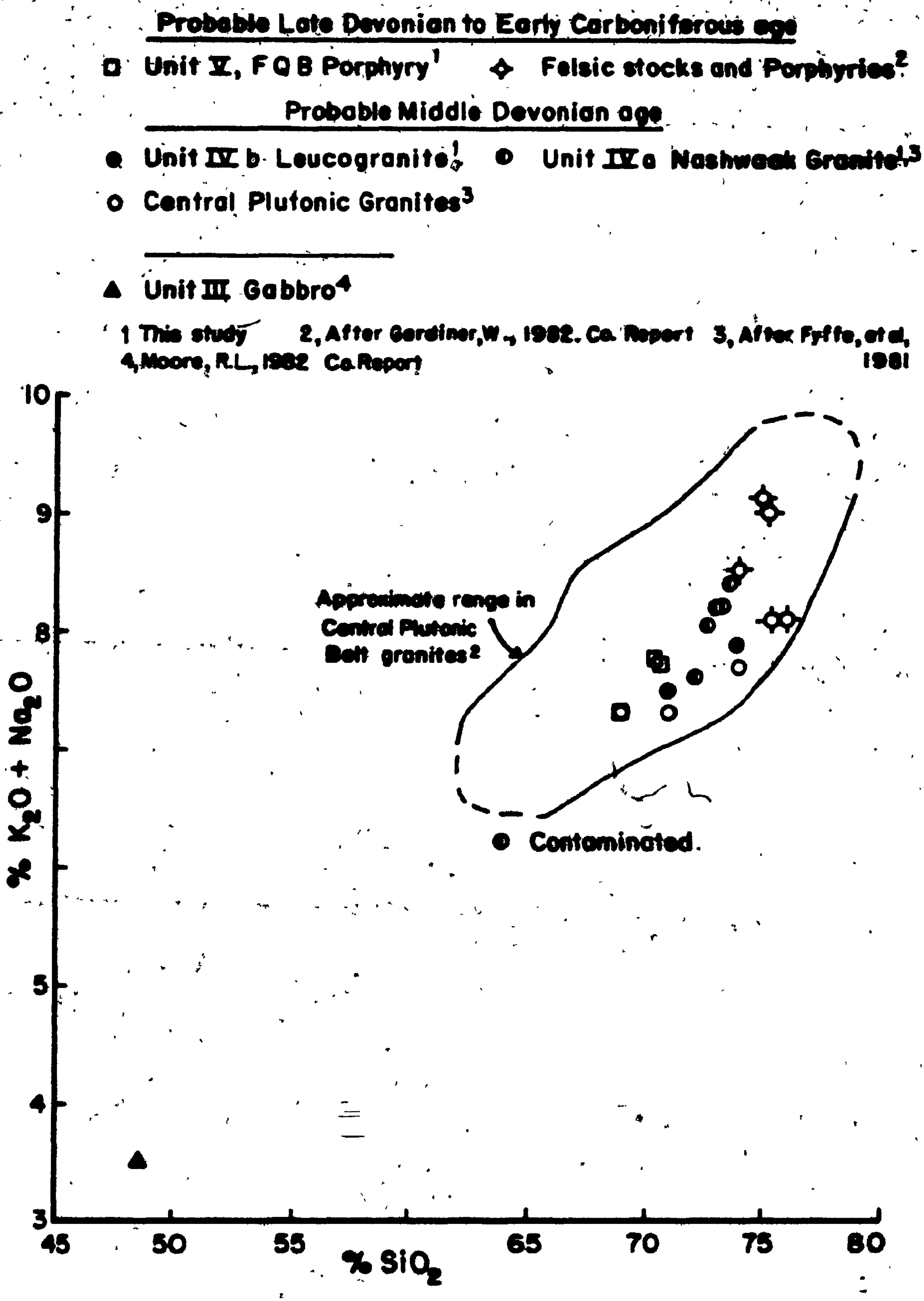
Probable Late Devonian to Early Carboniferous age
□ Unit V, F Q B Porphyry[1]
✧ Felsic stocks and Porphyries[2]
Probable Middle Devonian age
● Unit IV b Leucogranite[1,3]
◐ Unit IV a Nashwaak Granite[1,3]
○ Central Plutonic Granites[3]
▲ Unit III Gabbro[4]
1 This study
2, After Gardiner, W., 1982. Co. Report
3, After Fyffe, et al, 1981
4, Moore, R.L., 1982 Co. Report
Approximate range in Central Plutonic Belt granites[2]
◉ Contaminated.
% K₂O + Na₂O
% SiO₂
10
9
8
5
4
3
45
50
55
65
70
75
80

Table 2.2 Geochemical analyses of some Central Plutonic Belt Granites and Unit III gabbro. 1, this study; 2, Gardiner, W, 1982 co. rep't; 3, after Fyffe, et.al., 1981; Moore, R.L., 1982, co. rep't.[4]

Name	SiO_2	Al_2O_3	CaO	MgO	Na_2O	K_2O	Fe_2O_3	TiO_2
Nashwaak[1,3] (Unit IVa)	73.7	13.2	1.01	0.09	3.06	5.34	1.99	0.22
	72.6	14.6	0.59	0.33	3.27	4.78	1.82	0.24
	72.9	14.5	0.71	0.32	3.14	5.07	1.81	0.22
	73.3	14.7	0.60	0.33	3.31	4.91	1.76	0.23
	72.	13.	0.9	0.2	3.6	4.0	1.7	0.1
	71.	15.	2.9	1.3	3.2	4.3	3.5	0.6
Leucogranite[1] (Unit IVb)	73.8	12.5	1.02	0.57	2.70	5.16	2.14	0.25
Skiff Lake[3]	69.	15.	2.3	1.3	3.3	4.0	3.7	0.5
Burnthill[3]	74.	12.7	0.7	0.2	3.5	4.2	1.2	0.1
	76.	12.0	0.6	0.2	3.2	4.9	2.0	0.1
Dungarvon[3]	75.5	14.5	0.8	0.35	3.5	4.6	1.7	0.2
Porphyries								
Sisters Brook[2]	75.2	1.56			9.13			
Rocky Brook[2]	75.4	1.41			9.			
Moose Brook[2]	74.1	2.00			8.5			
FQB Porphyry[1] (Unit V)	69.2	14.5	2.5	0.92	3.65	3.64	2.66	0.41
	70.7	14.6	2.34	0.78	3.88	3.86	2.45	0.39
	70.3	14.6	2.17	0.81	3.81	3.95	2.52	0.39
Gabbro								
Unit IIIa[4]	48.7	19.4	9.79	5.00	2.82	0.82	8.95	1.46

2.2.1f UNIT IVb

Unit IVb comprises the leucogranite that crosscuts, engulfs, and/or assimilates Unit IIIb and c. It is found mostly in Unit III, and occurs in increasing amounts westward. One silicified outcrop, several meters wide and devoid of gabbro, occurs 600m east of the Nashwaak granite. A bulk rock analysis of the outcrop falls along the same regional trend of alkali enrichment and Ca depletion as the Nashwaak and other Central Plutonic granites, and near the upper evolved end of Nashwaak analyses (Fig. 2.3).

The leucogranite apparently does not have a thermal aureole. It is, however, associated with local pervasive brown biotite alteration of (Nashwaak-related) actinolite in gabbro. The evolved geochemistry, presence of hybridization and local alteration of (Nashwaak-related) actinolite, in the absence of a thermal aureole suggests that it intruded shortly after the Nashwaak into relatively hot country rocks.

2.2.1g UNIT V

Unit V consists of a gray to gray-green, unfoliated, feldspar-quartz-biotite (FQB) porphyry which contains large (<1 to 5cm), carbonate-filled miarolitic cavities. It is made up of plagioclase, K-feldspar, quartz, and biotite phenocrysts (48%) within a fine grained matrix of K-feldspar and quartz (52%). The phenocrysts consist of ~23% zoned plagioclase (An6 to 26) up to ~1cm across, 10% euhedral quartz crystal (1 to 7mm in width), 8% biotite (>0.05 to 0.3mm across), and 7% K-feldspar crystals (0.2 to 1.0cm wide). The quartz phenocrysts are gray in color and contain relatively low temperature fluid inclusions (Chap. 6) which might indicate that the original quartz was replaced.

The porphyry is found only in drill core within 100 to 200m of the gabbro-sediment contact (SSN 26,28, 30,31, 33, 36, 37, and 38; Fig. 2.4). The probable near-surface extent of the main porphyry body, which is inferred from geophysics, occurs to the east, and is discussed below (p. 17).

The porphyry post-dates intrusion of the Nashwaak and leuco- granites. It contains no Nashwaak-related contact metamorphic phases nor late brown biotite alteration, and intrudes along a late E-trending fault between drill holes SSN 28 and 31.

The porphyry falls along the Central Plutonic Belt granite trend. It is less evolved, (i.e., contains less Na2O + K2O) however, than the Nashwaak, leuco-granite or other late stage porphyries in the area. One reason for this may be that the porphyry formed from partial melting of, or was contaminated during ascension through, the gabbro. This occurs, for example, in the marginal phase of the Nashwaak (Fig. 2.3).

The porphyry is hydrothermally altered, in places. In least altered sections, the plagioclase is dusted with minor amounts of fine grained sericite. In more altered sections the plagioclase is moderately sericitized or replaced by epidote, chlorite or carbonate. In addition, the porphyry is associated with pervasive biotitization of surrounding country rocks. The biotite, which is reddish-brown in color, is optically and chemically different from the brown biotite associated with Unit IVa and is relatively easy to distinguish in thin section (below).

Figure 2.4 Distribution of mineralized Zones, A and B, about, and the inferred location of the FQB porphyry within (hatched area), the elliptical, torus-shaped region of high chargeability/low resistivity. Note that the hatched area coincides with the location of the FQB porphyry in drill hole 26, and is flanked to the west by numerous FQB porphyry dykelet(s) (in red), also found in drill core.

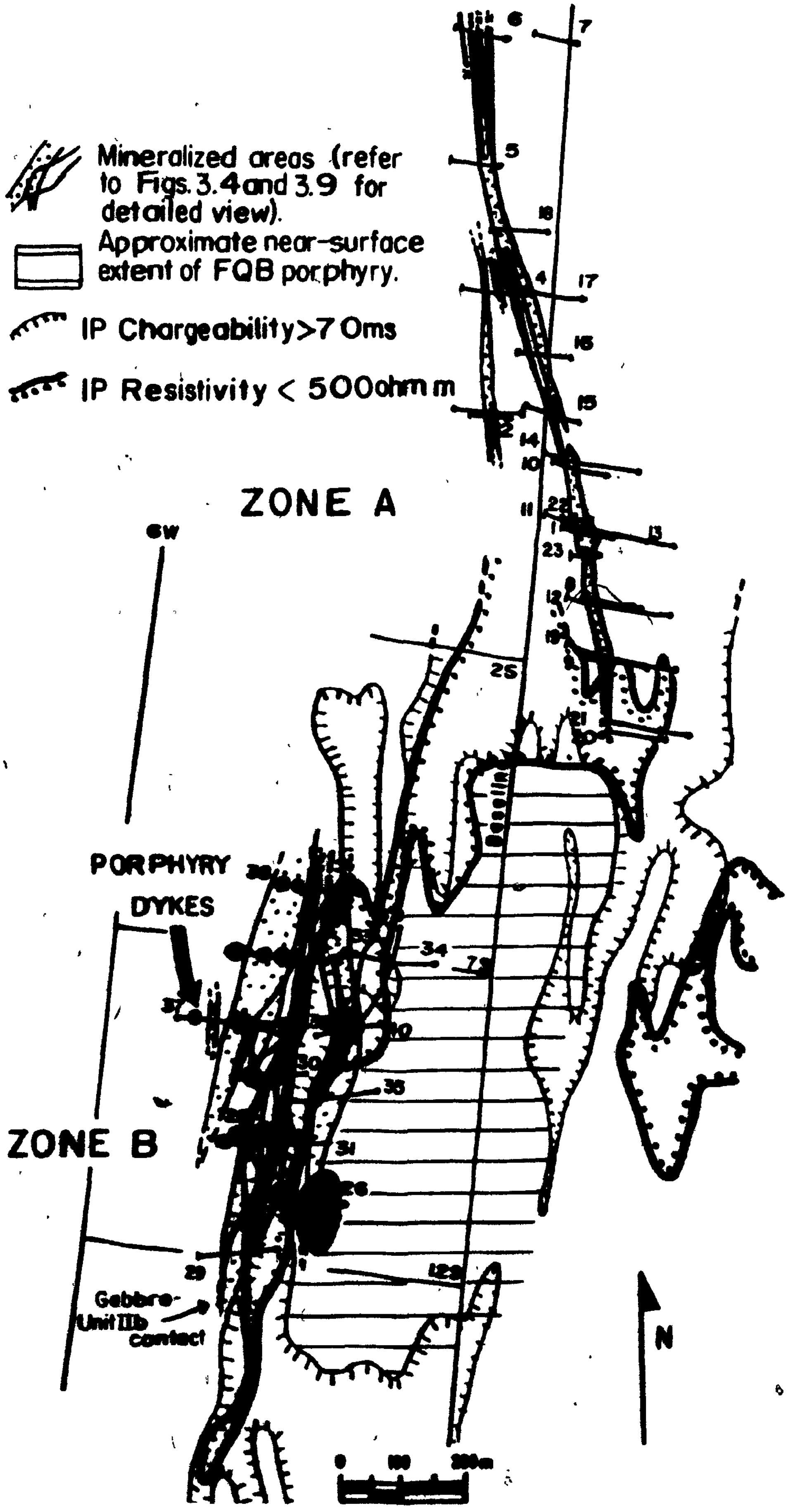
Mineralized areas (refer to Figs. 3.4 and 3.9 for detailed view).
Approximate near-surface extent of FQB porphyry.
IP Chargeability>7 Oms
IP Resistivity < 500ohm m
ZONE A
ZONE B
6W
PORPHYRY DYKES
Gabbro-Unit IIb contact
Baseline
N
0 100 200m
6
7
5
18
4
17
16
15
14
10
11
22
1
13
23
12
19
25
21
38
34
73
37
30
36
31
26
29
129

2.2.2 STRUCTURE

Three E-trending faults and two WNW-trending faults are found in the Sisson Brook area (Fig. 2.1). The northernmost fault subparallels L16N and is defined by a magnetic anomaly offset with no apparent displacement of the rock types (Fig. 2.5; Gasteiger, 1981; magnetic survey, north sheet).

The second most northerly fault subparallels L0+00, along Sisson Brook (Fig. 2.1), and is associated with intense silicification of surrounding country rocks. The fault has an observed right strike-slip displacement of up to 350m in Unit IIa near the Unit I-IIa contact. To the west, Zone A crosses the fault, but is not displaced, indicating that it formed after the fault. Further west, the fault dies out in, and is therefore older than, the Nashwaak granite.

To the south is a WNW-trending fault zone which extends from L1N/20W to L4S/2W and is defined by an en echelon array of offset northwesterly trending VLF anomalies (Figs. 2.1 and 2.5). No displacement of the rock units was observed.

Further south is an E-trending fault with a lateral displacement of <100m and limited extent (Fig. 2.1; see Fig. 3.4). The fault offsets the Unit III-IIb contact and early scheelite-mineralized zones, but does not displace late scheelite-molybdenite zones (Chap. 3). The offsets indicate that the fault formed after the first pulse of mineralization, but before the second.

The southernmost E-trending fault occurs within gabbro and extends from about L10S/22W to L16S/4W (Fig. 2.1). The

Figure 2.5 Compilation map of important geophysical features.

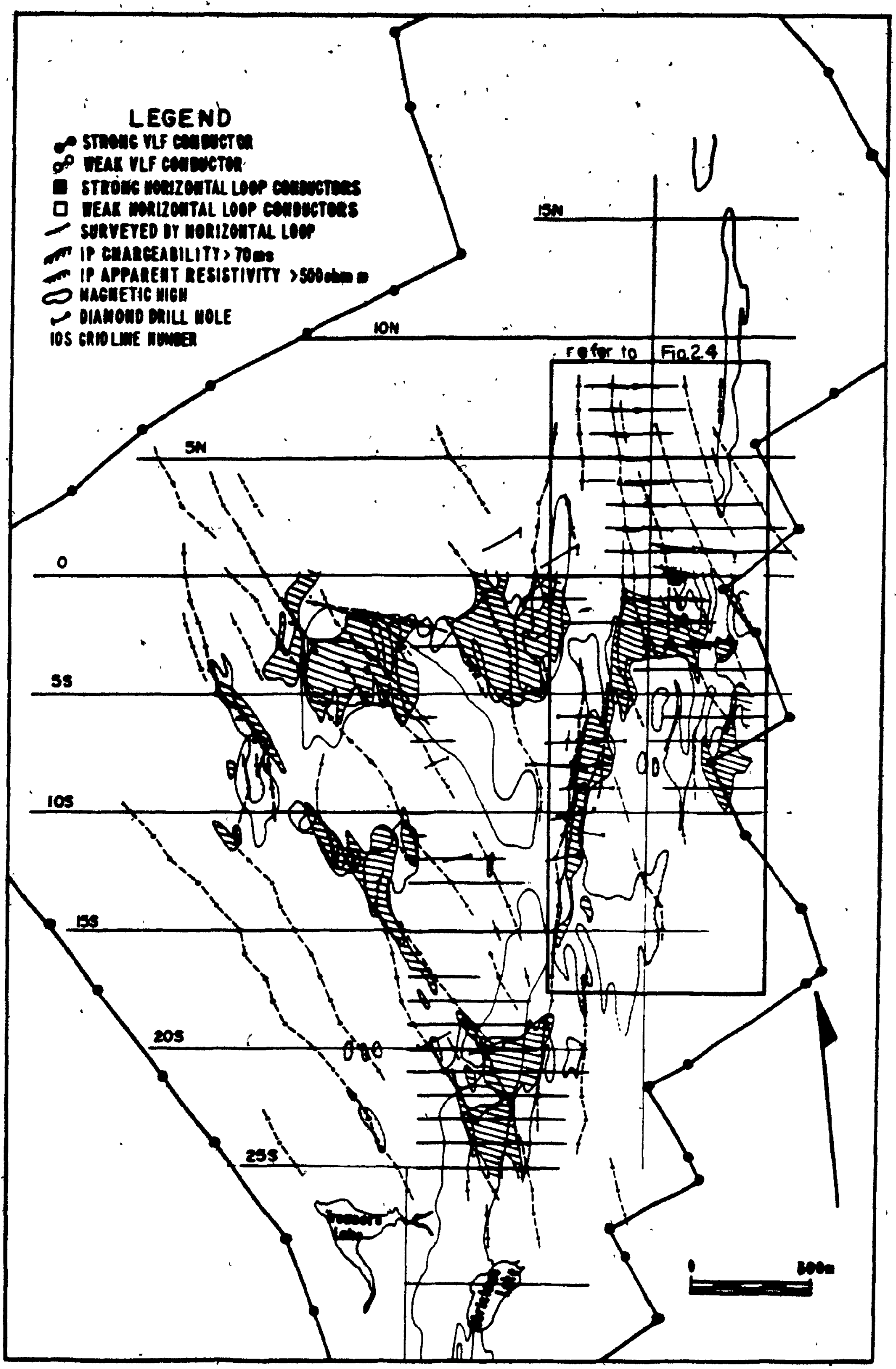
LEGEND
STRONG VLF CONDUCTOR
WEAK VLF CONDUCTOR
STRONG HORIZONTAL LOOP CONDUCTORS
WEAK HORIZONTAL LOOP CONDUCTORS
SURVEYED BY HORIZONTAL LOOP
IP CHARGEABILITY > 70ms
IP APPARENT RESISTIVITY >500ohm m
MAGNETIC HIGH
DIAMOND DRILL HOLE
10S GRIDLINE NUMBER
15N
10N
refer to Fig.2.4
5N
0
5S
10S
15S
20S
25S
0
300m

fault is inferred from an en echelon array of offsets in NNW-trending VLF structures (Fig. 2.5).

Two subsurface structures are inferred from geophysical data. A large elliptical zone, defined by anomalies in magnetic and chargeability measurements, occurs between L2S and L13S and 5W to 17W, and is postulated to be a gabbro rim about a subsurface intrusion centered at L8S/11W (Fig. 2.5; Ravenhurst, 1982).

An elongate torus-shaped region of high chargeability/low resistivity measurements subparallels the baseline from L3 to L13S, and is 400m across (Fig. 2.5). Dyke(let)s of FQB porphyry occur in drill core in the western rim and within 150m of the western flank of the anomalies in Zone B, but are absent in Zone A. The lack of dyke(let)s in Zone A and their concentration and coincidence along the western rim of the anomalies in Zone B, suggests that the anomalies represent the near-surface extent of the porphyry or related intrusion(s) (see Fig. 2.4). The elliptical shape of the anomalies, with the long axis parallel and slightly east of the gabbro-sediment contact, and the concentration of dyke(let)s along the gabbro-sediment contact, suggests further that intrusion of the porphyry was controlled by the contact.

2.2.3 METAMORPHISM AND MICROSTRUCTURE

Four periods of regional and contact metamorphism are recognized in the Sisson Brook area, M1 through M4 (Lutes, 1981). The first two events, M1 and M2, are attributed to the Taconic orogeny, and produced regional subgreenschist grade metamorphism and two, subparallel, steeply dipping, NE-trending foliation surfaces, S1 and S2.

The third event, M3, was associated with the intrusion of the post-Acadian Nashwaak and leuco- granites. Intrusion of the Nashwaak led to contact metamorphism of the country rocks, and intrusion of the leucogranite resulted in local hybridization and pervasive biotite alteration of the country rocks.

M4 led to the formation of a NW-trending, steeply SW-dipping S3 foliation surface, hydrothermal alteration and mineralization, predominantly E-trending faults, and intrusion of the FQB porphyry.

Events M1 and M2 are most clearly seen in Unit IIa shales and Unit I quartzites, which are furthest from the contact aureole of the Nashwaak, whereas M3 is most abundantly developed in Units IIb and III which flank it to the east. The S3 surface and E-trending faults, related to M4 are found in all units. M4 hydrothermal alteration appears to be present, however, only within 1km of the mineralized zones.

2.2.3a M1

The M1 event, of subgreenschist grade, resulted in development of steeply dipping, northeasterly trending hematite-filled fractures (S1) parallel to bedding surfaces (S0) that are outlined by black chloritic clays. The S1 surface was observed only in Unit IIa shales where it locally defines the dominant foliation surface, or occurs as relict, tightly folded pockets of black (M1) chloritic shales in M2-altered rocks (Fig. 2.9).

2.2.3b M2

The M2 event led to development of the dominant foliation surface, S2, which subparallels S1. The S2 foliation surface is defined by the M2 assemblage, fine grained muscovite + chlorite + quartz + opaques.

The gabbro locally contains a foliation in Units IIIb and c, defined by leuco- and melano-cratic zones, which may represent penetrative M2 deformation. The foliation strikes N17 to 40E and dips steeply, subparallel to the S2 surface. However, the zones appear to become increasingly well-developed westward, suggesting that they formed during intrusion of the leucogranite (M3; below).

2.2.3c M3

The M3 event is associated with intrusion of the Nashwaak and late leuco- granites. Intrusion of the Nashwaak produced a large thermal aureole. Most rocks at Sisson Brook lie within the andalusite-garnet (and-gt) isograd of the aureole, which is located in the western part of the shales (Lutes, 1981). The aureole is manifested by porphyroblasts of cordierite, andalusite, and garnet in the pelitic and volcanic metasediments in Units I, IIa, and IIb, and by actinolite in the bright green massive units (FGA), banded amphibolitic metavolcano-sediments, and gabbro (Unit III).

Intrusion of the leucogranite was associated with extensive dyking, assimilation and hybridization of gabbro. This produced minor metamorphic overprinting of M3 (Nashwaak-related) plagioclase and actinolite in gabbro, and replacement of M3 actinolite by brown biotite. The hydrothermal biotite alteration occurs as biotite reaction rims about leucogranite dykes in gabbro, and as 1 to 2cm biotite clots and fine grained pervasive alteration throughout western parts of the gabbro. The biotite, in all cases, is coarse grained, inclusion-free, and has brown- to yellow- or olive- colored pleochroism.

The intensity of dyking, minor metamorphic overprinting, and brown biotite alteration, increases westward across Unit IIIa into Unit IIIc. For example, Unit IIIa is relatively massive and contains minor amounts of leucogranite dykes and brown biotite alteration, and no metamorphic overprinting. Unit IIIb, however, comprises two subgroups which have equicrystalline and bimodal grain sizes, respectively. Both subgroups are foliated and contain up to 20% fine grained brown biotite and sphene, which replace M3 actinolite.

In contrast, M3 actinolite in Unit IIIc is, in places, completely altered to brown biotite and sphene, and plagioclase cores are locally obscured by sericite alteration. In addition, Unit IIIc, variant 1 rocks (p.20) locally contain fine grained undulose to serrate quartz and minor microcline, and some plagioclase crystals are abraded into small and large fragments. Late retrograde alteration in variant 1 rocks is evident by the presence of minor epidote and chlorite, which overgrows some of the brown biotite and plagioclase.

Intrusion of the leucogranite may also have produced microscopic strain and shock features in minerals in variant 2 gabbro blocks. This includes undulose to "protomosaic" quartz, shock twins in the actinolite, and extremely well-defined albite and/or Carlsbad twins which overprint primary concentric zoning in plagioclase. Shock twins in amphibole are rarely observed in nature, but have been produced in experimental studies of plastic rock deformation (Hawthorne, 1983, p.333).

The most extreme effects of the leucogranite are evident in the widespread assimilation and hybridization of Unit IIIc, variant 3 gabbro. Variant 3 gabbro is so completely hybridized by the leucogranite, in places, that it forms a felsic dioritic phase (p.22).

2.2.3d M4

The M4 event is associated with the formation of the S3 foliation surface, the mineralization and hydrothermal alteration, intrusion of the FQB porphyry, and development of E-trending faults. The S3 surface, which trends ~N50/70SW, is a crenulation cleavage in less competent units, e.g., shale, pelites, and volcanosediments, and a fracture cleavage in competent, massive units, e.g., gabbro, granite, blue quartzites (Unit I; Fig. 2.6).

The S3 surface locally disrupts M3 porphyroblasts in Units I and IIb. For example, andalusite, cordierite and

Figure 2.6 Outcrops of Unit I showing the development of S3 (yellow stripes) as a crenulation cleavage in the less competent intercalated pink quartzites and argillites (a), and as a fracture cleavage in the massive, more competent blue quartzites (b).

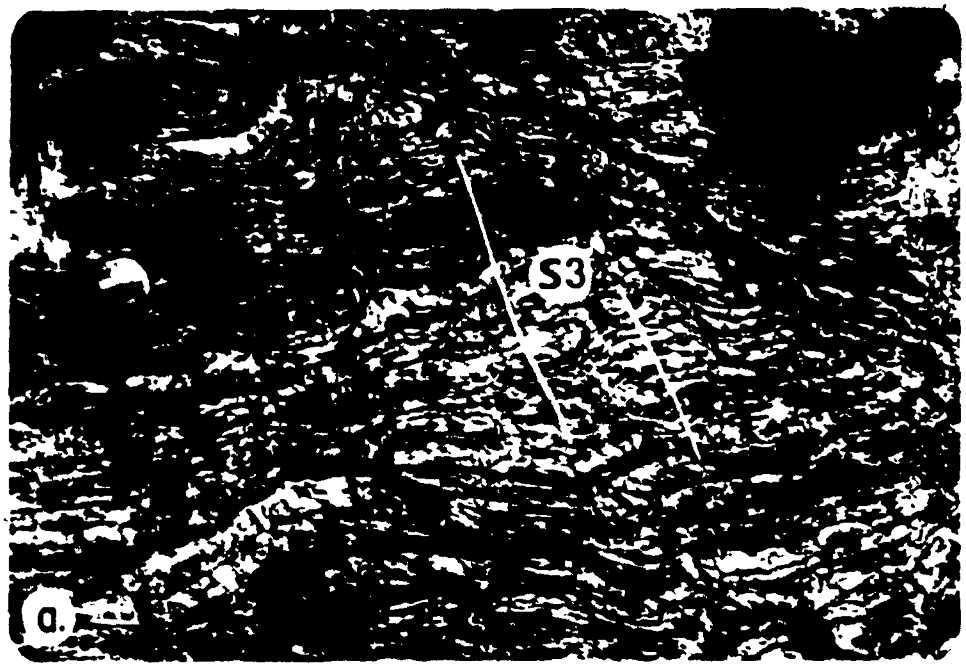
S3
a.

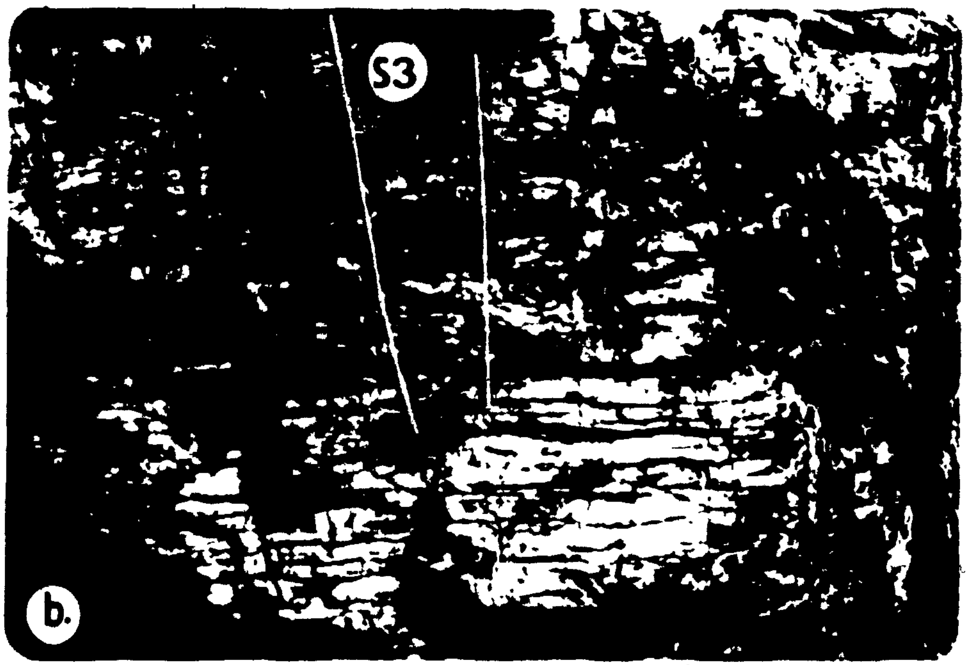
S3
b.

garnet porphyroblasts are bent locally along internal shear planes into or related to development of the S3 crenulation cleavage (Fig. 2.7).

In addition, the S3 surface hosts most of the mineralized veins in gabbro and metasediments in both zones (Chap. 3) The mineralization is locally associated with pervasive red-brown biotite alteration which crosscuts M3 porphyroblasts and brown biotite alteration. The biotite is concentrated locally as <1.0mm cryptocrystalline to crystalline spots along S3 crenulation hingelines, distal to the deposit, and intense pervasive alteration and vein haloes, in the deposit (Chap. 4). The red brown biotite is optically and geochemically identical to biotite in the veins and vein haloes. The red-brown biotite is also identical to the red brown biotite phenocrysts in the FQB porphyry (Chap. 5).

Extensive local faulting also occurred at this time. The faults trend E and WNW, and have a measured strike-slip component ranging from 0 to 350m. The faults locally crosscut the Nashwaak granite, displace early scheelite-mineralized zones in Zone B, but not the later molybdenite-scheelite- and wolframite-chalcopyrite- mineralized zones in Zones A and B (Chap. 3). In addition, FQB porphyry was found in drill core along the E-trending fault in Zone B (Fig. 2.4).

Figure 2.7 M3 garnet porphyroblast bent along internal shear planes which formed during development of the S3 surface.

CHAPTER 3. MINERALIZATION

3.1 INTRODUCTION

The mineralization at Sisson Brook occurs in two separate zones which contain nearly identical types of mineralized vein sets, denoted from oldest to youngest as, VI to VV. Zone A mineralization is found in Unit IIb metavolcano-sediments, only, and Zone B mineralization, which occurs south of Zone A, occurs within Unit IIb metavolcano-sediments and metagabbro (Unit III; Fig. 2.1).

VI mineralization consists of coarse to fine grained scheelite in bright green amphibole-filled vein(let)s, fractures, and massive clots, <1 to 10cm across. Vein set VI occurs almost entirely within gabbro, and hence, is almost exclusively found in Zone B. VII mineralization is composed of thin scheelite ± biotite ± sulfide-bearing quartz veinlets, and occurs in both Zones A and B. Biotite is notably absent in Zone B. VIII mineralization consists of molybdenite ± tr. pyrrhotite quartz veins in Zone A and scheelite ± molybdenite ± pyrrhotite quartz veins in Zone B. Both VII and VIII vein(let)s are associated with biotite haloes (potassic alteration; Chap. 4).

The VIV vein set consists of mineralized quartz veins and <1 to >30m wide, linear quartz-filled fracture zones up to 1km in length, hereafter called quartz stockworks. The veins and stockworks contain mostly wolframite, chalcopyrite, pyrrhotite ± trace molybdenite in Zone A, and scheelite, molybdenite ± wolframite ± chalcopyrite ± pyrrhotite in Zone

B. The veins and stockworks are characteristically associated with sericite (phyllic) alteration (Chap. 4).

The youngest vein set, VV, comprises pyrite ± arsenopyrite ± acanthite ± tr. hessite ± tr. native bismuth ± trace chalcopyrite, molybdenite, galena, and/or sphalerite in carbonate ± fluorite vein(let)s, fracture-fill, and pervasive, massive carbonate flood zones. VV veins are associated with sericite-clay (propylitic) alteration (Chap. 4).

The main differences between the mineralization in the two zones are that: 1) the potential ore minerals are wolframite and chalcopyrite in Zone A, and scheelite and molybdenite in Zone B and, 2) the mineralization of economic importance in Zone A is most abundant and contained within VIV quartz stockworks, whereas in Zone B, it is found in vein sets VI through VIV (Section 3.6, below).

3.2 RELATIONSHIP OF MINERALIZED ZONES TO GEOPHYSICS

Zones A and B are proximal to, and symmetrically disposed about a large, N- trending, elliptical and torus-shaped zone of high chargeability/low resistivity, >1km in length (Fig. 3.1; Chap. 2). The anomaly is believed to represent the near- surface extent of the FQB porphyry (Chap. 2, p.17). Zone A extends radially outward from its northern rim, following VLF and horizontal loop EM anomalies (below), pinching out ~1km to the north. Zone B, which also follows strong VLF anomalies, flanks and lies within its western rim (Fig. 3.1).

Figure 3.1 Relationship of important geophysical features to Zones A and B.

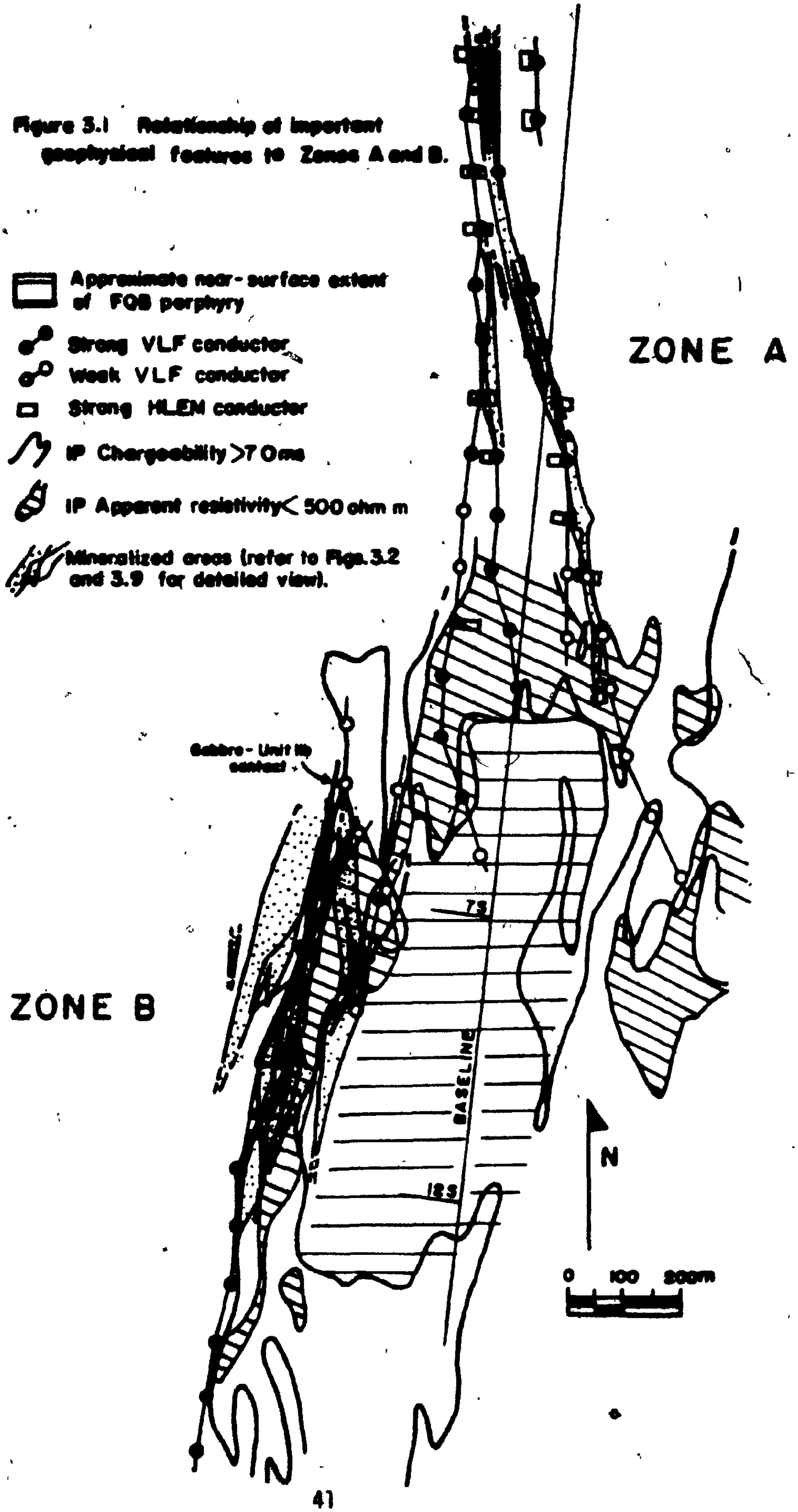

Figure 3.1 Relationship of important geophysical features to Zones A and B.

3.3 MINERALIZED FRACTURE ZONES WHICH COMPRISE ZONE B

Whereas the mineralization of economic importance in Zone A is contained within vein set VIV (see Fig. 3.8), the mineralization in Zone B is found throughout vein sets VI through VIV. Vein sets VI and VII are concentrated in four scheelite-mineralized zones, F1 to F4, and VIII and VIV veins are most abundant in three scheelite-molybdenite-mineralized zones, MZ1 to MZ3 (Fig. 3.2).

3.3.1 SCHEELITE MINERALIZED ZONES, F1 TO F4, ZONE B

Vein sets VI and VII largely occur in four NNE-trending scheelite-mineralized zones in Zone B, F1 to F4 (Fig. 3.2). The zones, which are 10 to 80m across, are defined by drill core intervals averaging ~0.10wt.% WO_3. They contain little molybdenite mineralization, generally <0.01wt.% MoS_2. The gabbro-hosted portions of the zones, i.e., all of F1 and F2 and approximately half of F3 are dominated by VI veins. Those portions which occur in Unit IIb metavolcano-sediments, i.e., approximately half of F3 and practically all of F4, contain mostly VII quartz veinlets.

The zones vary in strike from N19E in the west to N7E to the east, and appear to dip near vertically. The zones flank the western edge of the oblate zone of high chargeability-low resistivity (Fig. 3.1), and are proximal to and subparallel the gabbro-metavolcano-sediment contact. The latter suggests that the contact provided the main controlling structure for fluid focus.

F1, the westernmost and narrowest (~13m across)

Figure 3.2 Surface projection of scheelite-mineralized zones, F1 to F4, and late scheelite-molybdenite-mineralized zones, MZ1 to MZ3, in Zone B.

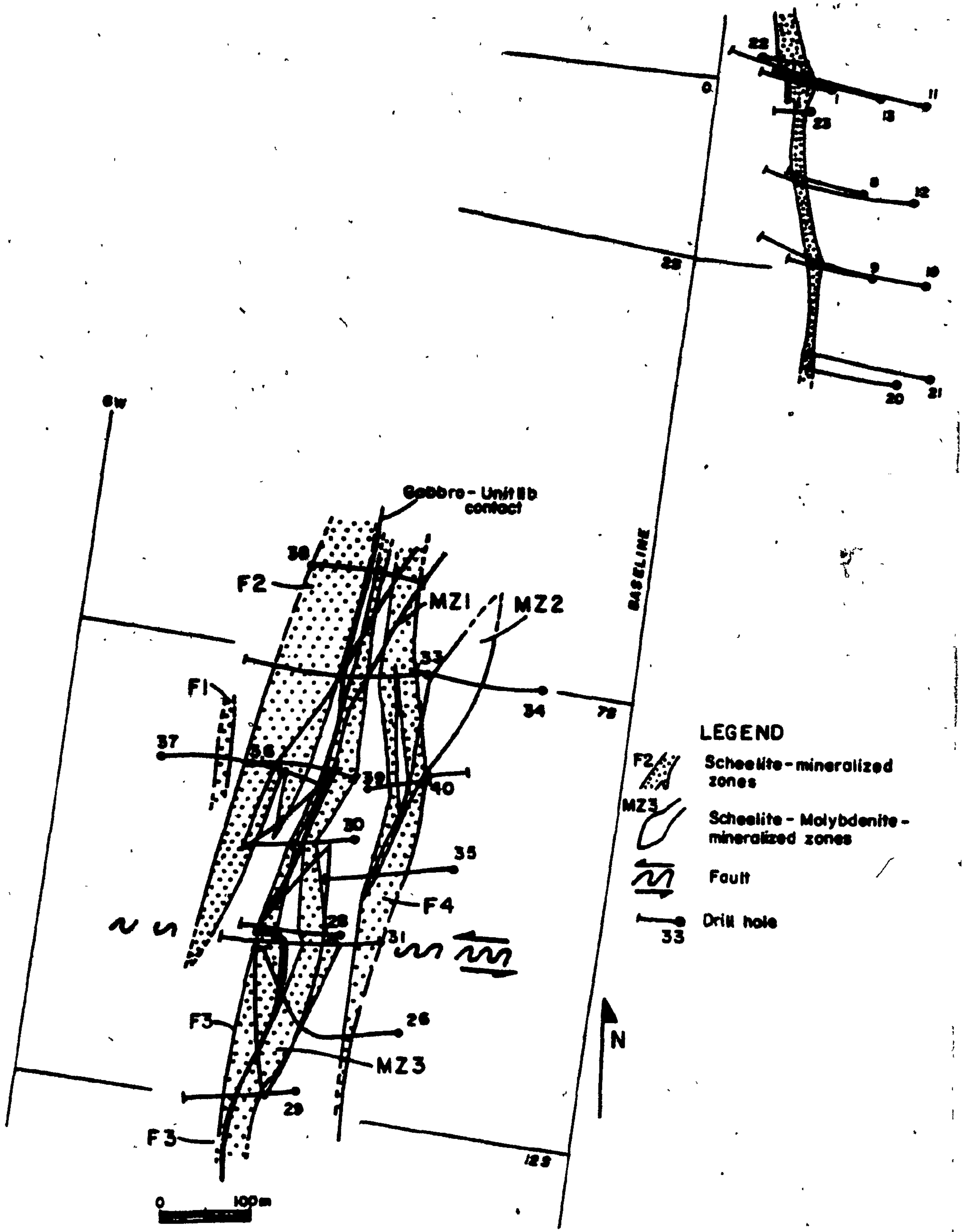
0
22
1
11
13
23
8
12
25
9
10
20
21
6W
Gabbro - Unit IIb contact
38
F2
MZ1
MZ2
33
BASELINE
F1
34
75
37
36
39
40
30
35
F4
28
31
26
F3
MZ3
29
F3
125
N
0
100m
LEGEND
F2
Scheelite-mineralized zones
MZ3
Scheelite - Molybdenite - mineralized zones
Fault
33
Drill hole

fracture, is entirely gabbro-hosted. F2, to the east, is the widest zone (~70m across), and also occurs entirely within gabbro. The zone appears to have a near vertical dip, based upon limited drill hole correlation from SSN 36 and 37.

F3 directly straddles the sediment-gabbro contact. The zone spans ~80m, bifurcates in its central part, and rejoins within 400m along its strike (Fig. 3.2). F3 crosses a small fault between drill holes SSN 28 and 31 which has a left strike-slip component of ~25m and unknown vertical displacement. The fault displaces F3 and the host rock by about the same amount, indicating that there was post-mineralization movement. The direction of dip is apparently steeply eastward according to drill hole data correlated directly across the fault. If one rotates the units westward to compensate for lateral displacement, the zone dips near vertically.

F4, which is the only zone that occurs completely within Unit IIb metavolcano-sediments, is ~50m across and bifurcates and rejoins within 150m along a zone of gabbro dykes. It contains the least number of VI veins.

The lateral extent of the mineralization in zones F1 to F4 is inferred from the geometry of the zones and geophysical data. The fractures pinch and swell and are open-ended in plan view, suggesting that the zones continue further north and south. The close correlation between VLF anomalies and mineralization (Fig. 3.1), and their relationship to the western flank of high resistivity/low chargeability, suggests that mineralization extends at least as far north and south as the VLF and elliptical anomalies overlap.

3.3.2 MOLYBDENITE-SCHEELITE ZONES, MZ1 to MZ3, ZONE B

Three NE-trending lensoid zones, comprised mostly of VIII- and lesser VIV- quartz-hosted scheelite and molybdenite mineralization (MZ1 to MZ3), crosscut the scheelite-mineralized zones, F1 to F4 (Fig. 3.2). The zones, which are 50 to 75m across, subparallel stratigraphy, trending from east to west, N29.5E, N13E, and N27.5E (Fig. 3.2). Drill hole data from SSN 28 and 31 indicate that the southernmost zone, MZ3, dips steeply eastward. The mineralization in the zones is discussed in Section 3.5.

3.4 VEIN ORIENTATIONS

A stereonet projection of poles to the planes of 347 VI vein(let)s and microfractures in Zone B, 144 VIII quartz veins in Zone A, and 37 VIII quartz veins in Zone B is shown in Figure 3.3. The figure shows that although the vein sets formed along a NW-trending conjugate fracture set, parallel to S3, VI veins dip steeply to the SW or NE, whereas VIII veins dip mostly to the SW.

In addition, Figure 3.3 shows that VIII veins have a smaller range in strike which appears to be rotated ~20° degrees counterclockwise, or north of that of VI vein(let)s. The strike rotation may help explain the ~15° difference in strike between early VI- and VII- scheelite-mineralized zones, which parallel the gabbro-sediment contact (F1 to F4; Fig. 3.2), and late VIII- and VIV- scheelite-molybdenite-

Figure 3.3 Orientation of poles to planes of VI vein(let)s in Zone B and VIII veins in Zones A and B. Note that VIII veins dip more consistently to the SW and are oriented about 15 in a more northward orientation than VI vein(let)s. The range in measured values of the S3 surface is shown as solid lines in each diagram, for reference.

VI Vein(let)s,
Zone B

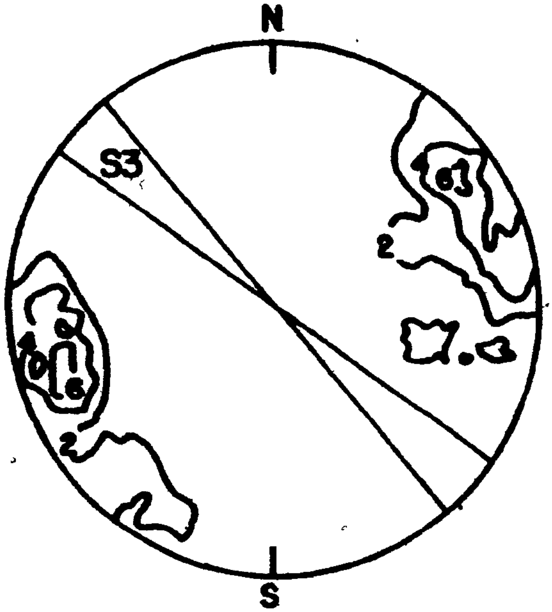

Contours at 2, 4, 6 %

342 Poles
1% area

VIII Veins,
Zone A

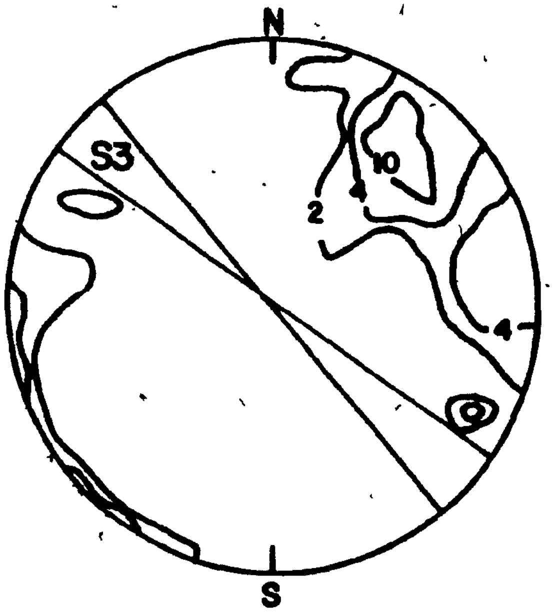

Contours at 2, 4, 10 %

144 Poles
1% area

VIII Veins,
Zone B

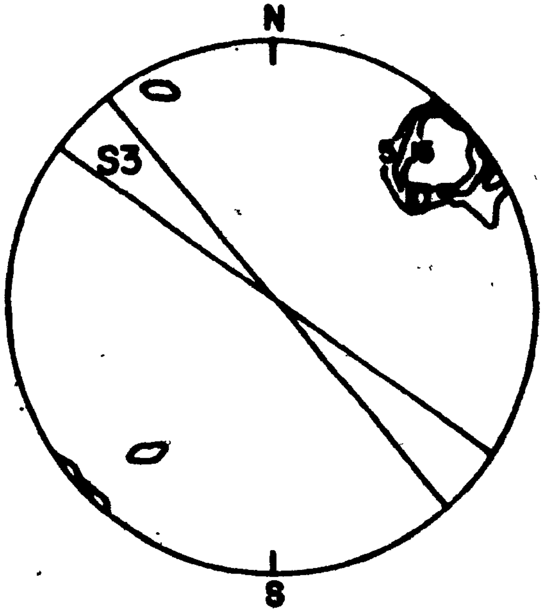

Contours at 5, 10, 15 %

37 Poles
1% area

mineralized zones, which subparallel stratigraphy (MZ1 to MZ3; Fig. 3.2).

Variations in orientation are apparently independent of vein(let) size. The smallest and largest veinlets, <1mm to 5mm and 1 to 1.8cm wide, for example, have almost identical ranges in orientation.

3.5 RELATIONSHIP OF VEIN ORIENTATION TO THAT OF THE MINERALIZED ZONES

Although the veins subparallel the steeply dipping, NW-trending S3 surface, the mineralized areas in Zones A and B, which are also steeply dipping, strike roughly N (Fig. 3.1). Hence, the veins intersect the mineralized zones obliquely. The oblique intersection suggests that the mineralized zones were gash fractures which may have resulted from shear coupling during formation of S3, and along which the fluids entered S3 foliation planes.

3.6 VEIN PARAGENESES

The vein parageneses and spatial distribution of the vein sets are discussed below in order of oldest, VI, to youngest, VV.

3.6.1 VEIN SET VI

3.6.1a VI MINERALOGY

The VI assemblage comprises scheelite-bearing hornblende ± albite ± tr. K-feldspar ± magnetite ± rare pyrrhotite vein(let)s, fractures and massive clots. In thin section, the hornblende, which typically comprises >90% of the assemblage, occurs as vibrant emerald to green-blue transparent blades and crystals <.05 to 2mm across. Microprobe analyses indicate that the amphibole varies in composition from actinolitic hornblende to ferro- and ferro-pargasitic hornblende (Chap. 5).

The albite, in thin section, appears as turbid, cloud-like masses interstitial to hornblende and magnetite crystals. Plagioclase of unknown composition was found on the walls or, less commonly, inside a minor number of large VI veins. K-feldspar was evident in a minor number of stained slabs, but was not found in thin section.

Magnetite is the most common accessory phase, and occurs as euhedral to subhedral cubic crystals up to 5mm in diameter, and as anhedral masses interstitial to vein amphibole. In one vein, large (3mm) crystals of pyrrhotite were found in apparent equilibrium with adjacent magnetite crystals. Minor disseminated specks and crystals of minor pyrrhotite, 0.05 to 2.0mm across, are present in a small number of VI clots, but are rare in VI veinlets. Pyrite was found in a rare number of clots which are crosscut by, or near, younger sulfide-bearing veinlets.

Scheelite is disseminated throughout most veins and in associated (A1) altered rocks (Chap. 4). The scheelite occurs as specks and less common, 1 to 2cm tetragonal crystals. The crystals are bipyramidal with approximately equidimensional lengths and widths, and have typically squarish outlines.

Most of the scheelite fluoresces canary yellow (y-scheelite). Microprobe analyses (this study; Scott, D., in-house co. report) indicate that the yellow fluorescence is due to minor (<2 to 3%) MoO2 in the scheelite structure. Some of the scheelite, however, is pure CaWO4 and fluoresces bright bluish white (w-scheelite).

3.3.1b VI MODE OF OCCURRENCE AND DISTRIBUTION

The VI assemblage occurs mostly in curved, discontinuous microfractures and veinlets, <2mm wide, and as dark green hornblende clots, <1 to 5cm in diameter, which are fed by hairline fractures (Mann, 1981). In addition, it is found less commonly, in more linear, continuous veins >3cm across, and rarely, in >18 to 50cm wide veins (Mann, 1982; SSN 33 and 36).

Vein set VI and associated (A1) alteration (Chap. 4), are highly host rock specific. Approximately 80% of VI clots and vein(let)s are hosted by gabbro and >16% are found in FGA units. The remainder, <4%, are found in Unit IIb metavolcano-sediments or felsic dykes (Fig. 3.4).

About 75% of the latter veins crosscut rocks which are highly silicified (Fig. 3.4, inset). Silicification is associated with the formation of vein sets VIII and VIV. Hence, the presence of VI veins in these units may indicate that a minor number of VI veinlets formed concurrently or later than vein set VIII. In most cases, however, VI vein(let)s are consistently crosscut by VII and VIII vein(let)s.

VI vein(let) density and the amount of associated scheelite mineralization apparently decreases abruptly within

Figure 3.4 Histograms showing distributions of VI density in gabbro and metavolcano-sediments in all drill holes in Zone B. The scale of the vertical axis in the histograms is, 1cm = 20 VI vein(let) or clot occurrences per 100m of drill core; "m" refers to FGA (mafic) units, "f" refers to all other "felsic" Unit IIb metavolcano-sediments. Inset shows relative amounts of VI vein(let)s and clots which occur in silicified versus unsilicified Unit IIb metasediments.

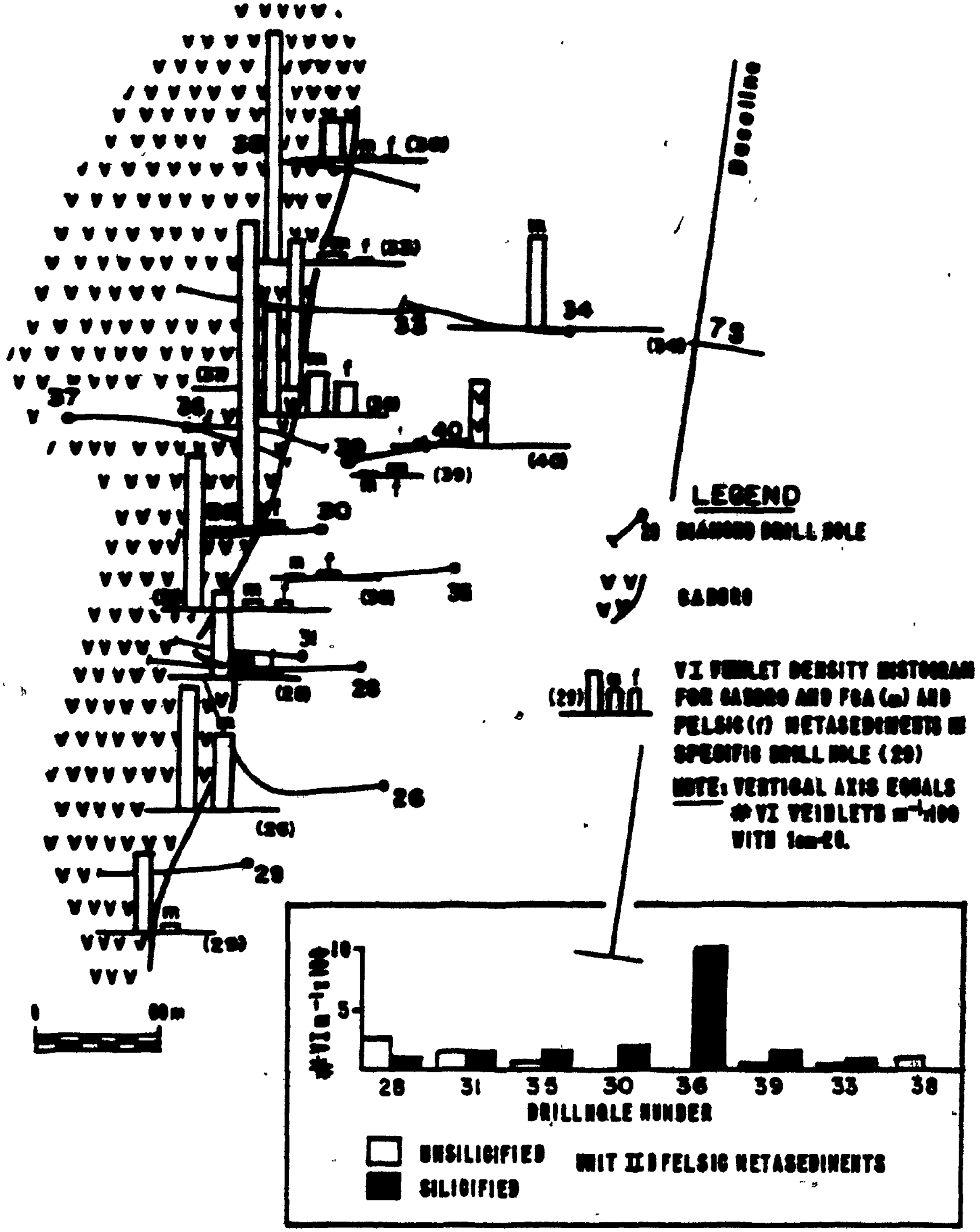
Baseline
7S
34
33
37
36
39
40
30
35
31
28
26
29
m
f
0
LEGEND
DIAMOND DRILL HOLE
GABBRO
VI VEINLET DENSITY HISTOGRAM FOR GABBRO AND FGA (m) AND FELSIC (f) METASEDIMENTS IN SPECIFIC DRILL HOLE (29)
NOTE: VERTICAL AXIS EQUALS # VI VEINLETS m⁻¹×100 WITH 1cm=20.
VI m⁻¹×100
10
5
28
31
35
30
36
39
33
38
DRILLHOLE NUMBER
UNSILICIFIED
SILICIFIED
UNIT IIB FELSIC METASEDIMENTS

several hundreds of meters outside F1 to F3. VI vein(let)s are rare and largely unmineralized in drill holes SSN 24 and 25, <800m to the southwest or in drill holes SSN 27 and 32, <400m to the west; no VI veinlets or clots were observed in any Unit IIIc gabbro outcrops to the west; and no VI features were found in any gabbro outcrops to the south (the first of which occurs ~200m south of SSN 25). Furthermore only minor, unmineralized VI clots and veinlets occur to the north in Unit IIIc gabbro outcrops, <400m west of Zone A, or in Zone A drill core of gabbro dykes.

These distribution patterns suggest that VI mineralization and most VI features probably die out along the gabbro-sediment contact near Zone B and south of Zone A. This agrees with the inferred extent of mineralization in fractures F1 to F3 (Section 3.3.1)

VI vein(let) density in FGA units is much lower than in gabbro (Fig. 3.4), although the units are mineralogically similar. The lack of vein(let) development implies that FGA units were not conducive to fracture formation. The only apparent differences between gabbro and FGA units, however, are the fine grained nature and presence of foliation surfaces in the FGA units. The foliation planes may have facilitated translation of compression into shear stress which moved along the planes and out of the units. This implies that points or planes of sustained stress, were needed to develop VI fractures and could not develop in FGA units. Alternatively, the larger crystals in gabbro may have acted as relatively large discrete bodies through which stress could propagate linearly to form fractures, whereas the fine grains of the FGA units refracted, and therefore dissipated linear stress outward from crystal interfaces.

3.6.2 VEIN SET VI-VII

Minor, possibly transitional veins, denoted VI-VII, were found in Zone B drill core and outcrop. These comprise thirty-four 1 to 3mm wide scheelite-bearing hornblende-quartz veinlets found in drill core (15) and the main trenched area west of F1 (19), and several *w*- and/or *y*- scheelite-bearing quartz veins with hornblende haloes, one of which contains biotite. The latter may, however, be a later VII veinlet which formed along the same VI fracture surface. Two VI microfractures and one VI veinlet which had biotite haloes (Mann, 1981; Mann, 1982), are also included in vein set VI-VII because biotite haloes normally characterize VII veins, only.

3.6.3 VEIN SET VII

3.6.3a VII MINERALOGY

Vein set VII comprises biotite-haloed scheelite ± biotite ± sulfide-bearing quartz veinlets, typically 1 to 3mm across, but locally up to 5cm in width. VII veinlets in five drill holes across Zone A and several drill holes in Zone B were studied in detail to determine and document general trends in the abundance, range in widths and parageneses of the veinlets.

VII veinlets in Zone A generally differ from those in

Zone B by being much less abundant and having a smaller range of vein widths. For example, numerous veins <3mm across are present in Zone B, whereas only a few (4) were found in Zone A, and Zone A veinlets typically contain biotite and/or Cu/Fe sulfides, whereas those in Zone B do not. In addition, molybdenite is common, albeit minor, in Zone B veinlets, whereas almost no VII molybdenite is present in Zone A.

It should be noted that most veinlets, which were observed in thin section, were found to contain various amounts of carbonate. One veinlet containing no carbonate, contained 1 to 2mm euhedral K-feldspar crystals and no sulfides. No K-feldspar was found, however, in the carbonate-bearing veinlets. Veinlets containing trace or moderate to relatively abundant amounts of carbonate typically host minor pyrrhotite and chalcopyrite or minor to moderate amounts of pyrite, minor epidote, and chlorite, respectively.

Most of the carbonate appears to be secondary, and crosscuts scheelite or other VII vein sulfides. In addition, some vein(let)s comprise quartz veinlet-carbonate stringer pairs. The carbonate member typically occurs as a hairline stringer which rims, subparallels, and/or enters the veinlet at a low angle. The stringers commonly contain pyrite, chalcopyrite and/or black chlorite which crosscut the quartz-hosted scheelite crystals and/or vein sulfides. In a minor number of veinlets containing moderate to low amounts of carbonate, however, crosscutting relationships are not present, and hence may indicate that some of the carbonate is primary.

3.6.3b SPATIAL DISTRIBUTION AND VARIATION IN PARAGENESES ZONE A

Within Zone A, VII veinlet density (# veinlets/100m) increases southward from ~12 to ~53, which suggests that the fluid source lay southward (Fig. 3.5b, solid line). The southward increase in Zone A veinlet density was examined in light of host rock lithology and destructive effects of late pervasive alteration (Fig. 3.5). Host rock effects were examined because veinlet density appears to be higher in FGA than in Unit IIb metavolcano-sediments. Hence, the southward increase in veinlet density may reflect the southward increase in the percentage of FGA units which increases from 0% to >22% of total rock units (Fig. 3.5a).

The percentage of mafic rocks, however, increases gradually across the zone, whereas veinlet density increases abruptly (Fig. 3.5a,b.), and veinlet density in drill hole SSN 9 is less than in drill hole SSN 13 although it contains a relatively greater amount of mafic units. The lack of correlation in the slopes of the two trends and abrupt increase in veinlet density south of drill hole SSN 4 (Fig. 3.5b), indicates that host rock effects cannot account entirely for the southward increase in veinlet density.

The lack of correlation may be due to southward decrease in late destructive A3 sericite alteration. The most intense destructive alteration (A3 sericite) occurs adjacent to large VIV quartz stockworks where it largely replaces previously

Figure 3.5 (a) percentage of FGA units in specific drill holes across Zone A. (b) VII veinlet density (# VII veinlets/100m) in all Unit IIb rock units (solid line), in FGA units, only (upper dashed line), and in unaltered and intensely (A3-) sericite-altered (lower dashed, and lower dashed-dotted line, respectively). (c) histogram showing percentage of total Unit IIb metavolcano-sediments which are highly sericite-altered (clear bar); stippled bar shows percentage of those units which are felsic units. The highly sericite-altered rocks are the most intensely altered, Level 1, rocks (see Chap. 4, pp. 11-13). Refer to Fig. 3.9 for drill hole locations.

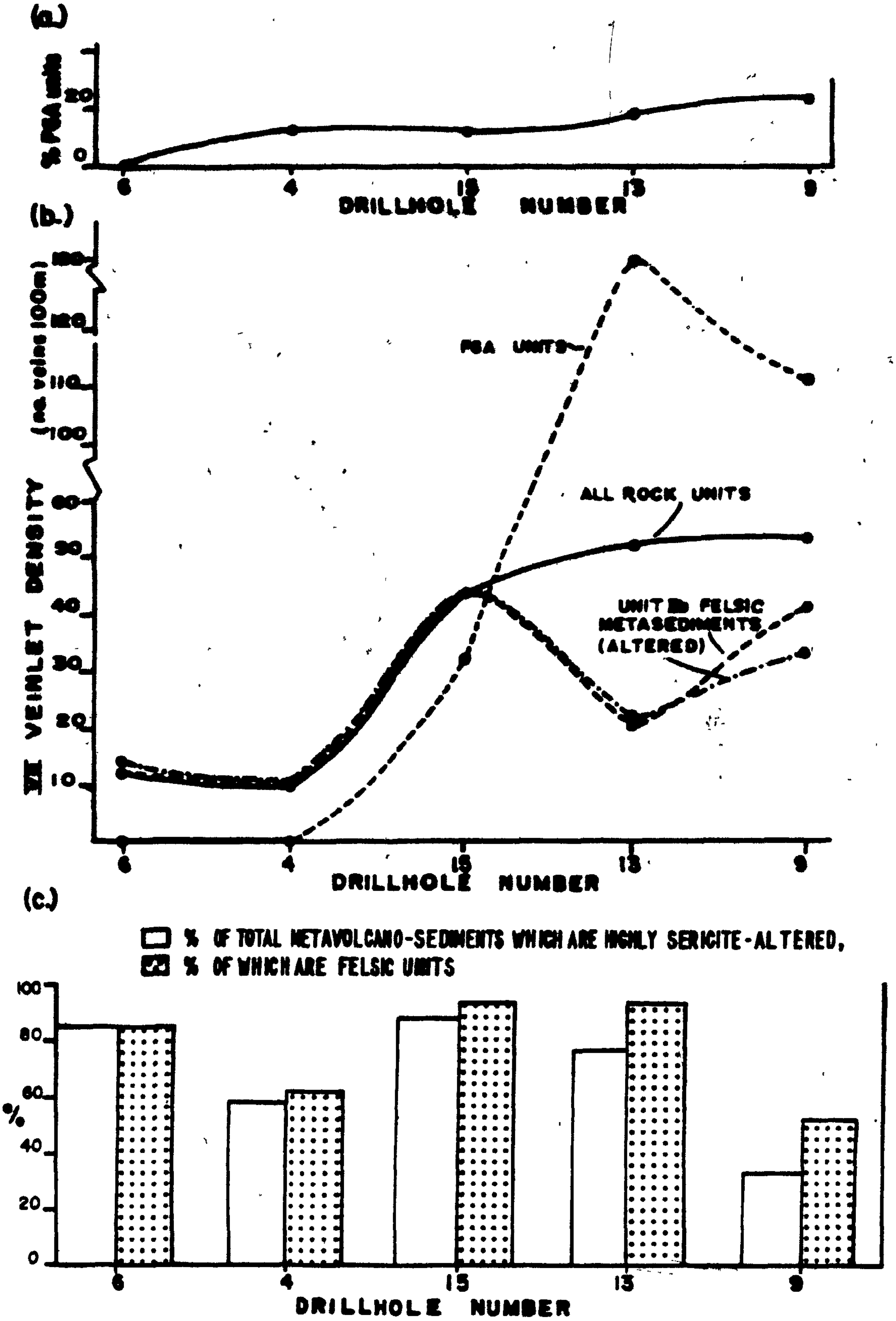
(a.)
% FGA units
0
20
6
4
15
13
9
DRILLHOLE NUMBER
(b.)
VI VEINLET DENSITY (no. veins/100m)
10
20
30
40
50
60
100
110
120
130
FGA UNITS
ALL ROCK UNITS
UNIT FELSIC METASEDIMENTS (ALTERED)
6
4
15
13
9
DRILLHOLE NUMBER
(c.)
☐ % OF TOTAL METAVOLCANO-SEDIMENTS WHICH ARE HIGHLY SERICITE-ALTERED,
▨ % OF WHICH ARE FELSIC UNITS
%
0
20
40
60
80
100
6
4
15
13
9
DRILLHOLE NUMBER

formed (A2 biotite) alteration (Chap. 4). The destruction of previous (biotite) alteration, may imply that the small (VII) veinlets, with which it is associated, were also destroyed. Hence, if destructive alteration decreases southward, the increase in VII veinlet density southward may only be apparent.

VII density in drill core of altered and unaltered felsic units* is nearly identical, however (Fig. 3.5c), which suggests that the number of veinlets destroyed by late sericite alteration is minimal. A possible exception is drill hole SSN 9 in which veinlet density is ∾10% less in highly sericite altered felsic rocks (Fig. 3.5b). Hence, the southward increase in veinlet density appears to be largely independent of host rock or alteration effects.

Many veinlets contain scheelite, only. Pure scheelite-bearing veinlets are most abundant in drill hole SSN 15, near the center of Zone A, and decrease in abundance abruptly northward over a small distance of 200m from 68 to 6 (Fig. 3.6); southward the scheelite veinlets decrease in number gradually over 400m from 68 to 9 with a concomitant large increase in the number of scheelite veinlets containing sulfides, 2 to 99. The southernmost drill holes, SSN 13 and 9, for example, contain abundant pyrite and SSN 9, contains abundant pyrite as well as chalcopyrite and pyrrhotite (Fig. 3.6).

* Mafic units were not considered. The units are substantially more resistant to alteration (Chap. 4)and hence the southward increase in the percentage of mafic units would distort the measured effects of sericite alteration on veinlet density trends.

Figure 3.6 Histograms showing main parageneses in VII scheelite-bearing quartz veinlets from a north-south sequence of drill holes across Zone A. Mineral(s) in parentheses represent the largest paragenetic subset of the main paragenesis written above it. 1cm = 10 occurrences.

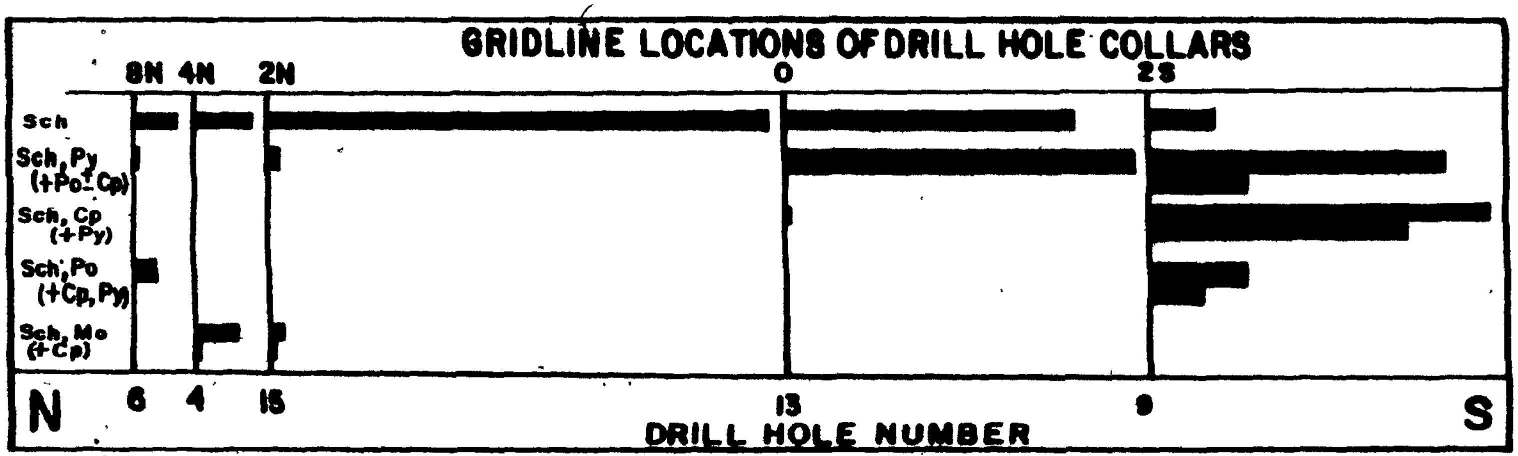
GRIDLINE LOCATIONS OF DRILL HOLE COLLARS
8N
4N
2N
0
2S
Sch
Sch, Py (+Po±Cp)
Sch, Cp (+Py)
Sch, Po (+Cp, Py)
Sch, Mo (+Cp)
N
6
4
15
13
9
S
DRILL HOLE NUMBER

Molybdenite is rare, occurring in <3% of all veinlets. No molybdenite-bearing veinlets were found in drill core north of drill hole SSN 4 or in the southernmost drill holes, SSN 9 and 20, and only a small number were found in drill core SSN 11 (Moore 1979) and 13 near the center of Zone A (Fig. 3.6). The erratic distribution of molybdenite is probably a statistical problem resulting from the high significance of minor fluctuations in the small number of molybdenite-bearing VII veinlets which were found; hence the variations in molybdenite distribution are not considered to be significant.

ZONE B

VII veinlets in Zone B are much more widespread and abundant than in Zone A. The veinlets occur up to 750m to the west but are largely concentrated in the metavolcano-sediment-hosted scheelite-mineralized zones, F3 and F4, and less so, in gabbro-hosted zones, F1 and F2 (Fig. 3.4). The northernmost drill hole in Zone B gabbro (SSN 38) however, contains relatively abundant VII veinlets, and an anomalously low amount of VI vein(let)s (Fig. 3.4).

VII veinlets in Zone B have a simpler and more consistent paragenesis than in Zone A. The veins typically contain only scheelite and minor to no molybdenite. This is reflected in drill core assays across F3 and F4, which commonly measure ~0.10wt%WO3, and <0.01wt% MoS_2.

The scheelite is made up mostly of 1 to 2mm crystals, and the molybdenite is fine grained and commonly concentrated along vein edges. Sulfides are relatively rare, except in the northernmost gabbro-hosted drill hole (SSN 38) where ~20% of the veinlets contain chalcopyrite and/or pyrite. The relatively sulfide-rich nature of these veins is similar to that found in the southern part of Zone A (Fig. 3.6).

3.6.4 VEIN SET VIII

3.6.4a VIII MINERALOGY

VIII is the smallest and least mineralized vein set in Zone A (only 178 VIII veins were found in all Zone A drill core), and the largest in Zone B. The veins comprise biotite-haloed molybdenite-bearing quartz veins in Zone A, and scheelite ± molybdenite-bearing quartz veins in Zone B. The veins are typically 1 to 3cm wide, but have a smaller range in widths in Zone A (0.5cm to 6cm) than in Zone B (up to 40cm). In contrast to VI and VII veins, many VIII veins contain vugs 3 to 4mm across.

The molybdenite is coarse grained, typically rims vein edges, and in Zone B, locally intergrows with coarse grained scheelite. Some composite veins, comprising several distinct quartz bands, which are separated by fine grained molybdenite "dust", were found in Zones A and B. Their presence indicates that there were several pulses of molybdenite mineralization.

3.6.4b SPATIAL DISTRIBUTION AND VARIATION IN PARAGENESES

ZONE A

VIII vein density generally increases southward across Zone A, from 0 to 8.34 (Fig. 3.7). VIII veins in Zone A

Figure 3.7 VIII vein density (# veins/100m) across Zone A. Upper coordinates correspond to grid lines shown in Fig. 3.9. Note that vein density generally increases southward.

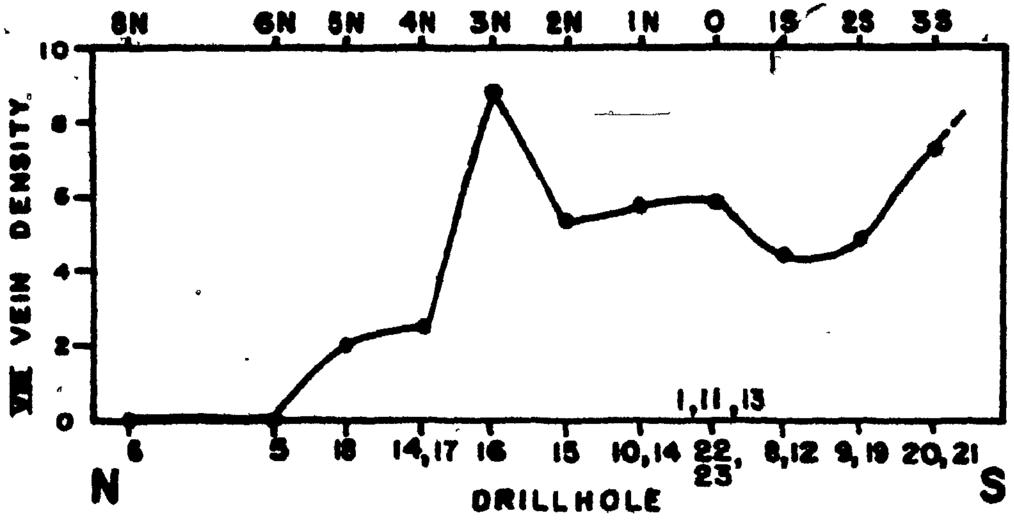
8N
6N
5N
4N
3N
2N
1N
0
1S
2S
3S
VII VEIN DENSITY
10
8
6
4
2
0
1,11,13
6
5
18
14,17
16
15
10,14
22, 23
8,12
9,19
20,21
N
DRILLHOLE
S

typically contain minor molybdenite, only, with almost all drill core containing VIII veins assaying <0.01wt.%MoS2. Three exceptions are found in drill holes SSN 2, 3, which each contain one 3m interval of relatively abundant molybdenite, assaying, 0.018wt.%, 0.14wt.%, and 0.047wt.% MoS2, respectively (Moore, 1979).

A minor number of molybdenite-bearing VIII veins containing chalcopyrite were found in the main trench. In addition, two molydenite-bearing VIII veins containing scheelite, and several containing fluorite were found in drill core. The latter are from the southernmost drill holes, and comprise five veins from drill holes SSN 20, 21, and 19, and apparently similar, but barren quartz-fluorite veins in drill hole SSN 21 and nearby Penarroya drill hole, NA-3 (Rabinovitch, 1969).

ZONE B

VIII veins in Zone B comprise the largest vein set and, with VIV veins and stockworks (below) are concentrated in the three molybdenite-scheelite zones, MZ1-MZ3 (Section 3.3).

The vein density, size, paragenesis, and orientation of VIII veins in MZ1 through MZ3 were studied using drill core data from SSN 37, 34, and 26 (Fig. 3.8). Drill hole SSN 37 is in gabbro and transects MZ1 which crosscuts parts of F2, F3 and F4. Drill hole SSN 34 occurs in Unit IIb and transects MZ2 which crosscuts part of F4; and SSN 26 transects MZ3 which overlaps the southern part of F3 (Fig. 3.8). Drill holes SSN 29, 33, 38, which occur peripheral to

Figure 3.8 Some measured sections in select drill holes across Zone B, showing vein density and percentage of chalcopyrite-bearing VIII veins in and outside fracture zones MZ1 to MZ3.

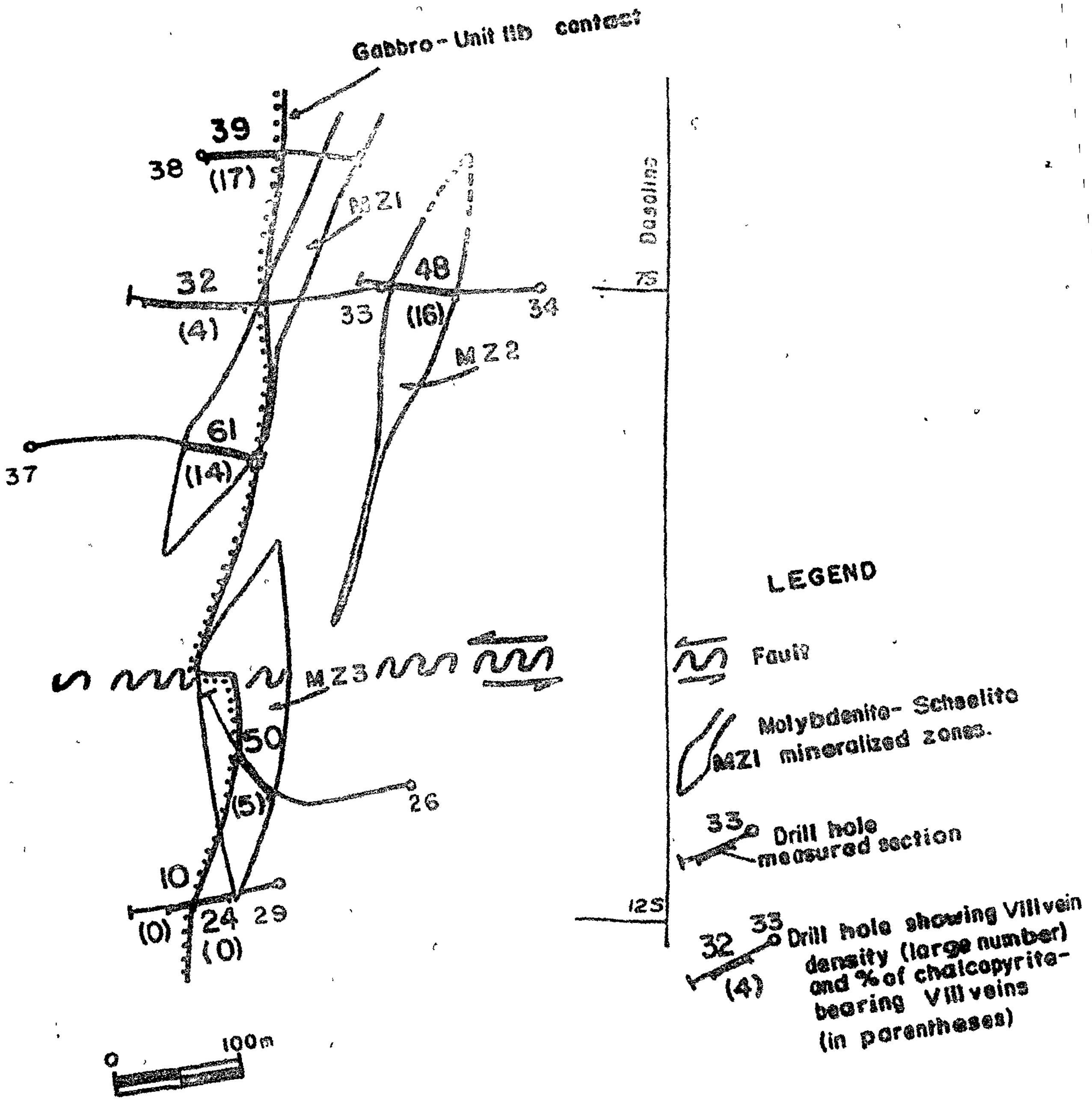
Gabbro - Unit IIb contact
39
38
(17)
MZ1
32
(4)
48
33
(16)
34
MZ2
Baseline
75
61
37
(14)
MZ3
50
26
(5)
10
(0)
24
29
(0)
125
0
100m
LEGEND
Fault
Molybdenite- Schaelite
MZ1 mineralized zones.
33
Drill hole
measured section
32
33
(4)
Drill hole showing VIII vein density (large number) and % of chalcopyrite-bearing VIII veins (in parentheses)

the zones (Fig. 3.8), were also studied to determine background vein density values and parageneses.

Drill hole data from SSN 26, 34 and 37 indicate that vein density may be higher in gabbro-hosted zones (61) than in metavolcano-sediment-hosted zones (48, 50; Fig. 3.8). However, vein widths in gabbro are generally narrower than in the metavolcano-sediments. For example, VIII veins in gabbro in drill holes SSN 29, 33, 37, and 38 are <0.5 to 6cm across, whereas those in Unit IIb metavolcano-sediments in drill holes SSN 26, 33, 34, and 37 range up to 50cm across.

Vein density in metavolcano-sediments across the deposit is approximately constant, and varies from 48 in MZ2 in the north (SSN 34), to 50 in MZ3 to the south (SSN 26; Fig. 3.8). In addition, vein density outside, but proximal to, fracture zones MZ1 through MZ3 is less and appears to decrease southward. Background vein density measures 39 in gabbro in the north, near MZ1 (SSN 38; Fig. 3.8), 32, about 100m southward (SSN 33), and 10 and 24 in gabbro and Unit IIb furthest south, outside MZ3 (SSN 29).

VIII vein density appears to drop off abruptly several hundreds of meters to the west and south of Zone B. A minor number of veins were found in drill core ~350m west of Zone B, (SSN 27 and 32); none were found in drill core further southwest (SSN 24, 25), and none were found in outcrop outside Zone B.

Most VIII scheelite is w- (molybdenum-free) scheelite, and is concentrated in gabbro. For example 65% (SSN 38) to 100% (SSN 37) of gabbro-hosted veins contain scheelite, composed of >50% (SSN 38) to 75% (SSN 33) w-scheelite. In contrast, minor (SSN 26) to 48% of metavolcano-sediment-hosted veins (SSN 34) contain scheelite, composed of 29% to 100% w-scheelite.

The scheelite occurs mostly as fine to coarse grained bipyramidal crystals with squarish cross sections up to 2cm across, and less commonly, as anhedral masses along vein walls and/or intergrown with molybdenite. Most y-scheelite occurs along quartz vein walls or as fine grained specks in associated biotite haloes.

The molybdenite is coarser grained and much more abundant in Zone B. It typically occurs along vein margins as fine grained amorphous masses, or apparently bladed rosettes, up to 1cm in diameter.

Pyrrhotite was found in minor amounts in many veins. In contrast, only minor to trace chalcopyrite and/or pyrite were found in a small number of veins. For example, only 15% of the veins in drill holes SSN 34 and 37 contain chalcopyrite or pyrite.

The percentage of gabbro- and metavolcano-sediment-hosted VIII veins containing chalcopyrite was measured in order to determine if it was preferentially deposited in a specific rock type. It occurs, however, in about the same percentage of veins in gabbro (14%; SSN 37) as in the metavolcano-sediments (16%; SSN 34). However, the percentage of chalcopyrite-bearing veins increases from south to north across the deposit (Fig. 3.8). No chalcopyrite was found in the southernmost drill hole, SSN 29; it was found in 5% of the veins in drill hole SSN 26, <100m to the north (MZ3); in 14% and 16% of the veins in MZ1 (SSN 37)and MZ2 (SSN 34), respectively; and in 17% of the veins outside MZ1, in the northernmost drill hole (SSN 38).

The mineralogy and paragenesis of vein sets VII and VIII in Zone B are similar, except that VIII veins are more mineralized, contain abundant molybdenite, and are concentrated in zones, MZ1 to MZ3. It was therefore difficult or impossible, in many cases, to distinguish between some of the wide molybdenite-poor VII veins and/or thinner molybdenite-rich VIII veins, especially where VI- and VII- mineralized fracture zones, F1 to F4, overlap MZ1 to MZ3.

In most cases, VII and VIII vein(let)s were distinguished by consistent differences in core intersection angles, relative amounts or grain size of molybdenite or scheelite, the presence of pyrrhotite, chalcopyrite and/or pyrite in VIII veins, and/or crosscutting relationships.

For example, in drill hole SSN 26, where MZ3 overlaps F4 completely, VII veinlets have a core intersection angle of 30 to 40 and are locally crosscut by large molybdenite-rich VIII quartz veins inclined 10 to 15 to the core axis (Mann, 1982). The similar mineralogies, vein parageneses, and presence of intermediate types of mineralized veins, however, indicate that the two vein sets probably represent a continuum in scheelite-molybdenite deposition.

3.6.5 VEIN SET VIV

3.6.5a VIV MINERALOGY

Vein set VIV comprises quartz veins and stockworks which in Zone A, contain abundant chalcopyrite, wolframite, and pyrrhotite, and in Zone B, minor similar mineralization, as well as abundant scheelite and molybdenite. The veins and stockworks commonly contain vugs, 1 to 4mm across. VIV vein(let)s and stockworks in both zones are associated with pervasive (A3) sericite alteration, which overprints previous amphibole and biotite alteration, associated with vein sets VI through VIII (Chap. 4).

3.6.5b VIV SPATIAL DISTRIBUTION

ZONE A

It is estimated that Zone A contains ~7.5 million tons grading 0.35% Cu as chalcopyrite and 0.21%WO3 as wolframite (Mann, 1980). The wolframite is typically surrounded by or intergrown with chalcopyrite which, in turn, surrounds or intergrows with pyrrhotite. Hence, it appears that wolframite was deposited first, followed by chalcopyrite (see Fig. 3.13) and later, pyrrhotite.

The wolframites have a generally high Fe to Mn ratio, and hence, are ferberites or manganiferous ferberites (Hak & Watkinson, 1982). No systematic variation in Fe/Mn os were found to occur across Zone A or with depth (op.cit).

Most of the VIV mineralization is contained within a NNW-trending, near vertical to steeply western dipping VIV quartz stockwork-filled fracture zone 13 to 35m wide and 1.2km in known length. A narrower (10 to 30m across) and apparently less mineralized quartz stockwork zone subparallels the main stockwork 33 to 63m to the west, where it is intersected in drill holes SSN 2 and 3 (Fig. 3.9).

A plan view of the main stockwork zone (Fig. 3.9) shows that it pinches and swells from L0+00 to L6N, where it branches out northward into several thin, mineralized, quartz stringer and small quartz stockwork zones. In addition, the zone strikes N12W and N8W, north and south across the silicified, E-trending fault at L0+00, but is not displaced. The lack of displacement and small strike change indicates that the stockwork zone formed after the fault.

Wolframite mineralization dies out at ~L5N, at the interface between Subunit IIb1, and the pelite-rich Subunit IIb2. Chalcopyrite mineralization, dies out ~200m further north. The stockwork tapers gradually from ~L0+00 to L4S, where it dies out. A vertical projection of the widest and most mineralized section of the eastern stockwork, near L0+00, shows that it nearly pinches out at ~300m depth, indicating that it may be lensoid or boudinage at depth (Fig. 3.10).

The two stockworks follow strong subparallel linear horizontal EM and/or VLF anomalies which flair out southward from 50m apart near 8N, to 130m apart near L3S (see Fig. 3.1). The western anomaly dies out abruptly at the northern interface, and the eastern anomaly dies out along the eastern flank of, the elliptical zone of high chargeability/low

Figure 3.9 Surface projection of Cu-W mineralized VIV stockwork-filled fracture zones in Zone A.

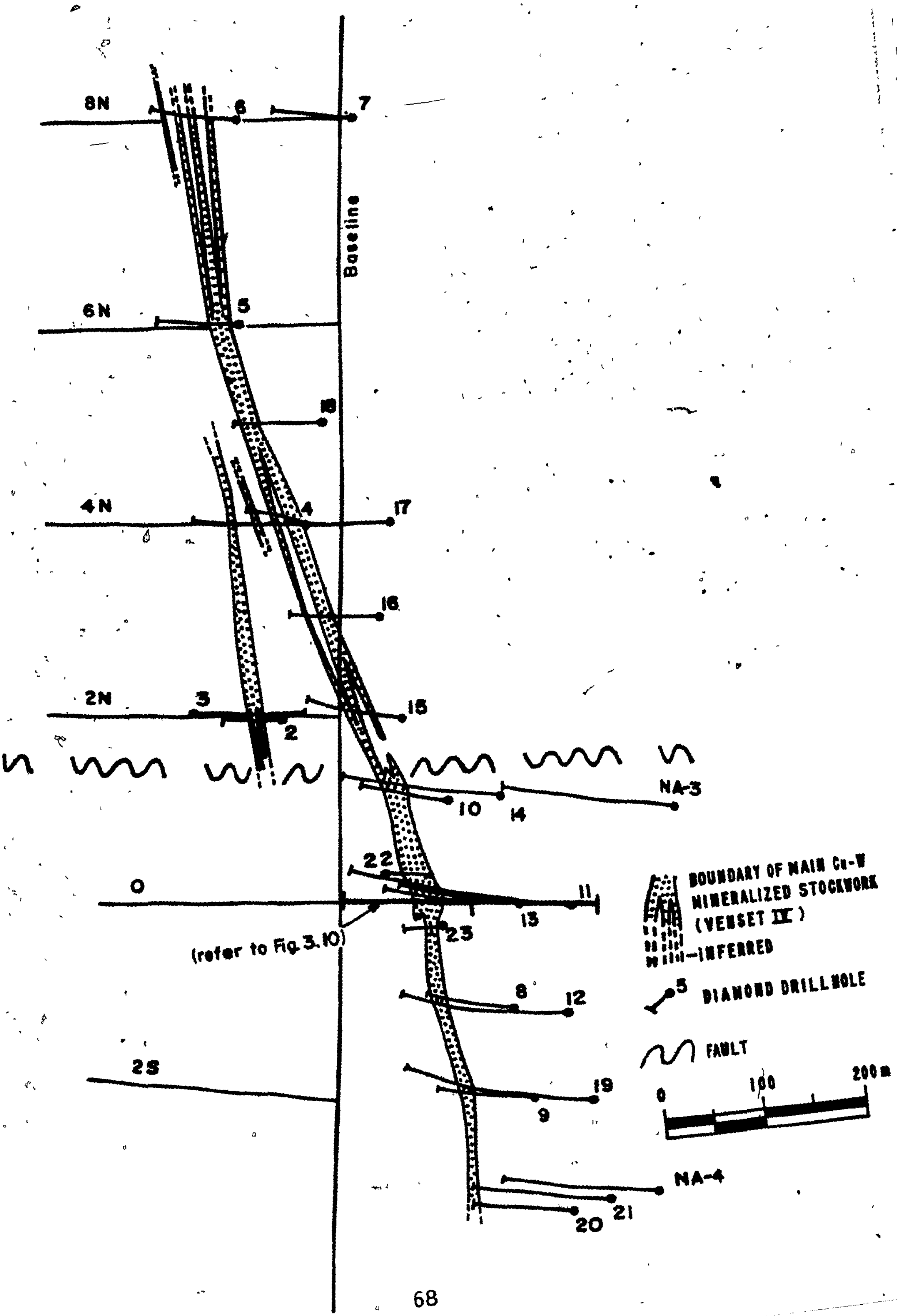
8N
6N
4N
2N
0
2S
Baseline
7
6
5
18
4
17
16
3
2
15
NA-3
10
14
22
11
13
23
(refer to Fig. 3.10)
8
12
19
9
NA-4
21
20
BOUNDARY OF MAIN Cu-W MINERALIZED STOCKWORK (VEINSET IX)
—INFERRED
5
DIAMOND DRILLHOLE
FAULT
0
100
200 m

Figure 3.10 Vertical cross section of the VIV stockwork at L0+00.

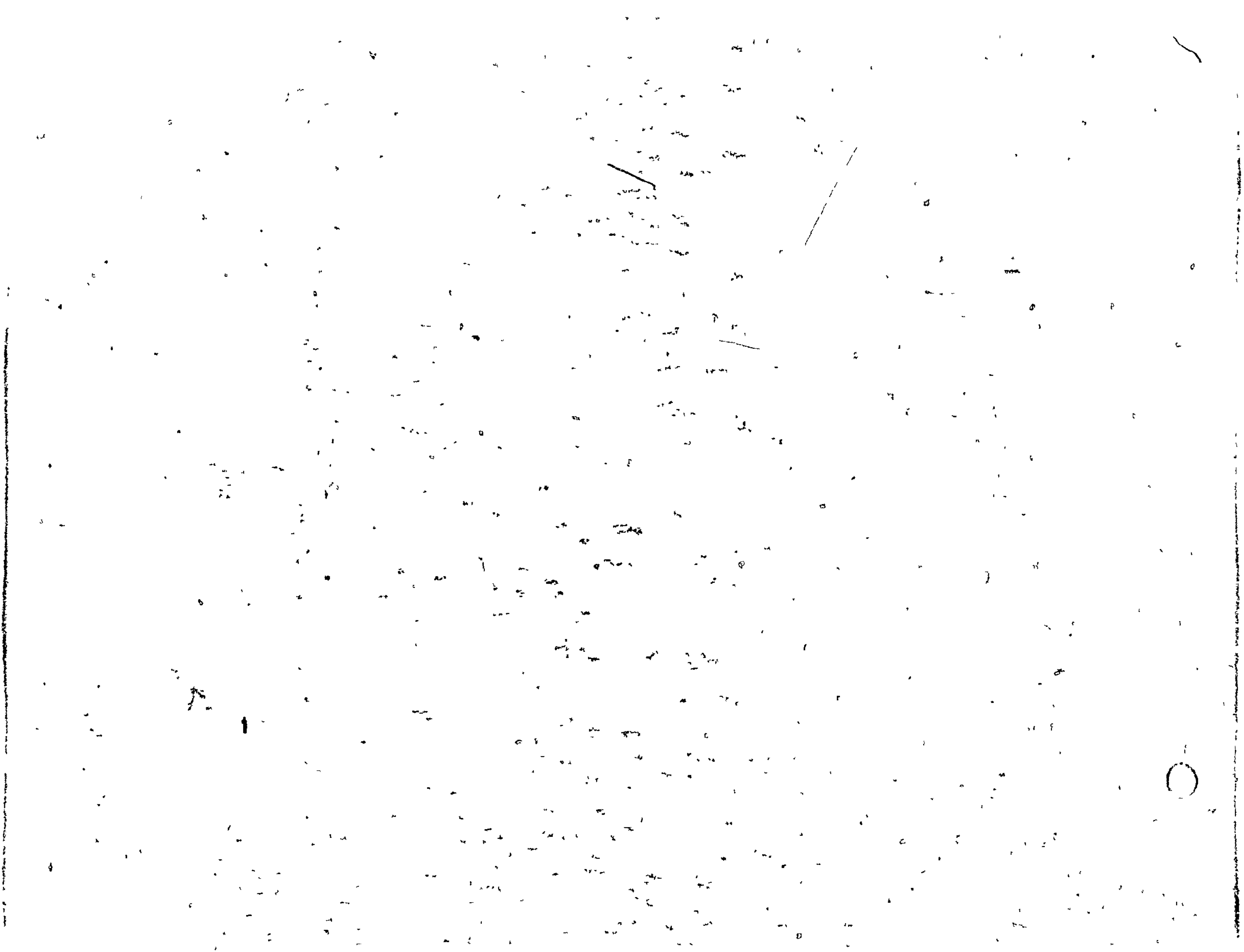

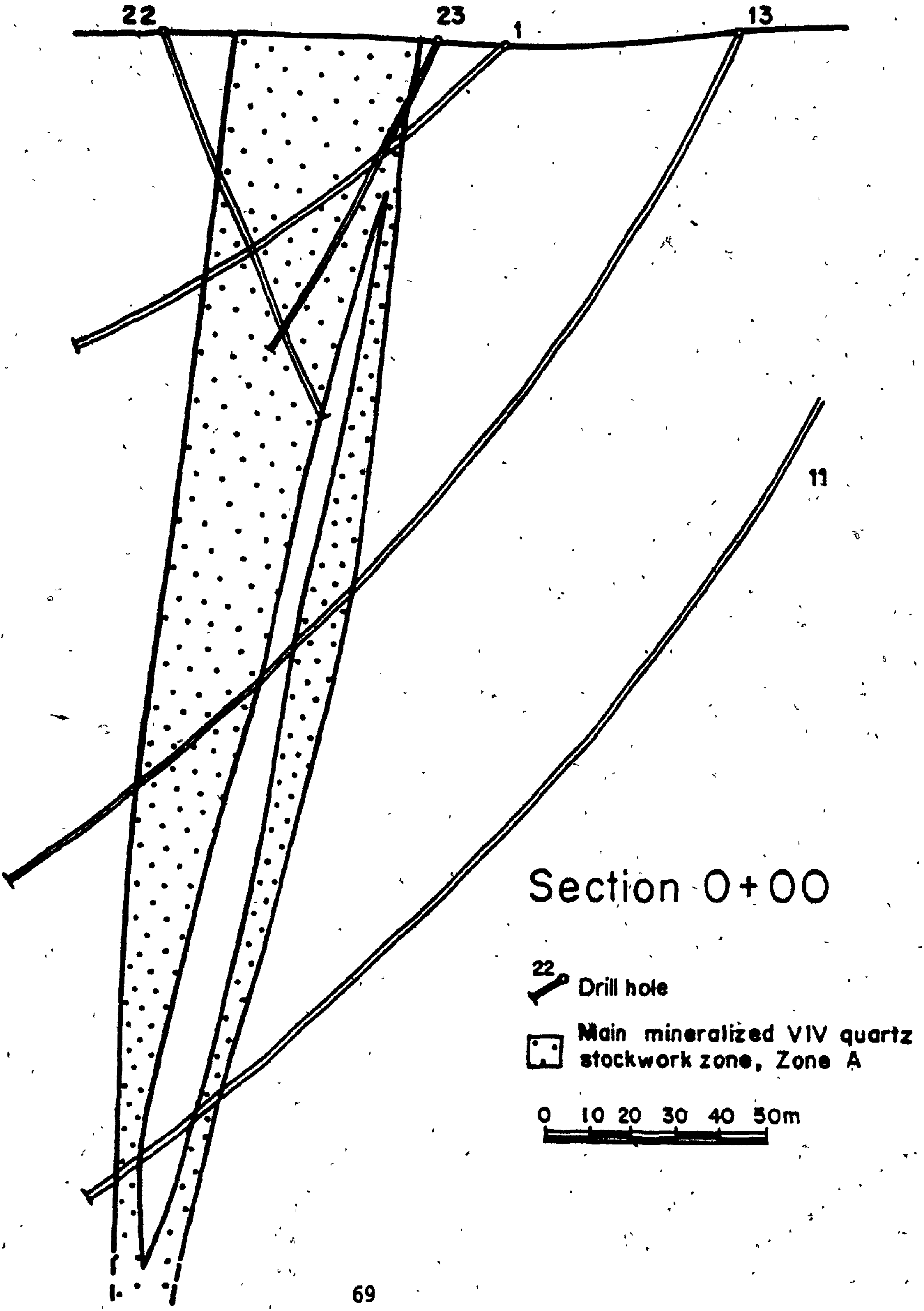
22
23
1
13
11
Section 0+00
22
Drill hole
Main mineralized VIV quartz stockwork zone, Zone A
0 10 20 30 40 50m

resistivity.

Two other linear VLF anomalies flair out southward from the west and east anomalies at L2N and L0N, respectively (see Fig. 3.1). The former dies out near L6S, and the latter dies out near L3S at the northwestern and northern interfaces, respectively, of the elongate geophysical anomaly. The latter VLF anomalies have not been drilled, but probably represent similarly mineralized stockwork-filled fracture zones. Another linear EM-VLF trend extends from L6 to L8N where the geophysical survey was discontinued. Drill hole SSN 7, drilled into the southern part of the anomaly contains sparsely mineralized, but highly (A3 sericite-; Chap. 4) altered rocks.

ZONE B

Vein set VIV in Zone B comprises numerous, less wide (½1-7m) scheelite ± molybdenite-mineralized stockworks and abundant, similarly mineralized quartz veins. Almost all of the scheelite is the white fluorescent variety. A single occurrence of bornite was recorded in drill hole SSN 34.

Wolframite and chalcopyrite, in contrast to Zone A, are present in only minor amounts. In addition, different amounts of VIV wolframite and chalcopyrite are found in Zone B metavolcano-sediment- versus gabbro- or FGA- hosted stockworks and veins. Wolframite is about one order of magnitude more abundant in metavolcano-sediments than in gabbro. This is evident in the difference in the average number of occurrences of wolframite in drill core of metavolcano-sediments, 0.10/m, versus gabbro, 0.01/m.

Chalcopyrite appears to be even more host rock specific, occurring mostly in felsic metavolcano-sediments. In the gabbro and mafic horizons in drill holes SSN 29 and 36, for example, chalcopyrite is absent; it is present in trace amounts in drill hole SSN 28 where the western stockwork occurs just outside the gabbro along the gabbro-sediment contact; it occurs in minor amounts in felsic metavolcano-sediments of drill hole SSN 30, 33; and it is relatively abundant in a metavolcano-sediment-hosted VIV quartz stringer zone near the gabbro-sediment contact in the north in drill hole SSN 38 (~0.10wt.% Cu) and in the eastern, totally metavolcano-sediment-hosted stockwork zone and associated quartz veins. In most cases, however, the amount of chalcopyrite in Zone B was considered too low to assay or measures <0.05wt.%Cu.

The apparent preferential deposition of chalcopyrite and wolframite in felsic metavolcano-sediments helps explain their relative abundance in metavolcano-sediment-hosted Zone A. However, the relative abundance of chalcopyrite in Zone A and molybdenite in Zone B, may also reflect metal zonation, with molybdenite being deposited closer to the fluid source (Barnes, 1975; Chap. 7). In addition, the abundance of wolframite in Zone A may reflect critical physico-chemical differences between the depositional environments of Zones A and B (Chap. 7).

The stockworks and vein(let)s are concentrated mostly in two large N-trending "composite stockwork zones", <5m to 60m in total width (Fig. 3.11). In addition, similarly mineralized VIV quartz stockwork zones, ∼30cm across, border several of the FQB porphyry dykes, and a quartz stringer zone is developed along the gabbro-sediment contact in the northern part of Zone B (Fig. 3.11).

Location of the composite stockwork zones is controlled structurally by lithologic contacts. Both stockwork zones are best developed in felsic metavolcano-sediments, and both die out within massive mafic units (Fig. 3.11). The western stockwork zone, has a relatively constant width of 20 to 30m, and largely straddles the gabbro - metavolcano-sediment contact, which occurs at a low angle to stratigraphy. The stockwork leaves the contact in two places, however: North of drill hole SSN 33, where it pinches out in a mafic metavolcano-sedimentary horizon; and south of drill hole SSN 28, where it extends undisturbed across a small fault between drill holes SSN 28 and 31 (Fig. 3.11). In the latter case, the stockwork continues into the eastward faulted block of gabbro where it dies out ∼175m to the south.

The eastern composite stockwork zone is located within a felsic metavolcano-sedimentary horizon, with no stockwork development in flanking mafic horizons, except at its southern extremity. There, the stockwork continues undisturbed across the fault between drill holes SSN 28 and 31, and dies out within 50m, in the eastward faulted block of a mafic horizon near drill hole SSN 26. In plan view, the eastern stockwork zone is open-ended to the north, pinches

Figure 3.11 Surface projection of main eastern and western IV composite quartz stockworks, minor quartz stockworks, and quartz stringer zone in Zone B.

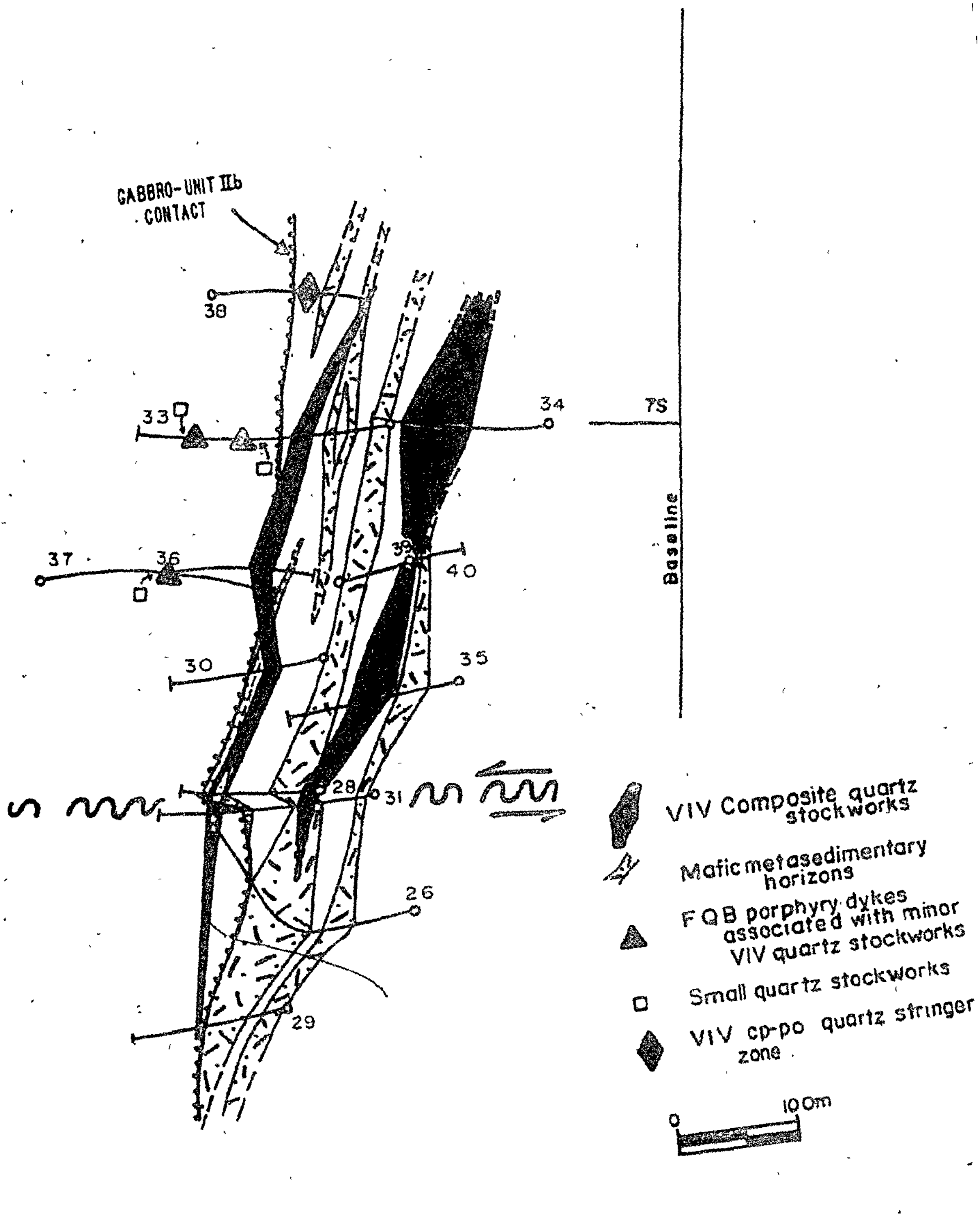
GABBRO-UNIT IIb CONTACT
38
33
34
7S
Baseline
37
36
39
40
30
35
28
31
26
29
VIV Composite quartz stockworks
Mafic metasedimentary horizons
FQB porphyry dykes associated with minor VIV quartz stockworks
Small quartz stockworks
VIV cp-po quartz stringer zone
0
100m

and swells southward along its length, and in its widest parts, extends out to the margins of the host felsic metavolcano-sedimentary horizon (Fig. 3.11).

Both stockwork zones, like MZ3, cross, but are not displaced by the late fault between drill holes SSN 28 and 31. A similar lack of displacement is seen in Zone A, where the eastern VIV quartz stockwork zone crosses a similar late fault (above). The lack of displacement of MZ3 and late VIV quartz stockworks by the late fault contrasts with the displacement observed in VI and VII scheelite-mineralized zone, F3, and indicates that the fault in Zone B formed after vein sets VI and VII, but before vein sets VIII and VIV.

The component stockworks along the eastern edge of the composite stockwork zones, especially the eastern one, are more numerous, wider and more mineralized than those in the west. The relative abundance of component stockwork zones and mineralization along the eastern contact suggest that the mineralizing fluid entered from the east, the direction inferred for the fluid source from the elongate geophysical anomaly (Chap. 2, p. 17).

The northern parts of the two composite stockwork zones parallel, overlap, and with vein set VIII, define scheelite-molybdenite zones, MZ1 and MZ2. MZ3, in contrast, is largely defined by VIII veins, only, with the western VIV stockwork overlapping it slightly along its western edge (see Fig. 3.8 and 3.11).

3.6.6 VEIN SET VV

3.6.6a VV MINERALOGY

VV, which is the youngest vein set, is the least important with respect to mineralization of economic interest. The vein set consists mostly of massive microcrystalline carbonate, as well as white or tan microcrystalline carbonate stringers, vein(let)s, and minor clear carbonate veins.

Three types of carbonate vein(let)s are recognized. One consists of white microcrystalline carbonate stringers typically containing massive pyrite ± trace amounts of small purple or rare green fluorite crystals ± molybdenite blebs <1mm across. The fluorite and molybdenite are locally in direct contact. A second type consists of tan to white carbonate + pyrite ± chlorite ± epidote stringers. The latter type locally comprises the carbonate member of quartz veinlet-carbonate stringer "pairs" discussed in Section 3.5.3.

A third vein(let) type consists of clear, coarse grained, barren carbonate which, in places, infills coarse grained VIV quartz veins, forming a comb texture. The latter may indicate that the fluids in vein sets VIV and VV were deposited continuously. Some of the carbonate is overgrown by turbid ankerite rhombs, which are gray-colored in thin section.

VV carbonate is also associated with the alteration of VIV quartz, wolframite, chalcopyrite, pyrrhotite, and previously formed hydrothermal alteration (Chap. 4). Clear coarse grained VIV stockwork quartz is recrystallized to fine grains and is grungy where crosscut by VV carbonate. VIV wolframite is altered to scheelite along its rims, cleavages and/or fracture planes, and VIV wolframite, chalcopyrite and pyrrhotite are locally rimmed or replaced by VV pyrite where crosscut by VV carbonate.

3.6.6b VV SPATIAL DISTRIBUTION

Massive carbonate comprises most of vein set VV. It infills S1, S2 foliation surfaces, fractures, and/or is concentrated along structural, stratigraphic or lithologic breaks. It is most abundant along the margins of VIV quartz stockworks (Zone A), or VIV composite quartz stockwork zones (Zone B). Abundant carbonate is also present along gabbro-Unit IIb contact and margins of some FQB porphyry dykes in Zone B. The carbonate in many of these areas is typically so abundant, that the rock is mechanically broken down and crumbly. Some drill core containing abundant carbonate along S2 foliation planes, for example, can be broken up into poker-chip like pieces (Moore, 1979). Much of the core from these areas is blocky, ground up, or lost.

The massive carbonate adjacent to the VIV quartz stockworks is associated with breccia zones. The breccias consist of <1 to 4cm, angular wall rock fragments set in massive microcrystalline carbonate containing abundant fine grained disseminated arsenopyrite, lesser amounts of pyrite, minor sphalerite and galena, and trace fluorite, molybdenite, chalcopyrite, and native bismuth (Moore, 1979). Arsenopyrite occurs locally as rare monomineralic patches in adjacent wall rock. The breccia zones are associated with abundant fine grained molybdenite along slickenside and/or fracture surfaces, which are common in Zone B, and less so, in Zone A.

Silver occurs in many of the brecciated carbonate zones, where it commonly assays up to 0.3 to 0.5 oz./ton in Zone A, but rarely more than 10ppm in Zone B. The silver minerals, scant and difficult to find, include acanthite, lesser hessite, and two unidentifiable phases in galena (Hak and Watkinson, 1981). The acanthite occurs in chalcopyrite, pyrrhotite, pyrite, galena, and sphalerite and hessite occur in galena, native bismuth, tellurobismutite, and acanthite. The unidentifiable phases occur in hessite or galena as tiny exsolution blebs (ibid.).

VV carbonate in Zone A is much less abundant than in Zone B and occurs mainly in areas adjacent to the two VIV quartz stockworks. In contrast, VV carbonate in Zone B, is abundant and concentrated in three N-trending zones, two of which occur along the eastern flanks of the VIV composite quartz stockwork zones (Fig. 3.12). In one place, however, the westernmost of the two VV carbonate zones diverges southward from the westernmost VIV stockwork zone to follow the gabbro-sediment contact. A third, less laterally continuous carbonate zone, ~300m in length, occurs between drill holes SSN 38 and 35, in between two mafic metavolcano-sedimentary horizons (Fig. 3.12).

Figure 3.12 Surface projection of VV carbonate zones in Zone B.

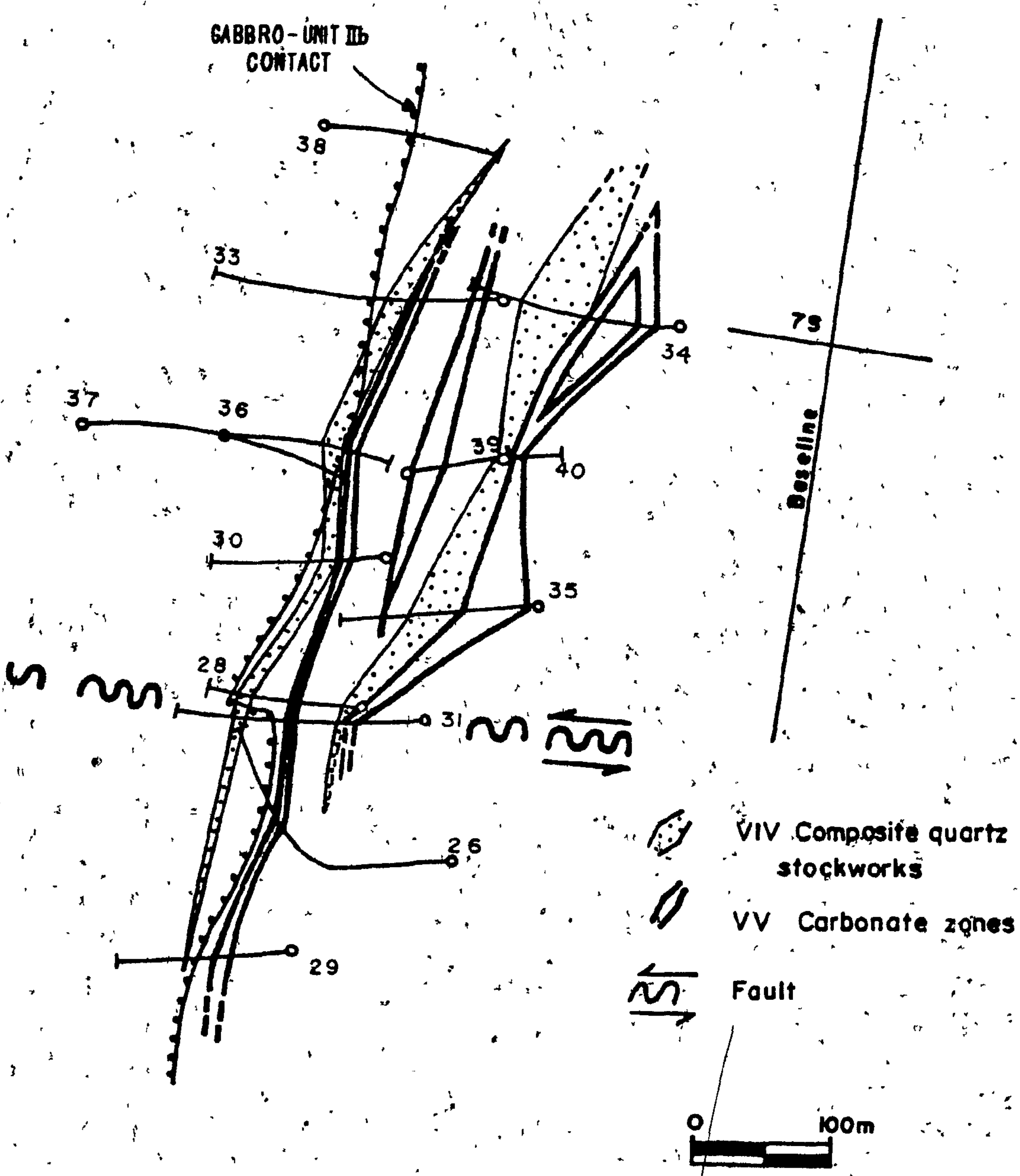
GABBRO-UNIT IIb CONTACT
38
33
37
36
30
28
31
26
29
39
40
35
34
79
Baseline
VIV Composite quartz stockworks
VV Carbonate zones
Fault
0
100m

3.7 SUMMARY

Similar vein parageneses and crosscutting relationships are present in Zones A and B (Fig. 3.13), and mineralization in both zones is associated with the same types of alteration (Chap. 4). VI amphibole veins occur almost exclusively in gabbro and contain mostly y-scheelite. VII quartz veinlets and VIII quartz veins crosscut VI veins and appear to represent continuous deposition of scheelite and molybdenite. VII veinlets contain mostly scheelite and trace to minor molybdenite, with a high percentage of y- to w-scheelite. VIII veins are wider, contain abundant scheelite and molybdenite, and a low percentage of y- to w-scheelite. Formation of VII and VIII quartz vein(let)s probably signals silica saturation of the hydrothermal system.

VI, VII and VIII vein(let)s are much more abundant and mineralized in Zone B than in Zone A. VII and VIII vein density in Zone A, however, increases southward. The relatively high vein(let) density in the southern part of Zone A and throughout Zone B suggests that the mineralizing fluid source is close to Zone B. This concurs with the geophysically inferred subsurface extent of the fluid source (Chap. 2, p.17).

Vein set VIV in Zone A is made up mainly of two quartz stockworks which host mostly chalcopyrite and wolframite and practically no molybdenite or scheelite. This contrasts with the VIV composite stockwork "zones" in Zone B that host relatively abundant w-scheelite and molybdenite, but only

Figure 3.13 Paragenesis of VL through VV mineralization in Zones A and B.

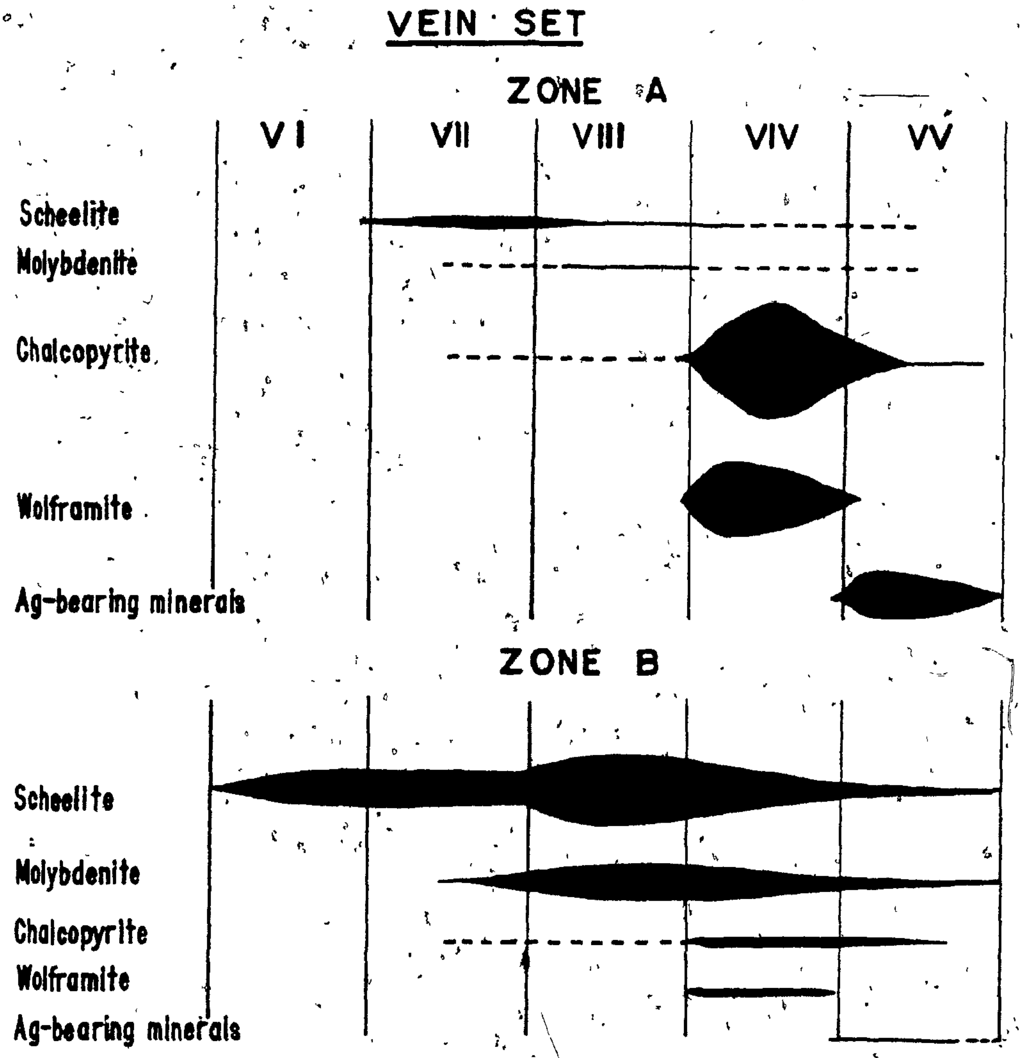
VEIN SET
ZONE A
V I
VII
VIII
VIV
VV
Scheelite
Molybdenite
Chalcopyrite
Wolframite
Ag-bearing minerals
ZONE B
Scheelite
Molybdenite
Chalcopyrite
Wolframite
Ag-bearing minerals

minor chalcopyrite or wolframite.

The difference in VIV mineralization between Zones A and B is probably due, in part, to effects of host rock lithology. However, it is probably more a function of proximity to the mineralizaing fluid source; Zone B, closer to the fluid source may represent the proximal molybdenite-rich silica zone, and Zone A, the distal chalcopyrite-rich facies. In addition, the presence of wolframite ($FeWO_4$) in Zone A and scheelite in Zone B ($CaWO_4$), may be due to differences between the physico-chemical conditions in the zones during mineralization (Chap. 7).

VV carbonate zones in both zones are similar. Most carbonate is massive and occurs adjacent to VIV stockwork zones (Zone B). Although VV carbonate is less abundant in Zone A, VV silver mineralization is much more abundant in Zone A than in Zone B. The relative abundance of silver mineralization in Zone A may also reflect greater distance of Zone A to the fluid source (Chap. 7).

VI and VII veins are most abundant in Zone B, where they are concentrated in four scheelite-mineralized zones in Zone B, F1 to F4. No mineralized VI veins and minor VII mineralization occur in Zone A. VIII veins are relatively rare in Zone B, but abundant in Zone B. Vein sets VIII and VIV in Zone B are concentrated in three scheelite-molybdenite mineralized zones in Zone B, MZ1 to MZ3.

Most mineralization of economic importance in Zone A comprises VIV chalcopyrite and wolframite which occurs in two steeply dipping, NNW-trending, continuous VIV quartz stockworks.

Vein set VIV in Zone B, comprises abundant small quartz stockworks concentrated in two composite quartz stockwork "zones". The component VIV quartz stockworks are more numerous in the eastern portion of the composite stockwork zones, than in the west. The VV massive carbonate zones are also located along the eastern margins of the VIV composite quartz stockwork zones.

The greater abundance of fracturing associated with formation of the composite VIV quartz stockwork zones as well as the presence of the relatively wide and laterally continuous VV massive carbonate zones, suggest that fluid volatile content was higher in Zone B. The concentration of component stockworks and massive VV carbonate zones along the eastern rims of VIV quartz stockwork "zones" in Zone B, suggests that the fluids entered from the east. A fluid source east of Zone B concurs with the geophysically inferred subsurface extent of the mineralizing fluid source, east of Zone B and south of Zone A (above; Chap. 2; Fig. 3.1).

CHAPTER 4. HYDROTHERMAL ALTERATION

4.1 INTRODUCTION

The mineralization at Sisson Brook is intimately associated with hydrothermal alteration which occurs locally about individual veins and fracture zones and pervasively throughout a large area surrounding the deposit. The alteration comprises four distinct alteration assemblages, denoted from oldest to youngest as A1 to A4. Each assemblage is characterized primarily by the presence of a particular hydrous silicate and associated host rock textures, and is vein-specific. The A1 assemblage haloes VI veins, the A2 assemblage haloes VII and VIII veins, the A3 assemblage haloes VIV veins, and the A4 assemblage is associated with VV veins.

A1 consists of hornblende + albitized plagioclase ± albite ± K-feldspar ± pyrrhotite ± magnetite, and occurs only in amphibole-bearing units. Most A1 alteration occurs in Unit IIIa gabbro where it is intimately associated with VI scheelite mineralization. A1 alteration also occurs in FGA and banded amphibolitic Unit IIb metavolcano-sediments.

A2 alteration comprises iron-rich, reddish brown-colored biotite + manganiferous ilmenite (Mn-ilmenite) + albitized plagioclase in mafic units, or albitized plagioclase + K-feldspar ± albite in Zone B felsic units. No K-feldspar alteration was observed in Zone A. A2 alteration is associated with the richest scheelite and molybdenite mineralization in Zone B and with minor, similar mineralization in Zone A (vein sets VII and VIII; Chap. 3).

Microstructural evidence shows that the reddish brown biotite, which crosscuts M3 porphyroblasts and brown biotite, formed contemporaneously with the S3 foliation surface.

A3 alteration is characterized by sericite + quartz ± pyrite, and is associated with the richest chalcopyrite and wolframite mineralization in Zone A, and minor similar mineralization and abundant molybdenite-scheelite in Zone B (vein set IV).

A4 is associated with late barren carbonate veins (vein set V V), and is recognized by the presence of fine grained sericite + massive carbonate ± pyrite ± chlorite ± epidote ± arsenopyrite ± kaolinite.

The extent of alteration about a specific vein or stockwork is proportional to the vein width, and to a lesser extent, depends on the relative permeability and composition of the host rock. An alteration halo about a large quartz stockwork-filled fracture, for example, is substantially larger in permeable and easily sericitized plagioclase lapilli tuffs than in refractory, less permeable FGA units. In both cases the halo is, however, much wider than that around a small veinlet.

Near the main zones of mineralization, where vein(let) and fracture density is high and vein size increases, intense local pervasive alteration occurs. Pervasive alteration is evident as epitaxial overgrowths or variable degrees of topotaxial replacement of primary or previously formed hydrothermal phases, and results in total or partial replacement of entire rock units. Local pervasive A1 and A2 alteration are the most widespread and extend up to 400m from the deposit. Local-pervasive A3 and A4 alteration, in contrast, are found within ~50m of VIV quartz stockwork zones and tens of centimeters from VV carbonate veins, respectively.

Local-pervasive A1 alteration grades gradually, and A2 alteration decreases abruptly, to a low level of distal pervasive alteration up to 1km from the deposit. Alteration distal to the deposit comprises only minor epitaxial or topotaxial replacement and occurs in the absence of vein(let)s or fractures. The latter suggests that the fluids moved via grain boundary diffusion or along regional cleavage surfaces. No distal A3 or A4 alteration was found.

4.2 MINERALOGY AND EXTENT OF ALTERATION TYPES

4.2.1 A1 ALTERATION

A1 alteration, which comprises hornblendic amphibole ± albitized plagioclase ± albite ± K-feldspar ± magnetite ± pyrrhotite, is found only in amphibole-bearing units, i.e., gabbro, FGA and amphibolitic sediments. Replacement of M3 by A1 amphibole is the most widespread alteration feature and appears to consistently decrease in intensity outwards from the deposit. For this reason, the degree of A1 alteration was contoured using the amount of observed A1 amphibole alteration.

A1 alteration is most intense in gabbro in Zone B and decreases in intensity outward from the deposit for ~0.75km

(Fig. 4.1). Contour 1 represents the lowest level of visible alteration. In thin sections of gabbro, this is expressed as clear green hornblendic replacement rims about primary actinolite centers. The centers are delineated by a slight brown coloration and are typically outlined and filled with numerous, minute, opaque inclusions. Similar brownish-colored cores and clear green-colored rims are found in Unit IIb FGA units and banded, amphibolitic metavolcano-sediments, except that the cores are not inclusion-filled. No alteration of the plagioclase was observed. Replacement rims in Zone B become slightly wider toward contour 2 and in some samples, the secondary phase replaces parts or all of the centers.

Contour level 2 was drawn where M3 amphibole cores are locally replaced in part or whole by hornblende, where microscopic blades of secondary hornblende are present, and/or at the first occurence of VI hornblendic amphibole patches or stringers. The latter is included as a criterion because vein set VI is characteristically associated with intense local pervasive Al alteration (Chap. 3). The hornblende blades, are generally <0.5mm long, and blue to blue-green or, less commonly, clear in color. The blades have chemical compositions identical to the replacement rims (Chap.5). The replacement rims locally intergrow with the blades, indicating that the two are co-genetic.

A minor number of rocks in Zone A occur in contour 2 (Fig. 4.1). These include several gabbro outcrops west of Zone A, minor gabbro dykes in drill holes SSN 2 and 3

Figure 4.1 Contour map of A1 alteration intensity. Contour 1 contains rocks showing the lowest level of visible alteration. In thin sections of gabbro, this is expressed as clear green hornblendic rims about primary actinolite cores. Contour 2 contains rocks showing intermediate amounts of alteration. This is evidenced by partial or whole replacement of M3 by A1 amphibole; where microscopic blades of secondary hornblende are present; and/or where V1 hornblende patches or stringers occur. Contour 3 contains the most pervasively altered rocks and is centered over Zone B. The primary amphiboles in the rocks are mostly altered to A1 hornblende, are bright green to green-blue in color, and are inclusion-free.

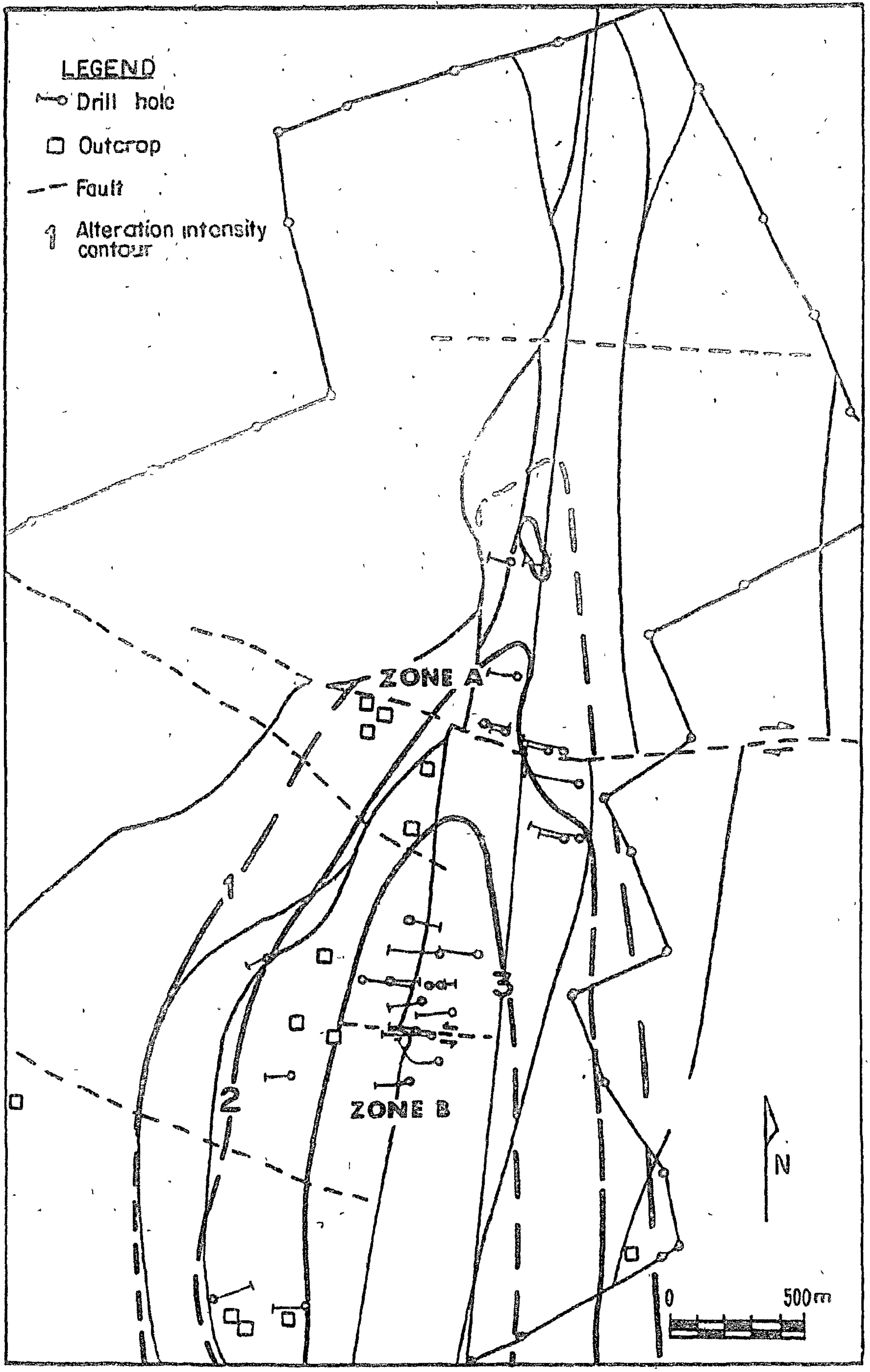
LEGEND
Drill hole
Outcrop
Fault
1 Alteration intensity contour
ZONE A
ZONE B
1
2
3
N
0
500m

containing rare, unmineralized hornblendic patches and stringers, some FGA units, and a green, amphibolitic, banded metasedimentary unit.

The most pervasively altered rocks lie within contour 3, which is centered over Zone B. The rocks commonly show total replacement of actinolite by hornblende, which in thin section, is bright green to green-blue in color and inclusion-free.

Plagioclase alteration is also common, but is patchy and less easy to identify or characterize. The most common alteration appears to comprise albitized M3 plagioclase, where M3 plagioclase crystals, having An contents between 50 and 65 (Chap. 2), are altered to compositions between An 5 and 50 (see Fig. 5.12). Another common alteration feature is the development of turbid, irregularly-shaped patches of albite which overgrow clear, concentrically zoned M3 plagioclase crystals. In addition, a small amount of K-feldspar alteration of M3 plagioclase was observed in a minor number of stained slabs.

The texture and composition of AI-altered rocks varies. Some altered rocks exhibit a heterogeneous texture, consisting of irregularly-shaped coarse grained AI-altered gabbroic patches, several centimeters across, in a fine grained and similarly altered gabbro matrix. In other places, the gabbro contains patches of coarse grained amphibole in a plagioclase-rich matrix. In addition, some VI veins in gabbro are rimmed by 2 to 100mm wide bleached (amphibole-absent) zones.

Disseminated scheelite is found throughout much of the highly A1-altered gabbro in contour 3, which is associated with a high density of scheelite-bearing VI fractures and clots. The scheelite is generally <1 to 10mm across, and commonly fluoresces bright canary yellow, and much less so, bluish-white. Microprobe analyses indicate that the yellow fluorescence is due to minor amounts of MoO_3 in the scheelite structure. The scheelite locally intergrows with, or is highly abraded and broken up by A1 amphibole which suggests that the two minerals are syngenetic.

Approximately the same ratio of y- to w- scheelite is present in the veins and associated altered rocks. The close spatial relationship and similar ratios of y- to w- scheelite in A1 and VI assemblages (Chap. 3) suggests that they formed contemporaneously from the same fluids.

Pyrrhotite is disseminated throughout most of the gabbro, and largely defines its regional aeromagnetic signature. Hence, most pyrrhotite in A1-altered gabbro is probably relict primary, or at least pre-M4 in age. Magnetite, in contrast, is coarse grained and euhedral, and is present in only the most intensely altered regions in contour 3. Magnetite is also a common VI constituent (Chap. 3).

4.2.2 A2 ALTERATION

The A2 assemblage is found in all rock types and comprises reddish brown, iron-rich biotite, manganiferous ilmenite (Mn-ilmenite; Chap. 5), and albitized M3 plagioclase in mafic units, and albitized M3 plagioclase, K-feldspar and albite in Zone B felsic units. The assemblage occurs locally as vein haloes and intense local-pervasive alteration, and as distal pervasive alteration up to 1km from the deposit where it comprises biotite, only (below).

The red brown biotite is the most widespread and characteristic mineral of the A2 assemblage. In thin section, the biotite is red-brown in color, relatively coarse grained, and commonly contains zircons and associated radiation burns.

The biotite is concentrated locally as <1.0mm cryptocrystalline to <1 to 3mm crystalline spots along S3 crenulation hingelines, distal to the deposit, and intense pervasive alteration and vein haloes, in the deposit. The apparently preferential nucleation of A2 biotite along crenulation hingelines shows that it is related genetically to formation of the S3 foliation surface.

The red brown biotite is optically and chemically identical to biotite in VII and VIII vein(let)s and the red brown biotite phenocrysts in the FQB porphyry (Chap. 5). The identical compositions suggest that the porphyry and hydrothermal fluids were the same. The concentration of all veins along tbe late S3 foliation (Chap. 3), and presence of the red-brown biotite in VII and VII vein(let)s and associated vein haloes, indicates further that the veins, alteration and S3 surface are co-eval.

4.2.2a A2 VEIN HALOES AND LOCAL-PERVASIVE ALTERATION

The most intense A2 alteration, occurs as VII and VIII vein(let) haloes and intense local-pervasive alteration near the main mineralized zones (Fig. 4.2; Contour 2). Biotite haloes are found mostly in amphibolitic or metavolcano-sedimentary units where the biotite replaces M3 and A1 amphiboles, or M2 sericite or chlorite, respectively.

A few veins which crosscut adjacent mafic and felsic units, have biotite haloes in the mafic unit and sericite haloes in the felsic units. The host rock specific nature of the haloes suggests that the fluids did not contain the ferromagnesian ions necessary for biotite formation, and that the halo-forming reactions were buffered by the host rock.

K-feldspar haloes were found in felsic dykes and lapilli tuffs in Zone B, only. The presence of the minor number of sericite haloes in felsic units (above) and K-feldspar haloes in Zone B, suggests that the fluids had a variable ratio of K^+/H^+. The absence of K-feldspar haloes in Zone A suggests further, that the K^+/H^+ ratio in Zone B was generally higher.

Haloes about a few carbonate-bearing VII vein(let)s contain minor chalcopyrite and/or pyrrhotite which locally mantles A2 Mn-ilmenite. Some VII veinlets which contain abundant carbonate and lesser amounts of chlorite, epidote and minor pyrite, have pyrite-bearing chlorite haloes which overgrow the A2 biotite haloes. In both cases, crosscutting relationships indicate that the carbonate and associated sulfides, chlorite and epidote are secondary.

Irregularly-shaped regions of especially intense

Figure 4.2 Contour map of A2 alteration intensity. Contour 2 outlines the area of most intense A2 alteration comprising abundant VII and VIII vein haloes and intense local-pervasive alteration. In many rocks M1, M2, and M3 platy and/or ferro-magnesian minerals are completely replaced by A2 biotite. The intensity of local-pervasive alteration decreases abruptly outside Contour 1, to a low level of distal pervasive alteration. Distal pervasive alteration occurs as biotite spots (less than 1 to 3mm across) and biotite stringers, locally concentrated along S3 surfaces.

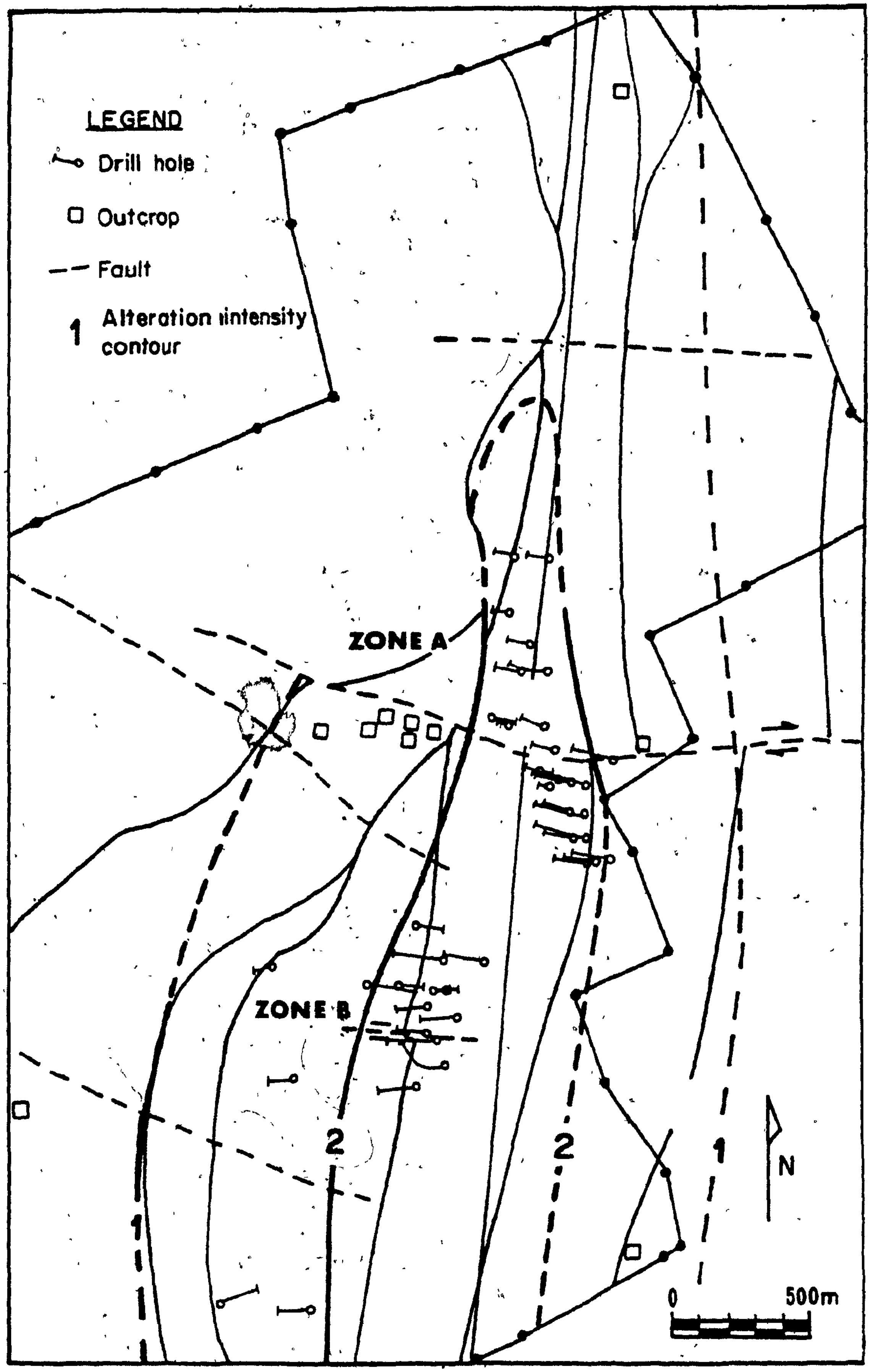
LEGEND
Drill hole
Outcrop
Fault
1 Alteration intensity contour
ZONE A
ZONE B
2
2
1
1
N
0
500m

alteration occur within Contour 2, near the gabbro-Unit IIb contact in Zone B, adjacent to dykes of FQB porphyry (Zone B), and near the main mineralized zones, especially in zone B. Pervasive alteration outside the irregularly-shaped, intensely altered regions, but inside Contour 2, is similar, but less intense.

Rocks on either side of the gabbro contact are in most cases completely biotitized to fine grained, dark brown-colored rocks such that the contact cannot be discerned. In the Unit IIb metavolcano-sediments crosscut by FQB porphyry (see Fig. 2.4, SSN 26), M2 chlorite and muscovite, and M3 cordierite and M3 and A1 amphibole are replaced completely by A2 biotite. In addition, most plagioclase in Unit IIb, Unit IVb (leuco-granite) and fine grained and pegmatitic felsic dykes is altered to K-feldspar and/or albite.

Especially intense alteration was also found in breccia zones adjacent to the FQB porphyry dykes in drill hole SSN 26. The breccia zones comprise <1 to 5cm diameter angular wall rock fragments in a dark brown-colored, fine grained matrix of A2 biotite, plagioclase, and quartz. Some of the felsic fragments are chalk white due to abundant K-feldspar and/or albite alteration.

In the intensely altered regions near the main mineralized zones, A2 biotite replaces M2 muscovite and chlorite along S1, S2 foliation surfaces, and occurs as topotaxial and minor epitaxial replacement of M3 and A1 amphibole by biotite (with Mn-ilmenite), and topotaxial replacement of M3 cordierite and brown biotite. The rocks also show pervasive disruption of primary sedimentary layering and less so, crystalline fabrics. Some primary host rock fragments and contact metamorphic porphyroblasts, for example, are sheared, kinked, rotated, fractured, split apart, and infilled and/or surrounded by A2 biotite (Figs. 4.3, 2.7).

FGA ~~units~~, which have a uniform grain size and fine crystalline texture (Chap. 2), proved to be optimum indicators of A2 alteration intensity. Units containing little to no alteration are dark green-colored (Chap. 2); moderately to more highly altered units are green-brown- and brown-green- colored, respectively; and the most altered or completely biotitized units are brown-colored. The relative degree of alteration intensity in Zones A and B was determined qualitatively by plotting the ratio of the number of meters of green- (fresh) against green-brown-, brown-green-, or brown- (altered) colored FGA units in several drill holes from each zone. The results show that the alteration in Zone B is approximately an order of magnitude more intense than in Zone A (Fig. 4.4).

FGA units in the southernmost drill holes in Zone A, however, contain anomalously high amounts of alteration, approaching that in Zone B (Fig. 4.4; SSN 20, 21). Similarly, the northernmost drill hole in Zone B (SSN 38), contains an anomalously low amount of alteration, similar to that in Zone A. Because the rocks in the drill holes contain intermediate levels of alteration, the drill holes were

Figure 4.3 M3 plagioclase which is abraded, sheared and infilled with A2 red-brown biotite.

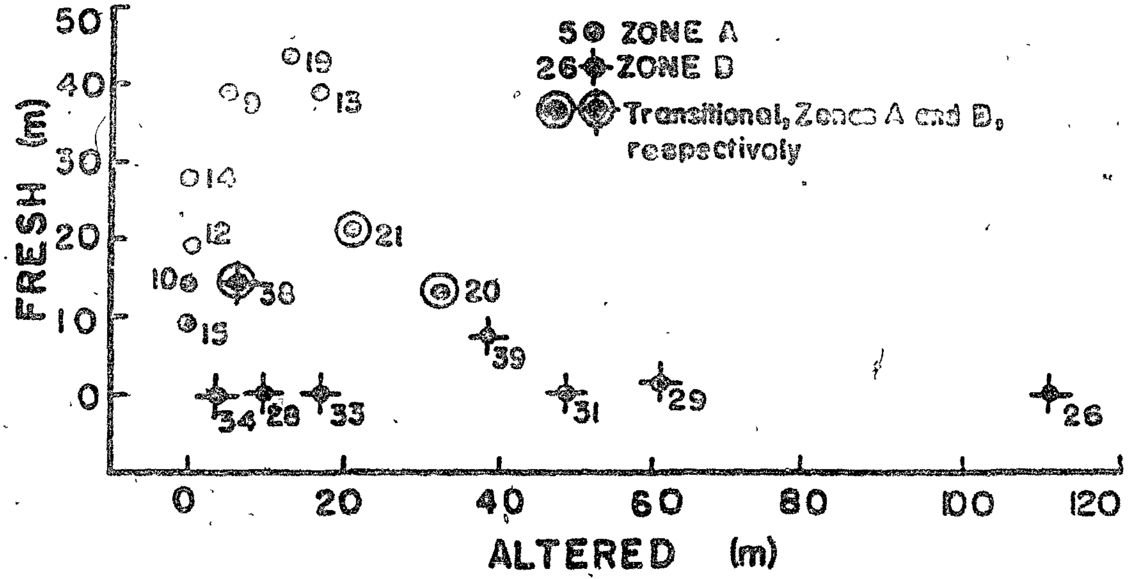

† drill holes which are not shown contain no FGA units, or none which are recognizable due to abundant destructive sericite alteration.

termed and plotted, "transitional" (Fig. 4.4).

4.2.2b DISTAL PERVASIVE ALTERATION

Local-pervasive alteration decreases abruptly outside Zones A and B (Contour 2) to a low level of distal pervasive alteration which extends up to ~1km from the deposit (Contour 1; Fig. 4.2). The distal alteration comprises mostly A2 biotite, which occurs as <0.05 to 1mm microcrystalline or crystalline biotite spots, < 1 to 3mm across, and biotite stringers. The spots and stringers are locally concentrated along S3 crenulation hingelines or subparallel S3 surfaces, respectively.

4.2.2c CRITERIA FOR PRESENCE OF A2 BIOTITE IN GABBRO

In most cases, A2 and M3 biotite are indistinguishable in hand sample or outcrop on the basis of color. They do, however, display characteristic modes of occurrence. For example, M3 biotite (brown in thin section; below) characteristically occurs as biotite in haloes about leucogranite dykes (Chap. 2) or in the 1-4cm pervasive splotches (Chap. 2), whereas A2 biotite (red-brown in thin section; below) occurs in rocks adjacent to the FQB porphyry or in vein haloes.

M3 biotite in thin section is coarse grained, inclusion-free, and ranges from pleochroic brown to olive-green or yellow, in color. The brown biotite characteristically replaces actinolite with sphene according to the general reaction,

amphibole ---> brown biotite + sphene,

A2 biotite, in contrast, is red-brown-colored, contains minute zircon inclusions with associated radiation burns, and crosscuts the brown variety. In addition, the biotite occurs with manganiferous ilmenite (Mn-ilmenite; Chap. 5) where it replaces amphibole, according to the general reaction,

amphibole ---> red-brown biotite + Mn-ilmenite.

The Mn-ilmenite is easily recognized in thin section by its metallic lustre and brown to tan and light blue anisotropy. Some Mn-ilmenite is also found locally in pervasively A2 altered metavolcano-sediments.

4.2.3 A3 ALTERATION

The A3 assemblage consists of sericite ± quartz ± pyrite and is associated with the formation of vein set VIV. The assemblage occurs in all rock types as VIV vein haloes or local-pervasive alteration adjacent to VIV quartz stockworks, and is areally more restricted than A1 or A2. It appears that A3 alteration is most intense in Zone A. No distal pervasive alteration was found in either zone.

The alteration in Zone A is mostly associated with the main VIV quartz stockwork which has a relatively simple and well-defined configuration (Figs. 3.9, 3.10). A3 alteration in Zone B, in contrast, is associated with numerous smaller stockworks and vein swarms, concentrated in stockwork "zones" (Chap. 3).

The intensity and extent of local pervasive A3 alteration in Zone A were determined using a color index. The most highly altered rocks are gray due to the abundance of A3 sericite, and are denoted as level 1 rocks (Fig. 4.5). Level 1 rocks are found mostly adjacent to the large VIV quartz stockworks, and grade outward into level 2 and 3 rocks over several tens of meters.

Level 1 alteration occurs as abundant sericite replacement of M2 platy minerals, M3 plagioclase, and A2 biotite, and most primary textures except lapilli outlines, are destroyed. Lapilli tuffs, which are the most permeable units, are typically the most altered and comprise ghost outlines of lapilli infilled with very fine grained sericite in a coarser grained sericite matrix. In hand sample, the lapilli have a distinct bluish hue and the matrix has a bleached white color. FGA units are rarely altered pervasively, and many retain original M3 amphibole and primary crystalline textures. A minor number of FGA units in level 1, are altered however, to pale green-colored rocks which contain abundant fine grained chlorite and sericite.

Level 2 and 3 rocks are mostly gray-brown and brown-gray in color, respectively, which reflects lesser amounts of sericite and greater amounts of relict A2 biotite. Most level 2 rocks show relatively well-preserved M2 and M3 mineralogies, foliations, and banding.

Rocks in level 3 are the least altered and represent the distal facies of alteration outward from the VIV quartz stockworks (Fig. 4.5). In addition, level 3 rocks are found in areas which contain a minor to moderate number of VIV veins.

Figure 4.5 Extent and intensity of A3 alteration about the eastern stockwork in Zone A. (see Fig. 3.9 for location of section line.)

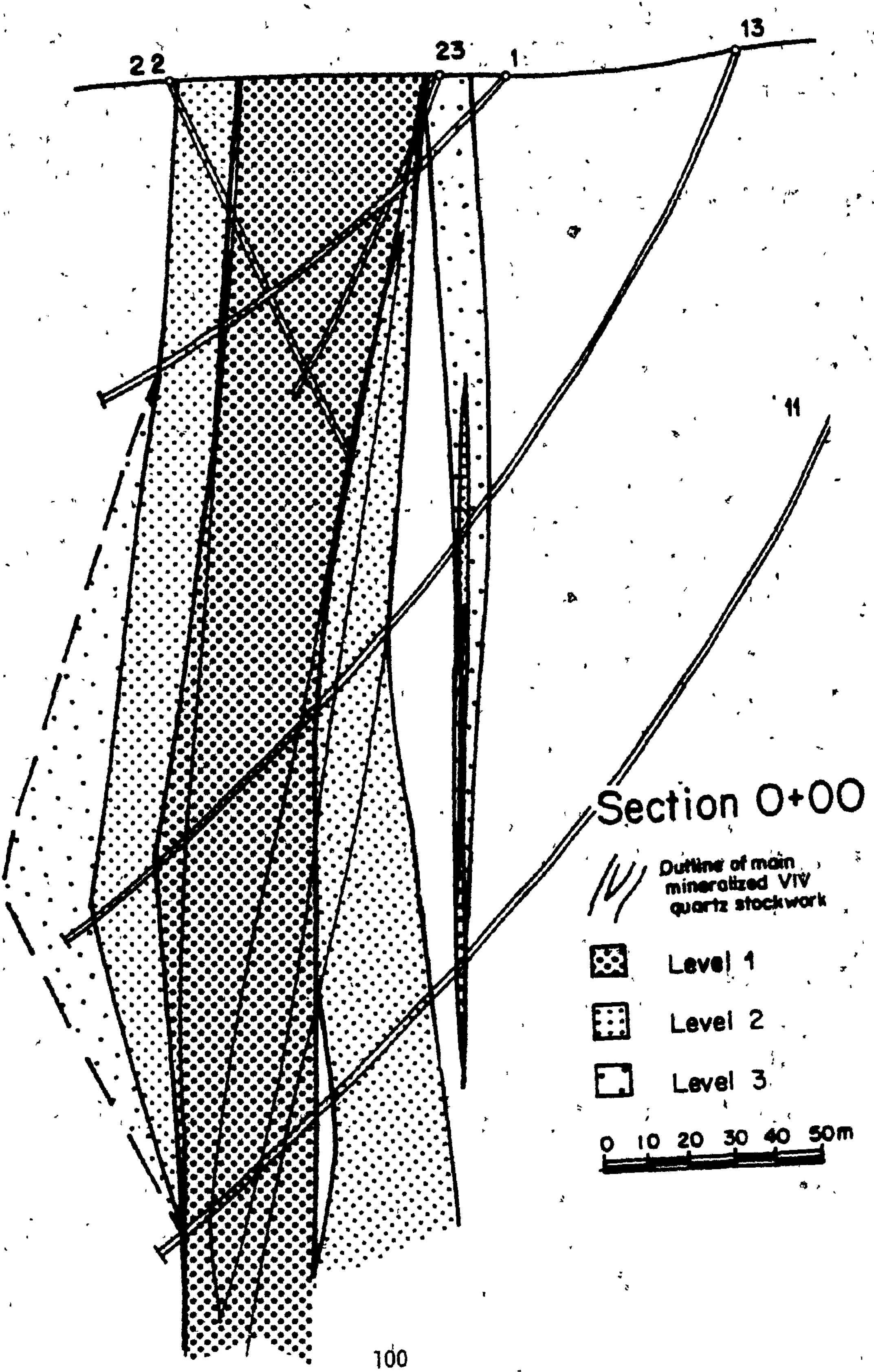
22
23
1
13
11
Section 0+00
Outline of main mineralized VIV quartz stockwork
Level 1
Level 2
Level 3
0 10 20 30 40 50m

The permeable lapilli tuffs and pelitic and quartzitic metasediments in levels 2 and 3 are the most altered. Practically no A3-altered FGA or gabbro units, however, are present in level 3.

It is noteworthy that the correlation coefficient between wt.%WO3 and Cu in the most intensely altered, level 1 rocks in Zone A is 0.90, whereas for all levels, it is only 0.41 (Moore, 1979). This suggests that alteration can be used as a discriminant to assess the different types, amounts, and extents of the various generations of mineralization.

4.2.4 A4 ALTERATION

A4 alteration consists primarily of fine grained sericite and fine grained massive carbonate with/without chlorite and pyrite, and comprises VV vein haloes and local pervasive alteration. VV vein haloes are almost 2X the width of haloes about VIV quartz veins of similar width, and the sericite is much finer grained than the A3 type. Local-pervasive A3 alteration is concentrated, like vein set VV, along pre-existing structural planes of weakness, such as the margins of VIV quartz stockworks, contacts beteen FGA- and metasedimentary-rich horizons, and along margins of FQB porphyry dykes (see Fig. 2.4).

The most intensely A4-altered rocks are converted mainly to fine grained sericite. The sericite replaces M2, M3, as well as previous alteration mineralogies, and obliterates relict crystalline textures, banding, and foliation surfaces.

Figure 4.6 Sequence and relative intensity of alteration types in Zones A and B. Note that each alteration type is vein specific and that A2 alteration is associated with vein sets VII and VIII.

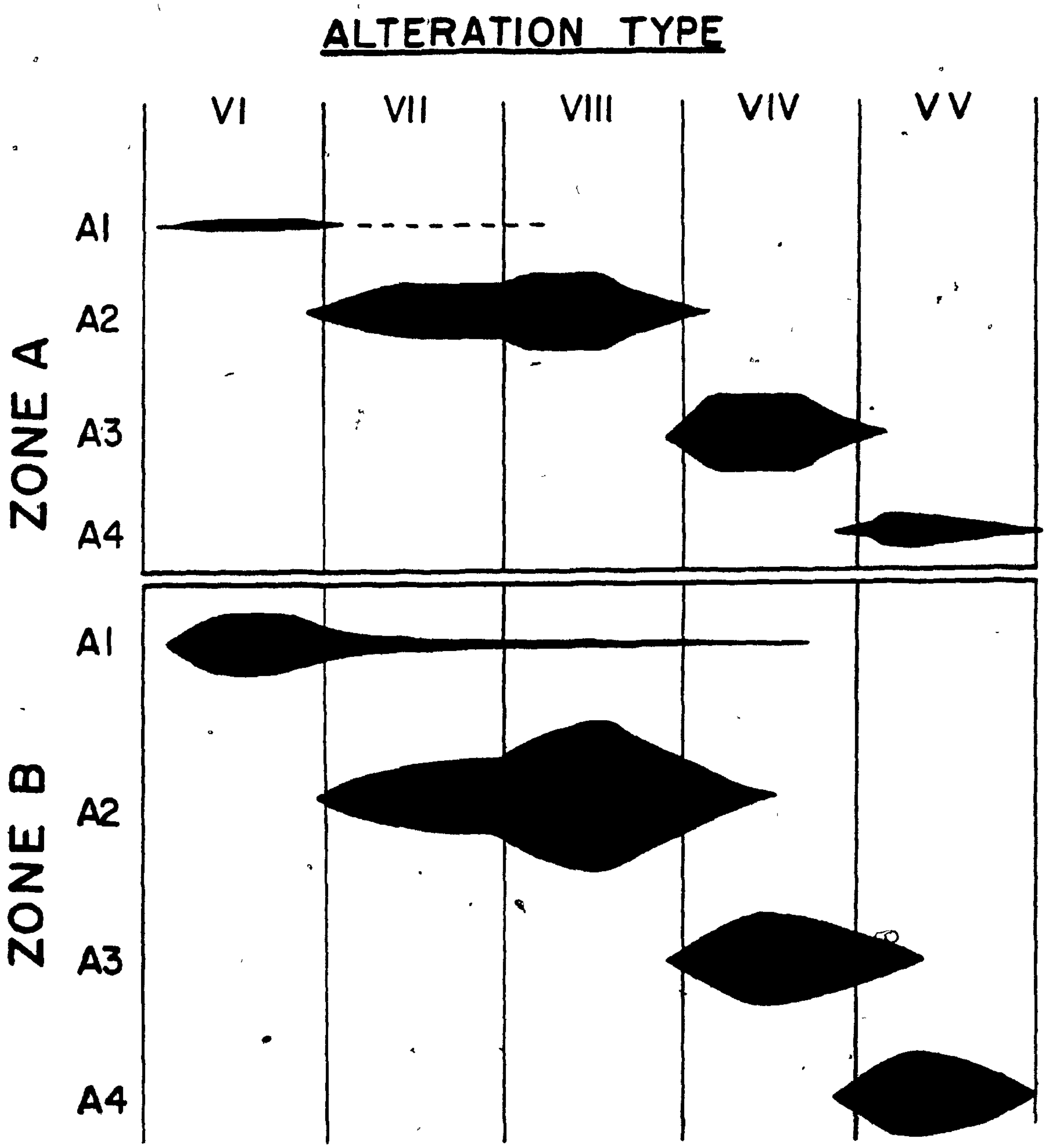
ALTERATION TYPE
VI
VII
VIII
VIV
VV
ZONE A
A1
A2
A3
A4
ZONE B
A1
A2
A3
A4

The most altered units are A3 sericite-altered lapilli tuffs adjacent to VIV quartz stockworks in level 1 (e.g., Fig. 4.5). The A4 sericite or carbonate in these areas patchily replaces A3 sericite and destroys lapilli outlines. FGA units, which are typically the units most resistant to alteration, are locally altered to light green chlorite-rich, or tan-colored carbonate and/or kaolinite-rich (below) units. The kaolinite, is tawn-colored, occurs locally, and in places, appears to post date the A4 sericite. The late nature of the kaolinite suggests that it formed during the waning stages of hydrothermal activity.

4.3 SUMMARY

Four types of alteration assemblages are found in Zones A and B, but in different amounts (Fig. 4.6). Each assemblage is associated with a specific vein set and is characterized by a particular hydrous silicate. A1 and A2 alteration is most abundant and associated with the most economically important mineralization in Zone B, i.e., VI through VIII scheelite and molybdenite. In contrast, A3 alteration is associated with almost all economically important mineralization in Zone A (VIV wolframite and chalcopyrite). In Zone B, A3 alteration is associated mostly with scheelite and molybdenite mineralization, and with only minor amounts of wolframite and chalcopyrite.

A1 alteration is restricted largely to gabbro and comprises mostly hornblendic amphibole replacement of M3 actinolite which increases in intensity into Zone B. Lesser amounts of A1 alteration are also found in the mafic FGA units. A1 alteration hosts moderate to abundant amounts of disseminated y-scheelite and less abundant w-scheelite. Gradual and increased replacement of amphibole occurs into the main VI-mineralized zones in Zone B (F1 to F4; Chap. 3), and VI veins contain similar high ratios of y- to w-scheelite; this suggests that A1 and VI assemblages are co-eval and are end-members of gabbro replacement.

A2 alteration is associated with vein sets VII and VIII, and like both vein sets, is much more abundant in Zone B. The alteration, which extends up to ~1km from the deposit, comprises mostly red brown biotite, shown to be co-eval with formation of the S3 surface, and K-feldspar. K-feldspar alteration was observed in Zone B, only, where it replaces plagioclase in felsic metavolcano-metasediments and felsic dykes.

The characteristic presence of A2 biotite and K-feldspar indicates that A2 alteration is a potassic alteration facies. The concentration of A2 biotite and apparently exclusive presence of K-feldspar alteration in Zone B indicates further, that the alteration in Zone B was more proximal to the fluid source. This agrees with the geophysically inferred location of the mineralizing intrusion(s) (Chaps. 2 and 3).

A3 alteration comprises mostly sericite, quartz, and pyrite, and signals a large change in fluid chemistry (Chap. 7). Its apparent concentration in Zone A may be the result of one or several factors. It may be due in small part to the abundance of mafic rocks in Zone B, which are typically most resistant to alteration.

Alternatively, more intense A3 alteration may have occurred in Zone A because of a higher fluid to rock ratio. As noted in Chapter 3, VIV quartz stockworks in Zone A are much wider, but smaller in number than those in Zone B. This suggests that the fluids were more focussed in Zone A. If fluid volumes in the two zones were similar, a higher fluid to rock ratio in Zone A would have resulted.

A3 sericite alteration may also represent a lower temperature/distal alteration facies. Hence its concentration in Zone A would indicate Zone A is more distal to the fluid source. This is consistent with its greater distance to the elongate geophysical anomaly, believed to represent the near-surface extent of the mineralizing intrusion (see Fig. 2.4).

A4 alteration, which comprises mostly fine grained sericite, carbonate, pyrite, chlorite, and epidote, is associated with the development of vein set VV. Kaolinite is also associated with the A4 assemblage, but appears to be a late phase.

CHAPTER 5. CHEMISTRY

5.1 INTRODUCTION

In this chapter, microprobe analyses of M3, A1, VI amphiboles, A2 biotites and manganiferous ilmenites (Mn-ilmenites), and A1 and A2 feldspars are presented and discussed. The chemistry of all mineral types is discussed in terms of relative cation, rather than oxide amounts. The stoichiometry of the amphiboles was derived using a computer program by Laird (1968); biotite stoichiometry was obtained using a modified version of a program by Laird and Albee (1969); and feldspar stoichiometry was obtained using an in-house program (**PL.BAS**, A. Hynes).

5.2 M3, A1, VI AMPHIBOLES

The chemistry of M3 and A1 amphiboles collected from 8 FGA samples in Zone A, and 9 gabbro and 1 FGA sample from Zone B were studied in detail. Amphiboles from gabbro and FGA units have similar ranges and variations in compositions which suggests that for the purpose of comparing amphibole analyses, the two rock types can be considered as one.

In thin section, the amphiboles comprise relict brownish-colored M3 cores, which commonly contain abundant opaque inclusions, as well as clear (inclusion-free) green A1 rims, completely A1-replaced crystals, and small discrete A1 blades, 1 to 3 microns across. The secondary blades were found in FGA units, only.

All amphibole analyses were examined in light of three main factors: 1) Mode of occurence, i.e., relict primary (M3) crystals, A1 blades, A1 replacement features, or VI veins; 2) the part of the crystal that was analyzed, i.e., core or rim and; 3) depth and proximity of the sample sites to the mineralized zones.

5.2.1 AMPHIBOLE CLASSIFICATION

The dominant M4 cations in Zone A and B amphiboles are Ca and Na, with sums of ≥ 1.34 and Na < 0.67. The amphiboles are therefore classified as calcic types (Leake, 1978). On a standard calcic amphibole grid (Leake, 1978), analyses from Zones A and B outline two broadly linear trends (Fig. 5.1).

Trend 1, defined by amphiboles distal to Zone B in drill hole SSN 25, extends from the actinolite to magnesio-tschermakitic hornblende fields and outlines a silica depletion trend at roughly constant Mg/Mg + Fe (Fig. 5.1b). The actinolite represents relatively pristine M3 cores, and the silica-depleted analyses comprise A1 rim (25.136.55) and totally A1-replaced (25.75) crystals.

Trend 2, outlines a Si + Mg depletion trend in amphiboles from both zones. The trend, which is more evolved in Zone B than in Zone A, extends from the actinolite field to the tschermakitic hornblende field (Fig. 5.1.a, b). No FGA units distal to either zone were measured. Hence, the least altered M3 core from FGA units in Zone A, sample 13.148, is probably slightly altered (i.e., hornblendic). In contrast, pristine M3 amphiboles were obtained from gabbro sample 25.136.55, located almost 1km southwest of Zone B.

Figure 5.1 Compositions of relict M3 and VI and Al amphiboles on a general hornblende classification diagram after Leake (1978), where Ca + Na $\geq$ 1.34 and Na < 0.67 in (a) Zone A, and (b) Zone B. Encircled samples contain analyses of amphiboles of the same type, e.g., core or rim, and from the same sample. The lines connect relict M3 and secondary amphibole compositions, or secondary amphiboles from different levels in the same drill hole. One tie line connects two VI vein analyses (0473 and 0466). Trend 1 and 2 amphiboles are outlined in green and red, respectively.

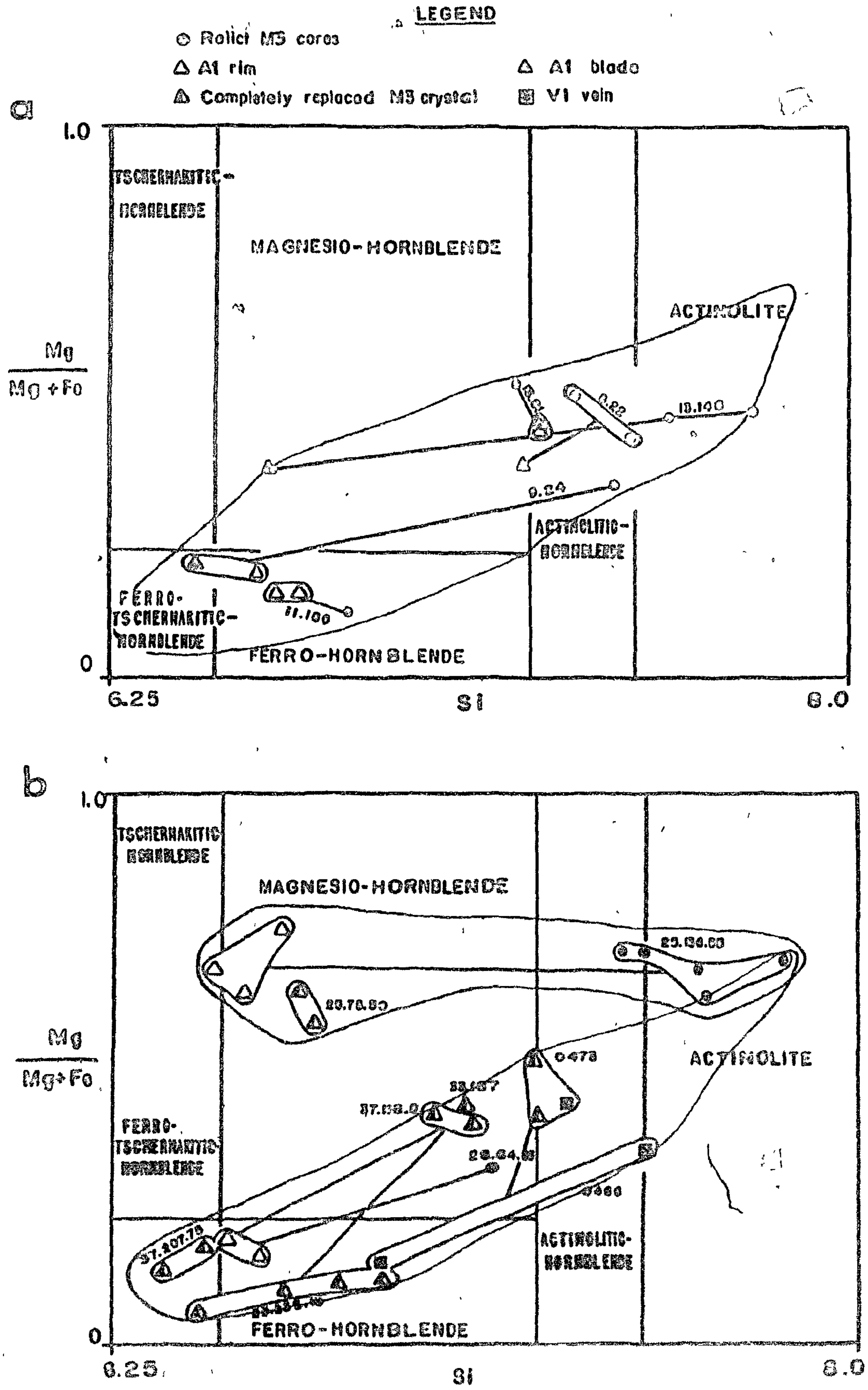
LEGEND
Relict M3 cores
Δ A1 rim
Completely replaced M3 crystal
Δ A1 blade
V1 vein
a
1.0
0
TSCHERMAKITIC-HORNBLENDE
MAGNESIO-HORNBLENDE
ACTINOLITE
ACTINOLITIC-HORNBLENDE
FERRO-TSCHERMAKITIC-HORNBLENDE
FERRO-HORNBLENDE
9.22
10.140
9.24
11.100
Mg / Mg + Fe
6.25
Si
8.0
b
1.0
0
TSCHERMAKITIC HORNBLENDE
MAGNESIO-HORNBLENDE
ACTINOLITE
FERRO-TSCHERMAKITIC HORNBLENDE
ACTINOLITIC-HORNBLENDE
FERRO-HORNBLENDE
25.130.00
23.78.80
0478
37.138.0
38.137
28.64.88
0480
37.207.75
Mg / Mg + Fe
6.25
Si
8.0

In order to show the chemical variations of Trend 2 amphiboles in plan view, Figure 5.1 was divided into 6 consecutively numbered "alteration zones" of equal width, along the trend axis (see Fig. 5.2). The most evolved analysis for each sample was considered representative of the furthest extent of alteration that the particular sample underwent, and was placed in the alteration grid (Fig. 5.2). The sample was assigned the number of the zone in which it occurs, and the zone numbers were transferred to the appropriate sample location site (Fig. 5.3).

5.2.2 DISCUSSION OF CHEMICAL VARIATIONS OF AMPHIBOLES

Figure 5.1 shows that some relict M3 cores, which are not visibly altered in thin section, are, in fact chemically altered to various degrees. In Zone B, the chemical alteration can be related to distance from the mineralized zones, i.e., the more proximal of the two relict core analyses has the more evolved composition (Sample 26.64 vs. 25.136.55; Figs. 5.1, 5.3). In addition, figure 5.1 shows that the compositions of A1 replacement rims and A1 blades in sample 9.24 are nearly identical, and that the compositions of VI vein and A1 alteration amphiboles from the same sample (0473) are practically the same.

Figure 5.3 shows that the most altered amphiboles, 33.235.10 and 37.207.75, are centered over the second most easterly scheelite-mineralized zone in Zone B, and the least altered amphiboles, with the exception of that from sample 33.157, occur outside Zone B. Figure 5.3 also shows that the

Figure 5.2 Hornblende classification scheme after Leake (1978) showing location of most altered analyses from each samplein alteration grid. See Figure 5.1 for legend.

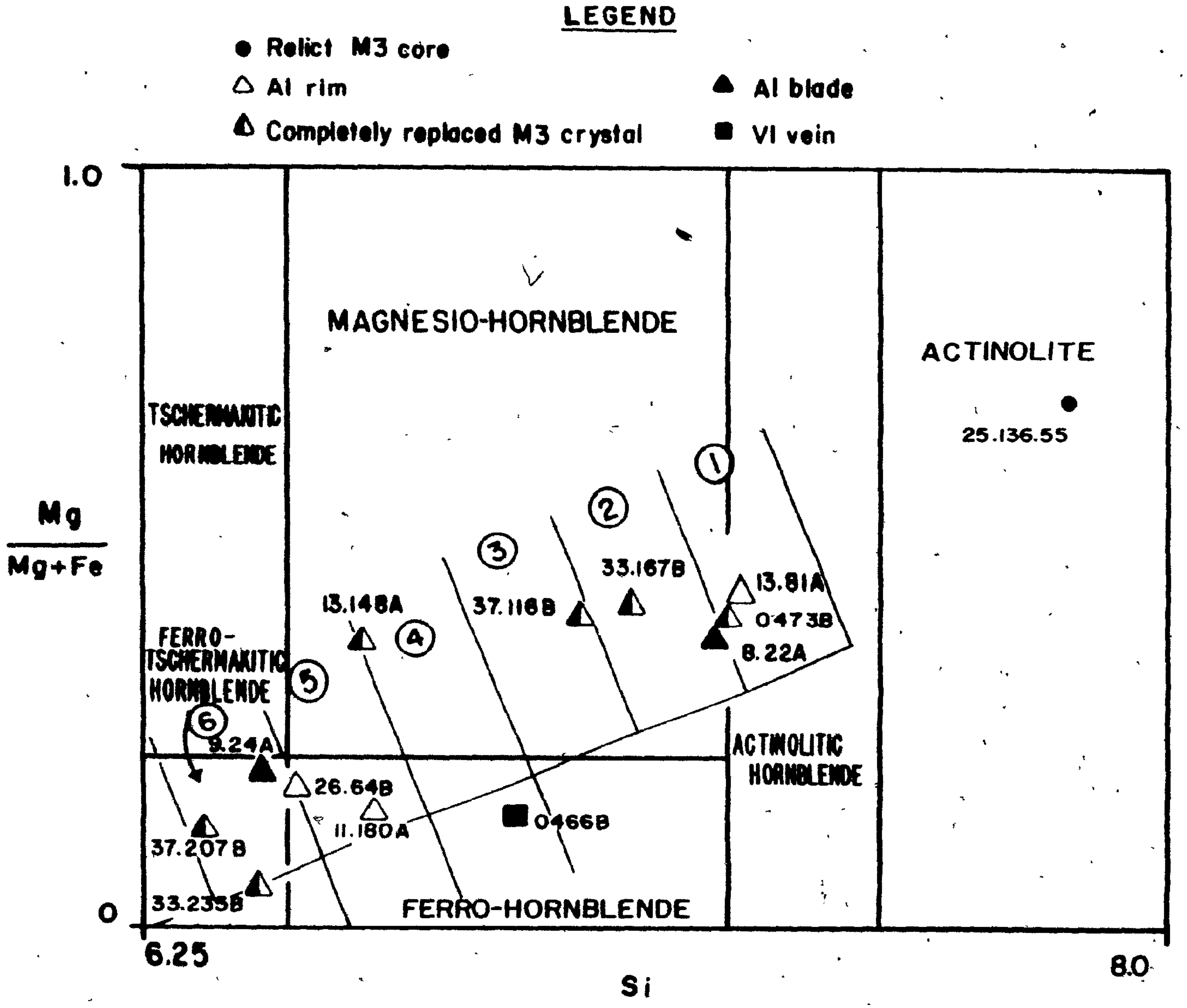
LEGEND
● Relict M3 core
△ Al rim
▲ Al blade
Completely replaced M3 crystal
■ VI vein
1.0
0
Mg / Mg+Fe
6.25
8.0
Si
MAGNESIO-HORNBLENDE
ACTINOLITE
TSCHERMAKITIC HORNBLENDE
FERRO-TSCHERMAKITIC HORNBLENDE
ACTINOLITIC HORNBLENDE
FERRO-HORNBLENDE
25.136.55
①
②
③
④
⑤
⑥
33.167B
13.81A
0473B
8.22A
37.116B
13.148A
9.24A
26.64B
11.180A
0466B
37.207B
33.235B

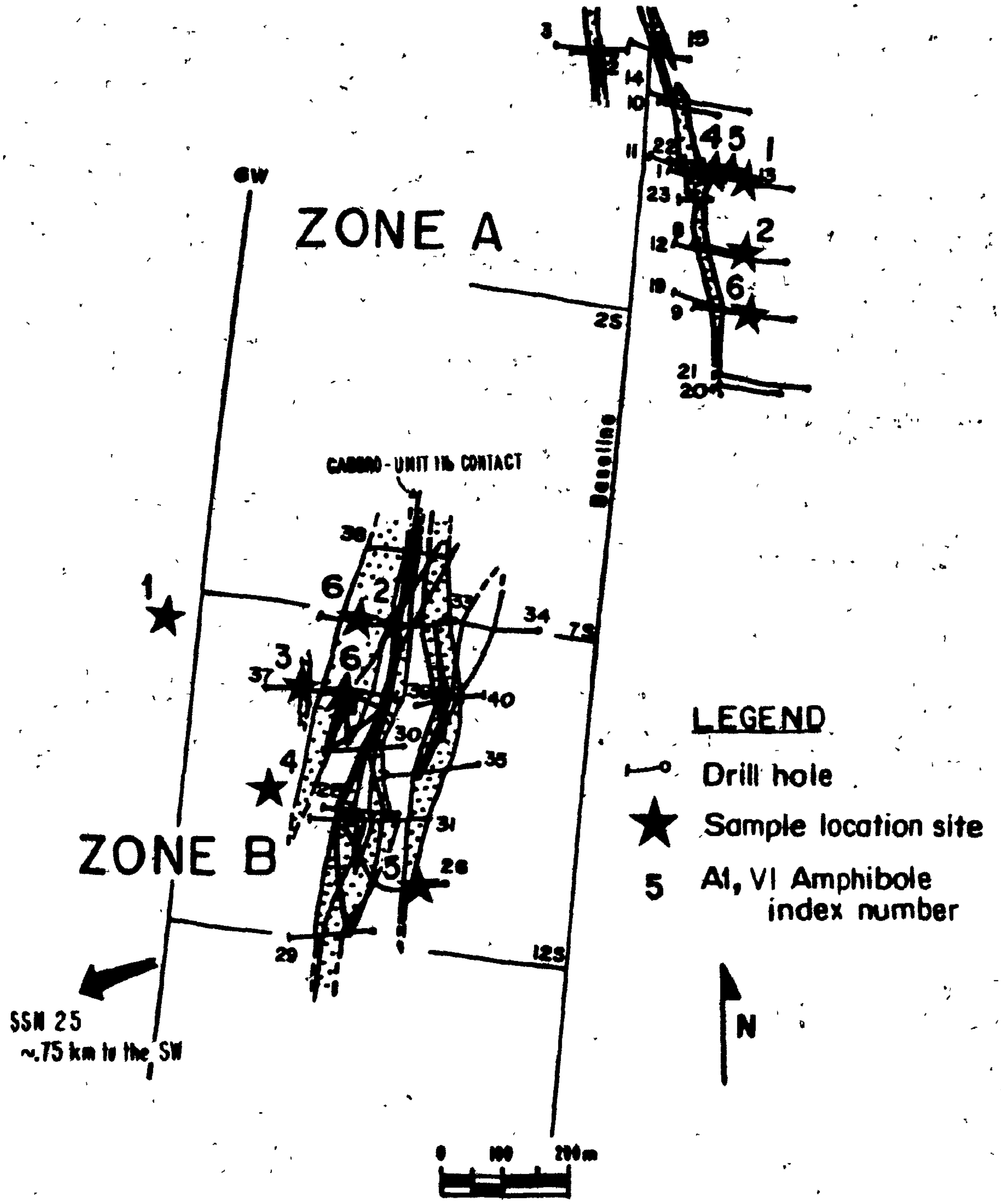

ZONE A
ZONE B
GW
Baseline
GABBRO - UNIT IIb CONTACT
25
75
125
3
15
14
10
11
22
1
23
8
12
19
9
21
20
13
4
5
1
2
6
38
33
34
37
39
40
30
35
28
31
26
29
1
6
2
3
6
4
5
SSN 25
~.75 km to the SW
LEGEND
Drill hole
Sample location site
5 Al, VI Amphibole index number
N
0
100
200m

most evolved Zone A sample occurs in drill hole SSN 9, furthest south and closest to Zone B. In addition, it appears that the most evolved Zone A analyses lie closest to the main VIV quartz stockwork, whereas the two furthest away are the least evolved.

5.2.3 COUPLED SUBSTITUTIONS

The alteration of actinolite to hornblende in Trend 1 and 2 amphiboles can be explained, in part, by two coupled substitutions represented by the actinolite-->tschermakite transition, where,

MgSi--> 2Al (Fig. 5.4) and,

the actinolite--> edenite transition, where,

Si--> NaAl (Fig. 5.5).

Together, the two, which can be written as,

MgSi --> NaAl3 (Fig. 5.6),

show that magnesium-silica depletion is associated with sodium and alumina enrichment.

In addition, Fig. 5.4 shows that the tschermakite trend is shallower, and hence less important, in Trend 2 versus Trend 1 amphiboles, which are distal to Zone B. In contrast, the edenite trend, defined by Trend 2 amphiboles, which are proximal to the mineralized zones, is steeper or more important than the one for Trend 1 amphiboles.

A cation plot of total Fe (TFe) versus TFe/TFe + Mg (Fig. 5.7) shows that Fe-enrichment accompanies the Mg-depletion in Trend 2 amphiboles, and also occurs to a lesser extent in Trend 1 amphiboles. Figure 5.7 also shows that the

Figure 5.4 Graphical depiction of Actinolite - Tschermakite transition where MgSi--> 2AlZ in amphiboles (a) in and near Zone A, and (b) Zone B. Trend 1 and 2 amphiboles are outlined in green and red, respectively (discussed in text). See Figure 5.1 for legend.

a

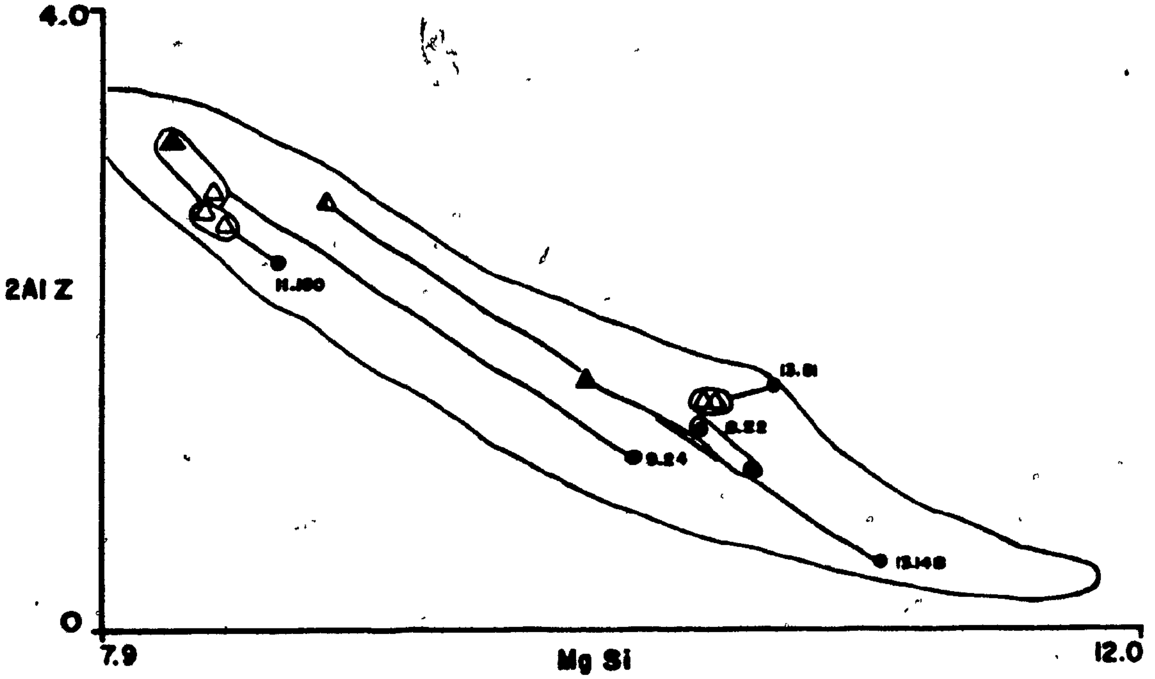
4.0
2Al Z
0
7.9
Mg Si
12.0
11.160
13.81
8.22
9.24
13.148

b

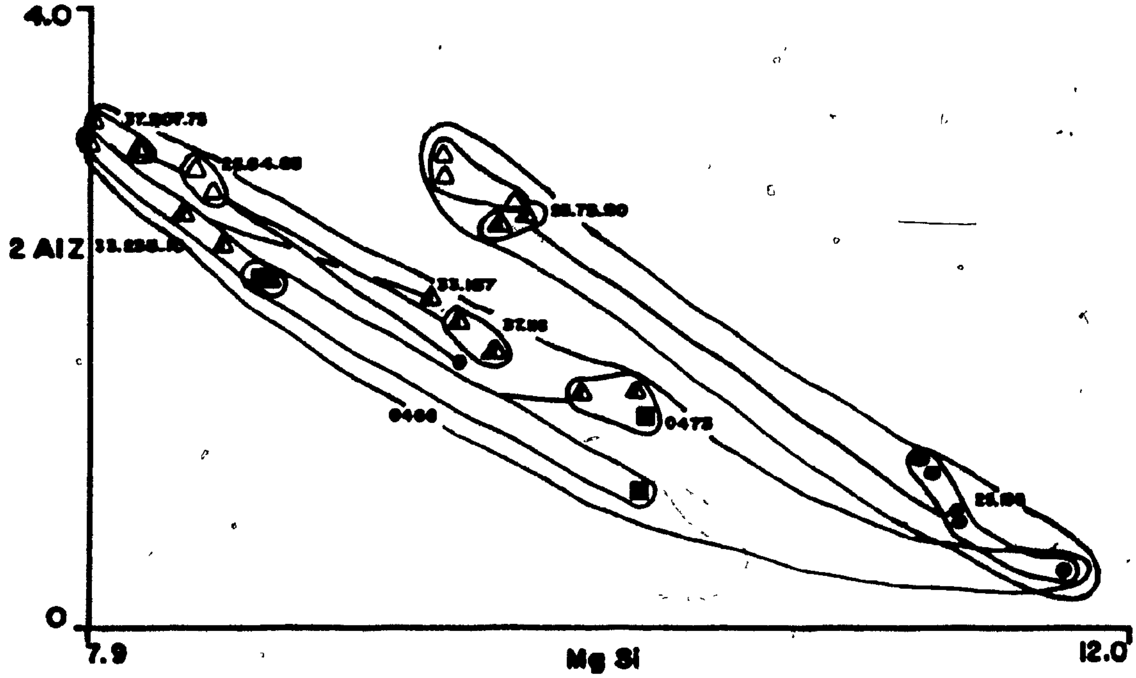
4.0
2 Al Z
0
7.9
Mg Si
12.0
37.207.75
25.64.65
33.226.10
33.157
37.16
25.73.90
0466
0475
25.196

Figure 5.5 Graphical depiction of Actinolite-Edenite transition, where, Si--> NaA AlZ in amphiboles (a) in and near Zone A, and (b) Zone B. Trend 1 and 2 amphiboles are outlined in green and red, respectively (discussed in text). See Figure 5.1 for legend.

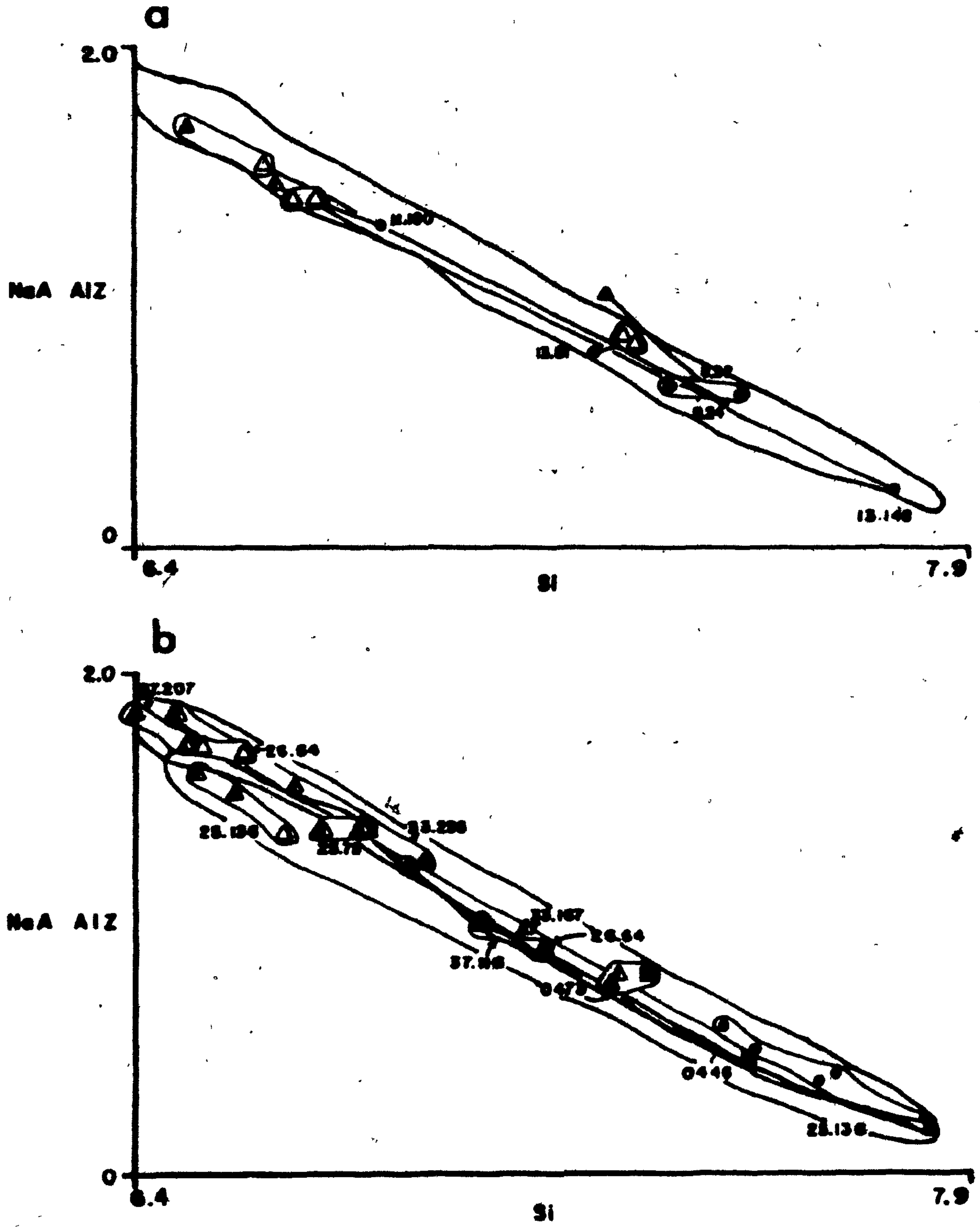
a
2.0
0
NaA AlZ
6.4
7.9
Si
11.190
13.81
8.32
8.24
13.146
b
2.0
0
NaA AlZ
6.4
7.9
Si
27.207
26.64
26.196
26.72
23.236
23.167
26.64
37.116
0473
0446
25.136

Figure 5.6 Graphical depiction of Actinolite-Tschermakite and Actinolite-Edenite transitions in amphiboles (a) in and near Zone A, and (b) Zone B. Trend 1 and 2 amphiboles are outlined in green and red, respectively (discussed in text). See Figure 5.1 for legend.

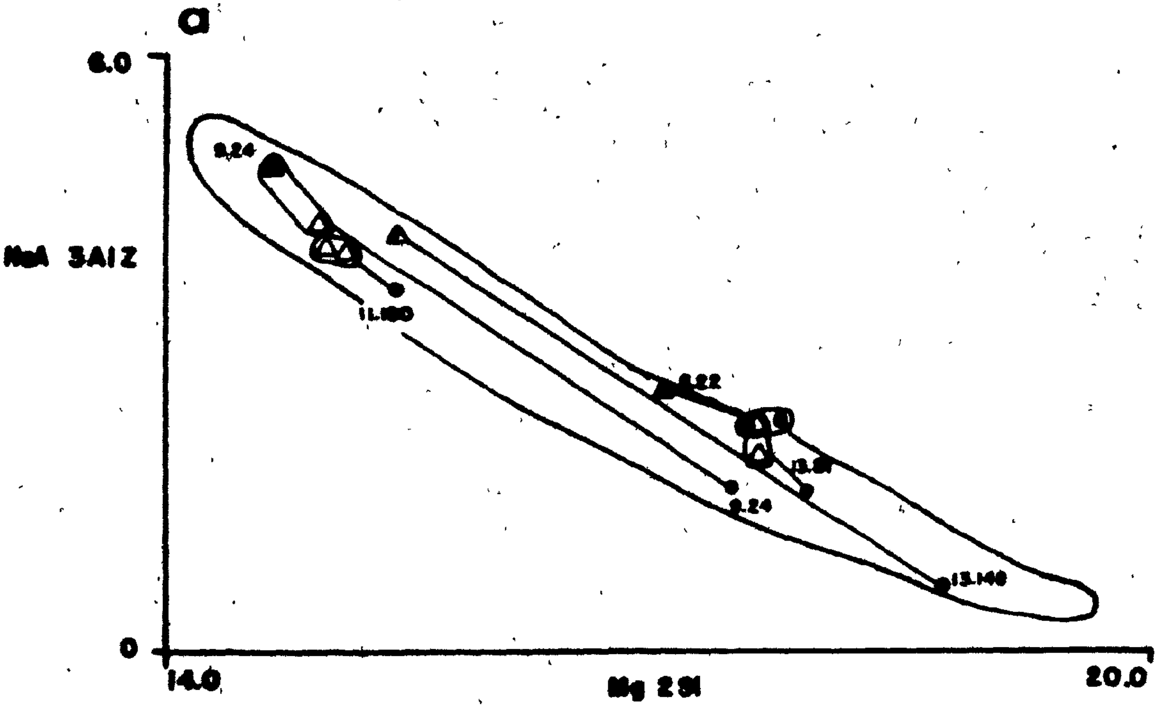
a
6.0
NaA 3AlZ
0
9.24
11.180
9.22
13.61
9.24
13.146
14.0
Mg 2Si
20.0

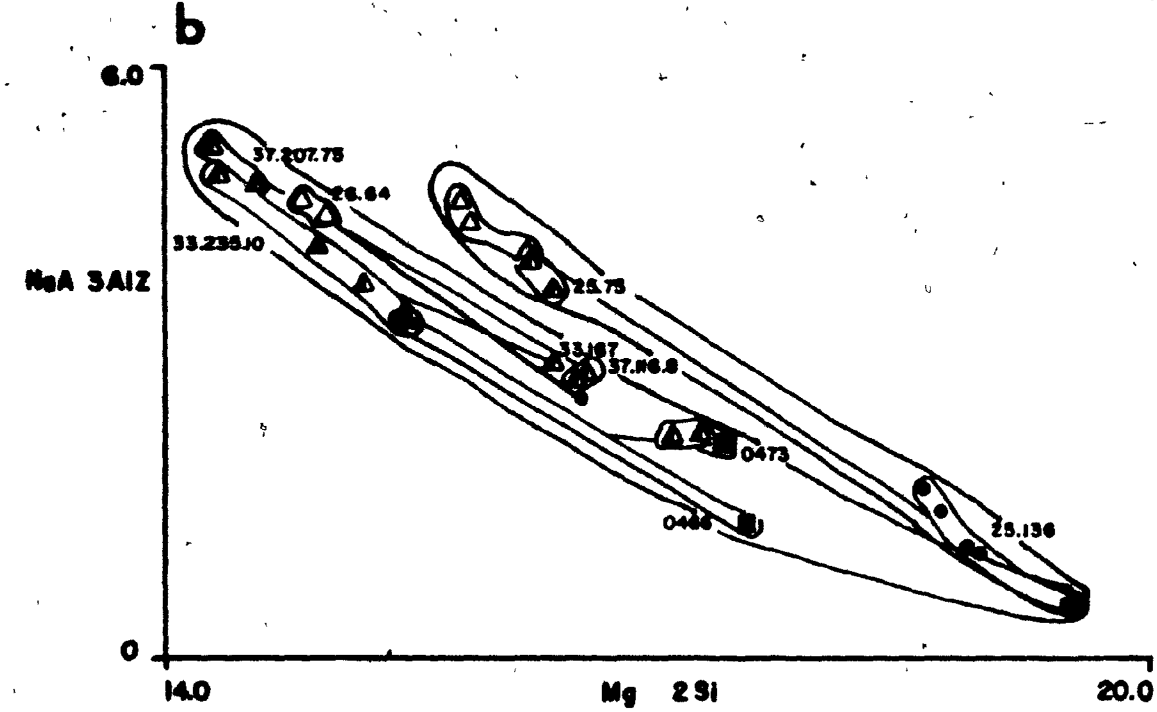
b
6.0
NaA 3AlZ
0
37.207.75
26.64
33.235.10
25.75
33.167
37.116.8
0473
0466
25.136
14.0
Mg 2Si
20.0

Figure 5.7 Cation plot of total Fe versus Fe/Fe + Mg, or XFe) in amphiboles from (a) Zone A, and (b) Zone B. See Figure 5.1 for legend.

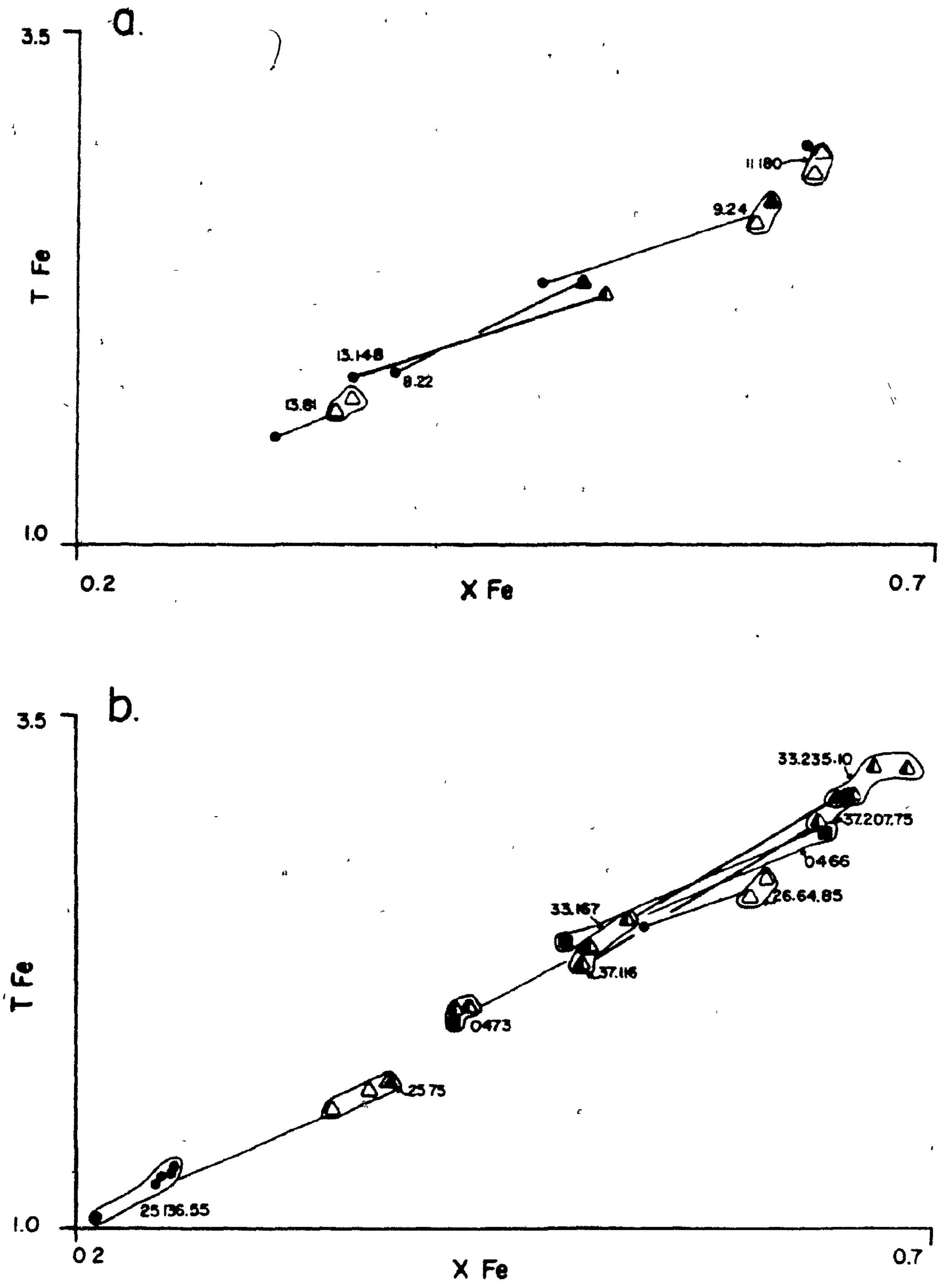
a.
3.5
T Fe
1.0
0.2
X Fe
0.7
11.180
9.24
13.148
8.22
13.81
b.
3.5
T Fe
1.0
0 2
X Fe
0.7
33.235.10
37.207.75
0466
26.64.85
33.167
37.116
0473
25 75
25 136.55

amphiboles in Zone A underwent less Fe-enrichment than those in Zone B.

A plot of K versus K + Na (Fig. 5.8) shows that the Na-enrichment associated with the edenite transition, is accompanied by K-enrichment. The plot also shows that amphiboles in Zone B are considerably more alkali-enriched than those in Zone A and that alkali enrichment occurs congruently with trends outlined by other variation diagrams, i.e., rim compositions are more evolved than cores, analyses close to Zone B are more evolved than those further away, etc.

5.2.4 SUMMARY AND CONCLUSIONS

All variation diagrams exhibit similar core-rim, alteration trends, and show that Trend 2 amphiboles in Zones A and B, start at roughly the same point of origin, and have approximately the same slope. In addition, the diagrams show that Zone A analyses outline slightly less evolved patterns than Trend 2 amphiboles in Zone B. The most striking example of this is seen in Figure 5.8 in which Zone A amphiboles are substantially less alkali-enriched than those in Zone B. The more evolved nature of Zone B amphiboles may indicate that Zone B underwent more intense alteration, and was closer to the fluid source.

5.3 VII, VIII, and A2 BIOTITE

Two different types of hydrothermal biotite are recognized in the map area and discussed in detail in chapters 2 and 3. Brown, M3 biotite occurs as fine grained

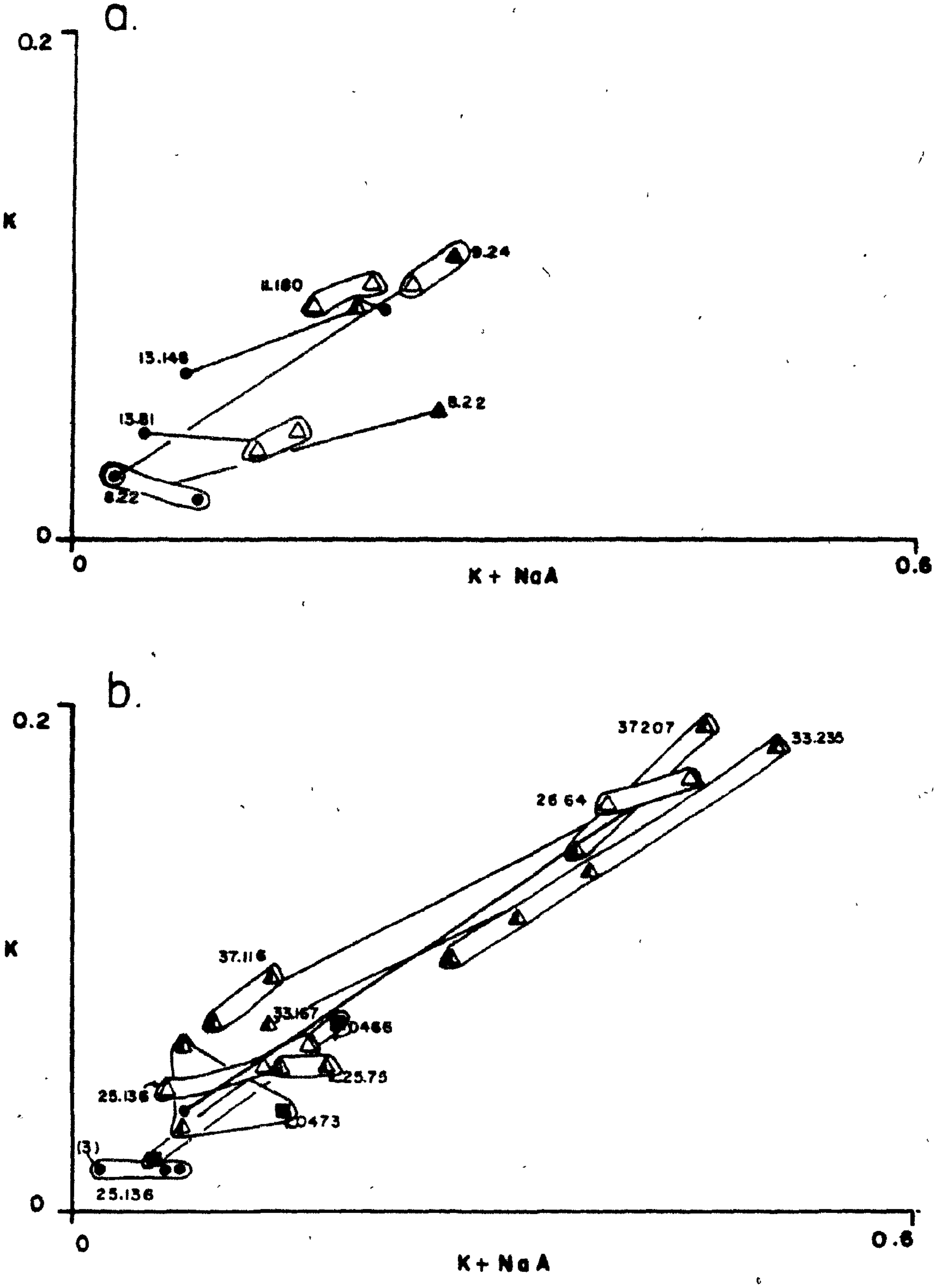
a.
0.2
K
0
0
K + NaA
0.6
9.24
11.180
13.148
13.81
8.22
8.22
b.
0.2
K
0
0
K+ NaA
0.6
37207
33.235
26 64
37.116
33.167
0466
25.75
25.136
0473
(3)
25.136

pervasive alteration and coarse grained clots as well as alteration envelopes about leucogranite dykes in gabbro and is believed to be related to intrusion of the leuco- granite (Chap. 2). The biotite has brown or olive green to yellow pleochroism and characteristically occurs with sphene at the expense of M3 amphibole.

A2 alteration biotite has reddish-brown pleochroism and typically contains zircons and associated radiation burns (Chap. 4). A2 biotite occurs as VII and VIII vein haloes and pervasive alteration (Chap. 4), and is locally concentrated along S3 crenulation hingelines, indicating that it formed during the M4 event (Chap. 2). The biotite is more abundant in Zone B where it is associated with locally intense K-feldspar replacement of felsic units. In addition, it typically occurs with manganiferous ilmenite (Mn-ilmenite) where it replaces amphibole.

Red-brown biotite, compositionally similar to A2 biotite, occurs within VII and VIII veins. The concentration of A2 biotite along S3 hingelines (Chap. 4) and all vein sets along the S3 surface (Chap. 3), as well as the similar compositions of VII and VIII vein, associated A2 vein halo, and pervasive A2 biotites suggests that the veins and alteration are co-genetic and co-eval with the S3 surface.

5.3.1 BIOTITE CLASSIFICATION

A microprobe study was conducted on A2 alteration, and VII and VIII vein biotites in 5 gabbro samples, 9 FGA units, 7 Unit IIb metavolcano-sediment samples, an A2-altered amphibole vein in gabbro, and biotite phenocrysts in the FQB porphyry (Figs. 5.9 and 5.10). In addition, brown, M3 biotite was analyzed in a gabbro sample distal to Zone B (25.75.50).

To facilitate discussion of biotite chemistry, the analyses are divided into gabbro, FGA, and sedimentary types and subdivided into two groups: 1) Analyses from pervasively altered rocks (Fig. 5.10 b,d,f) and, 2) VII or VIII veins and associated vein haloes (Fig. 5.10 c,e,g).

5.3.2 BIOTITE CHEMISTRY

The ranges in biotite compositions become more heterogeneous and more iron- and alumina- enriched from gabbro to FGA to sedimentary units (Fig. 5.10a). The different ranges in biotite compositions from the different rock types may partly reflect primary differences in host rock chemistry. For example, sediments are generally alumina-rich and heterogeneous in nature, which may explain why analyses from the metavolcano-sediments have the largest compositional field and are Al-rich.

In contrast, biotites from gabbro are Al-poor, and on the Fe-Mg-Al cation plot (Fig. 5.10), occupy the smallest compositional field. The low Al content and relatively homogenous chemistry may reflect the primary homogeneous and high temperature (relatively Mg-rich) nature of the gabbro. Biotite in an A2-altered VI amphibole vein in gabbro (0473) has the same composition as gabbro sample, 33.178.36.

Analyses from FGA units generally fall in betweenthose

Figure 5.9 Location map of biotite analyses.

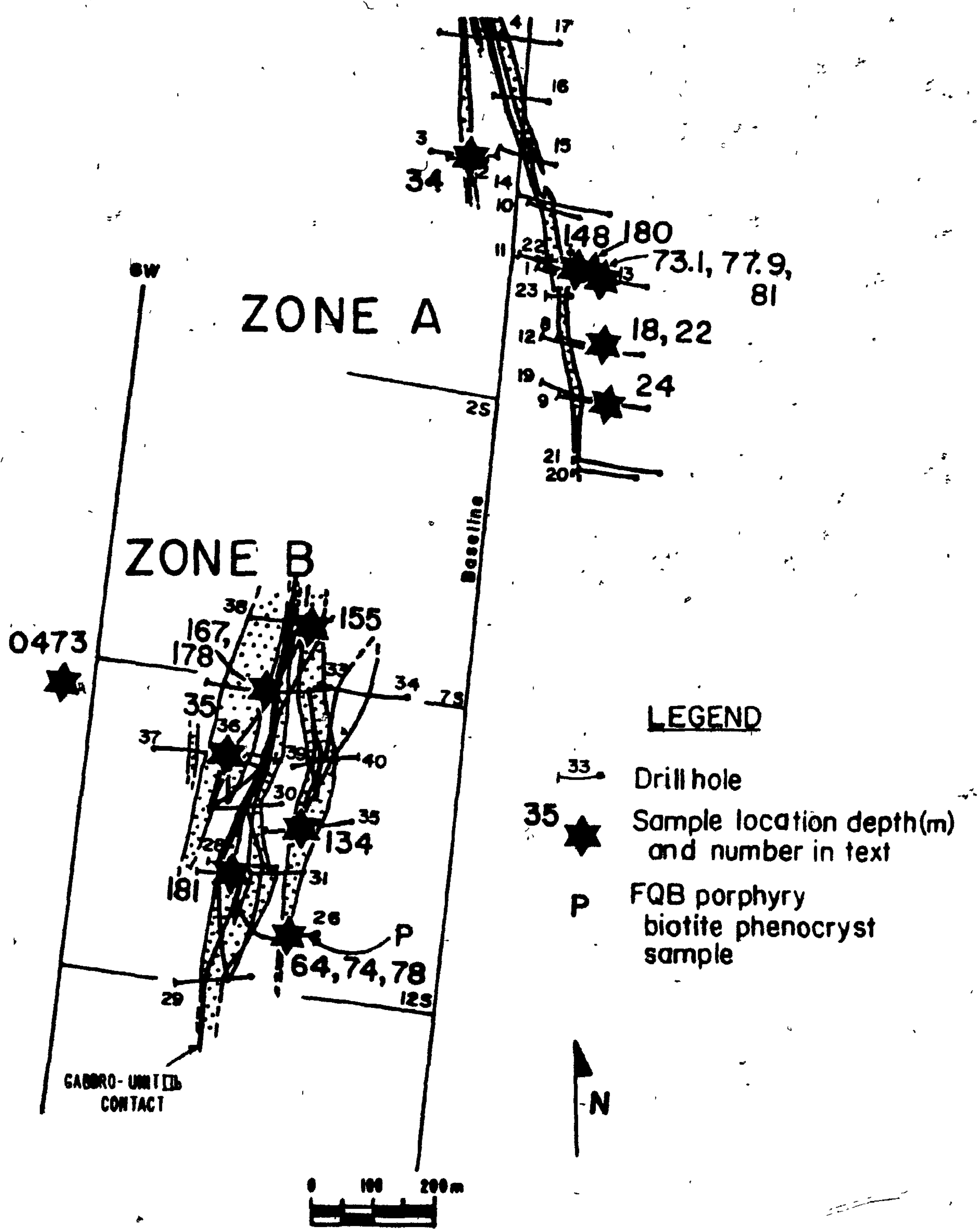
ZONE A
ZONE B
BW
Baseline
2S
7S
12S
34
148
180
73.1, 77.9, 81
18, 22
24
0473
167, 178
155
35
134
181
P
64, 74, 78
GABBRO-UNIT IIb CONTACT
0 100 200m
N
LEGEND
Drill hole
Sample location depth(m) and number in text
FQB porphyry biotite phenocryst sample

Figure 5.10 Al-Mg-Fe cation plots for biotite analyses. (a) Ranges of biotite from gabbro, FGA and metavolcano-sedimentary unit. (b-g) Ranges of each field are shown in detail. Left member of cation-plot pairs show subrange of samples which contain pervasive alteration. Right member shows subrange of biotites which were found in VII or VIII veins or vein haloes; Note: gabbro sample 25.75.50 comprises brown biotite from a leucogranite halo; "meta sediments" refers to all Unit IIb metavolcano-sediments exclusive of FGA units.

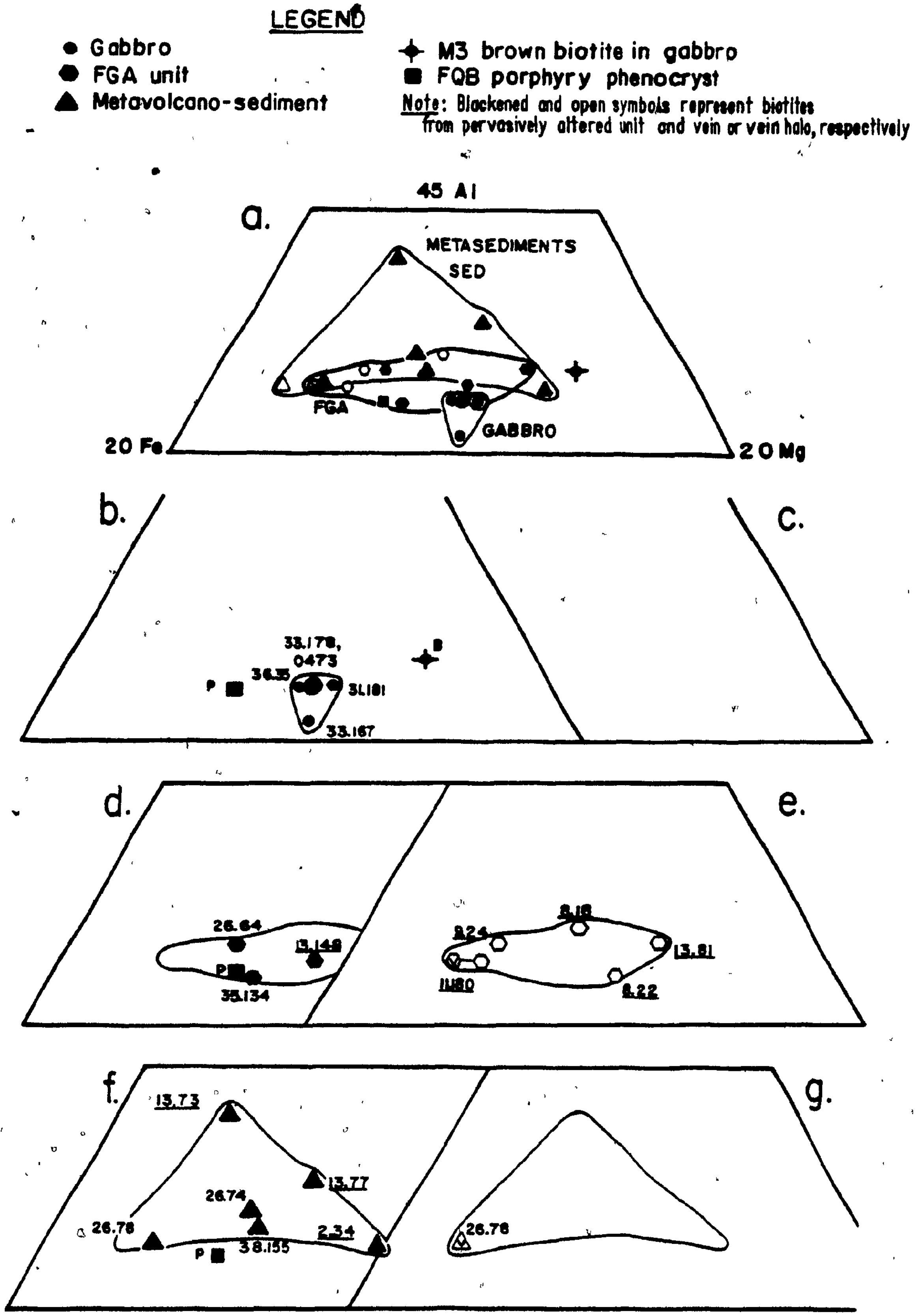
LEGEND
● Gabbro
⬢ FGA unit
▲ Metavolcano-sediment
✦ M3 brown biotite in gabbro
■ FQB porphyry phenocryst
Note: Blackened and open symbols represent biotites from pervasively altered unit and vein or vein halo, respectively
a.
45 Al
METASEDIMENTS
SED
FGA
GABBRO
20 Fe
20 Mg
b.
c.
33.178,
0473
36.35
P
31.181
33.167
B
d.
e.
26.64
13.149
P
35.134
8.18
8.24
13.81
11.80
8.22
f.
g.
13.73
13.77
26.74
26.78
2.34
P
38.155
26.78

from gabbro and metavolcano-sedimentary units. The intermediate composition of the FGA units suggests that the FGA units are not as homogeneous as the gabbro nor as heterogeneous as the sediments.

The least evolved, or most Mg-rich of all A2 biotites is from a pervasively altered metavolcano-sedimentary sample in Zone A, 2.34 (Fig. 5.10a, f). The sample was collected furthest north in Zone A, and is distal to the main Zone A stockwork zone and Zone B (Fig. 5.9). Metavolcano-sedimentary samples, 13.77.9 and 13.73.10, collected further south in Zone A, are more Fe-rich, and those from Zone B, the most enriched. The most Fe-rich metavolcano-sedimentary analyses are from a pervasively A2-altered unit and VIII vein from a sample in drill hole SSN 26 (Fig. 5.10 f,g, sample 26.78). The VIII vein analysis is, in fact, the most Fe-rich or evolved of all biotite samples (Fig. 5.10 a,g).

Analyses from FGA-hosted veins or vein haloes in Zone A also appear to be generally more Fe-rich and have a larger range in Al contents than pervasively altered FGA units (Fig 5.10 d,e). (Note: No vein or vein haloes from Zone B were measured). The most and least evolved analyses from pervasively altered FGA units are from drill hole SSN 26 in Zone B, and drill hole SSN 13, one of the furthest north samples in Zone A, respectively (samples 26.64 and 13.148). With the exception of sample 11.180, vein and vein halo biotites from Zone A appear to show iron-enrichment southward (13.81.90 to 9.24). The one exception, sample 11.180, is the most iron-rich of all FGA samples, and was collected from greatest depth.

Hence, it appears that within the general range of A2 biotite compositions from FGA and metavolcano-sedimentary units, some systematic variations are present. Zone B biotite is generally more evolved than that of Zone A; biotite from the southern part of Zone A is generally more evolved than that to the north, and the most evolved biotites are in drill hole SSN 26, which contains the FQB porphyry. In addition, vein and vein halo biotites are generally more Fe-rich than those from pervasively altered units.

Brown M3 biotite and biotite phenocrysts from the FQB porphyry were also analyzed. The M3 biotite, collected from a biotite-sphene halo in gabbro about a leucogranite dykelet distal to Zone B, is Mg-rich and plots clearly outside all the main fields (Fig. 5.10a). In contrast, the red-brown biotite phenocrysts have compositions which are similar to the Fe-rich analyses from FGA units (Fig. 5.10d).

5.3.3 Kd BETWEEN A1 AMPHIBOLE and A2 and VEIN BIOTITES

Biotites and amphiboles both display Fe-enrichment southward across Zone A and into Zone. This may indicate that the hydrothermal amphiboles and biotites formed from Fe-rich fluids which emanated from the same source region. Alternatively, the iron-enrichment of the biotites may be due to reactions in which fluids from the same or other regions were buffered by the compositions of the amphiboles that the biotites replace.

Analyses of A1 amphiboles and A2 and vein biotites are

Figure 5.11 Al-Mg-Fe cation plots for all FGA and gabbro samples from which biotites and M3 and A1 amphiboles were measured. (a) biotites from VII and VIII vein haloes and pervasive A2 alteration in FGA units and, (b) from pervasively altered gabbro and M3 brown biotite sample.

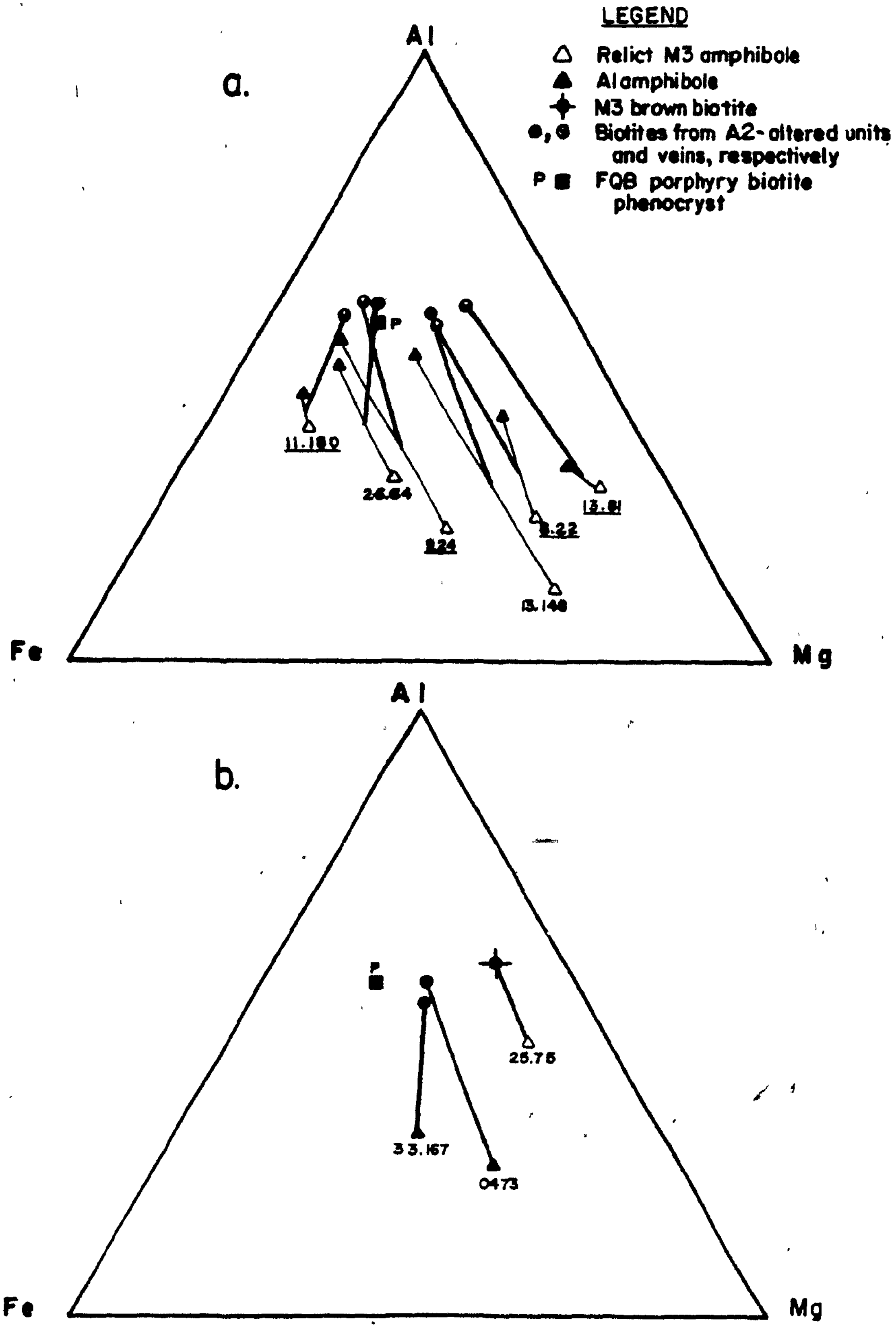
LEGEND
△ Relict M3 amphibole
▲ Al amphibole
✦ M3 brown biotite
●, ◐ Biotites from A2-altered units and veins, respectively
P ■ FQB porphyry biotite phenocryst
a.
Al
Fe
Mg
P
11.180
26.64
8.24
8.22
13.81
13.148
b.
Al
Fe
Mg
P
25.75
33.167
0473

compared in Figure 5.11. The slopes of the thick dark tie lines, which connect amphibole and biotite analyses from the same sample, change progressively from steeply negative in the right-hand-side of the diagram (Mg-rich), to steeply positive in the left-hand-side (Fe-rich).

The tie line rotation shows that biotites replacing relatively Mg-rich A1 amphiboles, have higher Fe/Mg ratios than those that replace Fe-rich A1 amphiboles. The tie line rotation suggests that although Fe to Mg ratios in A2 biotites generally reflect those of the amphiboles, the ratios are also partly independent of amphibole compositions.

This is also seen by the generally linear relationship between Fe/Fe + Mg ratio in the biotites and M3 and A1 amphiboles on a plot of XFe (A1 Amph) versus XFe (A2 Bi; Fig. 5.12). The slope of the line or Kd is less than 1 (.54), suggesting that the biotite-producing reactions were partly buffered by the fluid to lower XFe.

The slopes of the tie lines change from negative to positive about a point close to biotite phenocryst compositions in the FQB porphyry in drill hole SSN 26 (Fig. 5.11). This may indicate that the porphyry and altering fluids were the same.

5.4 A2 Mn-ILMENITE

A2 biotite is characteristically associated with manganiferous ilmenite (Mn-ilmenite) where it replaces amphibole. Minor Mn-ilmenite was also found in some

Figure 5.12 XFe in A2 biotite vs. XFe in relict M3 and A1 amphiboles, where XFe = Total Fe/ Total Fe + Mg. All amphiboles are from Trend 2, except sample 25.75 (see Fig. 5.1)

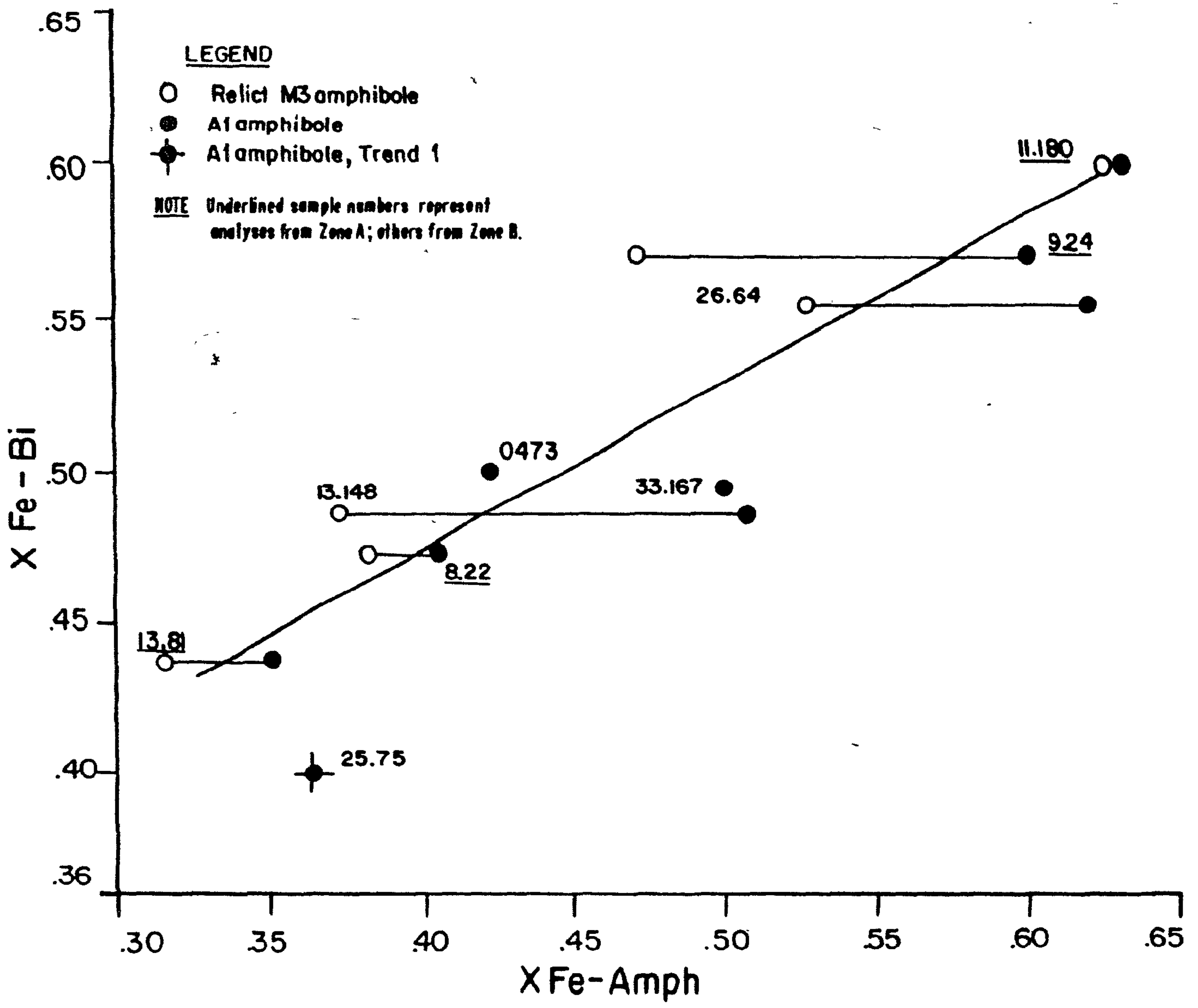
LEGEND
○ Relict M3 amphibole
● A1 amphibole
● A1 amphibole, Trend 1
NOTE Underlined sample numbers represent analyses from Zone A; others from Zone B.
11.180
9.24
26.64
0473
33.167
13.148
8.22
13.81
25.75
.65
.60
.55
.50
.45
.40
.36
X Fe - Bi
.30
.35
.40
.45
.50
.55
.60
.65
X Fe-Amph

pervasively A2-altered metasediments. The Mn-ilmenite, in thin section, has a metallic lustre and tan to brown and pale blue anisotropy under reflected light. A Mn-Fe-Ti plot shows that the compositions of the ilmenites in Zone A and B are essentially the same, and have a very small compositional range (Fig. 5.13). This implies that the fluids which produced them had similar compositions.

5.5 A1, A2 FELDSPAR CHEMISTRY

Plagioclase alteration appears to be less pervasive than amphibole or biotite alteration in the same drill hole. For example, one plagioclase-bearing sample from a drill hole which contains abundant amphibole and A2 biotite, is well-zoned and relatively unaltered (Figs. 5.14, 5.15, sample 33.178). In addition, A1 and A2 plagioclase alteration is similar and hence, difficult to discriminate in rocks which contain abundant A1 and A2 alteration.

In general, however, A1 alteration of plagioclase is not as intense as A2 alteration of plagioclase and comprises partially albitized plagioclase and minor K-feldspar alteration (observed in a minor number of stained sections, only; Chap. 4). In contrast, A2 feldspar alteration, appears to be more intense and pervasive, and consists mostly of K-feldspar alteration and minor albitized plagioclase.

Eleven unaltered and A1- and A2- altered plagioclase-bearing samples were analyzed to determine the general range of albitzation (Figs. 5.14, Fig. 5.15).

Figure 5.13 Compositional range of Mn-ilmenites in Zones A and B.

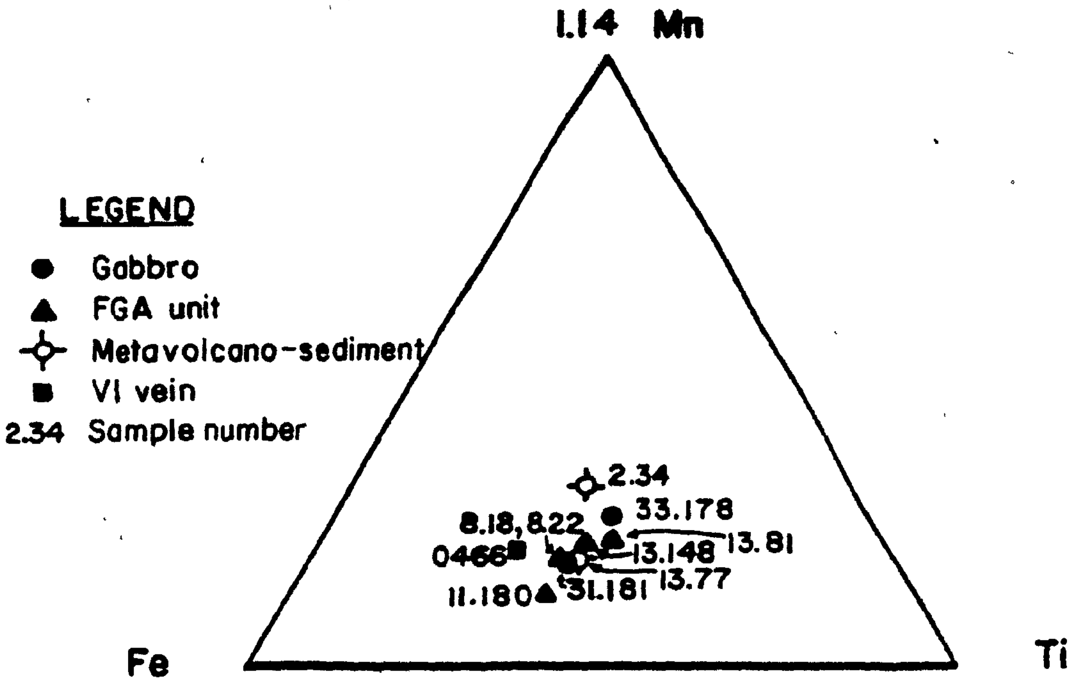
1.14 Mn
Fe
Ti
LEGEND
● Gabbro
▲ FGA unit
-◇- Metavolcano-sediment
■ VI vein
2.34 Sample number
2.34
33.178
8.18, 8.22
0466
13.81
13.148
13.77
11.180
31.181

Figure 5.14 Plan view of Zones A and B showing An contents and location of plagioclase samples.

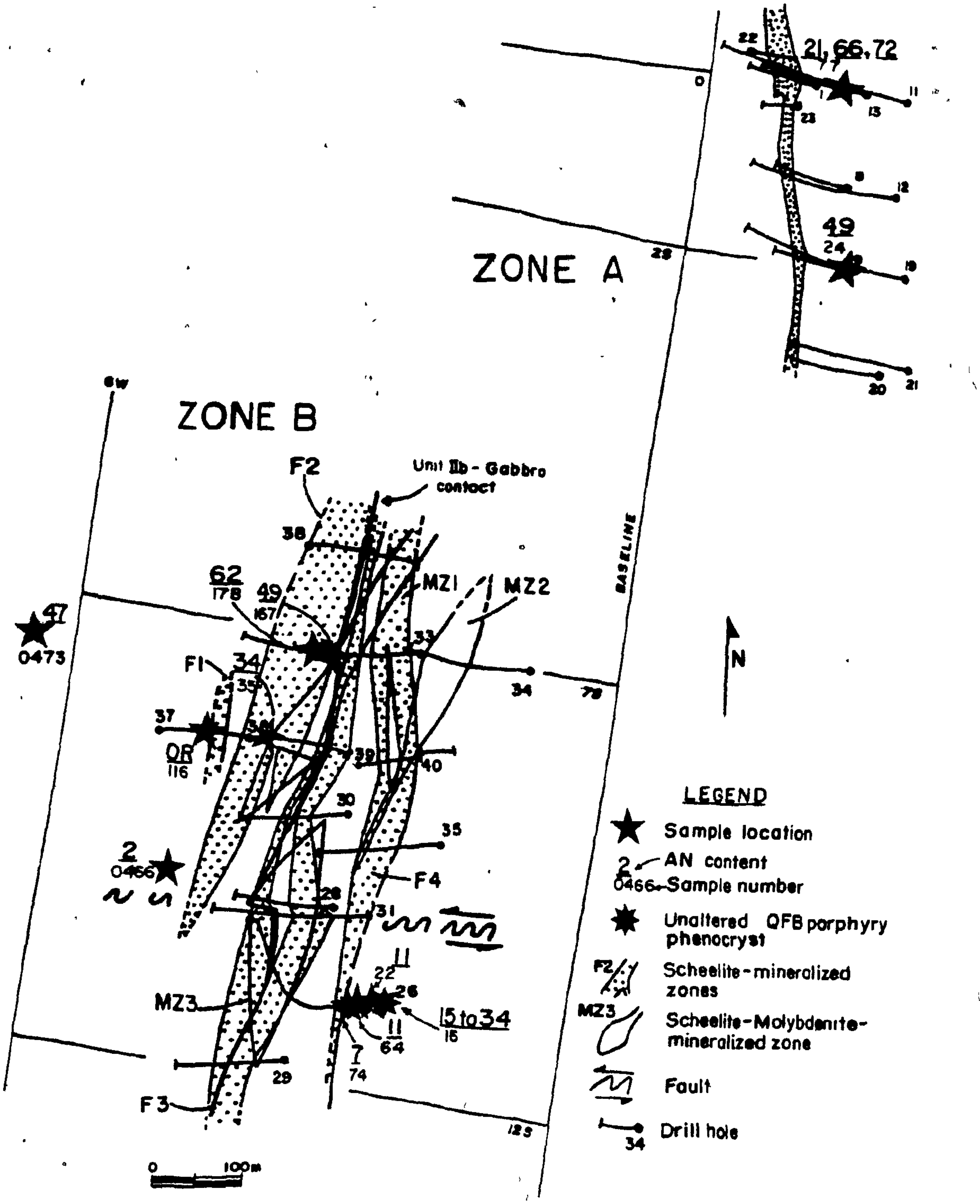
ZONE A
21,66,72
49
24
ZONE B
F2
Unit IIb - Gabbro contact
62
178
49
167
MZ1
MZ2
47
0473
F1
34
35
37
0R
116
33
34
39
40
30
35
2
0466
F4
28
31
MZ3
22
11
26
15 to 34
16
11
64
7
74
29
F3
BASELINE
N
0
100m
LEGEND
Sample location
2 AN content
0466 Sample number
Unaltered QFB porphyry phenocryst
F2 Scheelite-mineralized zones
MZ3 Scheelite-Molybdenite-mineralized zone
Fault
34 Drill hole

Figure 5.15 AB-AN-OR plots of plagioclase in A1- and A2 altered rocks, pristine M3 plagioclase in gabbro and a primary plagioclase phenocryst in the FQB porphyry.

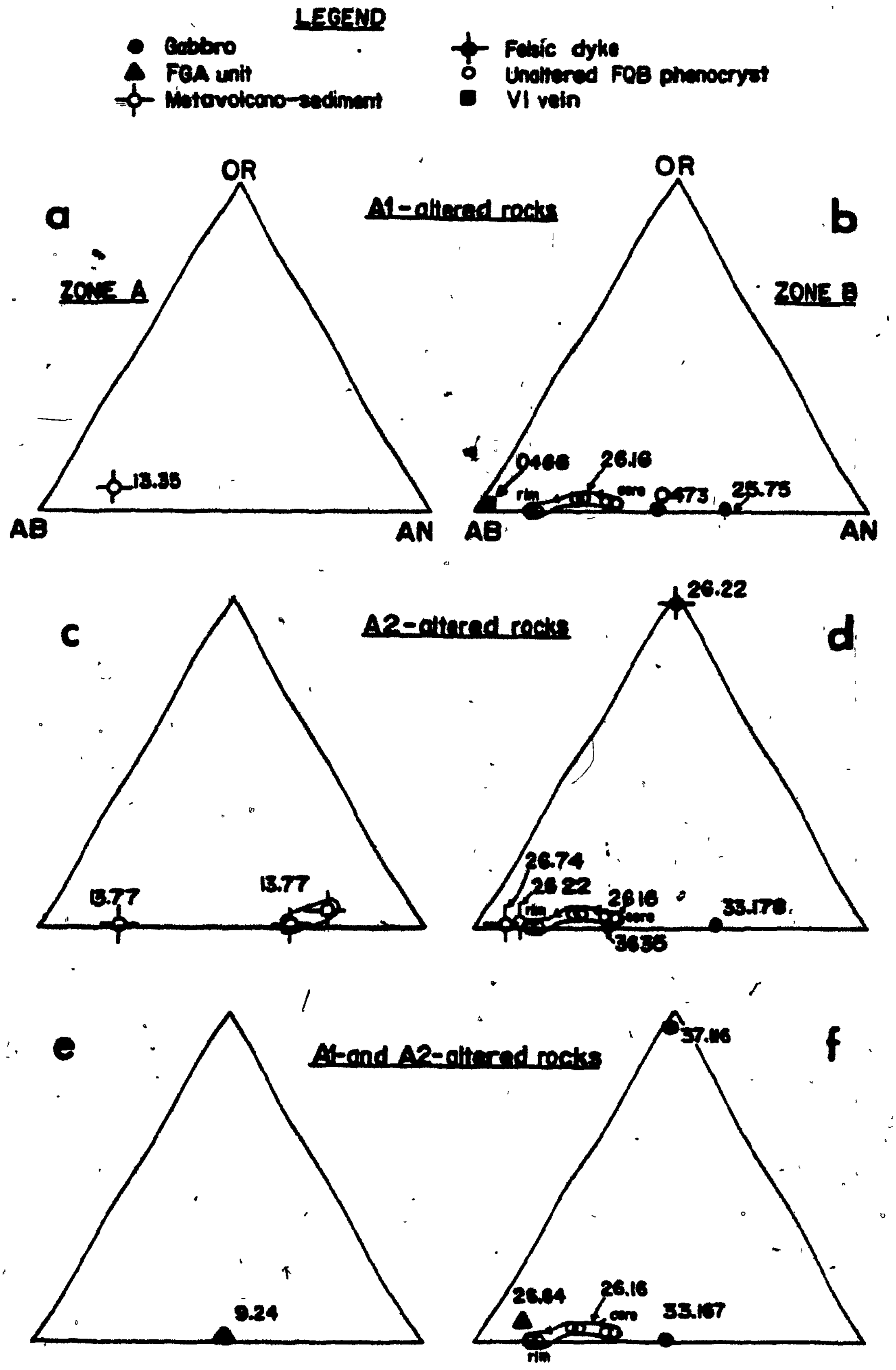
LEGEND
● Gabbro
▲ FGA unit
Metavolcano-sediment
Felsic dyke
○ Unaltered FQB phenocryst
■ VI vein
a
b
A1-altered rocks
ZONE A
ZONE B
OR
AB
AN
13.35
0466
26.16
rim
core
0473
25.75
c
d
A2-altered rocks
26.22
13.77
13.77
26.74
26.22
26.16
33.178
3635
e
f
A1-and A2-altered rocks
37.116
9.24
26.84
26.16
core
33.167
rim

5.5.1 A1-ALTERED ROCKS

Relatively unaltered plagioclase of composition An 64, was found in gabbro sample 25.75, collected about 750m southwest of Zone B. This contrasts with the moderately A1-albitized plagioclase in gabbro sample 0473, ~200m west of Zone B, which measures An 47. One A1-altered metavolcano-sedimentary sample from Zone A (13.35) was also studied and found to contain moderate to highly albitized plagioclase of An 21*. The albitizing nature of the fluids is perhaps most evident by the presence of relatively pure albite (An2) in a gabbro-hosted VI vein just west of Zone B (sample 0466).

5.5.2 A2-ALTERED ROCKS

Several plagioclase crystals from samples containing mainly A2 alteration were also measured and found to contain mostly K-feldspar and minor albite alteration. However, the two Zone B gabbro samples, both from scheelite-mineralized zone F2 (Fig. 5.14), show inconsistent amounts of albitization. Plagioclase from sample 33.178 has an An content of 62, whereas that from sample 36.35 measures An34.

In Zone A, a wide range of An contents was found in the one measured sample, 13.77. Plagioclase in a highly biotitized metasedimentary band, for example, ranges from An 66 to 72, whereas in the plagioclase lapilli-rich band, it measures An 21.

* The peristerite gap is believed to exist between An 0 and 25 (Smith, 1983). The so-called albitized plagioclase may therefore represent very fine scale albite replacement of plagioclase that was not resolvable on the microprobe or with a microscope (ibid., pp. 233-234 for further reference and discussion of the peristerite gap).

The most altered samples from both zones are from Zone B felsic dykes in drill hole SSN 26, which have An contents of 11 (sample 26.22) and 7 (sample 26.74). In addition, felsic dyke sample, 26.22 contains K-feldspar (Fig. 5.15a). A relatively high level of albitization in the plagioclase-rich felsic units is also evident in Zone A where the most highly albitized plagioclase is from a plagioclase lapilli-rich metavolcano-sedimentary unit (above). This may indicate that the plagioclase alteration was somewhat host rock dependent.

5.5.3 A1- and A2- ALTERED ROCKS

Plagioclase in five A1- and A2- altered samples were analyzed (Fig. 5.15e,f). The most sodic plagioclase is from an FGA unit (sample 26.64, An 11; Fig. 5.14) in drill hole SSN 26 in Zone B. The FGA sample from Zone A (9.24) is less altered and measures An 49. Gabbro sample 33.167, from scheelite-mineralized zone F2, is also less albitized and measures An 49. One K-feldspar altered gabbro sample was measured from Zone B (sample 37.116). The practical lack of K-feldspar in A1-altered rocks suggests that it formed during A2 alteration.

5.5.4 FQB PORPHYRY PHENOCRYSTS

Unaltered primary plagioclase phenocrysts from FQB porphyry in drill hole SSN 26 (Zone B) were analyzed and found to have An contents between 34, near phenocryst cores, and 15 at phenocryst rims (sample 26.16). The rim compositions are similar to the most albitized plagioclase analyses which, excluding vein sample 0466, are also from drill hole SSN 26 (Figs. 5.14, 5.15; 26.22, An 11; 26.64, An 11; and 26.74, An 7).

The similarities between altered plagioclase and phenocryst rim compositions suggest that the altering and porphyry fluids were the same. The similar compositions of A2 biotite and FQB porphyry biotite phenocrysts may imply further, that the porphyry was responsible for alteration and associated mineralization (see Chap 7).

5.6 SUMMARY

Amphiboles proximal to the mineralized zone define a Mg + Si depletion trend (Trend 2), whereas those distal to Zone B, define a Si-depletion trend, only (Trend 1; Fig. 5.1). The changes in amphibole composition into the mineralized zone are explained in terms of the tschermakite and edenite coupled substitutions (Figs. 5.4 to 5.6).

The edenite transition, which involved addition of Na (Fig. 5.5), is more important in amphiboles proximal (Trend 2), than in those distal (Trend 1) to, the mineralized zones. Conversely, the tschermakite substitution, which involved addition of Al (Fig. 5.5), is less important in Trend 2 versus Trend 1 amphiboles.

Addition of K is associated with that of Na (Fig. 5.8), and Fe-enrichment accompanied the Mg-depletion, associated with the tschermakite transition (Fig. 5.7).

All variation diagrams show that relict M3 cores are characteristically less altered than A1 rims. Some evidence suggests that A1 rims and blades, as well as A1 replacement and VI veins in the same sample, have identical compositions.

In addition, the diagrams show that amphiboles are possibly more evolved, southward across Zone A and into Zone B (Fig. 5.3), and that Zone A amphiboles are generally less evolved than those in Zone B. The latter is especially evident in the alkali-enrichment diagram (Fig. 5.8).

A2 biotite, which is red brown in thin section, is more Fe-rich than M3 biotite, which is brown in thin section. A2 biotite composition is apparently affected by that of the host rock in which it occurs, e.g., A2 biotites in metavolcano-sediments have the most heterogeneous compositions, whereas A2 biotite in gabbro is generally more Mg-rich, and has the most homogeneous chemistry.

The Fe-enrichment trend in FGA and metavolcano-sediments, appears to parallel that of A1 and VI amphiboles, but is in fact, partly independent of the amphibole composition, i.e., fluid buffered. This is evident by the Kd value of .54 between XFe-amph and AFe-A2 biot. Fluid buffering is perhaps also evident by the presence and relatively small and similar range in Mn-ilmenite compositions from both zones.

The most evolved biotite compositions are from drill hole SSN 26, which contains the largest amount of FQB porphyry. Biotite phenocrysts from the FQB porphyry fall within the range and near the most evolved of A2 biotites, suggesting that the porphyry and altering fluids were the same.

Feldspar alteration appears to be similar in Zones A and B, but less consistent than A1 amphibole or A2 biotite alteration. A1-altered feldspars are mostly albitized and appear to become more albitic into Zone B. Similar albitization occurs in A2-altered rocks, with the most albitic compositions from drill hole SSN 26. In addition, A2 altered rocks contain abundant K-feldspar alteration, whereas only a minor amount was observed in a few stained slabs of A1-altered rocks.

Primary FQB phenocrysts are progressively more albitic from the cores to rims. The rim compositions are similar to the most A1 and A2 albitized plagioclase samples (Fig. 5.15). This, as well as the similarity in compositions of A2 biotites and primary unaltered biotite phenocrysts in the FQB porphyry, may indicate that the porphyry and altering fluids were the same.

CHAPTER 6 FLUID INCLUSIONS

6.1 INTRODUCTION

A fluid inclusion study of vein sets VI through VIV was undertaken to examine the nature, evolution and genetic relationship of the mineralizing fluids in and between the two zones.

6.2 SAMPLE LOCATIONS

Sample collection was concentrated in drill holes SSN 13 and SSN 26 (Fig. 6.1). SSN 13 is the most heavily mineralized drill hole in Zone A. Drill hole 26, in Zone B, contains the largest intersection of FQB porphyry and the most complete overlap of VI and VII scheelite mineralization (F3) and VIII and VIV scheelite-molybdenite mineralization (MZ3; Chap. 3; Fig. 6.1).

A small number of fluid inclusion sections were made from material in drill holes 1, 3, 33, 36, and 37, within the main mineralized zones, as well as the main trenched area of Zone B (0466a and Q; Fig. 6.1). In addition, phase relationships in inclusions in quartz and scheelite in thin sections of VII veinlets from drill holes 2, 8, 9, and 13 were studied to supplement the fluid inclusion data obtained from those respective vein sets.

6.3 PRIMARY FLUID INCLUSION CLASSIFICATION, DESCRIPTION, AND IDENTIFICATION CRITERIA

A limited fluid inclusion study was conducted on quartz and y-scheelite from vein sets VI through VIV, and on amphibole from a VI amphibole vein and a VI-VII amphibole

Figure 6.1 Sample location map.

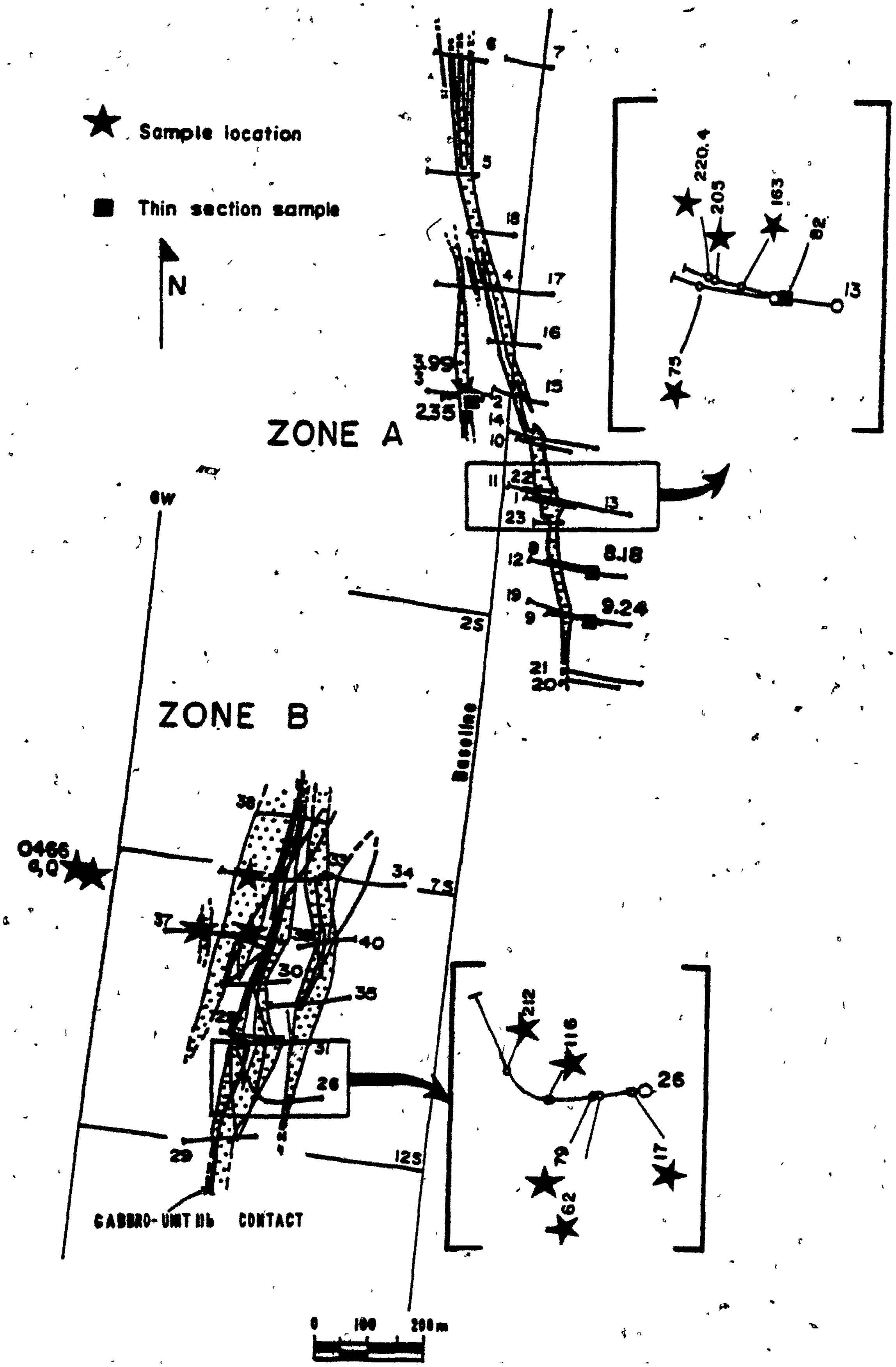
Sample location
Thin section sample
N
ZONE A
ZONE B
6W
Baseline
7
6
5
18
17
4
16
15
3.99
3
2.35
2
14
10
11
22
1
13
23
8
8.18
12
19
9
9.24
25
21
20
220.4
205
163
82
13
75
38
0466
4.0
34
75
37
40
30
35
31
26
29
125
212
116
26
70
17
62
GABBRO-UNIT IIb CONTACT
0
100
200 m

alteration halo.

Two major types of primary inclusions are recognized (Fig. 6.2). LV inclusions comprise liquid plus vapor phases which contain ~55 to 85% liquid; most however, contain 55 to 75% liquid. The second major type, LVS, comprises liquid, vapor, and one or more solid phases, and is subdivided into three types: (1) Type LVS-HA contains a cubic, non-birefringent, solid, and is relatively liquid-rich (Fig. 6.3e). During freezing, the cubic phase reacts with the liquid and forms a yellow birefringent hydrate. The cubic phase can therefore, not be sylvite, but is more likely halite, since sylvite does not form a hydrate, whereas halite does (Crawford, 1981). (2) Type LVS-B comprises vapor-rich and vapor-poor inclusions that contain 1 to 4, small, ~1 micron across, blue-birefringent, anhedral solids. (3) Type LVS-BHA contains both cubic and (1 to 3) blue phases (Fig.6.3d).

The blue phase does not dissolve upon cooling, and during heating, does not change size or shape prior to decrepitation. The apparent inability of the blue phase to dissolve prior to inclusion decrepitation, and the variable number of solids in any one inclusion suggests that the blue solid is a trapped phase.

Primary inclusions are larger and/or more isolated than secondary types. In some VIII and VIV quartz veins, an area 2 to 4 microns wide rimming blades or blebs of molybdenite, chalcopyrite, pyrrhotite and/or wolframite, contains isolated, primary, inclusions. Similar pockets of these

Figure 6.2 Major divisions and subdivision of primary inclusions.

LIQUID-VAPOR (LV)

Comprise >95% of primary inclusions

Variations in degree of filling

(a)

55 to 70 %

Most abundant type of fluid inclusion

(b)

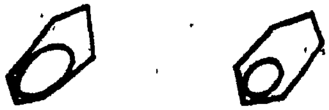

70 to 85 %

LIQUID - VAPOR - SOLID (LVS)

Comprise < 5% primary inclusions

(c)

LVS-HA **Halite-bearing**

(d)

LVS-B **Unidentified blue-solid, probably a trapped phase**

(e)

LVS-BHA **Halite- and blue-solid-bearing**

primary inclusions were also found in embayments or between blades of the aforementioned minerals, generally measuring <15 microns across.

Secondary inclusions, in contrast, are generally small, <1 to 5 microns across, liquid-rich, liquid-vapor inclusions. These are commonly distributed densely along numerous interconnected, parallel or isolated fracture planes.

Many LV and most LVS inclusions are also found along fracture planes. Some of the LV types are commonly elongate with the long axes oriented in the same direction within the plane of the fracture. The phase ratios of LV inclusions within the fractures are the same as isolated, apparently primary inclusions nearby. For this reason, they are considered to be pseudosecondary.

Many LVS inclusions within fractures, in contrast, do not have consistent phase ratios. The small percentage of LVS versus LV inclusions (<5% versus >95%, respectively; Fig. 6.2), and the predominance of LVS inclusions along fracture planes may indicate that LVS inclusions are secondary. The presence of some isolated halite-bearing inclusions along blades or blebs of mineralization, and alongside LV types with no apparent crosscutting relationships between them, however, makes it unclear whether LV and LVS inclusions are co-genetic or represent two separate fluid generations (see Section 6.8).

6.4 MORPHOLOGY AND DISTRIBUTION OF FLUID INCLUSIONS

Good primary inclusions were generally difficult to find and it was not possible to find representative material from several vein sets in both zones. For example, VI veins in Zone A were rare and too fine grained to study; no VI-VII veins were found in Zone A; VIII veins in Zone A drill core were uncommon and typically altered or broken up; most samples of VIV veins in Zone B contained mostly small secondary inclusions; and no primary inclusions were found in samples of VV carbonate.

Primary inclusions were most difficult to find in scheelite and amphibole. The softness of scheelite (H = 4.5-5) relative to quartz resulted, in most cases, in a highly scratched polished scheelite surface which effectively obscured inclusion observation. In addition, the high refractive index of scheelite resulted in abundant total internal reflection which made inclusion outlines and phase boundaries appear dark and thick. This was especially detractive in small inclusions where the outlines effectively merged, obscuring the interior. Scheelite-hosted inclusions which were suitable for study were <3 to 20 microns across, had thick, dark outlines, and irregular, anhedral shapes (Fig. 6.3a).

In amphibole, the dark green color commonly masks inclusion outlines and phase boundaries; very fine-grained samples contain no visible inclusions; and inclusions in coarse-grained samples are commonly disrupted by closely-spaced cleavage planes or are obscured by numerous minute opaque inclusions.

Coarse-grained amphibole samples containing widely-

Figure 6.3a-e LV inclusions in (a) VI scheelite (37.116), (b) VI amphibole (37.116) (c) VIII quartz (0466Q), an (d)LVS-BHA in VIII quartz (0466Q) and, (e) an LVS-HA inclusion in VIII quartz (0466Q). Note in (b) the well-defined cleavage surface along which one of the walls of the amphibole-hosted inclusion formed, as well as a lower cleavage surface which formed and resulted in leakage during heating.

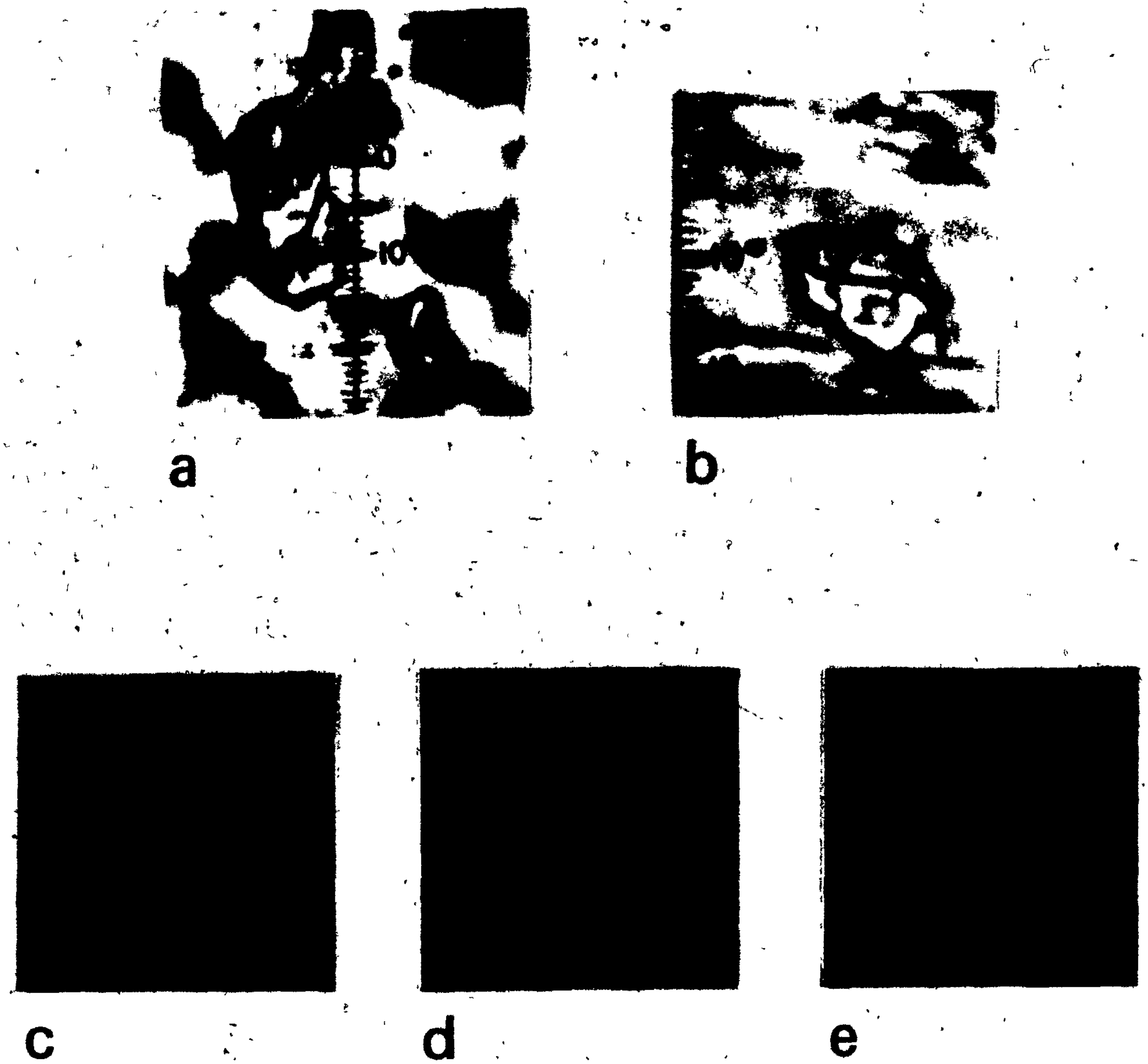
10
10
a
b
c
d
e

spaced cleavage planes proved the most suitable for fluid inclusion study. Most inclusions in these samples are large (10 to 20 microns across), irregularly-shaped, and oriented oblique to 010 or 001 cleavage surfaces. A minor number of small (5 to 10 microns), elongate inclusions, however, are oriented parallel to the cleavage planes. All of the larger, anhedral inclusions have highly variable liquid to vapor ratios, are interconnected and/or necked down. Both types, but especially the former, show evidence of leakage along cleavage planes.

Some of the inclusions oriented parallel to cleavage showed no evidence of leakage prior to study, but leaked during heating. Leakage occurred by microfracture development along 010 or 001 cleavage surfaces which grew into the inclusion cavity (Fig. 6.3b) or by the bending of cleavage planes and eventual disruption of the inclusion cavity.

Microfracture development and/or bending of cleavage surfaces during heating was commonly accompanied by brown discoloration. Barnes (1930 in Hawthorne, 1978, p.317) showed that during experimental heating of iron-bearing hornblende, much Fe^{2+} converts to Fe^{3+} with concomitant brown discoloration of the amphibole, and loss of water. Hence, the brown discoloration observed in this study probably represents similar oxidation.

Most suitable primary inclusions were found in quartz. The inclusions were relatively large (5 to 20 microns), abundant, and typically had clear, well-defined hexagonal outlines (Fig. 6.3c-e).

6.5 MINERAL- AND VEIN- SPECIFIC OCCURRENCES OF PRIMARY INCLUSIONS

All VI and VI-VII y-scheelite- and amphibole-hosted inclusions are LV types. LV inclusions also comprise most quartz-hosted inclusions in VI-VII through VIV veins. LVS inclusions were found only in quartz and mostly within vein sets VIII and VIV. One LVS inclusion was found in a VI-VII quartz vein and two were found in seven samples of VII quartz veinlets.

The absence of LVS inclusions in vein set VI, their rarity in vein sets VI-VII and VII, and their relative abundance in vein sets VIII and VIV suggests that influx of saline fluids may have increased with time.

6.6 LOW TEMPERATURE MICROTHERMOMETRY

Eutectic temperatures (Te) of LV inclusions range from -15° to -50° C with a mode at -25° to -30° C (Fig. 6.4a). Eutectic temperatures of halite-bearing inclusions, i.e., LVS-HA and LVS-BHA types are generally lower than LV types, and range from -32° to -74° C, with most values <-55°C (Fig. 6.4a). Freezing of LVS-HA and LVS-BHA inclusions typically resulted in dissolution of the cubic phase to form a hydrate phase. The blue phase in LVS-BHA or LVS-B inclusions, in contrast, did not change.

In most cases the hydrate phase melted between -60° and -70°C, forming numerous yellow, bleb-like, anhedral masses and larger pink, more coherent, interstitial masses of ice. The refractive indices of ice and hydrate could not be observed from relative Becke line movements due to poor

Figure 6.4 (a) Observed first melt temperatures for LV and LVS inclusions, and Tm-ice for halite-bearing LVS inclusions. (b) Salinity in eq.wt.% NaCl for LV and LVS inclusions. Salinity of LVS inclusions obtained from Th-Ha. All inclusions are quartz-hosted unless otherwise indicated.

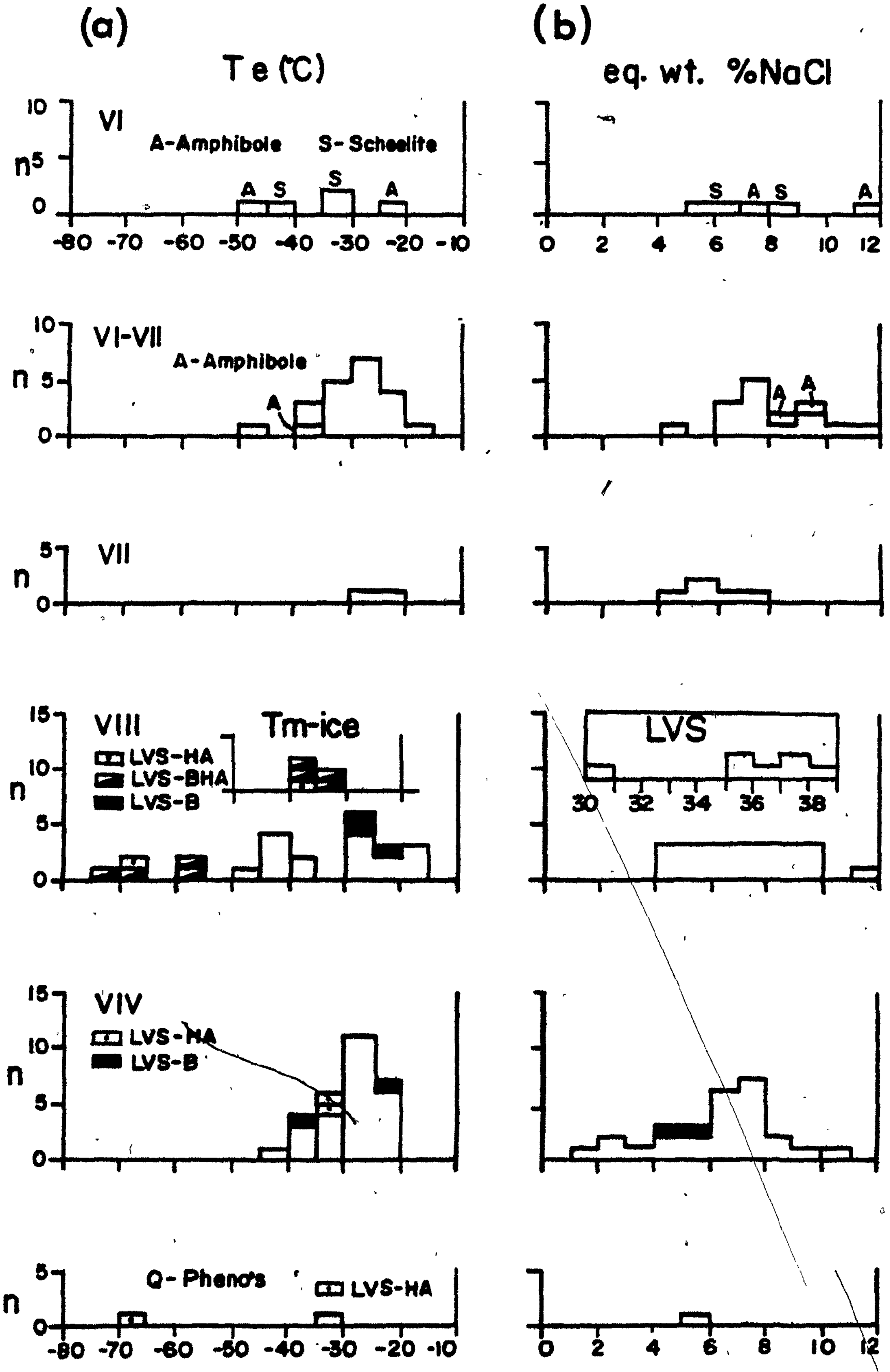
(a)
Te (°C)
(b)
eq. wt. %NaCl
VI
A-Amphibole
S-Scheelite
A
S
S
A
S
A
S
A
VI-VII
A-Amphibole
A
A
A
VII
VIII
Tm-ice
LVS-HA
LVS-BHA
LVS-B
LVS
30
32
34
36
38
VIV
LVS-HA
LVS-B
Q-Pheno's
LVS-HA
n
0
5
10
15
-80
-70
-60
-50
-40
-30
-20
-10
0
2
4
6
8
10
12

optical resolution. Outlines of ice fragments, however, appeared much darker than the outlines of anhedral hydrate blebs.

Continued heating and melting of the yellow hydrate in LVS inclusions was typically accompanied by growth of the cubic phase. In some cases a large, single cubic phase, present prior to a freezing run, recrystallized during heating to two or more smaller cubic solids.

The variation in Te probably reflects, in part, observational difficulties, as well as real chemical variations in the fluids. Observational difficulties include the dark color of amphibole, the high percentage of total internal reflection in scheelite, small inclusion size, inclusion orientation and/or shape (melting may begin in a part of the inclusion out of the view of the observer), and thickness and polish-quality of sectioned samples. In addition, the low amount of fluid generated at the eutectic of low salinity inclusions makes it more difficult to observe first melt in LV inclusions.

Last melt temperatures (Tm-ice) of vapor-rich LV and LVS-B inclusions range from -8° to -1.3°C, with a mode between ~-4° and -5° C. These temperatures correspond to salinity ranges of <2 to 12 and 6 to 8 eq.wt.% NaCl, respectively (Fig. 6.4b; Potter, et. al., 1978).

Last melt of ice in LVS-BHA and LVS-HA inclusions was observed in only four inclusions, all in sample 0466. The Tm-ice ranges from -38.5°C ± 3.5° to -30.5°C ± 2.5° (Fig. 6.4a). Melting of the hydrate, however, was not observed at temperatures <0°C, despite slow heating rates of 1°C per 3 to 4 minutes. The lowest temperature at which the hydrate was observed to melt was +8.8°C. In other inclusions, the hydrate melted after several hours at room temperature or at higher temperatures upon immediately beginning a heating run.

The high Tm of the hydrate implies that the hydrate comprises not only hydrohalite, but perhaps hydrohalite and/or a more complex hydrate such as NaCO3•10H20 (natron), which is stable at temperatures well above 0°C (Fig. 6.5). Heating of hydrohalite and natron, for example (Fig. 6.5, I), would result in melting of hydrohalite first (II; Fig. 6.5); natron would melt at temperatures up to ~20°C (III; Fig. 6.5). The two phases would probably be indistinguishable during melting because of similar refractive indices (hydrohalite, 1.42; natron, 1.41 to 1.44), and identical optical properties (both are monoclinic, hydrohalite is white and natron is colorless).

6.7 HOMOGENIZATION TEMPERATURES

LV inclusions homogenized by vapor disappearance and all LVS-HA inclusions, except one, homogenized by halite disappearance. The blue phase in LVS-B and LVS-BHA inclusions did not homogenize after vapor disappearance or prior to decrepitation, which generally occurred between 400° and 500° C. Homogenization temperatures (Th) of inclusions containing the blue solid were therefore, recorded at the disappearance of vapor (LVS-B) or halite (LVS-BHA).

LV and LVS-B inclusions homogenized between 80° and 385°

Figure 6.5 Phase diagram for part of the $NaCl$-Na_2CO_3-H_2O system showing a possible melting path for LVS inclusions. At the eutectic, E, (Point I) melting would begin. Melting may have continued along the indicated path to Point II, where hydrohalite and natron co-exist. Following complete disappearance of hydrobalite (II), natron would continue to melt up to ~20°C (Point III; modified after Samson, 1983).

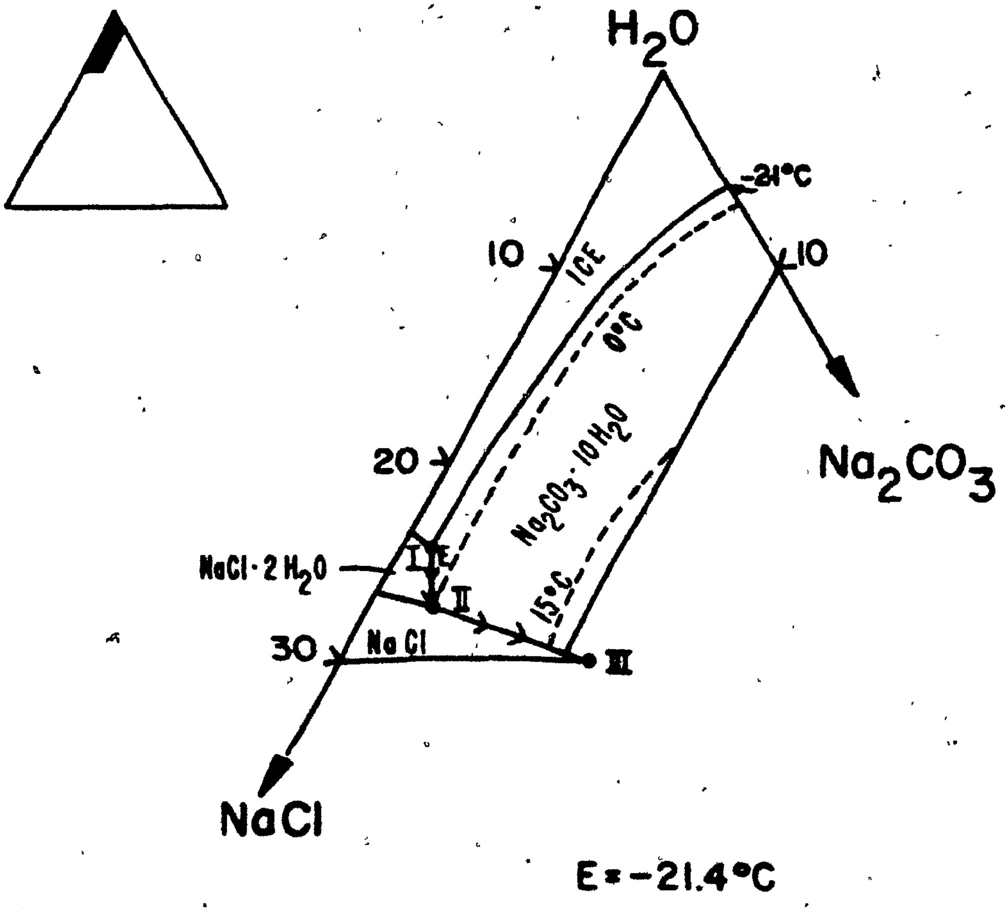
H$_2$O
-21°C
10
10
ICE
0°C
20
Na$_2$CO$_3$·10H$_2$O
Na$_2$CO$_3$
NaCl·2H$_2$O
I
E
II
15°C
30
NaCl
III
NaCl
E = -21.4°C

C, with modes for all vein sets lying between 300°and 380°C (Fig. 6.6). LV inclusions in vein sets VI through VII homogenized mostly between 310°and 340°C. Th of LV inclusions in vein set III are the highest of all vein sets and range mostly between 350°and 380°C. A smaller, slightly lower mode of Th of inclusions in VIV quartz veins and stockworks occurs between 330°and 350°C (Fig. 6.6).

Th of LV types suggests that temperatures increased from ~300°to 340°C to 350°to 380°C during formation of vein sets VI and VII, and VIII, respectively, and decreased to 330°to 350°C during formation of vein set VIV. In general, however, most mineralization occurred under a relatively small range of temperatures, averaging 350°C.

Because halite-bearing inclusions were rare, only a few halite homogenization temperatures were measured. In addition, the only two observed VII quartz-hosted LVS inclusions were found in thin sections and many inclusions were small or obscure and, hence, difficult to optically characterize or observe.

For example, the single VI-VII quartz-hosted LVS inclusion (see p.145) contained a small single solid phase which could not be adequately characterized due to poor optical resolution. V/L homogenization occurred at 268°C, but the inclusion decrepitated at 365°C, prior to melting of the solid. The latter may indicate that the solid was a trapped phase. In general, however, the number of LVS inclusions appears to increase from vein sets VI through VIV.

LVS inclusions, which are most common in vein sets VIII

Figure 6.6 Homogenization temperatures of LV and LVS inclusions. Inset shows Th-Ha for LVS inclusions. Vapor homogenization temperatures of halite-bearing inclusions in which Th-Ha was not observed are included with Th of LV inclusions, but are denoted using the LVS key in the same diagram.

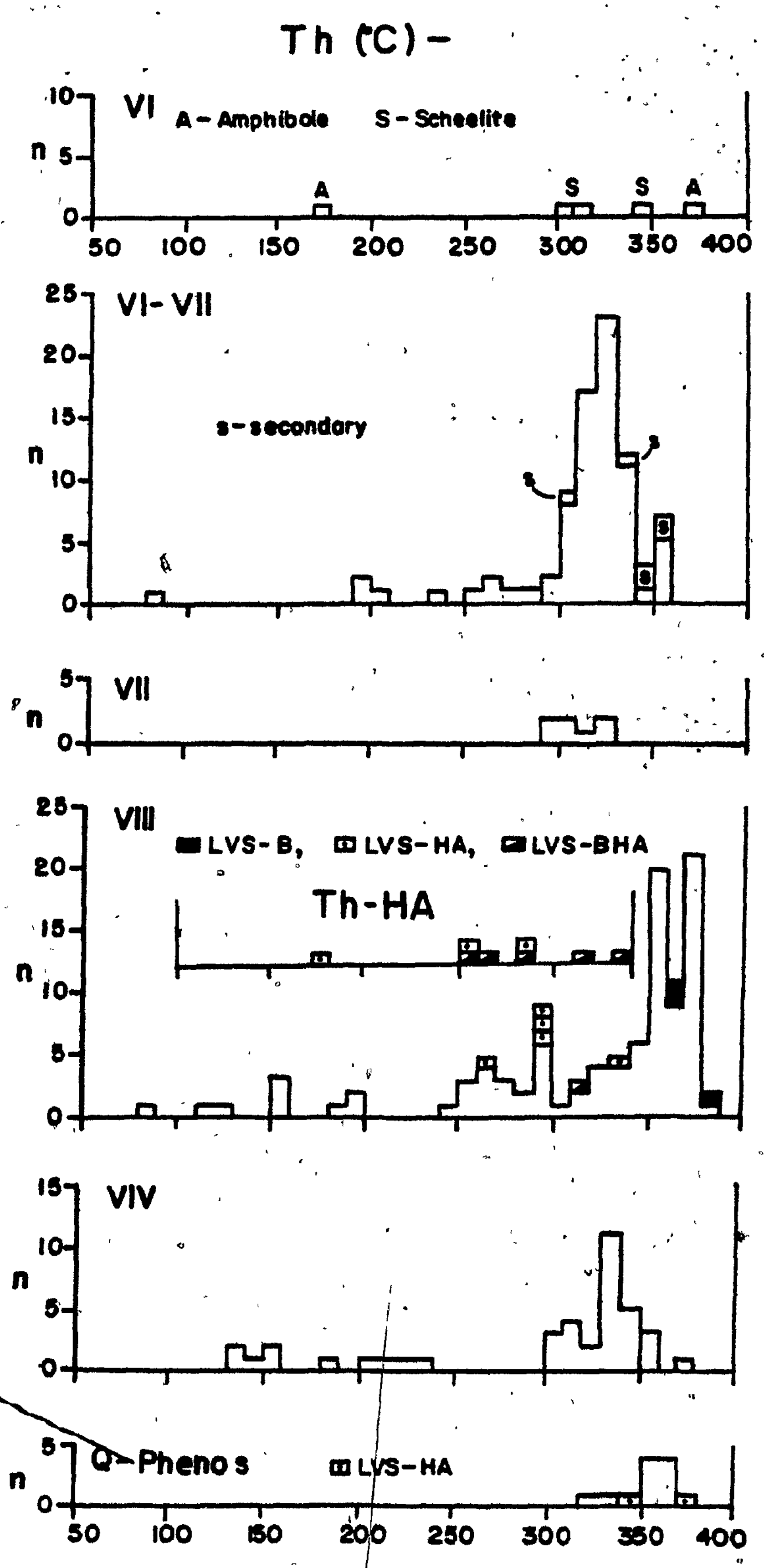
Th (°C) -
VI
A - Amphibole
S - Scheelite
n
10
5
0
A
S
S
A
50
100
150
200
250
300
350
400
VI - VII
s - secondary
s
s
25
20
15
10
5
0
VII
VIII
LVS-B,
LVS-HA,
LVS-BHA
Th-HA
VIV
Q-Phenos
LVS-HA

and VIV, homogenized mostly by halite disappearance. Th-Ha in inclusions in vein set III ranged from 171°to 340°C, 9°to 86°C higher than vapor disappearance. This corresponds to salinities between 30.61 and 39.84 eq.wt.% NaCl (Potter, et.al, 1978; Fig. 6.4b). One inclusion, however, homogenized by vapor disappearance, 7.6°C higher than Th-Ha.

Five LVS inclusions <4 to 5 microns across were found in a VIV quartz vein. Three of the inclusions contained small, apparently anhedral solids, and the other two contained solids with square outlines. One of the latter, however, decrepitated by 275°C, prior to homogenization of the solid, suggesting that the solid was a trapped phase. In addition, two halite-bearing, VIV quartz stockwork-hosted inclusions, decrepitated at <50°C for unknown reasons.

Several small (<4 microns), secondary liquid-vapor inclusions in scheelite were found along a plane crosscutting an adjacent amphibole and scheelite crystal in the amphibole halo of a VI-VII quartz vein. The inclusions homogenized between 300°and 360°C, near the modes of all primary LV inclusions (Fig. 6.6). The similarity in Th indicates that temperatures remained relatively constant for some time after VI deposition, which is also evidenced by the relatively constant Th modes in later vein sets.

6.8 DISCUSSION

Significant insight into the composition and temperature of the fluids was gained from this study. This includes the discovery of two distinct primary inclusion populations, LV and LVS, and recognition that the blue solid in LVS inclusions is a trapped phase. The latter suggests that LVS-B and LVS-BHA inclusions are LV and LVS-HA types, respectively, to which the blue phase was added, i.e., B + LV = LVS-B, and B + LVS-HA + LVS-BHA. The presence of the blue solid in both inclusion types may also be further evidence that LV and LVS types are co-genetic.

The range of Te observed in both inclusion types is lower than the eutectics of salt systems made up of 1- or 2-salt species which are most commonly found in hydrothermal systems (Crawford, 1981). The lowest measured Te of a common chloride in hydrothermal systems is -49.8° for CaCl2, which is <1°C lower than the lowest Te measured in LV inclusions and 21°C higher than the lowest Te measured in LVS inclusions. The proximity of the low CaCl2(aq) eutectic to the ones observed in this study, suggests CaCl2(aq) is present.

NaCl, which is present in LVS-(B)HA inclusions, is the most common salt species in hydrothermal systems, and may also be present in LV types. If present, NaCl would lower Te to -52°C (ibid.). At least 1 more species would therefore be needed in LVS inclusions, to account for the lowest observed Te, -70.1°C. The high Tm-hydrate implies that a complex hydrate such as natron may be present.

Fracture systems for all vein sets are moderately to well developed, especially in Zone B. For this reason, pressure corrections would probably not vary much between vein sets and hence, not effect the relative differences between modes in Th. Pressure corrections are derived and discussed in chapter 7.

VI and VII scheelite-bearing veins apparently formed at the lowest temperatures, 310° to 340° C, and contain practically no LVS inclusions. The latter suggests that VI and VII scheelite was deposited from heated, low salinity (4 to 9 eq.wt.% NaCl; Fig. 6.4), perhaps meteoric fluids. The presence of a single LVS inclusion in a VI-VII quartz vein may indicate that entry of saline fluids into the hydrothermal system was associated with onset of silica saturation and quartz vein development.

Vein set VIII formed under the highest temperatures, ranging mostly from 350° to 380°C, and contain relatively abundant LVS inclusions. The increase in temperature and number of LVS inclusions may reflect influx of highly saline, perhaps magmatic, fluids, associated with major molybdenite mineralization. Temperatures dropped slightly, to 330° to 350° C, during formation of vein set VIV, associated with quartz-sericite (A3) alteration, which may reflect initial cooling of the hydrothermal system. In general, however, VI through VIV mineralization occurred over a relatively small temperature range of 310° to 380°C.

The presence of the two apparently co-genetic, primary inclusion types poses a significant problem. There is no evidence that the two fluids evolved by boiling: No LV inclusions homogenized by liquid disappearance, and all, but one LVS inclusion homogenized by halite disappearance.

There is also no evidence that the fluids were generated from two separate fluid sources that interacted and mixed thoroughly. If the latter had occurred, a range in salinity and Th should be present. However, Th are similar for all inclusions and salinity ranges show little variation within inclusion types.

The predominance of LV inclusions and the location of most LVS inclusions along fracture planes suggests that LVS inclusions are secondary. However, the presence of isolated LVS inclusions, especially those along mineral edges or embayments suggests that at least some LVS inclusions are primary. Hence, the two fluids may reflect two different generations of fluid influx into the same veins. Alternatively the nature of the inclusion types may vary spatially. For example, primary, high salinity (>30eq.wt.% NaCl) inclusions in W-Mo mineralized veins and breccias occur in the Mt. Pleasant deposit, whereas in the peripheral chlorite-muscovite altered zones, highly saline inclusions are present, but are clearly secondary (Davis and Williams-Jones, 1985; Samson, 1985). It is not possible to make any conclusions, at present, however, due to the lack of sufficient data.

CHAPTER 7. PETROGENESIS OF THE VEIN AND ALTERATION ASSEMBLAGES

7.1 INTRODUCTION

In this chapter, petrographic phase relationships, fluid inclusion measurements, and microprobe data from the rocks and veins are used to estimate the physico-chemical conditions which existed during mineralization and hydrothermal alteration. In addition, phase diagrams are developed to help explain each major period of mineralization and alteration.

7.2 FLUID SOURCE

The increase in VII and VIII vein(let) density and mineralization (Chap. 3), and A2 alteration (Chap. 4), southward across Zone A suggests that the fluid source lay south of Zone A. This is supported by the geometry of the VIV quartz stockwork-filled fractures in Zone A, which flair out southward from <50m, near L8N, to >150m apart, along the northern rim of the elongate high chargeability/low resistivity anomaly (see Fig. 3.1).

The high, uniform VI through VIII vein(let) densities, mineralization, and associated A2 alteration in Zone B, imply that the fluid source lay close to Zone B. The abundance of component VIV stockworks and VV carbonate along the eastern edge of the VIV composite quartz stockwork "zones" in Zone B (Chap. 3), suggests further, that it lay east of Zone B. This coincides with the location of the FQB porphyry inferred from the elongate, torus-shaped high chargeability-low resistively geophysical anomalies (Fig.

3.1).

The compositions of the primary, unaltered biotite and plagioclase phenocrysts in the FQB porphyry are similar to those of the most evolved A2 biotite and plagioclase (Chap. 5). The similar mineral compositions suggest that the porphyry and altering fluids were the same, and may imply that the early fluids were derived in part, from the porphyry during its crystallization.

For these reasons, it is believed that the porphyry was responsible for initiation of the hydrothermal system which gave rise to the mineralization and alteration at Sisson Brook.

7.3 LITHOSTATIC PRESSURE

7.3.1 MINERALOGIC PRESSURE INDICATORS

The presence of M3 andalusite porphyroblasts in Unit IIa sediments, (M3 event; Chap. 2), places an upper pressure limit of 3.5kb (Holdaway, 1971) for the mineralized area. This corresponds to approximately 13km depth.

A range in lithostatic pressure can also be deduced using the mineral composition of the FQB porphyry. The presence of biotite and K-feldspar in the absence of muscovite implies that the porphyry probably cooled between 1 and 3kb pressure. This is inferred from the intersections of the lower stability boundaries of biotite and muscovite with the solidus of a "wet" granitic melt (see Fig. 2 in Fyfe, 1973).

7.3.2 FRACTURE INTENSITY IN HOST ROCKS AND ORIGINAL VOLATILE CONTENT IN MAGMA

Burnham and Ohmoto (1980) have shown that one can estimate confining pressure on an intrusion from an assessment of fracture intensity in the surrounding country rocks, and an estimate of the original volatile content of the magma. As a saturated melt cools, producing crystals and volatile phases, a volume increase results which gives rise to fracturing in the overlying rocks. The volume increase is proportional to the volatile content of the magma and inversely proportional to confining pressure (Burnham and Ohmoto, 1980).

A high fracture intensity is evident at Sisson Brook from the very high VI through VIII vein densities in Zone B, the numerous and/or relatively large VIV quartz stockworks in Zones A and B, and the widespread brecciation associated with vein set VV (Chap. 3). The high fracture intensity implies that either the volatile content of the porphyry was high, and/or confining pressure was low.

Some indication of original volatile content in the FQB porphyry may be obtained from the Fe/Mg ratio of the biotite phenocrysts. Biotite phenocrysts which have a relatively high Fe/Mg ratio >0.50, such as those in the FQB porphyry, are representative of melts with low $H2O$ contents (Trend II magmas, p.1263 in Wones and Eugster, 1965).

The volatile content of the original FQB porphyry melt may also be deduced from the percentage of hydrous phases and the $K2O + Na2O/CaO$ ratio of the rock which are 10 % and 3.3, respectively. These values are similar in magnitude to those of granites associated with molybdenite mineralization. Such granites are estimated to have had between 2.5 and 4 wt.%eq. H2O (Mutschler and Wright, 1981).

A plot of confining pressure versus fracture density about an intrusion is presented by Burnham and Ohmoto (1980, Fig. 3), and was drawn for 2.7 eq.wt.% H2O. If it is assumed that the volatile content of the FQB porphyry was similar, then use of the plot is justified and indicates that for the high fracture intensity evident at Sisson Brook, confining pressure was ~1kb. This pressure estimate is within the range of that made for other granite molybdenite systems (Mutschler, et.al., 1981; 0.3 to 1kb). A low confining pressure is supported by the presence of the large (1 to 5cm diameter) carbonate-filled vesicles in the porphyry (Chap. 2) and intrusion breccias along the contacts of some FQB porphyry dykes.

7.3.3 SUMMARY

The various mineralogic lines of evidence presented in Section 7.3.1 indicate that lithostatic pressure was <3.5kb and probably on the order of 1kb.

7.4 FLUID PRESSURE

A minimum estimate of fluid pressure of 380 bars was obtained from fluid inclusion microthermometric results using the data and technique presented by Roedder and Bodnar (1980). The pressure was derived using the average salinity of halite-bearing LVS inclusions (34 eq.wt.% NaCl), obtained from the average temperatures of halite-dissolution (243°C) and liquid-vapor homogenization (280°C; Chap. 6).

If the 380 bars represented pure hydrostatic pressure (i.e., the veins were completely open or interconnected to surface), corresponding lithostatic pressure would have been 970 bars, which is similar to the 1kb lithostatic pressure derived above (Section 7.3.3). This pressure is equal to a depth of 3 to 4km.

If, however, the 380 bars represented lithostatic pressure (i.e., the veins were isolated fractures at depth), the hydrostatic pressure would have been 161 bars, which equals 564m depth. These values were derived from the relationship: Phyd = -p x g x h where Phyd is lithostatic pressure, p equals the average density of the fluid, 1.06 g/cm3 (ibid.) or rock 2.7g/cm3, h equals the height of the water column (4km), and g equals the acceleration of the earth's gravitational field (9.81m/s2).

Hence, the 380 bars estimate of minimum fluid pressure corresponds to a range of pure hydrostatic (160 to 380bars) and pure lithostatic (380 to 970bars) values.

It is unlikely that all fractures were isolated at depth or were completely interconnected to surface. Instead, the veins (and wall rocks) were probably under pressures in between lithostatic and hydrostatic values. For this reason, an intermediate pressure of 700bars, was arbitrarily chosen to construct the phase diagrams and model, and as a minimum pressure correction factor for fluid inclusion data.

7.5 TEMPERATURE

Most homogenenization temperatures of LV inclusions range from 300°C to 370°C in vein set VI, 310° to 340°C in vein sets VI-VII and VII, 350° to 380° in vein set VIII, and 330° to 350°C in vein set VIV (Chap. 6; Table 7.1). Using the pressure correction factor (700 bars) and the average salinity of LV inclusions, i.e., 7 eq.wt.% NaCl (Fig. 6.5), the Th values in each vein set were raised 50° to 74°C. Hence, the pressure-corrected temperatures range between 350° and 454°C for LV inclusions in vein sets VI through VIV (Potter, 1977; Table 7.1).

Table 7.1 Principal ranges in Th, pressure correction factor, and pressure-corrected Th values, Th" for vein sets VI through VIV.

VEIN SET	**Th°C**	**Pcorr°C ***	**Th"°C**
VI	300 to 370	50 to 64	350 to 434
VI-VII, VII	310 to 340	59 to 65	369 to 405
VIII	350 to 380	66 to 74	416 to 454
VIV	330 to 350	62 to 67	392 to 417

*based upon average salinity of 7 eq.wt. %NaCl (Chap. 6; see Fig. 6.5).

7.6 PETROGENESIS OF VI AND A1 ASSEMBLAGES

7.6.1 INTRODUCTION

VI veins and A1 alteration comprise essentially the same mineral assemblage: hornblendized actinolite + albitized plagioclase (A1, only) ± minor albite ± minor K-feldspar ±

magnetite (mostly VI) ± pyrrhotite (mostly A1). Quartz is notably absent and both assemblages are associated with a characteristically high percentage of yellow (molybdenum-bearing) to white (pure $CaWO_4$) fluorescent scheelite (y-scheelite, w-scheelite; Chap. 3). Both assemblages are host rock specific. The A1 assemblage is found only in gabbro or FGA units, and VI veins are almost exclusively restricted to gabbro (Fig. 3.3).

7.6.2 PETROLOGIC RELATIONSHIPS BETWEEN A1 AND VI ASSEMBLAGES

The presence of A1 replacement rims about M3 actinolite cores in the absence of VI fractures, in areas distal to the mineralized zones, indicates that grain boundary diffusion was locally the sole means of fluid transport. Fracture-related diffusion/infiltration is more abundant and increases into Zone B where fluids were streamlined from hairline and (micro)fractures into vein(let)s and clots which were, in turn, concentrated into scheelite-mineralized zones, F1-F4.

The amount of replacement of M3 by A1 amphibole decreases outward from a fracture zone. This indicates that the A1 and VI assemblages are co-genetic and that the former probably formed via outward diffusion of VI vein fluids into the host rock. Co-genesis of the two assemblages is also evidenced by the similar ratios of y- to w- scheelite in VI veins and A1 altered rocks (Chaps. 3 and 4), as well as identical optical and chemical characteristics of VI and A1 amphiboles (Chap. 5).

Practically monomineralic replacement of gabbro by hornblende is evident in VI fractures and appears to have occurred incrementally and not by rapid or abrupt fracture-fill. Gradual replacement of gabbro along VI fractures is evidenced by the fine grained nature of VI fracture-fill, lack of VI mineral alignment into the veins, lack of coarse-grained, open-space filling textures, and diffuse vein boundaries.

7.6.3 EVIDENCE FOR OXIDATION

A common difference between the A1 and VI mineral assemblages is that relict disseminated pyrrhotite is common in A1-altered gabbro (Chap. 4), but rare in VI veins. In contrast, magnetite is common in VI veins, but is found in only the most intensely A1-altered rocks. The decreased abundance of magnetite outward from VI veins suggests that oxidizing vein fluids were progressively reduced as they diffused into pyrrhotite-bearing gabbro. The relative lack of magnetite in all but the most highly A1-altered host rocks implies that M3 pyrrhotite effectively buffered the oxygen fugacity of the fluids such that most host rock A1 reactions occurred within the pyrrhotite field, or near the magnetite-pyrrhotite boundary.

7.6.4 SIGNIFICANCE OF FE-ENRICHMENT IN AMPHIBOLES

VI veins and A1 alteration are most abundant, and A1 and VI amphiboles are the most chemically evolved (Al- and Fe-rich) in Zone B. Some highly evolved A1 amphiboles also occur in the southern part of Zone A (Chap. 5).

XFe in amphiboles is not only a function of iron activity in solution, but has been shown experimentally, for Fe-Mg amphiboles in the H-O-S-Fe system, to increase with, 1) decreasing temperature (Popp, et.al., 1977a), 2) increases in the ratio of oxygen to sulfur fugacities (fO2/fS2) for amphiboles which form within the pyrrhotite field of stability (Popp. et.al., 1977b) or, 3) decreases in fO2/fS2 for amphiboles which form within the magnetite stability field (ibid).

VI fractures in the mineralized zones were the main conduits for fluid and heat flow, and hence, would not have been regions of decreased temperature. The common presence of relict pyrrhotite in the Al-altered gabbro indicates, however, that most M3 amphibole replacement occurred within a reduced, pyrrhotite-bearing environment (i.e., the gabbro). Hence, increases in XFe in VI and Al amphiboles into Zone B and the southern part of Zone A (Chap. 5) may reflect increases in fO2/fS2 in the pyrrhotite-bearing gabbro (2, above).

Stability fields of Fe-Mg amphiboles having different XFe, in the system H-O-S-Fe at 700 bars and 450°C are shown in fO2-fS2 space in Figure 7.1, where they are superimposed over the stability fields of the common iron oxides and sulfides. Iron sulfide and oxide phase relationships were derived using standard thermodynamic data for iron oxides at 450°C and 1bar (Robie and Waldbaum, 1968) and experimental data for pyrrhotite-pyrite equilibria (Toulmin and Barton, 1964). The computed equilibria were corrected for a pressure

Figure 7.1 Stability fields of Fe-Mg amphiboles having different XFe, in the system H-O-S-Fe at 700 bars and 450°C. Points A through C show that the increase in XFe-Al amph can be explained in terms of increased fO_2/fS_2 conditions in the pyrrhotite-bearing gabbro.

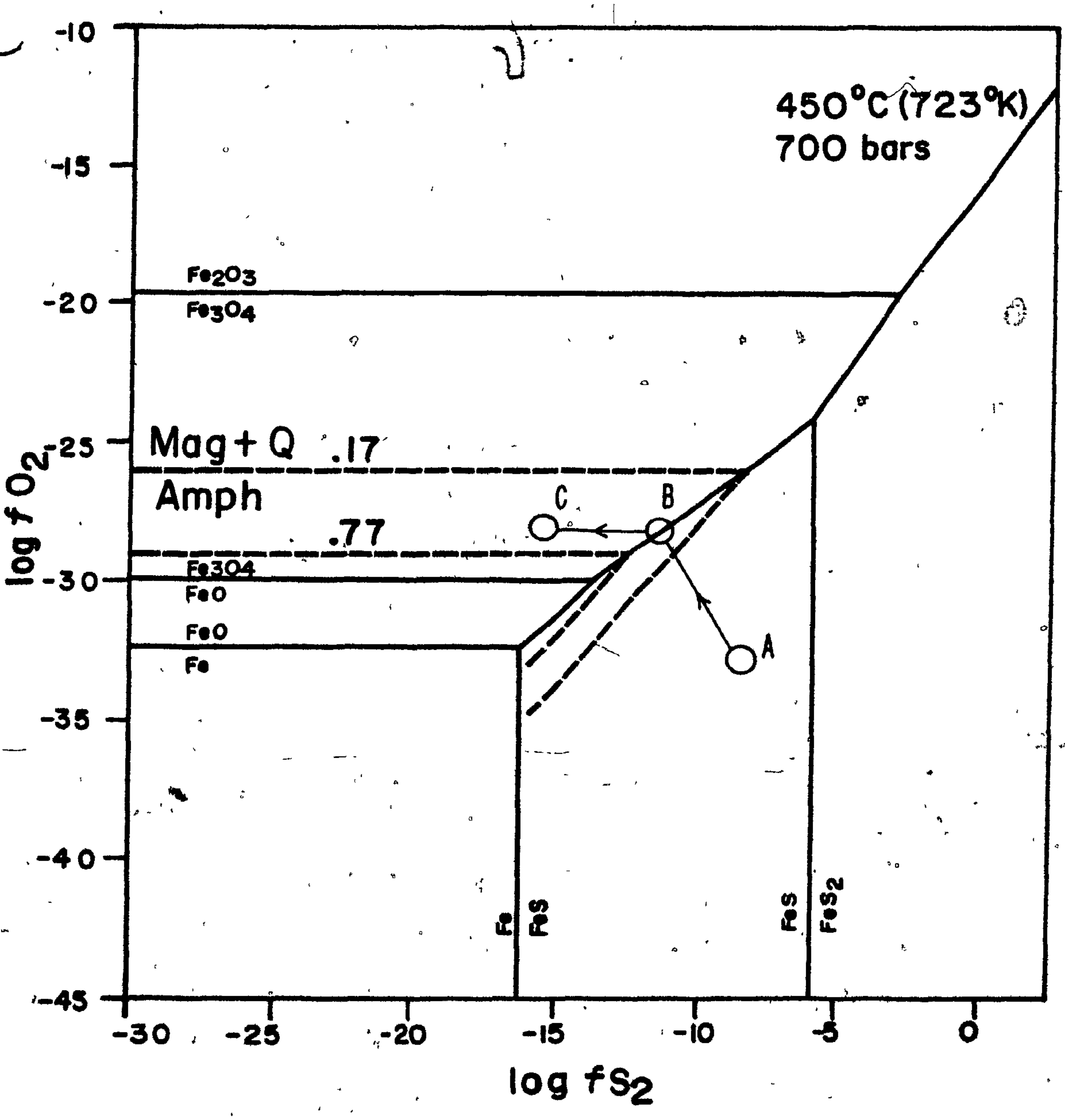
450°C (723°K)
700 bars
-10
-15
-20
-25
-30
-35
-40
-45
log f O2
Fe2O3
Fe3O4
Mag + Q
.17
Amph
.77
Fe3O4
FeO
FeO
Fe
C
B
A
Fe
FeS
FeS
FeS2
-30
-25
-20
-15
-10
-5
0
log fS2

of 700 bars using the equation, lnai, P = Vi(P-1)RT, where a = activity, i = the species under consideration, V = volume, P = pressure of interest, R = Boltzman's constant, and T = temperature. The equation assumes negligible volume change for solid species, i.e., dVP = 0 (see Anderson, 1977, for discussion of pressure corrections).

Lines of constant XFe-Amph were constructed and overlayed using the experimental data and technique of Popp et,al. (1977b). The technique is based upon experimentally established equilibria between pyrrhotite, Fe-Mg amphibole, magnetite, and quartz for various temperatures at 2kb. The four phase assemblage indicates that for particular XFe-amph, the simultaneous equilibria,

(1) amph + O_2 --> mag + q + H_2O and,

(2) amph + S_2 --> po + q + H_2O + O_2 .

occurred at a unique point along the pyrrhotite-magnetite boundary (q = quartz, amph = amphibole, mag = magnetite, and po = pyrrhotite). Keq values of reactions (1) and (2) are given by,

(3) $Keq(1) = 3\log fH_2O - 3\log aFe\text{-}amph - 5/2fO_2$ and,

(4) $Keq(2) = 7\log aFe\text{-}po + fH_2O + 7/2\log fO_2 - \log aFe\text{-}amph - 7/2\log fS_2$,

where aFe-amph and aFe-po represent activities of iron in amphibole and pyrrhotite, respectively.

Keq values for equations (3) and (4) at the T used in this study, i.e., 450°C, were obtained by graphically projecting along the best fit line of the log K versus 1/T

K*1000 plot in Popp, et. al., (1977, Fig.11) to 450°C.

At a given temperature, Keq values are constant, aFeS is a function of fS2 (Toulmin and Barton, 1964), and the variation of fH20 with f02 and fS2 can be derived mathematically using the technique of Eugster and Skippen (1976) *.

Hence, under constant temperature and pressure, but changing f02-fS2 condition, aFe-amph in equations 3 and 4 would be the only unknown. One can extrapolate from one set of f02-fS2 conditions to different ones along lines of constant amphibole compositions using relationships derived from equations 3 and 4.

In the magnetite field, log f02 for constant aFe-amph, is given by the relation,

$$(5)\quad 5/6\triangle \log f02 = \log \triangle fH20,$$

which is derived from equation 3 ($\triangle$ = the change in the fugacity or activity of a species from one set of f02-fS2 conditions to another). FH20 changes very little, however, (Fig. 8 in Popp, et.al., 1977), such that the curve for oxidation reaction (5) is largely independent of fH20 and hence, horizontal.

---

* The technique of Eugster and Skippen involves simultaneous solution of nine equations expressing the fugacities of the nine gas species present in the H-O-S-Fe system. Fugacity coefficients used in the equations were recalculated at 450°C and 700 bars using the same published sources cited by the authors. The nine equations were simultaneously solved using a FORTRAN iterative calculation program.

One can extrapolate to other fO_2/fS_2 conditions in the pyrrhotite field, for constant aFe-amph, by the relation,

$$(6)\ 7\,\Delta\log a_{FeS\text{-}po} + \log \Delta fH_2O + 7/2\,\Delta\log fO_2 = 7/2\,\Delta\log fS_2,$$

derived from equation (4). The aFeS-po is known (Barton and Toulmin, 1964), and log fH_2O is approximately constant (see Fig. 8 <u>in</u> Popp, et.al, 1977). Hence, the slope of the constant composition lines equal 1.

The resultant lines of constant XFe-amph in fO_2-fS_2 space (Fig. 7.1) show that increases in fO_2/fS_2 associated with A1 alteration of M3 amphiboles which formed in the pyrrhotite field (Fig. 7.1, Point A), result in Fe-enrichment (Point B). Once the magnetite-pyrrhotite boundary is reached and the magnetite field is entered, however (Point C), XFe-amph increases only with decreases in fO_2/fS_2.

7.6.5 fO_2/fS_2 CONTRAINTS OBTAINED FROM Y- AND W- SCHEELITE CHEMISTRY

The stability fields of scheelite ($CaWO_4$) - tungstenite (WS_2), and powellite ($CaMoO_4$) - molybdenite (MoS_2) at 450°C and 1kb are shown in Figure 7.2. The positions of the stability fields were determined experimentally in fO_2-fS_2 space at 577°C and 1kb, by Hsu (1977), and reconstructed at 450°C using positions of the solid buffer assemblages used in the experimental study (ibid., p.668). The phase relationships were not corrected to 700 bars, however, because volume changes in the molybdenite- and scheelite-producing reactions are so small ($\sim 0.009\ (P-1)*T$; ibid.) that the displacement in reaction curve positions is

Figure 7.2 The stability fields for scheelite, powellite, tungstenite molybdenite and ilmenite in f02-fS2 space for the system H-O-S-Fe 450°C and 700 bars. The scheelite/tungstenite and powellite/molydenite phase boundaries, shown in heavy lines, were derived at 450°C and 1kb pressure using the experimental data of Hsu (1977). Points A to C show that the inferred pathway of increased f02/fS2 into VI veins and Zone B explains the presence of y-scheelite, which precipitates above the pure CaW04 (w-scheelite) boundary. Points Dv and Dr represent approximate f02/fS2 conditions for the pyrrhotite-bearing VIII veins and associated (Mn-ilmenite-bearing) biotitized host rocks, respectively. The stippled pattern shows approximate stability field of Mn-ilmenite (discussed in detail in Section 7.7).

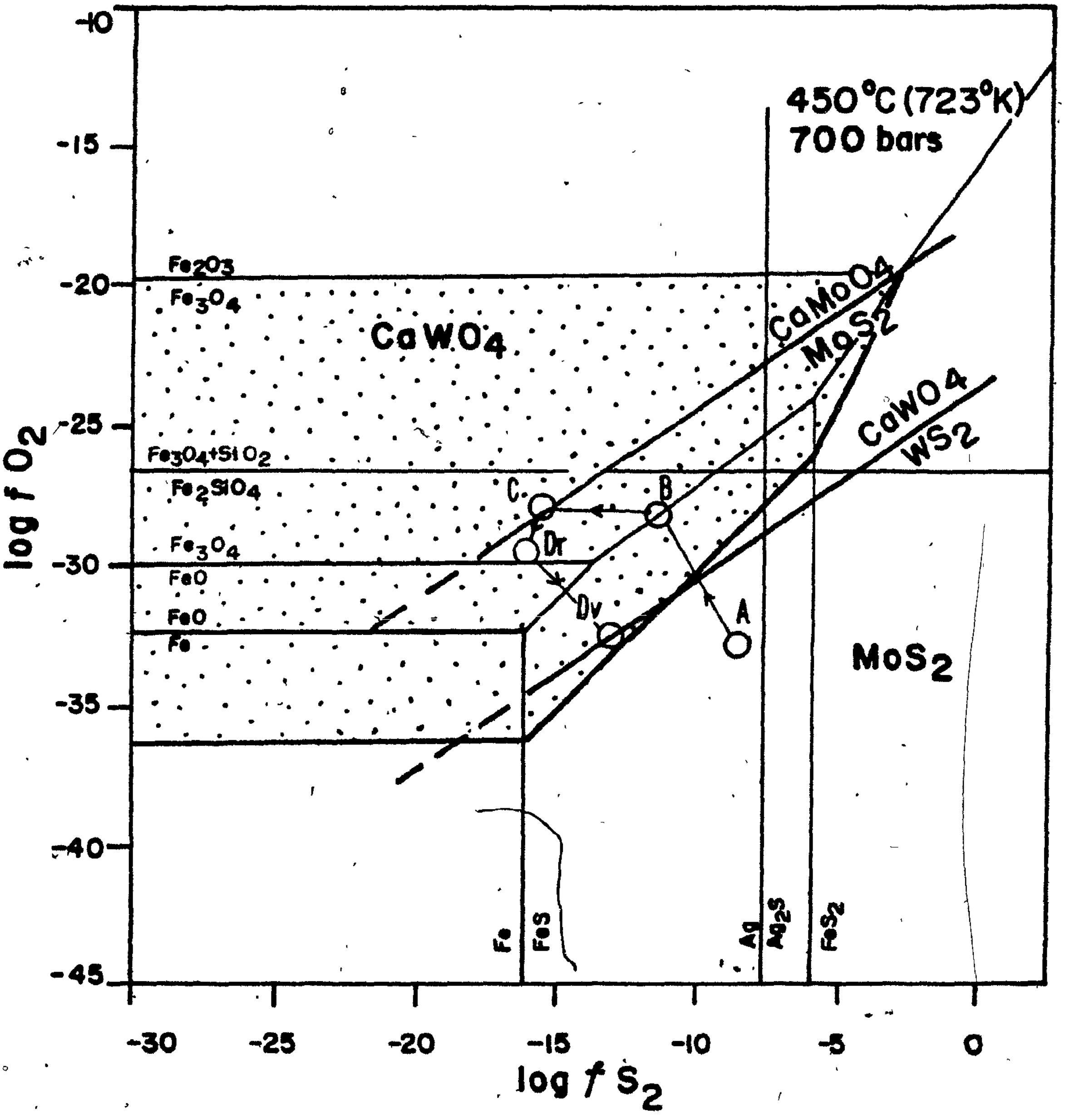
450°C (723°K)
700 bars
Fe2O3
Fe3O4
CaWO4
Fe3O4+SiO2
Fe2SiO4
Fe3O4
FeO
FeO
Fe
C
B
Dr
Dv
A
CaMoO4
MoS2
CaWO4
WS2
MoS2
Fe
FeS
Ag
Ag2S
FeS2
-10
-15
-20
-25
-30
-35
-40
-45
log f O2
-30
-25
-20
-15
-10
-5
0
log f S2

negligible.

The diagram shows that the CaMoO4 - MoS2 reaction occurs at higher fO2 and lower fS2 than the CaWO4 - WS2 reaction, and that the upper and lower stability fields of molybdenite and scheelite are parallel and overlap. The overlap forms a broad region of co-stability along the pyrrhotite-magnetite boundary, and explains why MoS2 and CaWO4 commonly occur together (Hsu and Galli, 1973; vein sets VII and VIII, below).

Most VI and A1 scheelite, however is y- (molybdenum-bearing) scheelite which is a solid solution between powellite and scheelite (Hsu, 1977). The y-scheelite is commonly associated with magnetite and occurs in the practical absence of sulfides or molybdenite. This indicates that the y-scheelite formed above the lower boundary of pure scheelite stability, where the scheelite and magnetite fields overlap. FO2/fS2 is probably sufficiently high in this area that molybdenum enters the scheelite structure (Hsu and Galli, 1973).

The relatively high fO2/fS2 conditions inferred for y-scheelite deposition supports the hypothesis that iron-enrichment in A1 and VI amphiboles was due to oxygenating conditions in the fluids (Fig. 7.2, Points B, C).

7.6.6 SIGNIFICANCE OF PLAGIOCLASE DEPOSITION

The presence of A1 and VI albite and A1 K-feldspar in the absence of sericite or paragonite indicates that the ratios of aK+/aH+ and aNa+/aH+ in the fluids which formed them were high (Fig. 7.3, Point A).

7.6.7 ESTIMATES OF MASS TRANSFER

The gabbro has the simplest mineralogy and is the most chemically homogeneous rock unit. For this reason, mass balance equations for A1 alteration of M3 amphibole and plagioclase were made using microprobe data from the gabbro.

The presence of topotaxial replacement of M3 plagioclase and especially amphibole, suggests that the equations can be estimated assuming constant volume. It should be noted, however, that these equations are only semi-quantitative; topotaxial replacement does not strictly apply in highly altered regions where the density of almost monomineralic VI amphibole veins is high, and textural inhomogeneiities occur (Chap. 4).

The mass balance equations are based upon microprobe data of relatively fresh M3 and moderately to highly A1-altered plagioclase and amphibole. M3 (An 62) and A1 albitic (An 34) plagioclase analyses are from gabbro samples, 33.178 and 36.35, respectively (see Fig. 5.16 for sample locations).

Although M3 plagioclase is apparently less consistently altered than M3 amphibole, most A1 alteration in Zone B appears to comprise Na-enriched plagioclase and minor albite and K-feldspar (Chaps. 4, 5). For this reason, a general reaction was written, assuming that approximately 70% (by volume) of M3 plagioclase of An content 62, was altered to an andesine composition (An34) and minor equal (15%) amounts of K-feldspar and al~~bite~~ (An 0), i.e.,

Figure 7.3 Plot of log Na+/H+ vs. log K+/H+ in the system KCl-NaCl-HCl-Al2O3-SiO2-H2O, showing stability fields of K- and Na-bearing silicates at 450°C and 700 bars. mHCl = 10 (E-2), assumes 2M KCl-NaCl. The stability fields were drawn assuming an ideal solution model where, (KCl) = mKCl = (K), and (NaCl) = mNaCl = (Na). Calculations were made at 450°C and P = 700bars, using the procedure outlined by Garrels and Christ (1965), except for the Ab-paragonite boundary, which drawn using the experimental data of Hemley et.al. (1961).

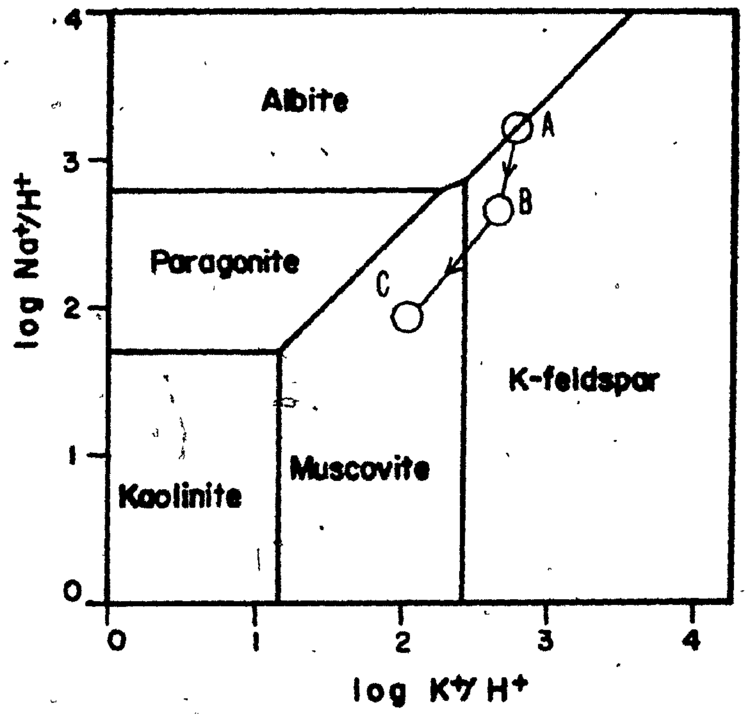
Albite
Paragonite
Kaolinite
Muscovite
K-feldspar
A
B
C
log Na⁺/H⁺
log K⁺/H⁺
0
1
2
3
4

$$(7)\ 1.0\text{Lab} \longrightarrow .15\text{Orth} + .15\text{AB} + .70\text{And}$$

This equation may also be considered to be balanced in terms of molar quantities. This is because the molar volume differences between the various feldspar phases are negligible, especially when compared with the possible errors in the volumetric exchange estimates.

A balanced reaction for this equation, using the analyses cited above is,

$$(8)\ .57\text{Si} + .22\text{K} + .22\text{Na} + 1.0\text{Lab} \longrightarrow .15\text{Ab} + .15\text{Or} + .70\text{And} + .38\text{Ca} + .31\text{Al}$$

or considering mobile elements, only,

$$(9)\ .57\text{Si} + .22\text{K} + .22\text{Na} \longrightarrow .38\text{Ca} + .31\text{Al}.$$

The general reaction for replacement of M3 by Al amphibole under conditions of constant volume was written using analyses from M3 actinolite sample, 25.136, and the most evolved Zone B hornblende sample, 33.235 (see Fig. 5.1 for sample locations), i.e.,

$$(10)\ \text{Act} + 2.17\text{Fe} + 1.41\text{Al} + .35\text{Na} + 2\text{K} + .05\text{Ca} + .07\text{Ti} + .06\text{Mn} \longrightarrow \text{Hbl} + 2.44\text{Mg} + 1.39\text{Si}$$

or considering mobile elements, only,

$$(11)\ 2.17\text{Fe} + 1.41\text{Al} + .35\text{Na} + .2\text{K} + .05\text{Ca} + .07\text{Ti} + .06\text{Mn} \longrightarrow 2.44\text{Mg} + 1.39\text{Si}$$

As in the case of the feldspars, the molar volume differences between hornblende and actinolite are negligible compared with the uncertainties in the volumetric exchange estimates.

The average amount of plagioclase and actinolite plus

M3 brown biotite is 57% and 43% respectively (Chap. 2; Table 2.1). By combining equations (9) and (11) in these proportions, the following general mass balance equation for A1 alteration in the gabbro is obtained,

$$(12)\ .93Fe + .43Al + .28Na + .21K + .03Ti + .03Mn \longrightarrow 1.05Mg + .28Si + .20Ca$$

Equation (12) therefore implies that relatively abundant amounts of Fe and Al and lesser Na and K were added to the host rock and that Mg, and to a lesser extent, Si and Ca were leached by the fluids.

The Ca released during plagioclase alteration (equation 9) may have controlled scheelite deposition. This would help explain its abundance and disseminated nature and implies that its deposition was host rock dependent, or buffered.

The lack of quartz veins or silicification is consistent with the conclusion that silica was leached during alteration, i.e., that the altering/vein fluids were undersaturated with respect to silica. The transitional hornblende-quartz veins of vein set VI-VII (Chap. 3) may have signalled the beginning of quartz saturation.

7.6.8 SUMMARY

VI and A1 assemblages appear to have formed under silica-undersaturated conditions from heated, low salinity, fluids, at temperatures that were generally between 350° and 434°C and at pressures between 150bars and 1kb. Fe-enrichment of A1 and VI amphiboles into Zone B was associated with the precipitation of y-scheelite and vein magnetite, and occurred in the practical absence of sulfides; this suggests that the fluids were oxygenating, and that reactions occurred within the magnetite field.

The presence of hornblende, only, in many veins may indicate that the fluids were alkaline. This is evidenced by the replacement of Ca^{2+} by Na^{+} and K^{+} (i.e., a cation with a high charge to radius ratio (acidic) replaced by cations with lower charge to radius ratios (basic)), and the replacement of Mg^{2+} (acid) by Fe^{2+} (base; the charge to radius ratio of Mg^{2+} is higher than Fe^{2+}; see Burt, 1979 for further discussion).

The alkaline nature of the reactions may have helped produce the high aK^{+}/aH^{+} and aNa^{+}/aH^{+} ratios which are inferred from the presence of K-feldspar and albite in the absence of muscovite or paragonite.

A1 reactions were, at least partly, host rock buffered. The presence of decreased amounts of relict pyrrhotite into the VI scheelite-mineralized zones, F1 to F4, suggests that fO_2/fS_2 conditions increased into Zone B. This implies that A1 and VI reactions moved progressively from the pyrrhotite field outside Zone B, towards the magnetite-pyrrhotite boundary into Zone B, where in many veins and some highly A1-altered rocks, reactions occurred in the magnetite field. The increasingly oxygenating conditions into Zone B are believed to have led to a concomitant increase in X_{Fe}-amph. The presence of y-scheelite in the absence of molybdenite or other sulfides supports the hypothesis that the hydrothermal fluids were oxidizing.

Host rock buffering is also evidenced by the formation of most VI veins and A1 alteration in the mafic gabbro and FGA units. In addition, mass balance equation 9 suggests that the Ca in VI and A1 y-scheelite may have been derived from M3 plagioclase. The evidence of host rock buffering suggests that the fluid to host rock ratio was relatively low.

7.7 PETROGENESIS OF VII, VIII AND A2 ASSEMBLAGES

7.7.1 INTRODUCTION

7.7.1a VII AND VIII VEIN(LET)S

VII and VIII vein(let)s are both associated with A2 biotite haloes, but have different widths and contain different modal amounts of the same types of mineralization. VII veinlets are typically 1 to 3mm wide, whereas VIII veins are 1 to 3cm across. VII veinlets contain mostly scheelite (with a high y- to w- scheelite ratio) ± minor to rare molybdenite, whereas VIII veins contain abundant w-scheelite + molybdenite. The similar vein parageneses, biotite alteration haloes, and presence of veins containing intermediate amounts of scheelite and molybdenite, suggest that vein sets VII and VIII represent a continuum in quartz-hosted scheelite-molybdenite deposition (Chap. 3).

VII and VIII vein density in Zone A is generally small, but increases southward. In contrast, the vein densities in Zone B are high and relatively uniform. In addition, VIII veins in Zone A contain minor mineralization, whereas VIII veins in Zone B help define three lens-like molybdenite-scheelite mineralized zones, MZ1-MZ3, averaging <0.30 wt.% $WO_3 + MoS_2$ (Chap. 3).

7.7.1b A2 BIOTITE

The biotite in VII and VIII veins is optically and chemically identical to the A2 biotite which occurs in biotite haloes and intense local-pervasive alteration proximal to the deposit, and minor pervasive alteration up to 1km from the deposit (Chaps. 4, 5).

Preferential nucleation of A2 biotite along S3 crenulation hingelines indicates that the biotite and S3 surface are co-genetic (Chap. 2). This, as well as the presence of chemically and optically identical biotite in VII and VIII veins (which are also concentrated along S3 surfaces; Chap. 3) and associated vein haloes (Chap. 5), indicate that the S3 surface, alteration, and mineralization were co-eval, and occurred during a late (M4) tectonic event (Chap. 2).

A2 biotite alteration intensity, like VII and VIII vein density, is significantly higher in Zone B than in Zone A (Chap. 4). A biotitization index developed for FGA units shows that A2 alteration in Zone B is almost an order of magnitude higher than in Zone A (see Fig. 4.4). In addition, A2 K-feldspar replacement of M3 plagioclase which apparently did not occur in Zone A, is abundant and widespread in Zone B.

7.7.1c Kd FOR Fe/Mg BETWEEN M3/A1 AMPHIBOLES AND VII, VIII, AND A2 BIOTITES

An approximately linear relationship occurs between the XFe in VII, VIII/A2 biotites, and the XFe in relict M3/A1 amphiboles, which defines a Kd of ∼.54 (see Fig. 5.12). The low Kd value suggests that A2 biotite-forming reactions were partly independent of host rock composition, or fluid-buffered (Chap. 5).

7.7.2 fO2/fS2 CONDITIONS

7.7.2a fO2/fS2 IN VEINS

The presence of rare to minor pyrrhotite in VIII veins in the absence of Mn-ilmenite or other vein oxides suggests that fO2/fS2 conditions in the veins decreased relative to magnetite-bearing VI veins. This is also inferred from the progressively greater amounts of molybdenite and w-scheelite and the increasingly smaller ratio of w- to y- scheelite (Section 7.5.1) in VII and VIII veins. The presence of locally intergrown w-scheelite and rare (VII) and abundant (VIII) molybdenite indicates however, that fO2/fS2 conditions did not decrease below the region of molybdenite-scheelite co-stability (Fig. 7.2; Point Dv).

7.7.2b fO2/fS2 IN HOST ROCKS

A2 Mn-ilmenite is present in pervasively altered mafic and some felsic units (Chaps. 4, 5). The field of Mn-ilmenite stability is shown in Figure 7.2 as the stippled region. The upper boundary is the same as that of magnetite (Rumble, 1976). The balanced reactions between ilmenite, pyrrhotite, and pyrite, however, i.e.,

(13) $FeTiO_3 + S_2 \rightarrow FeS_2 + TiO_2 + 1/2O_2$ and,

(14) $FeTiO_3 + 1/2S_2 \rightarrow FeS + TiO_2 + 1/2O_2$,

show that the lower boundary of the ilmenite stability field goes to lower fO_2 and higher fS_2 values than the magnetite one (Froese, 1976). The Mn content of A2 Mn-ilmenite would expand the field of ~~il~~menite further.

A2 Mn-ilmenite occurs in the absence of molybdenite or iron sulfides, implying that the fO_2/fS_2 conditions in the host rocks were higher than in the veins. This is supported by the presence of y-scheelite in some A2 biotite haloes or along VII and VIII vein walls (Scott, 1983). This indicates that the Mn-ilmenite precipitated above the lower boundary of pure (w-)scheelite, where y-scheelite is stable (Hsu, 1977; Fig. 7.2; Point Dr).

Pyrrhotite is present or overgrows Mn-ilmenite in some pervasively A2-altered rocks and in the inner portion of some multiple vein haloes. The presence of late A2 pyrrhotite suggests that the fO_2/fS_2 ratio decreased during late stages of A2 alteration (Fig. 7.2, path Dr to Dv). Alternatively, the aTi may have decreased such that the solution was undersaturated with respect to ilmenite and/or that Mn-ilmenite was not stable.

Fluid inclusion data shows that the range in Th of inclusions in VI veins (350° to 434°C) and VII and VIII veins (369° to 450°C) are similar (Table 7.1). This implies that changes in fO_2/fS_2 conditions were probably more important in affecting the XFe-Biot than temperature.

7.7.3 MASS BALANCE CALCULATION

An approximate mass balance equation was written for biotite replacement of amphibole in gabbro at constant volume conditions. The gabbro was chosen because it is more chemically homogeneous than the Unit IIb metavolcano-sediments. Constant volume was assumed because topotaxial replacement of amphibole in low to moderately altered gabbro is common (Chap. 4).

The equation was written for 50% amphibole replacement by biotite (sample 33.167), in a low to moderately Al-altered gabbro, in which the amphibole is a moderately evolved (i.e., Al- and Fe-rich) Al hornblende (sample 33.167), i.e.,

$$(15)\quad .5((\text{A1 amph} \dashrightarrow 1.82\ (\text{A2-biot})$$

where .5 = 50% of all amphibole and 1.82 equals the molar volume ratio between amphibole and biotite (Robie and Waldbaum, 1968) or,

$$(16)\quad \text{Hbl} + 2.15\text{Al} + 1.67\text{Si} + 1.60\text{K} + 1.33\text{Mg} + 1.28\text{Fe} + .18\text{Ti} \dashrightarrow \text{Bi} + .88\text{Ca} + .13\text{Na} + .01\text{Mn},$$

or considering mobile metal elements only,

$$(17)\quad 2.15\text{Al} + 1.67\text{Si} + 1.60\text{K} + 1.33\text{Mg} + 1.28\text{Fe} + .18\text{Ti} \dashrightarrow .88\text{Ca} + .13\text{Na} + .01\text{Mn}$$

Equation 17 shows that formation of A2 biotite required input of abundant alumina, silica, potassium, magnesium, and iron. The amount of potassium will be even higher if one includes the apparently abundant and widespread A2 K-feldspar alteration of plagioclase in Zone B. Lack of sufficient petrographic data on feldspar alteration, however, makes it difficult to assess how much more so. The small number of highly saline possibly primary (LVS) inclusions, in vein set VIII (~30 to 40 eq.wt. %/NaCl; Chap. 6), may indicate that the K was derived from potassic, possibly orthomagmatic fluids.

The Si and Mg needed to form A2 biotite contrasts with A1 amphibole alteration (equation 11) where Si and Mg were leached into the fluid. Silica addition is expected in light of VII and VIII quartz vein deposition, which indicates that the fluids were silica-saturated. Part of the Mg and Si may have been supplied by the M3-->A1 amphibole reaction (equation 11). Some or all remaining Mg, Al, and Fe may have come from leaching of adjacent rock units, i.e., the Unit IIa slates, Unit IIb metavolcano-sediments and/or gabbro, or from orthomagmatic fluids.

Although plagioclase alteration is not quantified, any K-feldspar or albite replacement would release Ca into the fluid (see equations 8 and 9). The amount of Ca released into the fluid from both plagioclase and amphibole alteration probably aided in deposition of the large amount of VII and VIII scheelite.

7.7.4 SUMMARY

A2, VII and VIII assemblages formed under silica-saturated conditions at temperatures between 369 to 454 C. Precipitation of VIII vein pyrrhotite and molybdenite in the practical absence of y-scheelite or accessory vein oxides, suggests that VII and VIII veins formed under lower fO2/fS2 conditions than vein set VI (Fig. 7.1, Point Dv). The presence of y-scheelite in some A2 haloes and characteristic presence of A2 Mn-ilmenite in mafic units and some Unit IIb metavolcano-sediments suggests that fO2/fS2 conditions in the host rocks were similar to those in VI veins and magnetite-bearing A1-altered rocks and higher than in the VII and VIII veins (Figs. 7.1, 7.2, Points Dv, Dr). The precipitation of Mn-ilmenite may also indicate that aMn and/or aTi were higher in the host rock.

The abundant Ca released by A2 alteration of amphibole and plagioclase probably accounts for the abundance of VII and VIII scheelite deposition. In addition, the relatively abundant A2 replacement of M3 plagioclase by K-feldspar and more sodic plagioclase (Chaps. 4, 5), suggests that the K+/H+ and Na+/H+ ratios were high (Fig. 7.3, Point B). The presence of LVS inclusions in VIII veins may indicate that the influx of potassic fluids was orthomagmatic in origin.

A molybdenite-rich zone commonly occurs near or over the apex of the fluid source in granite molybdenite systems (eg. Mutschler, et.al. 1981). The proximity of molybdenite mineralization to the fluid source may reflect its relatively low solubility (Barnes, 1975). The abundance of VIII molybdenite mineralization in Zone B might therefore be explained in terms of its inferred proximity to the fluid source, i.e., the FQB porphyry.

7.8 PETROGENESIS OF A3 AND VIV ASSEMBLAGES

7.8.1 INTRODUCTION

Vein set VIV is associated with abundant wolframite-chalcopyrite deposition in Zone A and minor similar mineralization as well as abundant molybdenite and scheelite mineralization in Zone B (Chap. 3). Vein set VIV is associated with A3 alteration which mainly alters the permeable Unit IIb metavolcano-sediments, and comprises mostly sericite, quartz and pyrite in felsic units. Lesser chlorite and pyrite is found in a minor number of mafic units (Chap. 4).

Fluid inclusion data indicates that maximum temperatures dropped from >450°C in vein set VIII to <420°C in vein set VIV. The presence of a minor number of LVS inclusions in VIV veins indicates that saline, possibly orthomagmatic fluids, may have been present (Chap. 6).

7.8.2 A3 SERICITE REPLACEMENT OF PLAGIOCLASE AND BIOTITE

The transition from A1/A2 sodic plagioclase and A2 K-feldspar alteration to A3 sericite alteration of M3 plagioclase, indicates that Na+/H+ and K+/H+ ratios decreased (Fig. 7.3, Point C). A3 alteration is associated mainly with silicification and sericitization of M3 plagioclase and A2 biotite in previously A2 biotitized metavolcano-sediments (Chap. 4). The alteration is most intense in the permeable and previously biotitized lapilli tuffs (Chap. 4).

It was not possible to determine whether volume was conserved during alteration. The obliteration of primary grain or crystal boundaries and presence of abundant silicification implies, however, that volume was not conserved.

The presence of abundant silicification and deposition of disseminated pyrite in A3-altered rocks suggests that replacement of A2-biotite and host rock plagioclase occurred under sulfidizing conditions, i.e.,

(18) Plag + A2 Biot + S_2 -->
A3 Ser + Py + 2Qtz + Ca + Na + Mg

The presence of A3 pyrite also indicates that the reactions occurred somewhere in the pyrite field (Fig. 7.4, Point Er).

7.8.3 fO_2/fS_2 CONTROLS ON VIV WOLFRAMITE AND SCHEELITE STABILITY

The Ca release by sericite replacement of plagioclase may have predominated in Zone B where plagioclase comprises over 60% of the gabbro (Chap. 2). This may help explain the relative abundance of VIV scheelite in Zone B, and its relative absence in Zone A. The relatively exclusive presence of wolframite in Zone A and scheelite in in Zone B, however (Chap. 3), may also reflect different fO_2/fS_2 conditions in each zone.

The relative stability fields of wolframite and scheelite in fO_2-fS_2 space were drawn using the positions of solid buffers used in the experimental studies of Hsu (1976, 1977; Fig. 7.4). The diagram shows that the wolframite, which locally intergrows or is surrounded by pyrrhotite, probably precipitated in or near the small region of

Figure 7.4 Stability fields of huebnerite and ferberite superimposed on the stability fields of the other minerals shown in Figure 7.3, at 450°C and 700 bars (after Hsu, 1976, 1977). Points Ev(A) and Ev(B) refer to approximate conditions in VIV veins in Zones A and B, respectively. Point Er represents fO_2/fS_2 conditions in associated A3-altered rocks. Striped pattern shows area of overlap of wolframite and pyrrhotite stability fields.

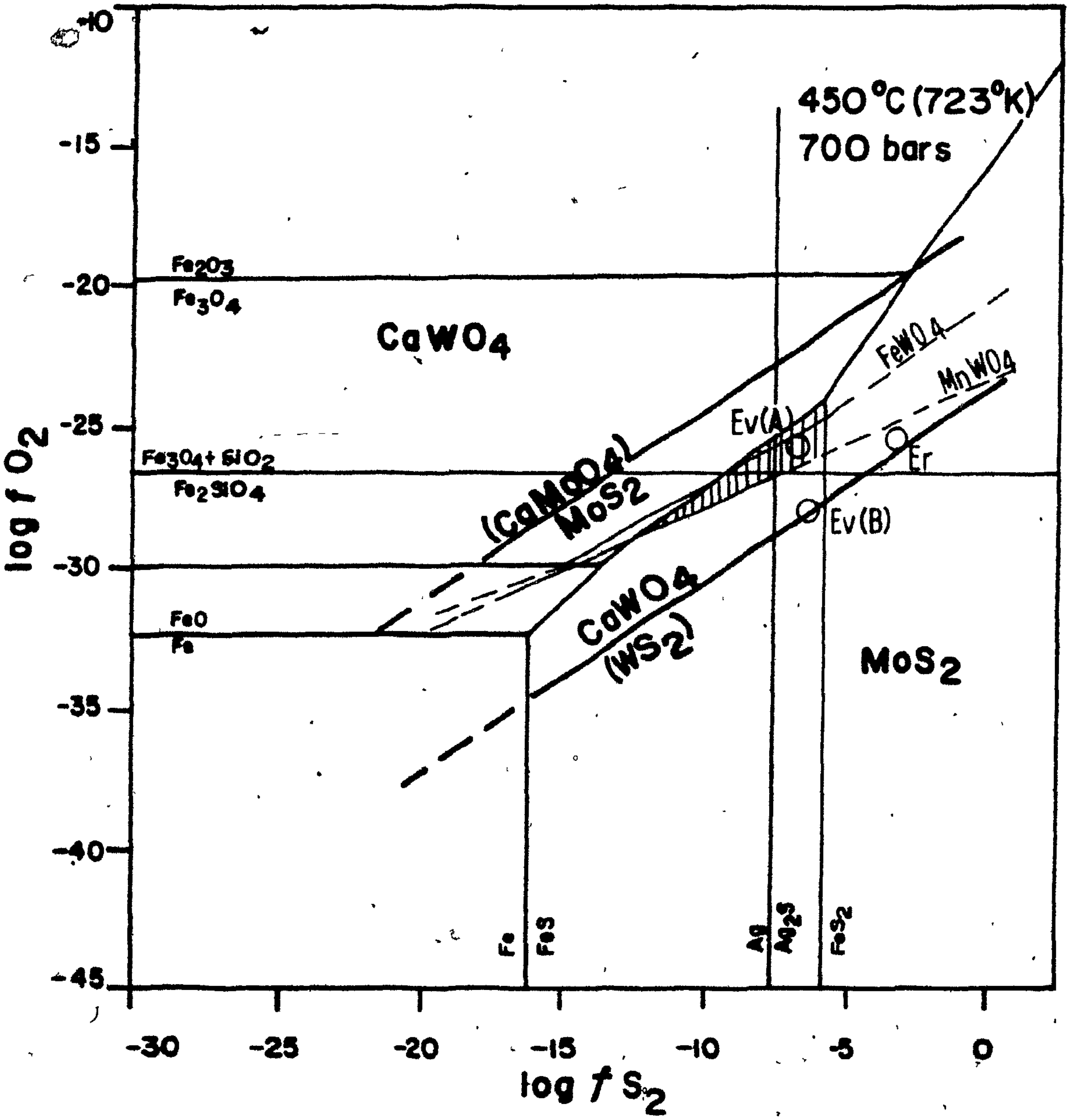
450°C (723°K)
700 bars
Fe2O3
Fe3O4
CaWO4
Fe3O4 + SiO2
Fe2SiO4
(CaMoO4)
MoS2
FeO
Fe
CaWO4
(WS2)
MoS2
FeWO4
MnWO4
Ev(A)
Er
Ev(B)
Fe
FeS
Ag
Ag2S
FeS2
log f O2
-10
-15
-20
-25
-30
-35
-40
-45
log f S2
-30
-25
-20
-15
-10
-5
0

wolframite-pyrrhotite overlap (Fig. 7.4, Point Ev(A)). The presence of VIV w-scheelite (i.e., pure CaWO4), molybdenite and/or pyrrhotite in Zone B, however, implies that the scheelite probably precipitated under a broader and generally lower range of fO2/fS2 conditions (Fig. 7.4, Point Ev(B)). Hence, if fO2/fS2 conditions were sufficiently low in Zone B, wolframite would not stable (Fig. 7.4, Point Ev(A)) but scheelite would be (Point Ev(B)). This suggests that Zone B was closer to a sulfidizing fluid source.

The higher fO2/fS2 needed for wolframite deposition may help explain its host rock specific nature (albeit rarity) in Zone B. There, the amount of wolframite measured in the relatively sulfide-free metavolcano-sediments (i.e., rocks having relatively high fO2/fS2 conditions), is 0.10 occurrences/100m, whereas in the pyrrhotite-bearing gabbro (i.e., a unit having a relatively low fO2/fS2), it is 0.01 occurrences/100m (Chap. 3). This implies that on a local scale, fO2/fS2 conditions were host rock-buffered.

7.9 PETROGENESIS OF A4 AND VV ASSEMBLAGES

7.9.1 INTRODUCTION

Vein set VV consists mostly of massive carbonate and carbonate vein(let)s and is associated with fine grained A4 sericite alteration. VV carbonate and associated alteration is found mainly adjacent to VIV quartz stockworks (Chaps. 3, 4).

7.9.2 EVIDENCE FOR A PRESSURE DROP

Vein set VV and A4 alteration are associated with numerous tension features which suggest that a pressure drop occurred. The tension features include numerous small horst and graben features in drill core which are several centimeters across and have 3 to 4cm displacements. Vuggy, fluorite-bearing VV carbonate breccia zones and slickenside surfaces adjacent to VIV quartz stockworks also indicate a drop in pressure.

7.9.3 EVIDENCE FOR A TEMPERATURE DROP

Minor but widespread native bismuth is associated with VV carbonate. The low melting point of native bismuth, 271.3°C (Weast, 1976) indicates that vein set VV formed at significantly lower temperatures than vein sets VI through VIV.

7.9.4 EFFECT OF DECREASED PRESSURE AND TEMPERATURE ON CO2 SOLUBILITY

The pressure and temperature drops probably occurred due to collapse of the hydrothermal system. The drops in pressure and temperature were accompanied by abundant volatile release, evidenced in part by the widespread explosive brecciation associated with vein set VV. CO2 would then have preferentially partitioned into the vapor phase leading to increased pH, decreased solubility of CO2 and precipitation of calcite (Holland and Malinin, 1979).

7.9.5 fO2/fS2 CONDITIONS

The presence of pyrite in the carbonate and associated host rock indicates that fS2 was generally high. The presence of rutile crystals and hematite alteration of VIV wolframite crystals in pervasively A4 altered rocks, indicates that fO2 was also high.

7.9.6 aK+/aH+ RATIOS

The abundance and fine grained nature of A4 sericite in the absence of K-feldspar or albite indicates that the Na+/H+ and K+/H+ ratios remained relatively low (Fig. 7.3, Point C).

7.9.7 SUMMARY

The association of VV carbonate with horst and graben features and brecciation, suggests a pressure drop occurred during the VV/A4 event. This would have led to increased pH and decreased CO2 solubility, which would explain the widespread and pervasive nature of carbonate deposition.

The deposition of native bismuth suggests that temperatures were, ≤ 271.3°C. The presence of pyrite and hematite suggests fO2 and fS2 were relatively high. The presence of A4 sericite indicates that Na+/H+ and K+/H+ ratios were low.

CHAPTER 8. PETROGENETIC MODEL

A late tectonic-hydrothermal event (M4) associated with intrusion of the feldspar-quartz-biotite (FQB) porphyry in the Sisson Brook area occurred during Upper Devonian-Lower Carboniferous times. The FQB porphyry intruded along the gabbro-sediment contact during development of a late NW-trending foliation surface (S3; Chap. 2).

Intersection of the stresses producing the S3 surface with those associated with the intruding porphyry, produced large N-trending, mineralized gash fractures which flank the porphyry to the west (Zone B), and which extend radially (up to 1km) outward from its northern edge (Zone A). Fluids associated with the porphyry entered the S3 surface along the gash fractures, producing five vein sets, oriented parallel to S3, and four periods of associated alteration (Chaps. 3, 4).

The mineralogy of the vein sets and alteration reflect different f02/fS2 conditions, fluid to rock ratios, and amounts of orthomagmatic to meteoric fluids. For example, VI vein/A1 alteration minerals and VI/A1 y-scheelite apparently formed from silica-undersaturated, alkaline fluids, in the presence of a low fluid to rock ratio (witness for example, the host rock specific nature of the VI/A1 assemblages and the host rock buffering of f02 reflected in A1 amphibole compositions; Chap. 7). This probably corresponded to an early stage in the crystallization of the porphyry prior to large-scale volatile separation from the magma and complete emplacement of the external hydrothermal system.

The porphyry continued to intrude during formation of vein sets VII, VIII/A2 alteration. This is evidenced by the presence of breccias along porphyry dyke interfaces, associated with abundant potassic alteration. It is perhaps also evident by the compositional similarities between primary unaltered biotite and plagioclase phenocrysts and VII, VIII vein/A2 alteration biotites and A2 plagioclases.

Movement of the porphyry and/or rotation of the stress field producing the S3 surface occurred during formation of vein set VIII. This resulted in the formation of a new set of gash fractures in Zone B and E-trending faults and widespread deposition of scheelite-molybdenite quartz veins and associated intense potassic alteration (Chaps. 2, 3, 4).

The presence of mostly w-scheelite, molybdenite, and/or pyrrhotite in VIII veins indicate that the fluids were more sulfidizing than during the VI/A1 event. The Kd value of 0.54 for Fe/Mg between relict M3/A1 amphiboles and A2 biotites which replace them, indicates that the fluid to rock ratio was substantially higher at this time (Chap. 7).

Fluid inclusion evidence indicates that temperatures peaked near 450°C during the VII, VIII/A2 event. In addition, the presence of relatively abundant LVS (saline) inclusions in VIII veins implies that orthomagmatic fluids may have been present (Chap. 6). The high salinity of the fluids and the relatively high fluid to rock ratio suggest that the hydrothermal system was largely orthomagmatic and well-established at this time.

Development of the VIV quartz stockworks and A3 sericite alteration probably signalled the beginning of meteoric fluid influx. This may help explain the even higher fluid to rock ratio evidenced by the large-scale nature of the quartz stockworks, as well as the slight cooling of the system (Chaps. 3, 6). Precipitation of VIV scheelite in Zone B, and VIV wolframite in Zone A implies that fO2/fS2 conditions were lower in Zone B, and also implies that the proportion of sulfidizing fluids was greater in Zone B.

Cooling and collapse of the hydrothermal system, evidenced in part, by the explosive brecciation and minor widespread deposition of native bismuth (Chap. 7), probably resulted from devolatilization and loss of CO2 from the fluid. This led to increased pH and consequent deposition of massive carbonate (vein set VV; Chap. 7). Rutile, hematite, and pyrite also precipitated at that time, indicating that both fO2 and fS2 were high (Chap. 7).

REFERENCES

ABBOTT, D., 1981. Petrographic Examination of Rock Specimens For Texas Gulf. Unpubl. company report (Fredericton) AS/82/150, Job 5001. Oct. 7, 1981.

ANDERSON, F.D., 1968. Woodstock, Millville and Coldstream map areas, Carleton and York counties, New Brunswick. Geol. Surv. Can. Mem. 353.

ANDERSON, G.M., 1977. Fugacity, activity and the equilibrium constant. In Greenwood, H.J. (ed.), Application of Thermodynamics to Petrology and Ore Deposits., Min. Assoc. Can. Short Course Notes, 17-37.

ANONYMOUS, 1960. (for, Nashwash Pulp and Paper Co.) New Brunswick Mineral Resource Assessment File 47028.

BARAGAR, W.R.A., and IRVINE, T.N., 1971. A guide to the classification of the common volcanic rocks. Can. Jour. Earth Sci., v. 8, 523-548.

BARNES, H.L., 1975. Zoning of ore deposits: types and causes. Trans. Roy. Soc. Edinburgh, v. 69, no. 13, 295-311.

BARTON, P.B.,Jr., and TOULMIN, P., III, 1964. The electron-tarnish method for the determination of the fugacity of sulfur in laboratory sulfide systems. Geochim. Cosmochim. Acta, v. 28, 619-640.

BURNHAM, C.W., and OHMOTO, H., 1980. Late-stage processes of felsic magmatism. Mining Geol. Spec. Iss., v. 8, 11.

CRAWFORD, M.L., 1981. Phase equilibria in aqueous fluid inclusions. In, Hollister,L.S., and M.L. Crawford (eds.), Min. Assoc. Can.: Short Course in Fluid Inclusions : Applications to Petrology. Calgary, May, 1981, 75-100.

DAVIS, W.J., AND WILLIAMS-JONES, A.E., 1985. A fluid inclusion study of the porphyry greisen, tungsten-molybdenum deposit at Mount Pleasant, New Brunswick, Canada. Mineralium Deposita, v.20, no. 2, 94-101.

DIETRICH, R.V., 1973. Migmatites - A Resume. Council on Educ. in the Geol. Sciences Short Reviews no. 24, 144-156.

EUGSTER, H.P., and SKIPPEN, G., 1967. Igneous and metamorphic reactions involving gas equilibria. In Abelson, P.H., (ed.), Researches in Geochemistry, v.2: John Wiley and Sons, New York, 663p.

FROESE, E., 1976. Oxidation and sulfidation reactions. In Greenwood, H.J., (ed)., Application of Thermodynamics to Petrology and Ore Deposits, Min. Assoc. Can. Short Course Notes, 84-98.

FYFE, W.S., 1973. The generation of batholiths. Tectonophysics, v. 17, 273-283.

FYFFE, L.R., PAJARI, G.E., and CHERRY, M.E., 1981. The Acadian plutonic rocks of New Brunswick. Maritime Sediments and Atlantic Geology, v. 17, 23-36.

GARRELS, R.M., and CHRIST, C.L., 1965. Solutions, Minerals, and Equilibria. Harper and Row, New York, 450p.

GASTEIGER, W.A., 1982. Report on geophysical work, Sisson Claims, Jan. 1982. Unpubl. company report.

HAK, J., and WATKINSON, D., 1981. Mineralogy and electron microprobe study of specimens from Sisson Brook, N.B. Unpubl. company report.

HAWTHORNE, F.C., 1983. The crystal chemistry of the amphiboles. Can. Min., v. 21, pt. 2, 173-480.

HEMLEY, J.J., MEYERS, C., and RICHTER, D.H., 1961. Some alteration reactions in the system $Na_2O-Al_2O_3-SiO_2-H_2O$. U.S. Geol. Surv. Prof. Pap. 424, 338-340.

HOLDAWAY, M.J., 1971. Stability of andalusite and the aluminum silicate phase diagram. Amer. Jour. Sci., v. 271, 97-131.

HOLLAND, H.D. and MALININ, S.D., 1979. The solubility and occurrence of non-ore minerals. In, Barnes, H.L. (ed.), Geochemistry of Hydrothermal Ore Deposits, 2nd ed.: Wiley-Interscience, New York, 461-501.

HSU, L.C., 1976. The stability relations of the wolframite series. Amer. Mineral., v.61, 944-955.

HSU, L.C., 1977. Effects of oxygen and sulfur fugacities on the scheelite-tungstenite and powellite-molybdenite stability relations. Econ. Geol., v. 72, 664-670.

HSU, L.C., and GALLI, P.E., 1973. Origin of the scheelite-powellite series of minerals. Econ. Geol., v. 68, 681-696.

LAIRD, J., and ALBEE, A.L., 1981. High pressure metamorphism in mafic schist from northern Vermont. Amer. Jour. Sci., v. 281, 97-126.

LEAKE, B.F., 1978. Nomenclature of amphiboles. Can. Min., v. 46, pt. 4, 501-510.

LOUGHEED, P.J., 1982. Geological and geochemical investigation of plutonic suites in the Sisson Brook Area, York county, New Brunswick. Unpubl. B.Sc. thesis, McMaster Univ., April 1982.

MANN, R.F., 1980. Report on diamond drilling at Sisson Brook (March - June, 1980). Texas Gulf Minerals Exploration Office, Fredericton, N.B. Unpubl. company report.

MANN, R.F., 1981a. Sisson Brook WO_3-Cu-Ag Property. Unpubl. company report. October 1981.

MANN, R.F., 1981b. Report on diamond drilling at Sisson Brook, 1981 Drilling Program. Unpubl. company report. November 1981.

McQUADE, B.N., 1979. Geological report of the Sisson claims, New Brunswick. Project 267. NTS21-J/16. Unpubl, company report.

MOORE, R., 1979. Geological report, Sisson claims, N.B. Unpubl. company report. January 1979.

MUELLER, R.F., 1972. Stability of biotite: discussion. Am. Min., v. 57, 300-316.

MUTSCHLER, F.E., WRIGHT, E.G., LUDINGTON, S., and ABBOTT, J.T., 1981. Granite molybdenite systems. Econ. Geol., v. 76, 847-897.

ORVILLE, P.M., 1963. Alkali ion exchange between vapor and feldspar phases. Amer. Jour. Sci., v. 261. 201-237.

POPP, R.K., GILBERT, M.C., and CRAIG, J.R., 1977a. Stability of Fe-Mg amphiboles with respect to oxygen fugacity. Amer. Mineral., v. 62, 1-12.

POPP, R.K., GILBERT, M.C., and CRAIG, J.R., 1977b. Stability of Fe-Mg amphiboles with respect to sulfur fugacity. Amer. Mineral., v. 62, 13-30.

POTTER, R.W., 1977. Pressure corrections for fluid inclusion homogenization temperatures based on the volumetric properties of the system NaCl-H_2O. Jour. Research U.S. Geol. Surv., v. 5, no. 5, 603-607.

POTTER, R.W., BABCOCK, R.S., and BROWN, D.L., 1977. A new method for determining the solubility of salts in aqueous solutions at elevated temperatures. Jour. Research U.S. Geol. Survey, v.5, no. 3, 389-395.

POTTER, R.W., and BROWN, D.L., 1977. The volumetric properties of aqueous sodium chloride solutions from 0 to 500 C at pressure up to 2000 bars based on a regression of available data in the literature. U.S. Geol. Surv. Bull. 142-C, 36p.

RABINOVITCH, M., 1969. New Brunswick mineral resources. Assessment file no. 470269.

RAVENHURST, C., 1982. Kidd Creek Mines Ltd. report on geophysical work (1982) Sisson Brook, New Brunswick. Unpubl. company report. September 1982.

RIBBE, P.H., and VEBLEN, D.R., (eds.), 1982. Amphiboles: petrology and experimental phase relations. Min. Soc. Amer., v. 9B.

RICHARDSON, F.D., and JEFFES, J.H.E., 1952. The thermodynamics of substances of interest in iron and steel making : III - Sulfides. Iron Steel Inst. J., v. 7, 165-175.

ROBIE, R.A., and WALDBAUM, D.R., 1968. Thermodynamic properties of minerals and related substances at 298.15^{o}K (250.0^{o}C) and one atmosphere (1.013 Bars) pressure and at higher temperatures. USGS Bull., v. 1259.

RODGERS, J., 1970. The Tectonics of the Appalachians. John Wiley and Sons, Inc., New York, 271 p.

RODGERS, J., 1971. The Taconic orogeny. Geol. Soc. Amer. Bull., v.82, 1141-1178.

ROEDDER, E., and BODNAR, R.J., 1980. Geologic pressure determinations from fluid inclusion studies. Ann. Rev. Earth Planet. Sci., v. 8, 263-301.

ROSE, A.W., and BURT, D.M., 1979. Hydrothermal alteration. In, Barnes, H.L. (ed.), Geochemistry of Hydrothermal Ore Deposits, 2nd ed.: Wiley-Interscience, New York, 173-235.

RUITENBERG, A.A., FYFFE, L.R., McCUTCHEON, S.R., ST. PETER, C.J., IRRINKI, R.R., and VENUGOPAL, D.V., 1977. Evolution of pre-Carboniferous tectono-stratigraphic zones in the New Brunswick Appalachians. Geoscience Canada, v. 4, no. 4, 171-181.

RUITENBERG, A.A., and FYFFE, L.R., 1982. Mineral deposits associated with granitoid intrusions and related subvolcanic stocks in New Brunswick and their relationship to Appalachian tectonic evolution. Can. Inst. Min. Bull., v., June 1982.

RUMBLE, D., III, 1976. Oxide minerals in metamorphic rocks. In Rumble, D., III, (ed.), Min. Soc. Am. Short Course Notes: Oxide Minerals, v. 3, R1-R20.

SAMSON, I.M., 1983. Fluid inclusion and stable isotope studies of the Silvermines ore bodies, Ireland, and comparisons with Scottish vein deposits. Unpubl. PhD. thesis, Univ. of Strathclyde, Glasgow, 290p.

SAMSON, I.M., 1985. Fluid inclusion studies on the Mount Pleasant W-Mo-Sn deposit, New Brunswick. Geol. Assoc. Can. Prog. with Abstr., v. 10.

SCOTT, D., 1983. Sisson Brook zone III - scheelite distribution and colour of fluorescence. Unpubl. company report.

SMITH, J.V., 1983, Phase equilibria of plagioclase. In Feldspar mineralogy. Ribbe, P.H. (ed.), Mineral. Soc. America, Reviews in Mineral., v.10, 233-239.

TOULMIN, P., III., and BARTON, P.B., Jr., 1964. A thermodynamic study of pyrite and pyrrhotite. Geochim. Cosmochim. Acta, v. 28, 641-671.

WEAST, R.C. (ed.), 1976. Handbook of Chemistry and Physics, 57th ed.: CRC Press, Cleveland Ohio.

WILLIAMS-JONES, A., 1981. A petrographic examination of three gabbroic rock specimens. Unpubl. company report.

WONES, D., and EUGSTER, H.P., 1965. Stability of biotite: experiment, theory and application. Am. Min., v. 50, 1228-1272.

APPENDIX A: AMPHIBOLE ANALYSES

ZONE A

Sample number	8.22	8.22	8.22	9.24	9.24	9.24
Amphibole type	core	core	blade	core	blade	rim
SiO_2	51.20	51.81	49.75	50.75	43.19	43.42
Al_2O_3	4.99	4.62	7.99	4.13	11.45	10.80
TiO_2	0.29	0.26	0.19	0.25	0.64	0.68
FeO	15.20	15.19	14.52	18.57	21.13	20.25
MnO	0.47	0.33	0.26	0.52	0.57	0.59
MgO	13.64	13.73	11.97	11.65	7.76	7.74
CaO	11.97	11.78	11.80	11.59	11.41	11.37
Na_2O	0.45	0.41	1.30	0.37	1.06	0.92
K_2O	0.18	0.11	0.30	0.15	0.68	0.62
Total	98.39	98.25	98.07	97.97	97.90	96.40

Sample number	11.180	11.180	11.180	13.81	13.81	13.81
Amphibole type	rim	rim	core	core	core	rim
SiO_2	45.25	44.39	45.75	51.75	51.50	51.19
Al_2O_3	8.41	9.58	7.90	5.93	6.74	6.19
TiO_2	1.46	1.19	1.52	1.03	0.35	1.05
FeO	23.54	22.43	23.78	13.16	13.86	14.26
MnO	0.59	0.54	0.71	0.34	0.52	0.53
MgO	7.67	7.41	8.00	16.05	14.41	14.26
CaO	10.96	11.07	10.21	11.29	11.57	11.76
Na_2O	1.24	1.00	0.95	0.44	0.62	0.43
K_2O	0.64	0.58	0.56	0.28	0.20	0.27
Total	99.75	98.18	99.39	100.27	99.77	99.93

Sample number	13.148	13.148	13.148
Amphibole type	core	core	s
SiO_2	54.71	53.30	46.07
Al_2O_3	1.58	3.16	11.14
TiO_2	0.10	0.15	0.44
FeO	15.27	16.08	18.47
MnO	0.50	0.40	0.48
MgO	15.18	14.27	10.09
CaO	12.17	11.94	11.74
Na_2O	0.07	0.29	1.00
K_2O	0.04	0.08	0.59
Total	99.61	99.68	100.02

ZONE B

Sample number	25.136.55	25.136.55	25.136.55	25.136.55
Amphibole type	core	core	core	core
SiO_2	46.88	46.83	44.56	45.53
Al_2O_3	9.75	9.74	10.12	9.62
TiO_2	1.47	1.45	1.74	1.28
FeO	13.58	13.73	13.91	13.00
MnO	0.38	0.45	0.22	0.34
MgO	13.18	13.35	12.64	13.50
CaO	12.04	11.65	11.14	10.72
Na_2O	0.94	1.09	1.12	1.18
K_2O	0.39	0.37	0.38	0.34
Total	98.61	98.64	95.84	95.51

Sample number	25.136.55	25.136.55	25.136.55	25.136.55
Amphibole type	rim	core	core	core
SiO_2	44.51	52.29	55.24	51.93
Al_2O_3	10.37	3.71	1.78	3.18
TiO_2	1.93	0.21	0.02	0.24
FeO	13.68	10.31	8.93	11.00
MnO	0.31	0.24	0.21	0.24
MgO	13.04	17.39	18.51	17.51
CaO	11.16	11.47	12.05	12.02
Na_2O	1.23	0.33	0.20	0.38
K_2O	0.42	0.10	0.08	0.12
Total	96.64	96.04	97.03	96.61

Sample number	25.136.55	25.136.55	26.64.85	26.64.85
Amphibole type	core	core	core	rim
SiO_2	53.98	53.76	49.13	43.33
Al_2O_3	3.12	2.95	6.03	10.19
TiO_2	0.03	0.00	0.20	0.78
FeO	10.19	10.60	20.58	21.73
MnO	0.19	0.19	0.55	0.48
MgO	17.53	17.26	10.33	7.99
CaO	12.34	12.36	11.76	11.38
Na_2O	0.23	0.25	0.74	1.33
K_2O	0.12	0.10	0.20	0.85
Total	97.72	97.47	99.52	98.07

Sample number	26.64.85	33.167(2)	33.235.10	33.235.10
Amphibole type	rim	s	s	s
SiO_2	43.44	47.32	44.77	45.49
Al_2O_3	10.19	6.17	7.48	6.55
TiO_2	0.86	0.28	0.37	0.25
FeO	20.73	19.70	24.49	24.43
MnO	0.56	0.70	0.68	0.77
MgO	7.90	10.58	7.31	7.60
CaO	11.52	11.37	11.50	11.79
Na_2O	1.37	0.90	1.06	0.82
K_2O	0.89	0.48	0.74	0.64
Total	97.44	97.51	98.39	98.34

Sample number	33.205.10	33.205.10	37.116.8	37.116.8
Amphibole type	s	s	s	s
SiO_2	43.38	42.30	48.71	47.82
Al_2O_3	7.55	9.51	6.33	6.64
TiO_2	0.39	0.63	0.12	0.14
FeO	25.16	25.33	18.98	19.31
MnO	0.72	0.72	0.75	0.78
MgO	7.05	6.46	10.97	10.83
CaO	11.68	11.56	11.46	11.12
Na_2O	0.98	1.35	0.78	1.01
K_2O	0.83	1.12	0.49	0.57
Total	97.72	98.97	98.58	98.21

Sample number	37.207.75	37.207.75	0466	0466	0473
Amphibole type	s	s	vein	vein	vein
SiO_2	42.06	42.86	46.15	51.68	49.92
Al_2O_3	10.00	9.28	7.56	2.55	4.89
TiO_2	0.57	0.41	0.19	0.13	0.10
FeO	24.59	24.44	23.90	20.18	16.50
MnO	0.88	0.85	0.67	0.73	0.42
MgO	6.98	7.34	7.69	11.81	12.56
CaO	11.41	11.15	11.64	11.83	12.00
Na_2O	1.28	1.34	0.82	0.48	0.79
K_2O	1.19	0.87	0.46	0.18	0.33
Total	98.93	98.53	99.08	99.57	97.39

Sample number	0473	0473
Amphibole type	matrix	matrix
SiO_2	49.95	49.99
Al_2O_3	5.70	4.82
TiO_2	0.36	0.16
FeO	17.25	16.95
MnO	0.36	0.46
MgO	12.02	13.01
CaO	11.94	11.68
Na_2O	0.65	0.67
K_2O	0.20	0.46
Total	98.43	98.21

APPENDIX B: BIOTITE ANALYSES

I GABBRO - ZONE B

Sample number	31.181	33.167	33.178	36.35	0473	25.75
Biotite type	-------------pervasive------------					N3
SiO_2	36.74	37.66	37.35	37.06	37.85	37.87
Al_2O_3	14.50	13.73	14.64	14.07	14.28	15.79
TiO_2	3.05	1.80	2.14	2.24	2.35	2.56
FeO	19.45	21.27	20.78	20.26	20.56	16.59
MnO	0.22	0.31	0.29	0.30	0.25	0.24
MgO	12.14	12.22	12.08	11.40	11.66	14.01
CaO	0.03	0.00	0.03	0.05	0.13	0.00
Na_2O	0.15	0.07	0.08	0.06	0.17	0.23
K_2O	9.78	9.30	10.06	9.30	9.91	8.33
Total	96.04	96.35	97.45	94.73	97.16	95.61

II FGA UNITS

ZONE A

Sample number	8.18	8.33	9.24	11.180	11.180	13.148
Biotite type	halo	halo	halo	halo	vein	pervasive
SiO_2	35.81	37.94	36.27	36.34	36.27	36.05
Al_2O_3	16.83	14.58	15.71	14.83	15.25	15.83
TiO_2	1.22	1.97	2.10	2.48	2.48	2.39
FeO	19.50	21.65	22.96	23.82	24.95	21.25
MnO	0.25	0.25	0.22	0.24	0.21	0.31
MgO	12.15	11.85	9.73	9.58	9.39	12.69
CaO	0.00	0.02	0.00	0.02	0.04	0.02
Na_2O	0.12	0.17	0.13	0.11	0.08	0.08
K_2O	9.93	8.87	9.33	9.34	9.61	8.05
Total	96.44	96.69	96.43	96.75	98.27	96.67

ZONE B

Sample number	26.64	35.134
Biotite type	---pervasive--	
SiO_2	36.45	36.50
Al_2O_3	15.20	14.40
TiO_2	3.30	2.74
FeO	22.09	22.37
MnO	0.35	0.38
MgO	10.00	10.58
CaO	0.01	0.03
Na_2O	0.12	0.05
K_2O	9.83	9.24
Total	97.36	96.29

III META-SEDIMENTARY

ZONE A

Sample number	2.34	13.74	13.77
Biotite type	------pervasive------		
SiO_2	37.87	36.85	37.69
Al_2O_3	15.38	18.51	17.04
TiO_2	1.84	2.22	1.77
FeO	18.15	20.05	19.02
MnO	0.30	0.19	0.16
MgO	13.63	9.10	11.65
CaO	0.00	0.00	0.00
Na_2O	0.04	0.26	0.11
K_2O	9.96	9.65	9.94
Total	97.18	96.83	97.37

ZONE B

Sample number	26.74	26.78	26.78	38.155
Biotite type	--pervasive--		vein	pervasive
SiO_2	35.58	35.52	33.13	37.19
Al_2O_3	16.06	14.91	16.23	15.29
TiO_2	2.47	2.25	1.82	3.20
FeO	20.97	25.91	26.32	20.58
MnO	0.39	0.39	0.68	0.36
MgO	10.40	8.08	9.68	10.61
CaO	0.00	0.00	0.00	0.00
Na_2O	0.13	0.10	0.01	0.08
K_2O	9.82	8.99	6.78	9.98
Total	95.82	96.14	94.66	97.29

IV FQB PORPHYRY PHENOCRYST

Sample number	26.16
SiO_2	35.40
Al_2O_3	14.65
TiO_2	3.89
FeO	23.49
MnO	0.30
MgO	10.44
CaO	0.06
Na_2O	0.21
K_2O	8.11
Total	96.54

APPENDIX C: PLAGIOCLASE ANALYSES

I A1-ALTERED CRYSTALS

Sample number	13.35	0466	0473	25.75
Zone	A	B	B	B
SiO_2	64.51	68.51	56.28	25.75
Al_2O_3	22.50	21.24	26.46	31.27
TiO_2	0.04	0.03	0.02	0.00
FeO	0.00	0.14	0.11	0.09
MnO	0.00	0.03	0.00	0.02
MgO	0.01	0.02	0.00	0.00
CaO	3.28	0.19	11.29	12.98
Na_2O	8.98	8.87	6.07	4.02
K_2O	1.12	0.42	0.12	0.07
Total	100.43	99.44	100.35	101.15

II A2-ALTERED CRYSTALS

Sample number	13.77a	13.77b	13.77b	26.22(4)	26.74
Zone	A	A	A	B	B
SiO_2	64.67	49.25	51.40	70.52	65.28
Al_2O_3	18.63	32.57	30.70	21.75	22.09
TiO_2	0.00	0.00	0.01	0.00	0.09
FeO	0.00	0.46	0.09	0.02	0.00
MnO	0.01	0.03	0.01	0.00	0.00
MgO	0.02	0.32	0.04	0.00	0.01
CaO	0.00	13.81	13.66	1.77	2.95
Na_2O	0.05	2.52	3.80	8.01	10.89
K_2O	17.56	0.86	0.10	0.16	0.25
Total	100.92	99.81	99.81	102.23	101.55

Sample number	33.178	36.35
Zone	B	B
SiO_2	53.03	59.59
Al_2O_3	30.34	25.10
TiO_2	0.03	0.00
FeO	0.13	0.12
MnO	0.01	0.03
MgO	0.00	0.00
CaO	12.63	6.84
Na_2O	4.34	7.42
K_2O	0.05	0.20
Total	100.57	99.30

III A1- and A2- ALTERED CRYSTALS

Sample number	9.24	26.64(4)	33.167
Zone	A	B	B
SiO_2	55.22	66.74	57.48
Al_2O_3	27.91	20.10	27.91
TiO_2	0.10	0.00	0.00
FeO	0.29	0.07	0.10
MnO	0.02	0.01	0.00
MgO	0.01	0.02	0.00
CaO	10.51	2.04	9.87
Na_2O	5.67	9.58	5.56
K_2O	0.19	0.38	0.13
Total	99.91	100.95	101.03

IV FQB PORPHYRY PHENOCRYST

Sample number	26.16	26.16	26.16	26.16	26.16	26.16
	core	----------	----------	----------	----------	½ rim
SiO_2	60.17	60.53	63.49	63.81	68.92	64.12
Al_2O_3	25.69	25.19	23.87	23.73	21.41	22.61
TiO_2	0.01	0.05	0.01	0.00	0.00	0.00
FeO	0.07	0.04	0.04	0.11	0.00	0.00
MnO	0.05	0.03	0.02	0.00	0.00	0.00
MgO	0.00	0.00	0.00	0.00	0.00	0.00
CaO	7.19	6.38	5.12	4.93	3.44	3.44
Na_2O	7.36	7.57	8.24	8.20	9.96	9.98
K_2O	0.45	0.51	0.73	0.69	0.04	0.04
Total	100.98	100.30	101.52	101.48	103.76	100.16

APPENDIX D: MANGANIFEROUS ILMENITE ANALYSES

I ZONE A

Sample number	2.34	8.18	8.22	11.180	13.77	13.81
Rock type	meta-sed	FGA	FGA	FGA	meta-sed	FGA
SiO_2	0.00	0.02	0.11	0.06	0.00	0.09
Al_2O_3	0.06	0.00	0.02	0.02	0.00	0.06
TiO_2	50.51	51.88	51.93	50.16	52.70	51.88
FeO	41.58	45.18	45.51	46.44	44.83	42.30
MnO	6.22	3.63	3.22	2.32	3.64	4.34
MgO	0.06	0.06	0.16	0.13	0.09	0.10
CaO	0.04	0.09	0.34	0.06	0.00	0.43
Na_2O	0.00	0.00	0.01	0.06	0.00	0.03
K_2O	0.09	0.01	0.01	0.00	0.03	0.01
Total	98.56	100.87	101.31	99.25	101.29	99.24

Sample number	13.148
Rock type	FGA
SiO_2	0.08
Al_2O_3	0.00
TiO_2	51.33
FeO	42.78
MnO	4.21
MgO	0.18
CaO	0.14
Na_2O	0.06
K_2O	0.02
Total	98.80

II ZONE B

Sample number	0466	31.181	33.178
Rock type	vein	FGA	gabbro
SiO_2	0.03	0.03	0.00
Al_2O_3	0.03	0.00	0.00
TiO_2	46.61	52.14	51.01
FeO	45.93	45.29	44.88
MnO	3.81	3.46	3.99
MgO	0.26	0.17	0.12
CaO	0.16	0.30	0.02
Na_2O	0.00	0.04	0.00
K_2O	0.00	0.02	0.01
Total	96.83	101.45	100.03

APPENDIX E: COMP

COMP is a program written in FORTRAN to calculate the fugacity of fH_2, given values for fO_2 and fS_2. The fH_2 was, in turn, used to calculate fH_2O, fSO_2, fSO, fH_2S, and fHS, fH_2SO_4.

The following equations define the logarithms of the fugacities of the gas species under consideration.

(1) $x_1 = \log fH_2O$

(2) $x_2 = \log fH_2$

(3) $x_3 = \log fO_2$

(4) $x_4 = \log fSO_2$

(5) $x_5 = \log fS_2$

(6) $x_6 = \log fSO$

(7) $x_7 = \log fH_2S$

(8) $x_8 = \log fHS$

(9) $x_9 = \log fH_2SO_4$

Using these equations, the rate equations (i.e.,K_{eq}) for formation of each species at 700 bars and 450°C (the conditions used in the phase diagrams of this study) become:

(10) $x_9 - 1/2x_5 - x_2 - 2x_3 = 22.93$

(11) $x_8 - 1/2x_5 - 1/2x_2 = -3.49$

(12) $x_7 - 1/2x_5 - x_2 = 2.29$

(13) $x_6 - 1/2x_5 - 1/2x_3 = 3.41$

(14) $x_5 = -12.50$

(15) $x_4 - 1/2x_5 - x_3 = 16.01$

(16) $x_3 = -29.00$

(17) $x_1 - x_2 - 1/2x_3 = 10.20$,

which are added together to describe the total internal pressure of the system, P (in this case, 700 bars),

$$(18)\quad P = 1/0.671\ 10^{x_1} + 1/1.461\ 10^{x_2} + 10^{x_3} + 10^{x_5} + 1/1.51\ 10^{x_4} + 10^{x_6} + 1/1.517\ 10^{x_7} + 10^{x_7} + 10^{x_8} + 10^{x_9}$$

The values for fO_2 (x_3) and fS_2 (x_5) were obtained directly by choosing one point along the magnetite/pyrrhotite boundary, constructed at 700 bars and 450°C. The latter was drawn using the thermodynamic and experimental data of Robie and Waldbaum (1968) and Toulmin and Barton (1964), respectively.

Equations 10 to 17 were simultaneously solved to leave a single free variable, which we chose as x_2. Substituting these results into equation 18, gives us a transcendental equation for x_2. COMP was written to calculate the function of equation 18 for a given value of x_2. We find the root of this equation by repeatedly choosing values of x_2 until the user deems the function sufficiently close to zero.

COMP

```
      IMPLICIT REAL*8 (A-H,O-Z)
      F(X) = DEXP(X*DX)*(T1+T2*DEXP(-0.5D0*DX*X))-C1
      DX=DLOG(10.D0)
      C1=700.D00-EXP(-DX*29.00D0)-DEXP(-DX*12.D0)-DXP(-DX*16.73D0)
      -(1*.D0/1.51D0)*DEXP(-DX*14.79D0)
      T1=(DEXP(-DX*0.57D0))/0.621D0+(1D0/1.461D0)+(DEXP(-DX*2.96D0))/1
      %57D0+DEXP(-DX*30.3D0)
      T2=DEXP(-DX*12.12D0)
      WRITE(6,900)C1, T1, T2
900   FORMAT(" ","C1=",F20.14,"   T1=",F20.14   T2="F20.14)
      XOLD=-2.D0
      YOLD=F(XOLD)
      WRITE(6,300)XOLD,YOLD
300   FORMAT("","X=",F10.6"   Y=",D13.6)
      XNEW=-1.D0
23    YNEW=F(XNEW)
C100  SLOPE=(YNEW-YOLD)/(XNEW-XOLD)
      WRITE(6,300)SNEW,YNEW
      READ(9,*)XNEW
      GO TO 23
      STOP
      END
C     XNEW=X2
C     CONSTANTS CHOSEN FOR PT = 700 BARS AND T = 450°C.
C     LOG FS2 AND LOG FO2 EQUAL -12.50 AND -29.00,
C     RESPECTIVELY.  THE LATTER ARE VALUES ALONG THE MAG/PO
C     BOUNDARY DRAWN AT 700 BARS AND 450°C USING THE
```

```
C     THERMODYNAMIC AND EXPERIMENTAL DATA OF ROBIE AND WALDBAUM
C     (1968) AND BARTON AND TOULMIN (1964), RESPECTIVELY.
```